ECSS-E-HB-31-01 Part 6A
5 December 2011

Space engineering

Thermal design handbook - Part 6: Thermal Control Surfaces

ECSS Secretariat
ESA-ESTEC
Requirements & Standards Division
Noordwijk, The Netherlands

Foreword

This Handbook is one document of the series of ECSS Documents intended to be used as supporting material for ECSS Standards in space projects and applications. ECSS is a cooperative effort of the European Space Agency, national space agencies and European industry associations for the purpose of developing and maintaining common standards.

The material in this Handbook is a collection of data gathered from many projects and technical journals which provides the reader with description and recommendation on subjects to be considered when performing the work of Thermal design.

The material for the subjects has been collated from research spanning many years; therefore a subject may have been revisited or updated by science and industry.

The material is provided as good background on the subjects of thermal design, the reader is recommended to research whether a subject has been updated further, since the publication of the material contained herein.

This handbook has been prepared by ESA TEC-MT/QR division, reviewed by the ECSS Executive Secretariat and approved by the ECSS Technical Authority.

Disclaimer

ECSS does not provide any warranty whatsoever, whether expressed, implied, or statutory, including, but not limited to, any warranty of merchantability or fitness for a particular purpose or any warranty that the contents of the item are error-free. In no respect shall ECSS incur any liability for any damages, including, but not limited to, direct, indirect, special, or consequential damages arising out of, resulting from, or in any way connected to the use of this document, whether or not based upon warranty, business agreement, tort, or otherwise; whether or not injury was sustained by persons or property or otherwise; and whether or not loss was sustained from, or arose out of, the results of, the item, or any services that may be provided by ECSS.

Published by: ESA Requirements and Standards Division
ESTEC, P.O. Box 299,
2200 AG Noordwijk
The Netherlands
Copyright: 2011 © by the European Space Agency for the members of ECSS

Table of contents

1 Scope....15

2 References....16

3 Terms, definitions and symbols....17

3.1 Terms and definitions....17
3.2 Abbreviated terms....17
3.3 Symbols....18

4 General introduction....21

5 Coatings....23

5.1 General....23
5.2 Solar reflectors....25
5.2.1 Titanium Dioxide-Polymethyl Vinyl Siloxane....25
5.2.2 Zinc Oxide-Potassium Silicate....32
5.2.3 Zinc Orthotitanate-Potassium Silicate....52
5.2.4 Zinc Oxide-Methylsilicone....136
5.2.5 Zinc Oxide-Potassium Silicate....163
5.2.6 Silver vacuum deposited on fused Silica....196
5.2.7 Silver vacuum deposited on fused Silica with a conductive coating....251
5.3 Total reflectors....274
5.3.1 Leafing Aluminium-Silicone....274
5.4 Total absorbers....279
5.4.1 Carbon black-Acrylic resin....279

6 Adhesive tapes....283

6.1 General....283
6.1.2 Adhesive properties....283
6.1.3 Curing of adhesive tapes....285
6.1.4 General purpose adhesive tapes....286
6.2 Application and handling....298
6.2.1 Application....298

6.2.2 Cleaning 298
6.2.3 Handling 299
6.2.4 Repairing 300
6.3 Degradation 300
6.3.1 Introduction 300
6.3.2 Terrestrial degradation 300
6.3.3 Space degradation 300
6.3.4 Blistering 304
6.4 Relevant properties of thermal control tapes 307
6.5 Past spatial use 331

Bibliography 333

Figures

Figure 4-1: Basic types of thermal control coatings. T_R [K] is the equilibrium temperature of a coated isothermal sphere at 1 AU. From Touloukian, DeWitt & Hernicz (1972) [126]. 21

Figure 4-2: Range of solar absorptance, α_S, and hemispherical total emittance, ε, covered by available thermal control coatings. From Touloukian, DeWitt & Hernicz (1972) [126]. 22

Figure 5-1: UV radiation effects on solar absorptance, α_S, of Thermatrol 2A-100 vs. exposure time, *t*. From Breuch (1967) [22]. 28

Figure 5-2: Change in solar absorptance, $\Delta\alpha_S$, of Thermatrol 2A-100, under various radiation conditions, vs. exposure time, *t*. From McCargo et al. (1971) [82]........ 28

Figure 5-3: Normal-hemispherical spectral reflectance, ρ_λ', of Thermatrol 2A-100, measured by two different methods, vs. wavelength, λ. From Cunnington, Grammer & Smith (1969) [33]. 29

Figure 5-4: Effect of Ultra-Violet Radiation on spectral reflectance, ρ_λ', of Thermatrol 2A-100 vs. wavelength, λ. Most of the data, concerning bidirectional reflectance, are from Rittenhouse & Singletary (1969) [105], while dashed line and dotted line, normal-hemispherical reflectance, are from Cunnington, Grammer & Smith (1969) [33]. 30

Figure 5-5: Variation of solar absorptance, α_S, with thickness, t_c. From Stevens (1971) [120]. 36

Figure 5-6: Estimated changes in the solar absorptance, α_S, of Z-93 during the total mission profile for a near-Earth orbit. From McCargo, Spradley, Greenberg & McDonald (1971) [82]. 45

Figure 5-7: Normal-hemispherical spectral reflectance, ρ_λ', of Z-93 vs. wavelength, λ. All data are from Touloukian, DeWitt & Hernicz (1972) [126] except solid and dashed lines which are from Cunnington, Grammer & Smith (1969) [33]. 47

Figure 5-8: Effect of Ultra-Violet Radiation on normal-hemispherical spectral reflectance, ρ_λ', of Z-93 vs. wavelength, λ. Data points are from Touloukian, DeWitt & Hernicz (1972) [126], while smooth curves are from Cunnington, Grammer & Smith (1969) [33]. 49

Figure 5-9: Effect of Proton Radiation on normal-hemispherical spectral reflectance, ρ_λ', of Z-93 vs. wavelength, λ. From Touloukian, DeWitt & Hernicz (1972) [126]. 50

Figure 5-10: Hemispherical total emittance, ε, of Zinc Orthotitanate-Potassium Silicate Coatings vs. temperature, T. ○: SSR pigment,> phosphated. From Keyte (1975) [70]. ●: MOX pigment,> YB-71. From Harada & Wilkes (1979) [58]. □: YB-71.> AESC. From Ahern & Karperos (1983) [4]. 60

Figure 5-11: Solar absorptance, α_S, of YB-71 vs. thickness, t_c. ○: From Harada & Wilkes (1979) [58]. ▨: From measurements on 16 panels by AESC. Scatter is due to t_c variation. From Ahern & Karperos (1983) [4]. 60

Figure 5-12: Solar absorptance, α_S, of Zinc Orthotitanate-Potassium Silicate coating vs. incidence angle, β. SSR pigment, phosphated. From Keyte (1975) [70]. 63

Figure 5-13: Solar absorptance, α_S, of several YB-71 coatings vs. exposure time, t, as deduced from data of various spacecraft in geosynchronous orbits. Numbers corresponds to sample designations. 74

Figure 5-14: Normal-hemispherical spectral reflectance, ρ'_λ, of Zinc Orthotinanate-Potassium Silicate coatings vs. wavelength, λ. 76

Figure 5-15: Effect of Ultra-Violet Radiation on normal-hemispherical spectral reflectance, ρ'_λ, of Zinc Orthotitanate- Potassium Silicate coatings vs. wavelength, λ. 78

Figure 5-16: Effect of Protons Radiation on normal-hemispherical spectral reflectance, ρ'_λ, of Zinc Orthotitanate-Potassium Silicate coatings vs. wavelength, λ. From Gilligan & Zerlaut (1971) [46]. 79

Figure 5-17: Hemispherical total emittance, ε, of S-13 G coating vs. temperature, T. 2 x 10^{-4} m thick coating on molybdenum substrate. From Spisz & Jack (1971) [119]. 85

Figure 5-18: Hemispherical total emittance, ε, of S-13 and S-13 G coatings vs. exposure time, t, at 1-Sun level and 395 K. From Cunnington, Grammer & Smith (1969) [33]. Equal symbols correspond to the same sample. ○ :> Sample 27; ● :> Sample 43; □ :> Sample 28; ■ :> Sample 44. 87

Figure 5-19: Variation of solar absorptance, α_S, of S-13 coating with coating thickness, t_c. ○ :> Nominal composition. Sprayed on primed surface. Air dryed. T = 298 K. (Designation in the ref.: 119 to 127). □ :> ZnO in silicone binder. T = 298 K. (Designation in the ref.: 29, 30). From Touloukian, DeWitt & Hernicz (1972) [126]. 89

Figure 5-20: Solar absorptance, α_S, of S-13 G coating vs. incidence angle, β. From Keyte (1975) [70]. 90

Figure 5-21: Change in solar absorptance, $\Delta\alpha_S$, of S-13 and S-13 G coatings due to Protons and Alpha Particles Radiation vs. integrated flux, n. 94

Figure 5-22: Change in solar absorptance, $\Delta\alpha_S$, of S-13 G coating due to Electrons Radiation vs. integrated flux, n. Data taken in situ. Compiled by Bourrieau, Paillous & Romer (1976) [21]. 96

Figure 5-23: Changes in solar absorptance of S-13 and S-13 G coatings. OSO III experiment. From Millard (1969) [84]. 98

Figure 5-24: Change in solar absorptance, $\Delta\alpha_S$, of S-13 coatings vs. flight time in ESH as measured in orbital flight. Prepared by the compiler after Touloukian, DeWitt & Hernicz (1972) [126]. 99

Figure 5-25: Change in solar absorptance, $\Delta\alpha_S$, of S-13 G coating vs. flight time in ESH as measured in orbital flight. Prepared by the compiler after Touloukian, DeWitt & Hernicz (1972) [126]. 100

Figure 5-26: Position on the sample holder of the samples 1 and 2, for irradiation and measurement. From Paillous (1976) [96]. 104

Figure 5-27: Solar absorptance, α_S, of S-13 G/LO coating vs. flight time, ... 105

Figure 5-28: Variation of absorptance to emittance ratio, α/ε, of S-13 coating vs. flight time. Prepared by the compiler after Touloukian, DeWitt & Hernicz (1972) and Triolo (1973) [126] 106

Figure 5-29: Variation of absorptance to emittance ratio, α/ε, of S-13 G coating vs. flight time. Prepared by the compiler after Touloukian, DeWitt & Hernicz (1972) [126]. 107

Figure 5-30: Normal-hemispherical spectral reflectance, ρ'_λ, of S-13 coating vs. wavelength, l, for five different values of P-VC. G.E. LTV-602 binder. From Touloukian, DeWitt & Hernicz (1972) [126]. 108

Figure 5-31: Effect of Ultra-violet Radiation on normal-hemispherical spectral reflectance, ρ'_λ, of S-13 coating vs. wavelength, λ. LTV-602 silicone binder. Two different pigment-binder ratios (PBR). From Touloukian, DeWitt & Hernicz (1972) [126]. 109

Figure 5-32: Effect of Ultra-Violet Radiation on normal-hemispherical spectral reflectance, ρ'_λ, of S-13 coating vs. wavelength, λ. Several binders and PBRs. From Touloukian, DeWitt & Hernicz (1972) [126]. 110

Figure 5-33: Effect of Ultra-Violet Radiation on normal-hemispherical spectral reflectance, ρ'_λ, of S-13 coating vs. wavelength, λ. From Touloukian, DeWitt & Hernicz (1972) [126]. 111

Figure 5-34: Effect of Ultra-Violet Radiation on normal-hemispherical spectral reflectance, ρ'_λ, of S-13 coating vs. wavelength, λ. From Zerlaut, Rogers & Noble (1969) [144]. Drawn from Touloukian, DeWitt & Hernicz (1972) [126]. 112

Figure 5-35: Effect of Ultra-Violet Radiation on normal-hemispherical spectral reflectance, ρ'_λ, of S-13 G coating vs. wavelength, λ. Two different pigment treatment processes. From Zerlaut, Rogers & Noble (1969) [144]. Drawn from Touloukian, DeWitt & Hernicz (1972) [126]. 113

Figure 5-36: Effect of Ultra-Violet Radiation on normal-hemispherical spectral reflectance, ρ'_λ, of S-13 G coating vs. wavelength, λ. Sweated pigment. Two different solvent systems. From Zerlaut, Rogers & Noble (1969) [144]. Drawn from Touloukian, DeWitt & Hernicz (1972) [126]. 114

Figure 5-37: Effect of Ultra-Violet Radiation on normal-hemispherical spectral reflectance, ρ'_λ, of S-13 G coating vs. wavelength, λ. Two different pigment treatment processes. Owens-Illinois 650 binder. From Zerlaut, Rogers & Noble (1969) [144]. Drawn from Touloukian, DeWitt & Hernicz (1972) [126]. 115

Figure 5-38: Effect of Ultra-Violet Radiation on normal-hemispherical spectral reflectance, ρ'_λ, of S-13 G coating vs. wavelength, λ. Pigment was sifted prior to wet grinding. Paint grind time 3 h. From Zerlaut, Rogers & Noble (1969) [144]. Drawn from Touloukian, DeWitt & Hernicz (1972) [126]....... 116

Figure 5-39: Effect of Ultra-Violet Radiation on normal-hemispherical spectral reflectance, ρ'_λ, of S-13 G coating vs. wavelength, λ. Silicated pigment with five mechanical perturbations. From Zerlaut, Rogers & Noble (1969) [144]. Drawn from Touloukian, DeWitt & Hernicz (1972) [126]. 117

Figure 5-40: Effect of Ultra-Violet Radiation on normal-hemispherical spectral reflectance, ρ'_λ, of S-13 G coating vs. wavelength, λ. Plasma annealed and potassium silicate treated pigment. From Gilligan & Zerlaut (1971) [46]. 118

Figure 5-41: Protons exposure effects on normal-hemispherical spectral reflectance, ρ'_λ, of S-13 coating vs. wavelength, λ. LTV-602 silicone binder. From Gillette, Brown, Seiler & Sheldon (1966) [54]. Drawn from Touloukian, DeWitt & Hernicz (1972) [126]. 120

Figure 5-42: Protons exposure effects on normal-hemispherical spectral reflectance, ρ'_λ, of S-13 G coating vs. wavelength, λ. Plasma annealed and potassium silicate treated pigment. From Gilligan & Zerlaut (1971) [46]. 121

Figure 5-43: Electrons exposure effects on normal-hemispherical spectral reflectance, ρ'_λ, of S-13 G coating vs. wavelength, λ. Radiation intensity 20 keV. Recovery after exposure. From Fogdall, Cannaday & Brown (1970) [43]. Drawn from Touloukian, DeWitt & Hernicz (1972) [126]. 122

Figure 5-44: Electrons exposure effects on normal-hemispherical spectral reflectance, ρ'_λ, of S-13 G coating vs. wavelength, λ. Radiation intensity 80 keV. Recovery after exposure. From Fogdall, Cannaday & Brown (1970) [43]. Drawn from Touloukian, DeWitt & Hernicz (1972) [126]. 124

Figure 5-45: Electrons exposure effects on normal-hemispherical spectral reflectance, ρ'_λ, of GSFC, 101-7 coating vs. wavelength, λ. Radiation intensity 20 keV. Different integrated fluxes. 101-7 is a coating, similar to S-13 G, developed by NASA Goddard. From Fogdall, Cannaday Brown (1970) [43]. Drawn from Touloukian, DeWitt & Hernicz (1972) [126]. 125

Figure 5-46: Electrons exposure effects on normal-hemispherical spectral reflectance, ρ'_λ, of GSFC, 101-7 coating vs. wavelength, λ. Radiation intensity 80 keV. Different integrated fluxes. 101-7 is a coating, similar to S-13 G, developed by NASA Goddard. From Fogdall, Cannaday & Brown (1970) [43]. Drawn from Touloukian, DeWitt & Hernicz (1972) [126]. 126

Figure 5-47: Electrons exposure effects on normal-hemispherical spectral reflectance, ρ'_λ, of GSFC, 101-7 coating vs. wavelength, λ. Radiation intensity 20 keV. Recovery after exposure. 101-7 is a coating, similar to S-13 G, developed by NASA Goddard. From Fogdall, Cannaday & Brown (1970) [43]. Drawn from Touloukian, DeWitt & Hernicz (1972) [126]. 127

Figure 5-48: Electrons exposure effects on normal-hemispherical spectral reflectance, ρ'_λ, of GSFC, 101-7 coating vs. wavelength, λ. Radiation intensity 80 keV. Recovery after exposure. 101-7 is a coating, similar to S-13 G, developed by NASA Goddard. From Fogdall, Cannaday Brown (1970) [43]. Drawn from Touloukian, DeWitt & Hernicz (1972) [126]. 128

Figure 5-49: Effect of Combined Exposure on normal-hemispherical spectral reflectance, ρ'_λ, of S-13 G coating vs. wavelength, λ. Plasma annealed and potassium silicate treated pigment. From Gilligan & Zerlaut (1971) [46]. 130

Figure 5-50: Effect of Combined Exposure, simulating up to three years in geosynchronous orbit, on normal- hemispherical spectral reflectance, ρ'_λ, of S-13 G/LO coating vs. wavelength, λ. From Paillous (1976) [96]. 131

Figure 5-51: Effect of O_2 bleaching, after Combined Exposure, on normal-hemispherical spectral reflectance, ρ'_λ, of S-13 G/LO coating vs. wavelength, λ. Curves of ▬▬▬ and ▬▬•▬▬ are those shown in Figure 5-19. From Paillous (1976) [96]. 132

Figure 5-52: Effect of Combined Exposure, simulating up to three years in geosynchronous orbit, on normal- hemispherical spectral reflectance, ρ'_λ, of S-13 G/LO coating vs. wavelength, λ. Curves of ▬ ▬ and — — are those shown in Figure 5-50. From Paillous (1976) [96]. 133

Figure 5-53: Change in normal-hemispherical spectral absorptance, $\Delta\alpha'_\lambda$, of PSG 120 coating, due to Ultra-Violet Radiation, vs. exposure time, *t*. Wavelength, λ = 0,46x10^{-6} m. From Simon (1974) [118]. 140

Figure 5-54: Change in normal-hemispherical spectral absorptance, $\Delta\alpha'_\lambda$, of PSG 120 coating, due to Ultra-Violet Radiation, vs. exposure time, *t*. Wavelength, λ = 2,5x10^{-6} m. Shaded zone in *a* is enlarged in *b*. See Explanation in the caption of Figure 5-53. From Simon (1974) [118]. 141

Figure 5-55: Change in solar absorptance, $\Delta\alpha_S$, of PSG 120 coating, due to UV radiation, vs. exposure time, *t*. Shaded zone in *a* is enlarged in *b*. From Simon (1974) [118]. 142

Figure 5-56: Estimated change in solar absorptance, α_S, of PSG 120 vs. time, t. From Paillous (1976) [96]. ○: From Guillaumon & Guillin (1981) [52]. 148

Figure 5-57: Bidirectional total radiation intensity of reflected flux, *i*'', vs. cone angle, β', for several values of the cone angle of the incident flux, β. PSG 120 coating. Incident and reflected fluxes are coplanar. *i*'' is measured by the response of a photocell attached to a photogoniometer. From ASTRAL (1976)a [6]. 148

Figure 5-58: Effect of Ultra-Violet Radiation on normal-hemispherical spectral reflectance, ρ'_λ, of PSG 120 coating vs. wavelength, λ. Thick line: Before irradiation. $p<1{,}3\times10^{-5}$ Pa. T = 348 K. Thin line: After irradiation. $p<1{,}3\times10^{-5}$ Pa. T = 348 K. A Sun level. t = 212 ESH. From Simon (1973) [117]. 149

Figure 5-59: Effect of Protons radiation on normal-hemispherical spectral reflectance, ρ'_λ, of PSG 120 coating vs. wavelength, λ. Radiation intensity ≅ 45 keV. See Explanation in the caption of Figure 5-61. From Paillous, Amat, Marco & Panabiere (1977) [97]. 150

Figure 5-60: Effect of Protons radiation on normal-hemispherical spectral reflectance, ρ'_λ, of PSG 120 coating vs. wavelength, λ. Radiation intensity ≅ 75 keV. See Explanation in the caption of Figure 5-61. From Paillous, Amat, Marco & Panabiere (1977) [97]. 151

Figure 5-61: Effect of Protons radiation on normal-hemispherical spectral reflectance, ρ'_λ, of PSG 120 coating vs. wavelength, λ. Radiation intensity ≅ 150 keV. From Paillous, Amat, Marco & Panabiere (1977) [97]. 151

Figure 5-62: Effect of Electrons Radiation on normal-hemispherical spectral reflectance, ρ'_λ, of PSG 120 coating vs. wavelength, λ. Radiation intensity ≅ 40 keV. See Explanation in the caption of Figure 5-63. From Paillous, Amat, Marco & Panabiere (1977) [97]. 153

Figure 5-63: Effect of Electrons Radiation on normal-hemispherical spectral reflectance, ρ'_λ, of PSG 120 coating vs. wavelength, λ. Radiation intensity ≅ 80 keV. From Paillous, Amat, Marco & Panabiere (1977) [97]. 153

Figure 5-64: Effect of Electrons Radiation on normal-hemispherical spectral reflectance, ρ'_{λ}, of PSG 120 coating vs. wavelength, λ. Radiation intensity ≅ 210 keV. From Paillous, Amat, Marco & Panabiere (1977) [97]. 154

Figure 5-65: Change in normal-hemispherical spectral reflectance, ρ'_{λ}, of PSG 120 coating, due to particulate irradiation, vs. penetration range, X_d. Wavelength, λ = 2,05x10^{-6} m. From Bourrieau (1978) [19]. 157

Figure 5-66: Effect of Combined Exposure, simulating up to three years in geosyncronous orbit, on normal-hemispherical spectral reflectance, ρ'_{λ}, of PSG 120 coating vs. wavelength, λ. From Paillous (1976) [96]......................... 157

Figure 5-67: Effect of O_2 bleaching, after Combined Exposure, on normal-hemispherical spectral reflectance, ρ'_{λ}, of PSG 120 coating vs. wavelength, λ. Curves ▬▬▬ and — — are those shown in Figure 5-66. From Paillous (1976) [96]. 158

Figure 5-68: Change in normal-hemispherical spectral absorptance, $\Delta\alpha'_{\lambda}$, of PSZ 184 coating, due to UV Radiation, vs. exposure time, *t*. Wavelength, λ = 0,46x10^{-6} m. See Explanation in the caption of Figure 5-69. From Simon (1974) [118]. 166

Figure 5-69: Change in normal-hemispherical spectral absorptance, $\Delta\alpha'_{\lambda}$, of PSZ 184 coating, due to UV Radiation, vs. exposure time, *t*. Wavelength, λ = 2,5x10^{-6} m. From Simon (1974) [118].. 167

Figure 5-70: Change in solar absorptance, $\Delta\alpha_S$, of PSZ 184 coating, due to UV Radiation, vs. exposure time, *t*. Shaded zone in *a* is enlarged in *b*. From Simon (1974) [118]. 168

Figure 5-71: Estimated change in solar absorptance, α_S, of PSZ 184 vs. time, *t*. From Paillous (1976) [96]. 173

Figure 5-72: Effect of Ultra-Violet Radiation on normal-hemispherical spectral reflectance, ρ'_{λ}, of PSZ 184 coating vs. wavelength, λ. Thick line: Before irradiation. p<1,3x10^{-5} Pa. Thin line: After irradiation. p<1,3x10^{-5} Pa. 1 Sun level. Neither sample temperature nor exposure time are given. From Simon (1974) [118]. 174

Figure 5-73: Effect of Protons Radiation on normal-hemispherical spectral reflectance, ρ'_{λ}, of PSZ 184 coating vs. wavelength, λ. *a* Coating on P 131 primer. *b* Coating on silicated primer. Radiation intensity ≅ 45 keV. See Explanation in the caption of Figure 5-74. From Paillous, Amat, Marco & Panabiere (1977) [97]. 175

Figure 5-74: Effect of Protons Radiation on normal-hemispherical spectral reflectance, ρ'_{λ}, of PSZ 184 coating, on silicated primer, vs. wavelength, λ. Radiation intensity ≅ 75 keV. From Paillous, Amat, Marco & Panabiere (1977) [97]. 176

Figure 5-75: Effect of Protons Radiation on normal-hemispherical spectral reflectance, ρ'_{λ}, of PSZ 184 coating, on silicated primer, vs. wavelength, λ. Radiation intensity ≅ 150 keV. From Paillous, Amat, Marco & Panabiere (1977) [97]. 177

Figure 5-76: Effect of Electrons Radiation on normal-hemispherical spectral reflectance, ρ'_{λ}, of PSZ 184 coating, on silicated primer, vs. wavelength, λ. Radiation intensity ≅ 40 keV. From Paillous, Amat, Marco & Panabiere (1977) [97]. 178

Figure 5-77: Effect of Electrons Radiation on normal-hemispherical spectral reflectance, ρ'_{λ}, of PSZ 184 coating, on silicated primer, vs. wavelength, λ.

Radiation intensity ≅ 80 keV. From Paillous, Amat, Marco & Panabiere (1977) [97]. 179

Figure 5-78: Effect of Electrons Radiation on normal-hemispherical spectral reflectance, ρ'_{λ}, of PSZ 184 coating, on silicated primer, vs. wavelength, λ. Radiation intensity ≅ 210 keV. From Paillous, Amat, Marco & Panabiere (1977) [97]. 180

Figure 5-79: Effect of Combined Exposure, simulating up to three years in geosynchronous orbit, on normal-hemispherical spectral reflectance, ρ'_{λ}, of PSZ 184 coating, vs. wavelength, λ. From Paillous (1976) [96]. 181

Figure 5-80: Effect of O_2 bleaching, after Combined Exposure, on normal-hemispherical spectral reflectance, ρ'_{λ}, of PSZ 184 coating, vs. wavelength, λ. Curves ▬▬▬ and— — are those shown in Figure 5-79. From Paillous (1976) [96]. 182

Figure 5-81: Solar absorptance, α_s, of PCBZ coating vs. UV Radiation exposure time, *t*. From Guillaumon (1982) [48]. 189

Figure 5-82: Normal-hemispherical spectral reflectance, ρ'_{λ}, of PCBZ coating, sample A, vs. wavelength, λ. Effect of Ultra-Violet radiation. 192

Figure 5-83: Normal-hemispherical spectral reflectance, ρ'_{λ}, of PCBZ coating, sample C, vs. wavelength, λ. Effect of Ultra-Violet radiation. 193

Figure 5-84: Hemispherical total emittance, ε, of OCLI Type SI-100 Thermal Control Mirrors as a function of temperature, *T* . ○ :> From Breuch (1967) [22]. □ :> From Marshall & Breuch (1968) [80]. △ :> From Cunnington, Grammer & Smith (1969) [33]. Uncertainty limits are from Marshall & Breuch (1968) [80]. 201

Figure 5-85: Solar absorptance, α_s, of OCLI Type SI-100 Thermal Control Mirrors vs. incidence angle, β. The full lines in *a* correspond to the analytical geometries sketched in *b*. Circles are from solar reflectance measurements, and the dotted line is based on flight temperatures of the NEMS radiator. From Stultz (1976) [123]. 203

Figure 5-86: Change in solar absorptance, $\Delta\alpha_s$, of OCLI Type SI-100 Thermal Control Mirror vs. incidence angle, β, as deduced from data of COMSTAR D-1, D-2 and D-3 satellites. The envelopes contain all the data points. ○ :> Integrated sphere spectroreflectometer measurements made on a single mirror. From Hyman (1981) [62]. 204

Figure 5-87: Change in solar absorptance, $\Delta\alpha_s$, of OCLI Type SI-100 Thermal Control Mirrors vs. exposure time, *t*. 207

Figure 5-88: Solar absorptance, α_s, of OSR Fused Silica Mirrors vs. orbital time, *t*, as deduced from data of NavStar 5. 215

Figure 5-89: Solar absorptance, α_s, of OCLI Type SI-100 Thermal Control Mirrors vs. exposure time, *t*, as deduced from data of COMSTAR D-1, D-2 and D-3 satellites. ▬▬▬: Derived from> temperature telemetry. ▬ ▬: Corrected to> normal solar incidence. 220

Figure 5-90: Solar absorptance, α_s, of OCLI Type SI-100 Thermal Control Mirrors vs. exposure time, *t*, as deduced from data of SCATHA spacecraft. 223

Figure 5-91: Change in solar absorptance, $\Delta\alpha_s$, of OCLI Type SI-100 Thermal Control Mirrors vs. exposure time, *t*, as deduced from data of HELIOS-A and B spacecraft. 227

Figure 5-92: Summery data on the change in solar absorptance, $\Delta\alpha_S$, of OCLI Type SI-100 Thermal Control Mirrors vs. exposure time, *t*. 229

Figure 5-93: Normal-hemispherical spectral reflectance, ρ'_λ, of OCLI Type SI-100 Thermal Control Mirrors vs. wavelength, λ. From Cunnington, Grammer & Smith (1969) [33]. 230

Figure 5-94: Effect of Ultra-Violet radiation on normal-hemispherical spectral reflectance, ρ'_λ, of OCLI Type SI-100 Thermal Control Mirrors vs. wavelength, λ. From Cunnington, Grammer & Smith (1969) [33]. 231

Figure 5-95: Effect of Combined Exposure, simulating up to seven years in geosynchronous orbit, on normal-hemispherical spectral reflectance, ρ'_λ, of OCLI Type SI-100 Thermal Control Mirrors vs. wavelength, λ. *a* Bonded sample. *b* Sample fastened bare. From Paillous (1975) [95]. 240

Figure 5-96: Effect of Combined Exposure, simulating up to seven years in geosynchronous orbit, on normal-hemispherical spectral reflectance, ρ'_λ, of OCLI Type SI-100 Thermal Control Mirrors vs. wavelength, λ. Sample fastened bare. From Paillous (1975) [95]. 241

Figure 5-97: Solar absorptance, α_S, of OCLI Type CC-SSM vs. incidence angle, β. Circles are calculated values. From Winkler & Stampfl (1975) [139]. 255

Figure 5-98: Estimated change in solar absorptance, $\Delta\alpha_S$, of OCLI Type CC-SSM vs. exposure time, *t*. The tests simulate geosynchronous orbit exposure of the Orbital Test Satellite (OTS) equatorial faces. 256

Figure 5-99: Change in solar absorptance, $\Delta\alpha_S$, of OCLI Type CC-SSM vs. exposure time, *t*. The insert shows the changes in α_S which suddenly results when ultra-violet exposure, at 16 Suns, begins. 258

Figure 5-100: Solar absorptance, α_S, of OCLI Type CC-SSM vs. exposure time, *t* as deduced from data of SCATHA spacecraft. 260

Figure 5-101: Change in solar absorptance, $\Delta\alpha_S$, of OCLI Type CC-SSM vs. exposure time, *t* as deduced from data of HELIOS-A and B spacecraft. Line of circles: First HELIOS-A orbit. Simplified model of data analysis. 261

Figure 5-102: Summary on the change in solar absorptance, $\Delta\alpha_S$, of OCLI Type CC-SSM vs. exposure time, *t*. The estimated values of the initial solar absorptance, α_{SO}, are shown near each curve. 262

Figure 5-103: Effect of Combined Exposure, simulating up to three years in geosynchronous orbit, on normal-hemispherical spectral reflectance, ρ'_λ, of OCLI Type CC-SSMs vs. wavelength, λ. From Paillous (1976) [96]. 263

Figure 5-104: *a*. Electrical resistance, R, of six CC-SSM samples as a function of temperature, *T*. *b* shows the two alternative configurations of the electrical contacts set for performing the measurements. From Joslin & Kan (1975) [67]. 264

Figure 5-105: *a*. Sheet electrical resistance, *R*, of three OCLI Type CC-SSMs vs. time in simulated geosynchronous orbit, *t*. *b*. Configuration of the electrical contacts and position of the mirrors on the sample holder for irradiation and measurements. From Paillous (1976) [96]. 269

Figure 5-106: Normal-hemispherical spectral reflectance, ρ'_λ, of Fuller 172A1, vs. wavelength, λ. From Touloukian, DeWitt & Hernicz (1972) [126]. 277

Figure 5-107: Normal-hemispherical spectral reflectance, ρ'_λ, of Fuller 172A1, exposed to gamma radiation, vs. wavelength, λ. From Touloukian, DeWitt & Hernicz (1972) [126]. 278

Figure 5-108: Normal-hemispherical spectral reflectance, ρ'_λ, of Kemacryl M49BC12, vs. wavelength, λ. From Touloukian, DeWitt & Hernicz (1972) [126]. 281

Figure 5-109: Normal-hemispherical spectral reflectance, ρ'_λ, of Kemacryl M49BC12, exposed to gamma radiation, vs. wavelength, λ. Points of white circles are those represented in Figure 5-108. From Touloukian, DeWitt & Hernicz (1972) [126]. 282

Figure 6-1: Peel force, probe tack and rolling ball tack, *F*, as functions of resin concentration, *c*, for a rubber adhesive on a polyethylene terephthalate (polyester) film. 284

Figure 6-2: Peel adhesion, *F/w*, measured at 393 K as a function of curing temperature, *T*. Rubber based adhesive. From Toyama & Ito (1974) [127]....285

Figure 6-3: Space degradation of second surface mirrors based on $1{,}27\text{x}10^{-4}$ m thick FEP Teflon. All data are from Triolo (1973) [128] except those corresponding to IMP-I which are from Hoffman (1973) [61]....303

Figure 6-4: Sketch of a blistering tape. From Brown & Merschel (1970) [23]....304

Figure 6-5: Solar absorptance, α_S, vs. total hemispherical emittance, ε, of several thermal control tapes. 307

Tables

Table 5-1: Ultra-Violet Radiation Effects on Spectral Absorptance of Thermatrol 2A-100....27

Table 5-2: Solar Absorptance of Zinc Oxide-Potassium Silicate Paint....34

Table 5-3: Ultra-Violet Radiation Effects on Spectral Absorptance of Zinc Oxide-Potasium Silicate Paint....36

Table 5-4: Ultra-Violet Radiation Effects on Solar Absorptance of Zinc Oxide-Potassium Silicate Paint....43

Table 5-5: Literature Search for Thermal radiation Properties of ZOT Coatin 55

Table 5-6: Solar Absorptance of Zinc Orthotitanate-Potassium Silicate Coatings[a]....61

Table 5-7: Ultra-Violet Radiation Effects on Solar Absorptance of Zinc Orthotitanate-Potassium Silicate Coatings[a]....63

Table 5-8: Hemispherical Total Emittance of S-13 and S-13 G Coating....85

Table 5-9: Ultra-Violet Radiation Effects on Hemispherical Total Emittance of S-13 and S-13 G Coating....86

Table 5-10: Normal Total Emittance of S-13 G and S-13 G-LO Coatings....88

Table 5-11: Ultra-violet radiation effects on spectral absorptance of S-13 coating (samples 27 & 28)....90

Table 5-12: Ultra-Violet Radiation Effects on Solar Absorptance of S-13 and S-13 G Coatings....93

Table 5-13: Combined Exposure Effects on Solar Absorptance of S-13 G/LO Coating 102

Table 5-14: Outgassing Characteristics of PSG 120 Coating 138

Table 5-15: Protons Radiation Effects Solar Absorptance of PSG 120 Coating 144
Table 5-16: Electrons Radiation Effects on Solar Absorptance of PSG 120 Coating 145
Table 5-17: Combined Exposure Effects on Solar Absorptance of PSG120 Coating 146
Table 5-18: Application of the Degradation Model to PSG 120 Coating 156
Table 5-19: Test Conditions Simulating up to Three Years in Geosynchronous Orbit 159
Table 5-20: Hemispherical Total Emittance, ε, and Solar Absorptance, α_S, of PSZ 184 165
Table 5-21: Protons Radiation Effects on Solar Absorptance of PSZ 184 Coating 169
Table 5-22: Electrons Radiation Effects on Solar Absorptance of PSZ 184 Coating 170
Table 5-23: Combined Exposure Effects on Solar Absorptance of PSZ 184 Coating 171
Table 5-24: Outgassing Characteristics of PCB Z Coating 187
Table 5-25: Ultra-Violet Radiation Effects on Solar Absorptance of PCBZ Coating 189
Table 5-26: Charging Tests with PCBZ Coating 194
Table 5-27: Candidate Adhesives for OSR Fused Silica Application 198
Table 5-28: Ultra-Violet Radiation Effects on Spectral Absorptance of OCLI Type SI-100 Thermal Control Mirrors 205
Table 5-29: Test Conditions Simulating up to Seven Years in Geosynchronous Orbit 232
Table 5-30: Combined Exposure Effects of Reflectance of OCLI Type SI-100. Thermal Control Mirrors. 234
Table 5-31: Charging-Arcing Tests with OCLI Type SI-100 Thermal Control Mirrors 243
Table 5-32: Normal Total Emittance, ε', and Solar Absorptance, α_S, of Several OCLI Type Thermal Control Mirrors 255
Table 5-33: Effects of Simulated Geosynchronous Orbit Exposure on Solar Absorptance of OCLI Type CC-SSM 257
Table 5-34: Protons (Electrons) Only Exposure Effects on Sheet Resistance of OCLISolar Cell Cover Slides 265
Table 5-35: Protons (Electrons) Only Exposure Effects on Resistance of Conductive Coated Fused Silica 266
Table 5-36: Change in the Specific Electrical Cross Resistance, ρ_c, of OCLI Type CC-SSMs by Outgassing Silastic Materials 268
Table 5-37: Charging Tests with OCLI Type CC-SSMs 271
Table 5-38: Hemispherical Total Emittance and Solar Absorptance of Leafing Aluminium-Silicone 275
Table 5-39: Hemispherical Total Emittance and Solar Absorptance of Carbon Black-Acrylic Resin 280
Table 6-1: Thermosetting Cure Cycles and Useful Temperature Range of Several MYSTIK Adhesive Tapes. 286
Table 6-2: Properties of Double-Faced Adhesive Tapes[a] 287
Table 6-3: Properties of Unsupported Adhesive Tapes [a] 296
Table 6-4: Several Solvents of the Adhesives 299
Table 6-5: Rubbing Degradation of the Optical Properties of Aluminized Films 299

Table 6-6: Thermal radiation Properties of Second Surface Silver-Teflon (1,27x10^{-4} m thick) 301
Table 6-7: Exposure Conditions of Silver-Teflon on IMP-I Spacecraft 304
Table 6-8: Blistering Temperatures of Tapes Applied to an Aluminium Substrate [a] 305
Table 6-9: Properties of First Surface Metallized Tapes [a] 308
Table 6-10: Properties of Second Surface Metallized Tapes [a] 314
Table 6-11: Properties of Clear Tapes [a] 324
Table 6-12: Mass-Area Ratio of Several Foils and Tapes 328
Table 6-13: Characteristics of Low-Outgassing Tapes [a] 329

1

Scope

This Part 6 of the spacecraft thermal control and design data handbooks, provides information on coatings on spacecrafts for the purposes of thermal and thermo-optical regulation.

Properties of pigmented and contact coatings, are described and are classified according to their thermal radiation characteristics.

Also included in this Part are the properties and characteristics of foils and tapes with particular emphasis on their adhesive characteristics; these are not classified according to their thermal radiation properties.

In addition to the data provided in this Part, information on aluminium coatings can be found in Part 5.2: Composite materials.

The Thermal design handbook is published in 16 Parts

ECSS-E-HB-31-01 Part 1	Thermal design handbook – Part 1: View factors
ECSS-E-HB-31-01 Part 2	Thermal design handbook – Part 2: Holes, Grooves and Cavities
ECSS-E-HB-31-01 Part 3	Thermal design handbook – Part 3: Spacecraft Surface Temperature
ECSS-E-HB-31-01 Part 4	Thermal design handbook – Part 4: Conductive Heat Transfer
ECSS-E-HB-31-01 Part 5	Thermal design handbook – Part 5: Structural Materials: Metallic and Composite
ECSS-E-HB-31-01 Part 6	Thermal design handbook – Part 6: Thermal Control Surfaces
ECSS-E-HB-31-01 Part 7	Thermal design handbook – Part 7: Insulations
ECSS-E-HB-31-01 Part 8	Thermal design handbook – Part 8: Heat Pipes
ECSS-E-HB-31-01 Part 9	Thermal design handbook – Part 9: Radiators
ECSS-E-HB-31-01 Part 10	Thermal design handbook – Part 10: Phase – Change Capacitors
ECSS-E-HB-31-01 Part 11	Thermal design handbook – Part 11: Electrical Heating
ECSS-E-HB-31-01 Part 12	Thermal design handbook – Part 12: Louvers
ECSS-E-HB-31-01 Part 13	Thermal design handbook – Part 13: Fluid Loops
ECSS-E-HB-31-01 Part 14	Thermal design handbook – Part 14: Cryogenic Cooling
ECSS-E-HB-31-01 Part 15	Thermal design handbook – Part 15: Existing Satellites
ECSS-E-HB-31-01 Part 16	Thermal design handbook – Part 16: Thermal Protection System

2
References

ECSS-S-ST-00-01	ECSS System - Glossary of terms
ECSS-E-HB-31-01 Part 9	Thermal design handbook – Part 9: Radiators
ECSS-E-HB-31-01 Part 12	Thermal design handbook – Part 12: Louvers
ECSS-E-HB-31-01 Part 15	Thermal design handbook – Part 15: Existing Satellites

All other references made to publications in this Part are listed, alphabetically, in the **Bibliography**.

3
Terms, definitions and symbols

3.1 Terms and definitions

For the purpose of this Standard, the terms and definitions given in ECSS-S-ST-00-01 apply.

3.2 Abbreviated terms

The following abbreviated terms are defined and used within this Standard.

AU	astronomical unit, 1 AU = 1,495x10^{11} m
CC	conductive coated
COP	coprecipitation
CVCM	collected volatile condensable materials
ESH	equivalent sun hours
EWH	equivalent (solar) wind hours
GY	gray, 1 $GY = 1$ J.kg^{-1}
IR	infrared
ITO	indium-tin oxide
LDEF	long duration exposure facility
MLI	multilayer insulation
MOX	mixed oxalate process
OSR	optical solar reflector
PBR	pigment to binder ratio by weight
RML	remainder mass loss
RMS	root mean square

RTV	room temperature vulcanizing
SCATHA	spacecraft charging at high altitudes
SSM	second surface mirror
SSR	solid state reaction
TML	total mass loss
TWL	total weight loss
UV	ultra-violet
VCM	volatile condensable materials

3.3 Symbols

A	area of the sensor, [m^2]
C	conductive thermal coupling constant between sensor and tray, [W.K^{-1}]
D	irradiation dose, [GY/particle]
F	view factor from the sun
F	adhesive force, [N]
F_a	view factor for Albedo
F_{sp}	view factor for earth infrared radiation
K	radiative thermal coupling constant between sensor and tray, [W.K^{-4}]
P	earth infrared radiation, [W.m^{-2}]
Q	heat transfer rate through sensor insulation from external sources, [W]
Q_i	internal dissipated power or heat load, [W]
R	sheet electrical resistance, [Ω per square, Ω/square]
S	solar flux, [W.m^{-4}]
T	temperature, [K]
T_R	equilibrium temperature for an isothermal sphere at 1 AU, [K]

T_c	tray or sample-housing temperature, [K]
T_s	equivalent surrounding temperature, [K]
T_{max}	maximum temperature, [K]
T_{min}	minimum temperature, [K]
X_d	irradiation penetration range, [kg.m^{-2}]
X_u	photon absorption and scattering range, [kg.m^{-2}]
a	mean Albedo of the Earth
c	specific heat of a sample, [J.kg^{-1}.K^{-1}]
c	resin concentration in an adhesive
p	pressure, [Pa]
t	thickness, [m]
t_c	coating thickness, [m]
t	time, [h] or [ESH]
n	number of experimental data points
w	width, [m]
α	hemispherical total absorptance
α_p	Earth infrared radiation absorptance
α_s	solar absorptance
$\alpha'_\lambda(\lambda,\beta,\theta)$	directional-hemispherical spectral absorptance
β	angle between surface normal and direction of incident flux, [angular degrees]
β'	angle between surface normal and direction of emitted, reflected or transmitted flux, [angular degrees]
ε	hemispherical total emittance
$\varepsilon'(\beta',\theta')$	directional total emittance
θ	azimutal angle of incident flux, [angular degrees]
θ'	azimutal angle of emitted, reflected or transmitted flux, [angular degrees]
λ	wavelength, [m]

ρ	electrical resistivity, [Ω.m]
ρ_c	specific electrical cross resistance, [Ω.m^2]
ρ_s	solar reflectance
ρ_{sIR}	solar reflectance in the infrared range
ρ_{sUV}	solar reflectance in the UV range
ρ_{sV}	solar reflectance in the visible range
$\rho'_\lambda(\lambda,\beta,\theta)$	directional-hemispherical spectral reflectance
σ	Stefan-Boltzmann constant, $\sigma = 5{,}6697\text{x}10^{-8}$ W.m^{-2}.K^{-4}
σ	standard deviation
ω	solid angle of incident radiation beam, [steradians]
ω'	solid angle of emitted, reflected or transmitted radiation beam, [steradians]

Subscripts

o	refers to initial values
f	refers to after-exposure values

Superscripts

–	mean value

Angles used to define directional emittance.

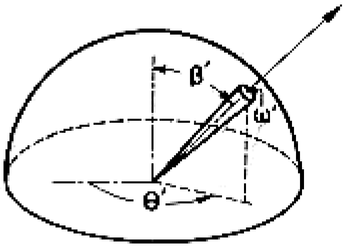

Angles used to define bidirectional reflectance.

4
General introduction

A coating consists of a layer (or layers) of any substance (s) upon a substrate.

Optical coatings have been used to control the temperature of satellites since the first successful orbital flight in 1958. Since then coating materials have been developed to the point where reasonably stable coatings are available, that give any desired value of the hemispherical total emittance, ε, between 0,1 and 0,9 for any desired value of the solar absorptance, α_s, between 0,1 and 0,9.

According to Touloukian, DeWitt & Hernicz (1972) [126] three types of coatings can be identified:

1. Pigmented coatings which are mixtures of a pigment and a vehicle.
2. Contact coatings, formed by layers of a substance coated on a substrate without chemical reaction occurring between the coating material and the substrate.
3. Conversion coatings which are layers of compounds formed by a chemical reaction of the substrate with another material.

Figure 4-1, from Touloukian et al. (1972) [126] is a plot of solar absorptance, α_s, vs. hemispherical total emittance, ε. For each ray from the origin two values are given. The first one, T_R, is the equilibrium temperature for an isothermal sphere at 1 AU; the second value is the ratio α_s/ε.

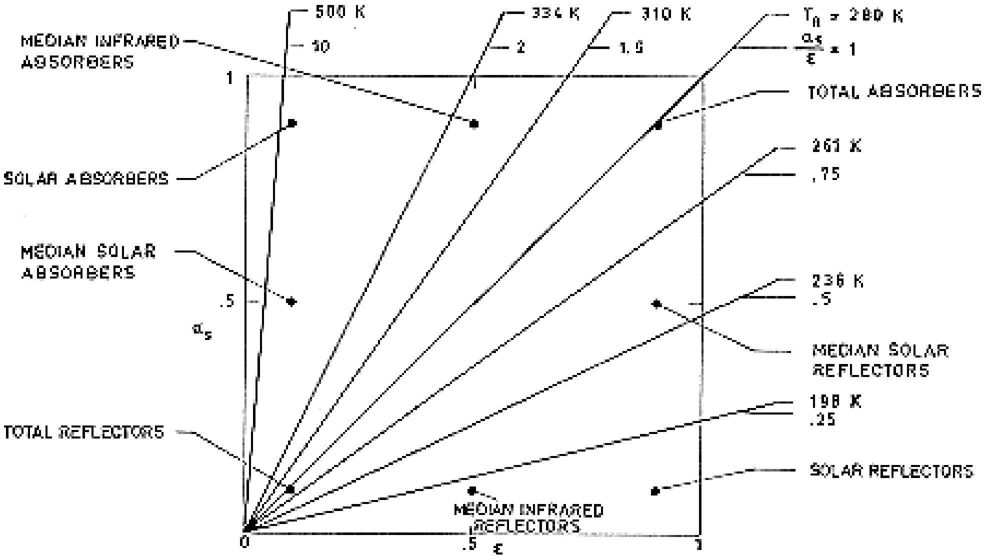

Figure 4-1: Basic types of thermal control coatings. T_R [K] is the equilibrium temperature of a coated isothermal sphere at 1 AU. From Touloukian, DeWitt & Hernicz (1972) [126].

Figure 4-2, from the same source, indicates how to obtain the various types of surfaces exhibiting the characteristics shown in the previous figure.

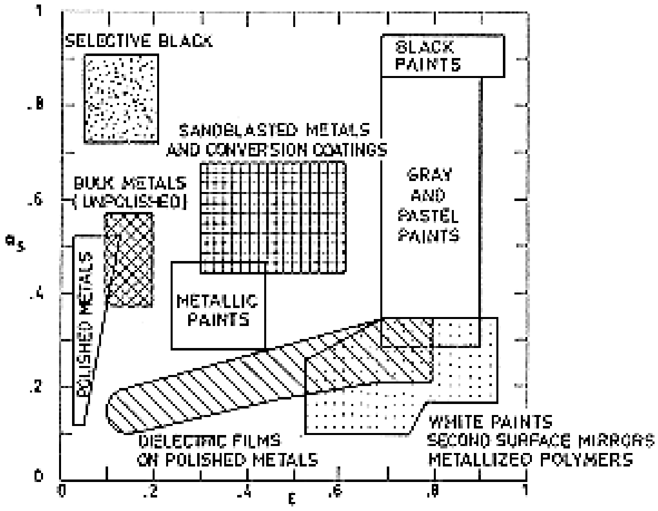

Figure 4-2: Range of solar absorptance, α_s, and hemispherical total emittance, ε, covered by available thermal control coatings. From Touloukian, DeWitt & Hernicz (1972) [126].

The basic requirement for a coating to be used in spacecraft is long-term space stability for periods of months and even of years. This objective, however, has not yet been achieved in many instances.

The problem of selecting the specific coating for a given α_s/ε is somewhat circumvented by the use of mosaics or coating patterns, normally combining white and black paints. Nevertheless, the possibility of using a single paint should not be lay aside; for example, Triolo (1973) [128] reports that encouraging results have been obtained by using green paints to take the place of white and black paint patterns.

This data item, which is intended to give information on several pigmented and contact coatings, has two clearly different parts. In the first one data concerning several coating materials are gathered. These coatings are classified according to their thermal radiation characteristics.

The second part deals with coated foils and tapes. The main characteristic of these coating is that they are flexible and can be applied to a surface by mere pressure, although a double-faced adhesive tape can be used in several case. Since ease of application and removal is the peculiar feature of these coatings, particular emphasis has been placed on their adhesive characteristics.

No attempt has been made to classify foils and tapes according to their thermal radiation properties. On the other hand, this classification is by no means obvious in several cases. For example: Series Emittance Tapes are coatings whose emittance is controlled by the thickness of a Teflon Type A film, and their solar absorptance by a metallic second surface. By choosing the proper Teflon thickness and the appropriate metal it is possible to specify a thermal control surface within a wide range of α_s/ε values.

In addition to the data collected here, information concerning aluminium coating can be found in G, Clause 5.2.

5
Coatings

5.1 General

The data concerning each coating have been arranged, whenever possible and meaningful, as indicated below. When no data on a given property are available the corresponding heading has been normally omitted.

1. COMPOSITION

2. FORMULATION

3. USUAL DESIGNATION

4. SUBSTRATE

5. METHOD OF APPLICATION

5.1. Preparation of paint for application

5.2. Preparation of surfaces for painting

5.3. Application of paint

5.4. Coating thickness

5.5. Curing process

6. SOLVENTS RESISTANCE

7. PHYSICAL PROPERTIES

7.1. Density

7.2. Outgassing

7.3. Thermal radiation properties

7.3.1. Emittance

7.3.1.1. Hemispherical total emittance

7.3.1.2. Variation of hemispherical total emittance with coating thickness

7.3.1.3. Effects of the space environment on hemispherical total emittance

7.3.1.3.1. Ultra-violet radiation

7.3.2. Absorptance

7.3.2.1. Solar absorptance

7.3.2.2. Variation of solar absorptance with coating thickness

7.3.2.3. Variation of solar absorptance with incidence angle

7.3.2.4. Earth albedo normal absorptance

7.3.2.5. Effects of space environment on absorptance

7.3.2.5.1. Ultra-violet radiation

7.3.2.5.2. Gamma radiation

7.3.2.5.3. Protons only exposure

7.3.2.5.4. Electrons only exposure

7.3.2.5.5. Contamination

7.3.2.5.6. Combined exposure

7.3.2.6. Effects of the space environment on solar absorptance to emittance ratio

7.3.3. Reflectance

7.3.3.1. Normal-hemispherical spectral reflectance

7.3.3.2. Effects of the space environment on reflectance

7.3.3.2.1. Ultra-violet radiation

7.3.3.2.2. Gamma radiation

7.3.3.2.3. Protons only exposure

7.3.3.2.4. Electrons only exposure

7.3.3.2.5. Contamination

7.3.3.2.6. Combined exposure

7.4. Electrical resistance

7.4.1. Effects of temperature on electrical resistance

7.4.2. Effects of the space environment on electrical resistance

7.4.2.1. Ultra-violet radiation

7.4.2.2. Gamma radiation

7.4.2.3. Protons only exposure

7.4.2.4. Electrons only exposure

7.4.2.5. Contamination

7.4.2.6. Combined exposure

7.4.3. Charging

8. ENVIRONMENTAL BEHAVIOR

8.1. Prelaunch

8.2. Postlaunch

8.2.1. Ascent

8.2.2. Orbital

9. THERMAL CYCLING

10. SOURCE

11. COST

12. PAST SPATIAL USE

5.2 Solar reflectors

5.2.1 Titanium Dioxide-Polymethyl Vinyl Siloxane

1. COMPOSITION

Pigment: Titanox Ra-NC, Titanium Pigment Corp. proprietary, calcined rutile TiO_2, 93% TiO_2.

Vehicle: Dow-Corning proprietary, Q 92-007. 33% nonvolatile content by weight after 24 h at 343 K.

From Cunnington, Grammer & Smith (1969) [33], Cunnington (1974) [32].

2. FORMULATION

1:1 by weight of pigment and vehicle (Cunnington et al. (1969) [33]).

3. USUAL DESIGNATION

LMSC/Dow-Corning Thermatrol 2A-100.

4. SUBSTRATE

Any clean substrate, either rigid or non-rigid (Breuch (1967) [22]).

5. METHOD OF APPLICATION

5.2. Preparation of surfaces for painting. The entire surface is primed with one coat of silicone primer, Dow Corning Corp. A-4094 or equivalent, to a thickness of approximately 5×10^{-6} m. The primer is air cured 30 min minimum prior to application of top coats.

5.3. Application of paint. By spray techniques.

5.4. Coating thickness. For internal application, where emittance is of primary interest, a minimum thickness of $2,54 \times 10^{-5}$ m should be maintained. For external surfaces, where both α_s and ε are important, the minimum thickness for opacity is $0,9 \times 10^{-4}$ to $1,3 \times 10^{-4}$ m.

5.5. Curing process. 24 h minimum at room temperature and normal pressure, after final coat.

From Breuch (1967) [22], Cunnington, Grammer & Smith (1969) [33].

6. SOLVENTS RESISTANCE

The following data, concerning resistance of elastomeric silicones to chemical attack, have been reported by the producer of the vehicle.

Solvent and Fuels (after 7 d at room temperature) Volume Variation (per cent)

Acetone	15 to 25
Carbon tetrachloride	above 150
Ethyl alcohol	0 to 20
Isooctane	above 150
Xylene	above 150
B type fuel	above 150
JP-4 jet fuel	above 150

Oils (after 70 h at $T = 423$ K)

ASTM No. 1 Oil	5 to 10
ASTM No. 3 Oil	35 to 60

Hydraulic fluid Mil-0-5606 (Univis J-43)............................ above 150

Oronite 8200 (silicate ester)... above 150

From DOW-CORNING (1970) [37].

7. PHYSICAL PROPERTIES

7.1. Density. 1500 kg.m^{-3} after curing (Cunnington et al. (1969) [32]).

7.2. Outgassing. Negligible after coating has been fully cured (Cunnington, Grammer & Smith (1969) [33]).

7.3. Thermal radiation properties

7.3.1. Emittance.

7.3.1.1. Hemispherical total emittance.

T [K]	ε^a	ε^b
295	0,86± 0,03	0,84
395	0,86± 0,02	0,84

[a] Determined calorimetrically. Chamber pressure: 1,33x10^{-5} Pa.

[b] From spectral reflectance data in the range 2x10^{-6} to 2,5x10^{-5} m and the blackbody function corresponding to the temperature quoted.

NOTE From Cunnington et al. (1969) [33].

7.3.1.3. Effects of the Space Environment on hemispherical total emittance.

7.3.1.3.1. Ultra-Violet Radiation.

t[h]	0,25	5	69	117	168	250	360	410	457	486	550
ε	0,87	0,87	0,87	0,85	0,88	0,88	0,87	0,85	0,86	0,85	0,85

Degrading Source: 2x10^{-7} to 4x10^{-7} Xenon lamp, 1 Sun level.

Method of obtaining data: Calorimetric. Chamber pressure: 1,33x10^{-5} Pa.

Probe temperature 395 K.

t, exposure time.

From Cunnington et al. (1969) [32].

7.3.2. Absorptance.

7.3.2.1. Solar Absorptance.

T [K]	α_s
278	0,16 ± 0,03[a]
295	0,15 ± 0,02[b]
389	0,16 ± 0,03[a]
395	0,18 ± 0,01[b]

[a] From Breuch (1967) [22].

[b] From Cunnington, Grammer & Smith (1969) [33].

7.3.2.5. Effects of the Space Environment on absorptance.

7.3.2.5.1. Ultra- Violet Radiation. Laboratory data concerning the effects of UV radiation on spectral absorptance are given in Table 5-1. Calculated values of α_s are also included.

Table 5-1: Ultra-Violet Radiation Effects on Spectral Absorptance of Thermatrol 2A-100.

T [K]	*t* [h]	α for Xenon Lamp					α_s
		Range of λ x 10^7 [m]					
		2-4,1	4,1-6	6-8,5	8,5-	Total	
395	0,25	0,70	0,12	0,07	0,13	0,18	0,18
395	5	0,70	0,17	0,07	0,19	0,21	0,21
395	69	0,85	0,25	0,16	0,22	0,29	0,29
395	117	0,85	9,24	0,18	0,26	0,30	0,31
395	168	0,85	0,25	0,18	0,28	0,31	0,32
395	360	0,80	0,24	0,17	0,27	0,29	0,31
395	410	0,85	0,25	0,18	0,26	0,30	0,31
395	457	0,85	0,24	0,18	0,26	0,30	0,31
395	486	0,90	0,25	0,18	0,27	0,31	0,32
395	550	0,90	0,25	0,19	0,27	0,31	0,32
Before Exposure[a]		0,69	0,08	0,06	0,07	0,14	0,15
After Exposure[a]		0,79	0,27	0,15	0,13	0,24	0,26

[a] Values deduced from spectral reflectance data.

Degrading Source: 2x10^{-7} to 4x10^{-7} Xenon lamp, 1 Sun level.

Method of obtaining data: Calorimetric in situ absorptance.

Chamber pressure: 1,33x10^{-5} Pa.

From Cunnington, Grammer & Smith (1969) [33].

Similar laboratory data are compared with those corresponding to orbital flight in Figure 5-1.

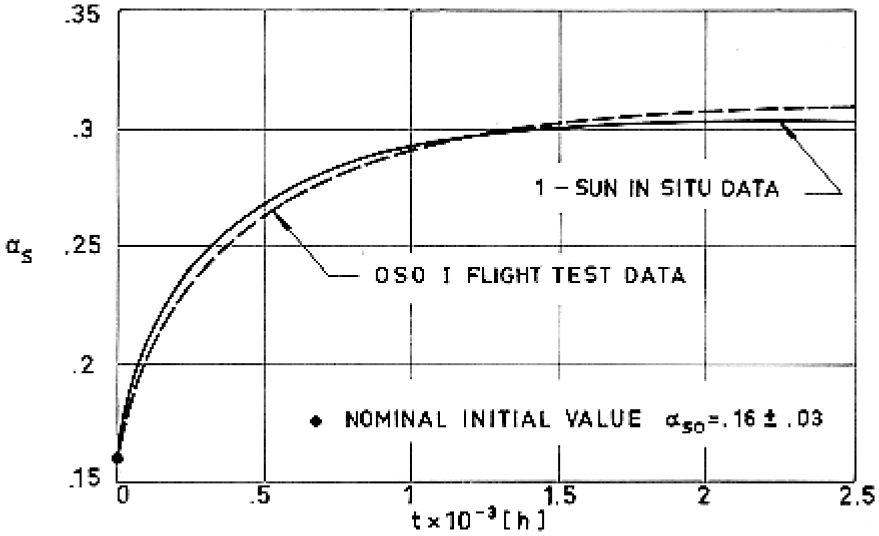

Note: non-si units are used in this figure

Figure 5-1: UV radiation effects on solar absorptance, *α_s*, of Thermatrol 2A-100 vs. exposure time, *t*. From Breuch (1967) [22].

The influence of different radiation conditions on the degradation of solar absorptance is represented in Figure 5-2. It can be deduced from this figure that the intensity of the radiating source does not affect significantly the results, since the difference between the curves labeled 5 Suns and 10 Suns seems to be smaller than the experimental error.

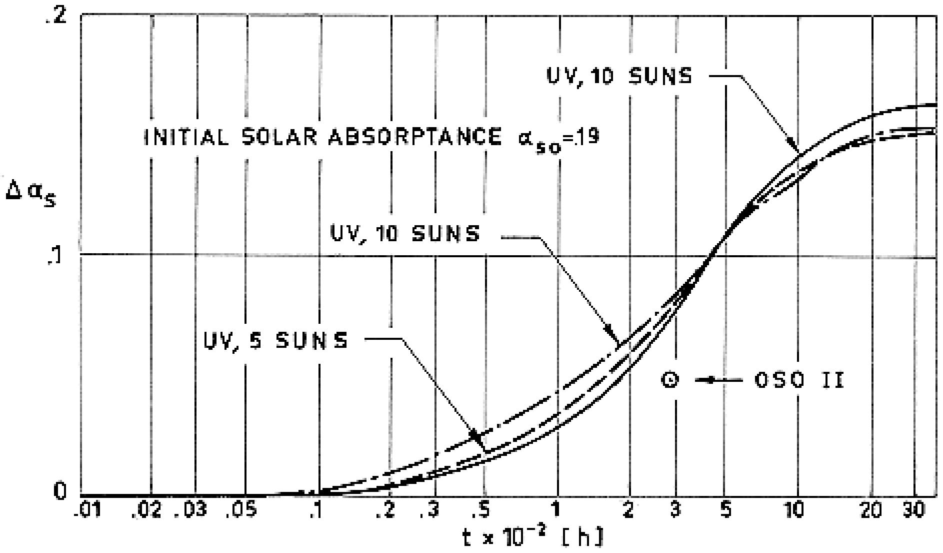

Note: non-si units are used in this figure

Figure 5-2: Change in solar absorptance, *$\Delta\alpha_s$*, of Thermatrol 2A-100, under various radiation conditions, vs. exposure time, *t*. From McCargo et al. (1971) [82].

7.3.3. Reflectance.

7.3.3.1. Normal-hemispherical spectral reflectance: Figure 5-3.

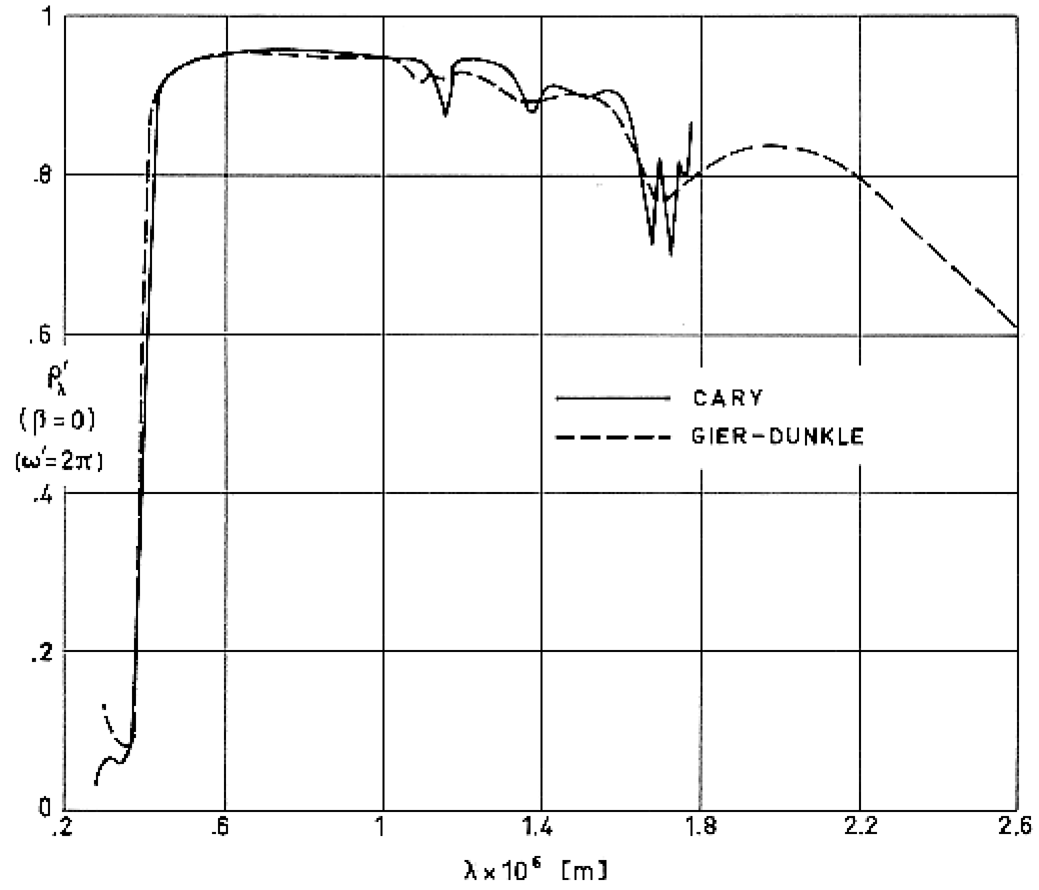

Note: non-si units are used in this figure

Figure 5-3: Normal-hemispherical spectral reflectance, ρ_λ', of Thermatrol 2A-100, measured by two different methods, vs. wavelength, λ. From Cunnington, Grammer & Smith (1969) [33].

7.3.3.2. Effects of the Space Environment on reflectance.

7.3.3.2.1. Ultra-Violet Radiation: Figure 5-4.

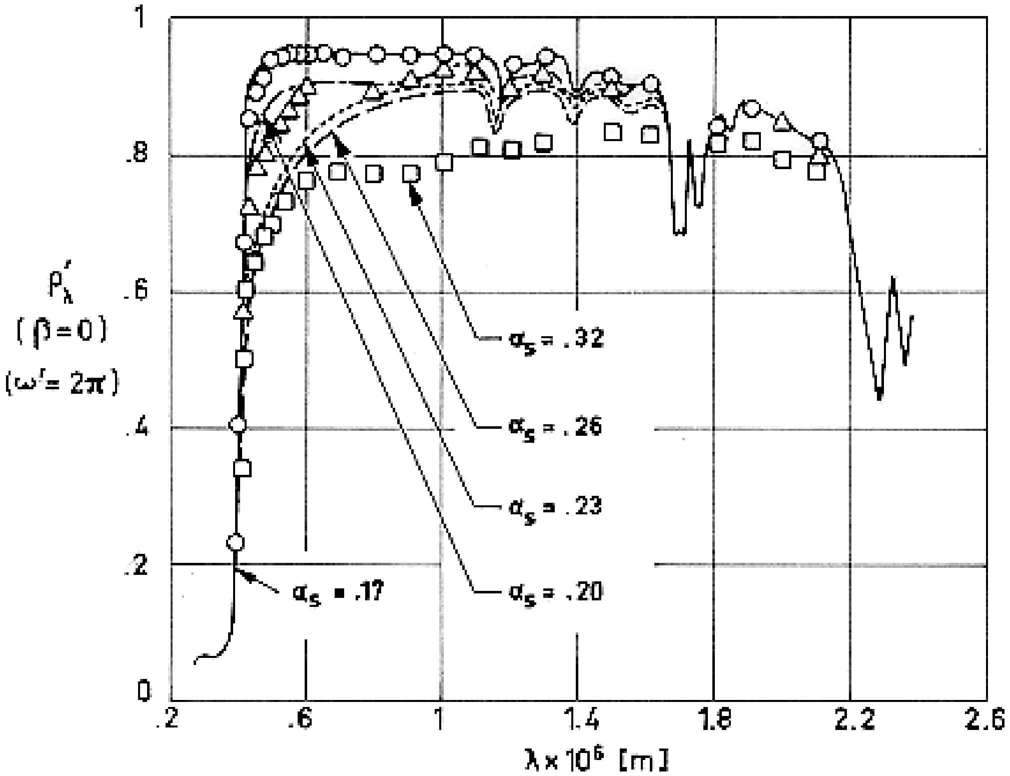

Note: non-si units are used in this figure

Figure 5-4: Effect of Ultra-Violet Radiation on spectral reflectance, ρ_λ', of Thermatrol 2A-100 vs. wavelength, λ. Most of the data, concerning bidirectional reflectance, are from Rittenhouse & Singletary (1969) [105], while dashed line and dotted line, normal-hemispherical reflectance, are from Cunnington, Grammer & Smith (1969) [33].

Explanation

Key	Description	Comments
—		T = 313 K. Near-normal reflectance (Cary).
○		T = 313 K. Measured in vacuum (6,65x10^{-5} Pa).
□		Same as ○ except exposed to UV radiation (PEK Type C(A-H6) lamp, 20 Suns). ESH 1330. During exposure p = 9,3x10^{-5} Pa.
△		Same as □ except sample in air at 40 Pa for 24 h after exposure.
—·—		Same as — except exposed to the same radiation as □.

Key	Description	Comments
▬ ▬	6061-T6 Al substrate polished and then machined to a (30± 3)x10^{-6} m RMS finish.	T = 395 K. Exposed to UV radiation (900 W Hanovia, Xenon lamp, 1 Sun) ESH 550. Sample in air for 5 min after exposure.
....	Same as ▬ ▬.	Same as ▬ ▬.> Sample in air for 30 min.

8. ENVIRONMENTAL BEHAVIOR

8.1. Prelaunch. The surface is soft and rubbery and should be protected from abrasion or scratches. Since this paint is electrostatic, contamination should be avoided.

8.2. Postlaunch. In order to avoid blistering during ascent heating, the paint is be cured, at room temperature, at least for 24 h. In this manner, volatile materials are removed.

8.2.1. Ascent. Ascent heating histories with peak temperatures below 615 K cause an increase in α_s of 0,03 or less, while ε is unaffected.

8.2.2. Orbital. The primary source of degradation appears to be the near-ultra-violet portion of incident solar and albedo radiation.

From Breuch (1967) [22].

9. THERMAL CYCLING

The maximum and minimum temperatures at which the paint has been tested without major changes in properties were:

T_{min} = 211 K

T_{max} = 366 K

(Rittenhouse & Singletary (1969) [105]).

10. SOURCE

Lockheed Missiles and Space Company Inc. 3251 Hanover Street. Palo Alto, California 94304.

11. COST

Varies depending on quantity; Cunnington et al. (1969) [33] indicate that the nominal price is 16 US $ per litre.

12. PAST SPATIAL USE

Thermatrol 2A-100 has been used for thermal control in Explorer 33 (launched July 1, 1966), Rittenhouse & Singletary (1969) [105]. According to Neel (1967) [91], this paint has been tested on board OSO I (launched March 7, 1962) and OSO II (Feb. 3, 1965). The results obtained have been presented in

5.2.2 Zinc Oxide-Potassium Silicate

1. COMPOSITION

Pigment: New Jersey Zinc Co., SP500 zinc oxide; calcined at 873 to 973 K for 16 h. (Heating and cooling rates are not critical).

Binder: Sylvania Electric Products Corp., PS7 potassium silicate.

From Cunnington, Grammer & Smith (1969) [33].

2. FORMULATION

4,3:1 by weight of pigment and binder (Cunnington et al (1969) [33]).

3. USUAL DESIGNATION

Z-93. IIT Research Institute.

4. SUBSTRATE

All metals except noble; Aluminium is preferred (IITRI (1974)).

5. METHOD OF APPLICATION

5.1. Preparation of paint for application. The components are mixed in a pigment to binder ratio of 4,3 with a solids content of 56,9%. A typical batch may be 0,1 kg of ZnO, 50 cm^3 of PS7 (35% solution), and 50 cm^3 distilled water.

The paint should be prepared just before use. Shelf life is limited. Actual shelf life should exceed 24 h. The mixture should be shaken to maintain the pigment in suspension (Cunnington et al. (1969) [33]).

5.2. Preparation of surfaces for painting. The substrate should be abraded and thoroughly washed with detergent and water.

According to the supplier, chromate treatments are not permissible.

5.3. Application of paint. By spray-painting. Because of the porous nature of the cured coating, heavy spraying upon application of a second coat is required to achieve a satisfactory finished texture (Breuch (1967) [22]).

For process specification see Stevens (1971) [120].

5.4. Coating thickness. A thickness of about $2{,}54\times10^{-5}$ m is achieved per cycle. Total thickness should be of the order of $1{,}1\times10^{-4}$ to $1{,}5\times10^{-4}$ m.

5.5. Curing process. Satisfactory physical properties are obtained by an air-drying cure for 4 h. The supplier recommends, as optional, a cure at 366 K for 16 h, while Cunnington et al. (1969) [33] indicate that improved hardness is obtained by heat curing at 413 K.

6. SOLVENTS RESISTANCE

Not attacked by the solvents.

7. PHYSICAL PROPERTIES

7.2. Outgassing. Initial weight loss in 20 h: $8{,}0\times10^{-4}$ kg.m^{-2}.

Stationary loss rate: $5{,}6\times10^{-10}$ kg.m^{-2}.s^{-1} (McCargo, Spradley, Greenberg & McDonald (1971) [82]).

7.3. Thermal radiation properties

7.3.1. Emittance.

7.3.1.1. Hemispherical total emittance.

T [K]	ε^a	ε^b	Ref.
295	0,90± 0,05	0,87	c
310	0,96		d
394		0,88	c
533		0,88	c

[a] Determined calorimetrically. Chamber pressure: 1,33x10^{-5} Pa.

[b] From spectral reflectance data in the range 2x10^{-6} m to 2,5x10^{-5} m and the blackbody function corresponding to the temperatures quoted.

[c] From Cunnington, Grammer & Smith (1969) [33].

[d] From Westcott (1968) [132].

7.3.1.3. Effects of the Space Environment on hemispherical total emittance.

7.3.1.3.1. Ultra-Violet Radiation. The following table has been prepared using data given by Cunnington et al. (1969) [33].

T [K]	*t* [h]	*n*	ε_0	ε_f	$\bar{\varepsilon}$	σ
300	2001	28	0,90	0,88	0,882	0,012
366	2024	33	0,89	0,88	0,887	0,007
422	10517	140	0,88	0,87	0,878	0,010
450	1004	19	0,87	0,87	0,871	0,004
534	502	12	0,81	0,81	0,811	0,009

Degrading Source: 2x10^{-7} to 4x10^{-7} m Xenon Lamp, 1 Sun level.

Method of obtaining data: Calorimetric. Chamber pressure: 1,33x10^{-5} Pa.

t, total exposure time. [h].

n, number of data points given in the source.

ε_0, ε_f, initial and after-exposure values of the hemispherical total emittance.

$\bar{\varepsilon}$, mean value.

$$\bar{\varepsilon} = \frac{\sum_{1}^{n} \varepsilon_i \Delta t_i}{t} \qquad [5\text{-}1]$$

σ standard deviation.

$$\sigma = \sqrt{\frac{\sum_{1}^{n} (\varepsilon_i - \bar{\varepsilon})^2 \Delta t_i}{t-1}} \qquad [5\text{-}2]$$

7.3.2. Absorptance.

7.3.2.1. Solar absorptance: Table 5-2.

Table 5-2: Solar Absorptance of Zinc Oxide-Potassium Silicate Paint

No	*T* [K]	α_s	Comments
1	278	0,114	Measured in vacuum (1,2x10^{-4} Pa).
2	278	0,112	Similar to above specimen and conditions.
3	279	0,153	Air dried at 100% relative humidity; measured in vacuum (1,3x10^{-4} Pa).
4	279	0,168	Similar to above specimen and conditions except air dried at 0% relative humidity.
5	279	0,161	Similar to No. 3 specimen and conditions except air dried at 35% relative humidity.
6	279	0,147	Spray application; measured in vacuum (1,3x10^{-4} Pa); fresh preparation.
7	279	0,150	Similar to above specimen and conditions except measured in vacuum (6,7x10^{-4} Pa).
8	279	0,150	Similar to No. 6 specimen and conditions except measured in vacuum (4,7x10^{-4} Pa).
9	279	0,138	Spray application; measured in vacuum (1,3x10^{-4} Pa); preparation aged 120 d.
10	279	0,119	Above specimen and conditions except heat-treated at 773 K for 2 h.
11	279	0,131	Similar to No. 9 except measured at pressure of 6,7x10^{-4} Pa.
12	279	0,126	Above specimen and conditions except heat-treated at 773 K for 2 h.
13	279	0,140	Similar to No. 9 specimen ad conditions except measured at pressure of 4,7x10^{-4} Pa.
14	279	0,119	Above specimen and conditions except heat-treated at 773 K for 2 h.
15	279	0,120	Spray application; measured in vacuum (1,3x10^{-4} Pa); preparation aged 120 d.
16	279	0,133	Similar to above specimen and conditions except measured in vacuum (6,7x10^{-4} Pa).
17	279	0,124	Similar to No. 15 specimen and conditions except measured at pressure of 4,7x10^{-4} Pa.
18	298	0,164	Substrate abraded with No. 60 Aloxite cloth. Sample cured at 413 K for 18 h.
19	298	0,158	Above specimen and conditions except heat-treated (418 K for 16 h); time lapse, 1 d.
20	298	0,149	Similar to No. 18 specimen and conditions except heat-treated (773 K for 2 h); time lapse, 6 h.
21	298	0,160	Similar to No. 18 specimen and conditions except after time lapse of 90 d.

No	T [K]	α_s	Comments
22	298	0,165	Abraded magnesium silicate substrate.
23	298	0,158	Similar to above specimen and conditions except heat-treated (418 K for 16 h); time lapse, 1 d.
24	298	0,158	Similar to No. 22 specimen and conditions except heat-treated (973 K for 2 h); time lapse, 1 d.
25	298	0,159	Similar to No. 22 specimen and conditions except heat-treated (1073 K for 2 h); time lapse, 6 h.
26	298	0,161	Similar to No. 22 specimen and conditions except after time lapse of 90 d.
27	298	0,168	Abraded alumina substrate.
28	298	0,159	Similar to above specimen and conditions except heat-treated (418 K for 16 h); time lapse, 1 d.
29	298	0,160	Similar to No. 27 specimen and conditions except heat-treated (973 K for 2 h); time lapse, 1 d.
30	298	0,160	Similar to No. 27 specimen and conditions except heat-treated (1073 K for 2 h); time lapse, 6 h.
31	298	0,165	Similar to No. 27 specimen and conditions except after time lapse of 90 d.
32	298	0,153	Measured in vacuum (4×10^{-3} Pa).
33	298	0,120	Aluminium substrate; supplied by IITRI.
34	298	0,220	Similar to above specimen and conditions except supplied by ESRO I Project Group; coating thickness $8{,}9 \times 10^{-5}$ m.
35	298	0,260	Similar to above specimen and conditions except soiled.
36	298	0,184	Property calculated from reflectance; lab data taken on sample to be tested on Lunar Orbiter V.
37	293	0,14± 0,02	Substrate abraded with No. 60 Aloxite cloth. [a]
38	289	0,14± 0,02	Same as above[a].
39	533	0,14± 0,02	Same as above[a].

[a] From Breuch (1967) [22].

NOTE All data, unless otherwise stated, are from Touloukian, DeWitt & Hernicz (1972) [126].

7.3.2.2. Variation of solar absorptance with coating thickness: Figure 5-5.

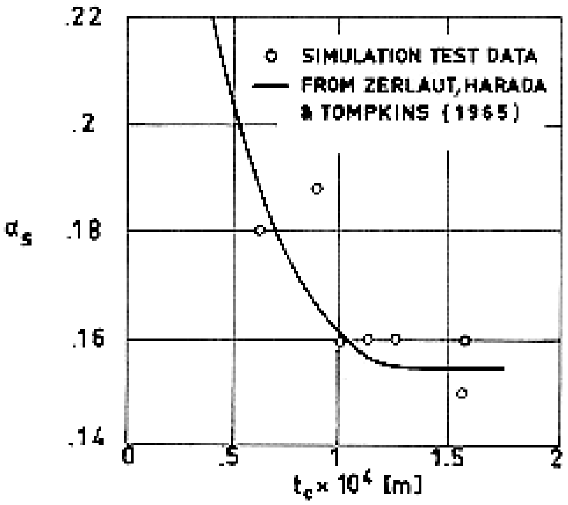

Note: non-si units are used in this figure

Figure 5-5: Variation of solar absorptance, α_s, with thickness, t_c. From Stevens (1971) [120].

7.3.2.4. Earth Albedo normal absorptance. The value α = 0,26 has been obtained by Westcott (1968) [132] from spectral data. Albedo radiation is approximated by the solar spectrum truncated below 3,5x10^{-7} m. Aluminium substrate.

7.3.2.5. Effects of the Space Environment on absorptance.

7.3.2.5.1. Ultra-Violet Radiation. Fairly detailed laboratory data on the effects of UV radiation on spectral absorptance are given in Table 5-3. Table 5-4 has a broader scope, it is intended to illustrate how the experimental conditions influence the results.

Changes in solar absorptance during the total mission profile for a near-Earth orbit, as estimated by McCargo, Spradley, Greenberg & McDonald(1971) [82] are shown in Figure 5-6.

Table 5-3: Ultra-Violet Radiation Effects on Spectral Absorptance of Zinc Oxide-Potasium Silicate Paint

T [K]	*t* [h]	α for Xenon Lamp					α_s
		Range of λ x 10^7 [m]					
		2-4,1	4,1-6	6-8,5	8,5-	Total	
300	0	0,72	0,10	0,05	0,08	0,14	0,14
300	43	0,70	0,09	0,05	0,09	0,14	0,14
300	293	0,67	0,11	0,06	0,08	0,15	0,14
300	365	0,67	0,15	0,04	0,09	0,14	0,15
300	461	0,66	0,15	0,05	0,09	0,15	0,15
300	509	0,65	0,14	0,06	0,09	0,15	0,15
300	605	0,69	0,14	0,06	0,09	0,15	0,16
300	701	0,70	0,16	0,07	0,09	0,15	0,16
300	773	0,67	0,19	0,09	0,08	0,16	0,16
300	821	0,71	0,18	0,05	0,09	0,15	0,17
300	869	0,70	0,19	0,08	0,09	0,16	0,17

T [K]	t [h]	α for Xenon Lamp					α_s
		Range of λ x 10^7 [m]					
		2-4,1	**4,1-6**	**6-8,5**	**8,5-**	**Total**	
300	941	0,65	0,19	0,08	0,09	0,15	0,17
300	989	0,70	0,15	0,09	0,08	0,16	0,17
300	1039	0,65	0,19	0,09	0,08	0,15	0,17
300	1109	0,66	0,20	0,08	0,08	0,16	0,17
300	1157	0,73	0,19	0,10	0,08	0,16	0,17
300	1205	0,69	0,20	0,09	0,08	0,16	0,18
300	1277	0,68	0,20	0,07	0,09	0,16	0,17
300	1325	0,63	0,23	0,07	0,09	0,16	0,18
300	1373	0,65	0,22	0,10	0,08	0,16	0,17
300	1445	0,66	0,23	0,10	0,08	0,16	0,18
300	1545	0,65	0,22	0,08	0,09	0,16	0,18
300	1617	0,68	0,22	0,10	0,08	0,16	0,19
300	1665	0,67	0,24	0,08	0,08	0,16	0,18
300	1713	0,67	0,22	0,08	0,09	0,16	0,18
300	1785	0,69	0,22	0,09	0,09	0,17	0,18
300	1953	0,69	0,21	0,09	0,08	0,17	0,18
300	2001	0,68	0,21	0,09	0,09	0,17	0,18
After Exposure[a]		0,75	0,17	0,06	0,08	0,16	0,17
366	0	0,84	0,05	0,04	0,08	0,14	0,14
366	17	0,88	0,10	0,06	0,08	0,16	0,16
366	70	0,89	0,14	0,08	0,08	0,17	0,18
366	93	0,89	0,16	0,06	0,08	0,17	0,18
366	161	0,90	0,14	0,09	0,08	0,17	0,18
366	233	0,90	0,16	0,07	0,08	0,18	0,18
366	329	0,91	0,16	0,10	0,08	0,18	0,19
366	377	0,90	0,16	0,10	0,08	0,18	0,19
366	425	0,90	0,16	0,09	0,08	0,18	0,19
366	497	0,89	0,16	0,09	0,09	0,18	0,19
366	545	0,85	0,17	0,10	0,09	0,17	0,19
366	593	0,85	0,20	0,09	0,09	0,18	0,20
366	665	0,82	0,18	0,08	0,09	0,18	0,18
366	713	0,87	0,18	0,10	0,09	0,19	0,20
366	761	0,87	0,19	0,10	0,09	0,19	0,20
366	833	0,85	0,19	0,11	0,09	0,18	0,20
366	881	0,85	0,18	0,11	0,09	0,18	0,19
366	939	0,80	0,20	0,12	0,09	0,19	0,20
366	1011	0,80	0,19	0,10	0,09	0,17	0,20
366	1059	0,83	0,19	0,10	0,09	0,18	0,19
366	1179	0,84	0,18	0,09	0,09	0,17	0,19
366	1227	0,85	0,19	0,13	0,09	0,19	0,20
366	1275	0,82	0,21	0,12	0,08	0,181	0,19
366	1347	0,84	0,21	0,11	0,09	0,183	0,20

T [K]	t [h]	α for Xenon Lamp					α_s
		Range of $\lambda \times 10^7$ [m]					
		2-4,1	**4,1-6**	**6-8,5**	**8,5-**	**Total**	
366	1395	0,84	0,19	0,13	0,09	0,187	0,20
366	1443	0,85	0,18	0,11	0,09	0,173	0,19
366	1575	0,85	0,18	0,10	0,09	0,173	0,19
366	1621	0,82	0,19	0,12	0,09	0,183	0,20
366	1693	0,82	0,19	0,12	0,09	0,183	0,20
366	1741	0,81	0,22	0,11	0,09	0,187	0,20
366	1909	0,80	0,22	0,11	0,09	0,183	0,20
366	1957	0,80	0,22	0,12	0,085	0,183	0,20
366	2024	0,80	0,22	0,11	0,085	0,185	0,20
After Exposure[a]		0,75	0,25	0,12	0,10	0,18	0,21
422	0	0,75	0,11	0,05	0,05	0,0126	0,137
422	22	0,90	0,16	0,05	0,05	0,15	0,16
422	96	0,92	0,16	0,07	0,07	0,17	0,18
422	144	0,87	0,17	0,07	0,07	0,16	0,18
422	192	0,80	0,20	0,07	0,07	0,16	0,18
422	264	0,80	0,18	0,10	0,07	0,16	0,19
422	312	0,78	0,20	0,07	0,08	0,16	0,18
422	360	0,80	0,17	0,08	0,09	0,16	0,18
422	432	0,76	0,19	0,07	0,08	0,16	0,18
422	480	0,76	0,20	0,09	0,08	0,16	0,18
422	528	0,76	0,19	0,08	0,08	0,16	0,18
422	600	0,80	0,17	0,10	0,08	0,16	0,19
422	648	0,80	0,19	0,09	0,08	0,16	0,19
422	768	0,77	0,18	0,07	0,08	0,15	0,18
422	816	0,80	0,17	0,08	0,08	0,15	0,19
422	864	0,75	0,18	0,07	0,08	0,14	0,17
422	936	0,78	0,16	0,08	0,08	0,14	0,17
422	984	0,78	0,18	0,08	0,08	0,15	0,18
422	1032	0,78	0,18	0,08	0,08	0,14	0,18
422	1152	0,70	0,16	0,08	0,08	0,14	0,17
422	1200	0,72	0,17	0,09	0,08	0,15	0,17
422	1272	0,73	0,17	0,08	0,08	0,14	0,17
422	1320	0,72	0,18	0,08	0,08	0,14	0,17
422	1488	0,70	0,19	0,08	0,08	0,14	0,17
422	1536	0,68	0,21	0,09	0,09	0,15	0,18
422	1608	0,66	0,18	0,09	0,09	0,15	0,17
422	1656	0,65	0,18	0,10	0,08	0,15	0,17
422	1704	0,67	0,18	0,10	0,08	0,15	0,17
422	1776	0,68	0,20	0,09	0,08	0,15	0,18
422	1824	0,70	0,18	0,11	0,08	0,16	0,18
422	1872	0,70	0,19	0,09	0,09	0,16	0,18
422	1944	0,70	0,18	0,09	0,09	0,16	0,18

T [K]	t [h]	α for Xenon Lamp					α_s
		Range of λ x 10^7 [m]					
		2-4,1	**4,1-6**	**6-8,5**	**8,5-**	**Total**	
422	2016	0,68	0,19	0,10	0,08	0,16	0,18
422	2256	0,69	0,19	0,09	0,08	0,16	0,17
422	2424	0,69	0,17	0,11	0,08	0,15	0,17
422	2472	0,66	0,19	0,10	0,08	0,15	0,17
422	2560	0,68	0,17	0,11	0,08	0,15	0,18
422	2644	0,67	0,18	0,10	0,09	0,15	0,17
422	2736	0,68	0,18	0,10	0,08	0,15	0,17
422	2784	0,68	0,18	0,11	0,09	0,15	0,18
Xenon Lamp off 2832 to 3335 h.							
422	3336	0,66	0,17	0,10	0,09	0,16	0,17
422	3408	0,64	0,16	0,11	0,09	0,15	0,17
422	3508	0,64	0,18	0,10	0,09	0,15	0,17
422	3580	0,64	0,18	0,11	0,09	0,15	0,17
422	3678	0,62	0,16	0,12	0,09	0,16	0,17
422	3676	0,64	0,20	0,11	0,09	0,16	0,18
422	3798	0,63	0,17	0,12	0,09	0,16	0,18
422	3866	0,66	0,17	0,11	0,09	0,16	0,18
422	3914	0,64	0,20	0,12	0,09	0,16	0,18
422	3962	0,61	0,17	0,13	0,09	0,16	0,17
422	4034	0,65	0,20	0,12	0,09	0,17	0,18
422	4082	0,66	0,21	0,12	0,09	0,17	0,18
422	4202	0,65	0,20	0,13	0,09	0,16	0,19
422	4298	0,66	0,20	0,12	0,09	0,17	0,19
422	4370	0,65	0,20	0,12	0,09	0,17	0,18
422	4466	0,63	0,20	0,13	0,09	0,17	0,18
422	4530	0,62	0,21	0,13	0,09	0,17	0,19
422	4634	0,61	0,20	0,13	0,10	0,17	0,19
422	4706	0,61	0,25	0,12	0,09	0,17	0,19
422	4754	0,66	0,22	0,12	0,09	0,17	0,19
422	4802	0,65	0,23	0,12	0,09	0,17	0,19
422	4874	0,62	0,21	0,12	0,10	0,17	0,20
422	4921	0,63	0,22	0,11	0,10	0,17	0,19
422	4969	0,66	0,20	0,11	0,10	0,17	0,19
422	5089	0,62	0,22	0,10	0,11	0,17	0,18
422	5137	0,59	0,24	0,11	0,09	0,17	0,18
422	5209	0,63	0,24	0,10	0,10	0,17	0,19
422	5329	0,60	0,25	0,11	0,10	0,17	0,19
422	5401	0,61	0,25	0,11	0,11	0,17	0,19
422	5449	0,64	0,25	0,13	0,09	0,17	0,20
422	5497	0,59	0,26	0,12	0,09	0,17	0,20
422	5617	0,62	0,25	0,12	0,10	0,18	0,20
422	5665	0,58	0,25	0,11	0,10	0,17	0,19

T [K]	*t* [h]	α for Xenon Lamp					α_s
		Range of λ x 10^7 [m]					
		2-4,1	**4,1-6**	**6-8,5**	**8,5-**	**Total**	
422	5737	0,59	0,26	0,12	0,09	0,17	0,19
422	5785	0,58	0,26	0,14	0,09	0,17	0,20
422	5833	0,59	0,25	0,11	0,10	0,17	0,19
422	5905	0,58	0,22	0,14	0,10	0,17	0,19
422	5953	0,58	0,25	0,11	0,10	0,17	0,19
422	6001	0,61	0,25	0,11	0,10	0,17	0,19
422	6073	0,62	0,22	0,11	0,10	0,17	0,19
422	6121	0,60	0,26	0,09	0,10	0,17	0,19
422	6169	0,63	0,22	0,11	0,09	0,17	0,19
422	6241	0,64	0,23	0,09	0,10	0,17	0,19
422	6289	0,64	0,22	0,08	0,10	0,16	0,19
422	6457	0,68	0,20	0,10	0,10	0,17	0,19
422	6505	0,64	0,23	0,08	0,10	0,17	0,19
422	6577	0,63	0,22	0,11	0,09	0,17	0,19
422	6625	0,65	0,20	0,11	0,10	0,17	0,19
422	6673	0,62	0,24	0,10	0,09	0,17	0,19
422	6745	0,62	0,22	0,11	0,10	0,16	0,19
422	6793	0,62	0,22	0,10	0,09	0,16	0,19
422	6913	0,62	0,23	0,10	0,09	0,17	0,19
422	6961	0,62	0,23	0,10	0,10	0,16	0,19
422	7009	0,62	0,20	0,10	0,10	0,16	0,19
422	7081	0,66	0,19	0,10	0,10	0,16	0,18
422	7129	0,63	0,19	0,09	0,10	0,16	0,19
422	7177	0,65	0,21	0,09	0,10	0,16	0,18
422	7249	0,65	0,18	0,10	0,10	0,16	0,18
422	7345	0,60	0,18	0,11	0,10	0,16	0,18
422	7417	0,62	0,18	0,10	0,10	0,16	0,18
422	7465	0,63	0,19	0,09	0,10	0,16	0,18
422	7513	0,65	0,20	0,11	0,10	0,16	0,19
422	7585	0,62	0,22	0,10	0,10	0,16	0,19
422	7633	0,65	0,20	0,10	0,10	0,17	0,19
422	7681	0,63	0,17	0,10	0,10	0,16	0,18
422	7753	0,64	0,18	0,12	0,10	0,16	0,18
422	7801	0,60	0,19	0,10	0,10	0,16	0,18
422	7849	0,62	0,20	0,11	0,09	0,17	0,18
422	7921	0,63	0,20	0,09	0,09	0,17	0,18
422	8017	0,62	0,21	0,09	0,10	0,16	0,18
422	8029	0,62	0,20	0,10	0,10	0,16	0,18
422	8125	0,62	0,20	0,10	0,10	0,16	0,18
422	8251	0,57	0,17	0,12	0,10	0,16	0,18
422	8301	0,56	0,17	0,12	0,10	0,16	0,18
422	8349	0,57	0,18	0,11	0,10	0,16	0,18
422	8421	0,55	0,17	0,13	0,10	0,16	0,18
422	8517	0,54	0,17	0,12	0,10	0,16	0,18

T [K]	**t [h]**	**α for Xenon Lamp**					**α_s**
		Range of $\lambda \times 10^7$ [m]					
		2-4,1	**4,1-6**	**6-8,5**	**8,5-**	**Total**	
422	8589	0,57	0,17	0,12	0,10	0,16	0,18
422	8781	0,59	0,19	0,13	0,10	0,16	0,18
422	9021	0,54	0,21	0,11	0,11	0,17	0,18
422	9093	0,57	0,19	0,11	0,10	0,16	0,17
422	9189	0,50	0,20	0,09	0,10	0,15	0,17
422	9285	0,53	0,21	0,11	0,10	0,16	0,18
422	9357	0,54	0,23	0,14	0,10	0,17	0,19
422	9424	0,54	0,21	0,12	0,10	0,17	0,18
422	9501	0,52	0,20	0,09	0,10	0,16	0,17
422	9597	0,54	0,19	0,13	0,10	0,16	0,18
422	9645	0,52	0,21	0,11	0,10	0,15	0,18
422	9693	0,52	0,19	0,11	0,10	0,16	0,18
422	9789	0,59	0,19	0,09	0,11	0,16	0,18
422	9861	0,50	0,19	0,11	0,11	0,15	0,17
422	9885	0,53	0,20	0,12	0,10	0,15	0,18
422	9975	0,50	0,18	0,11	0,11	0,16	0,17
422	10071	0,48	0,19	0,10	0,11	0,15	0,17
422	10143	0,50	0,17	0,13	0,10	0,14	0,17
422	10239	0,49	0,19	0,12	0,10	0,15	0,17
422	10431	0,49	0,21	0,11	0,10	0,15	0,17
422	10454	0,49	0,19	0,12	0,10	0,14	0,17
422	10517	0,45	0,19	0,13	0,10	0,15	0,17
422	10517	0,62	0,22	0,14	0,12	0,17	0,19
Before Exposure[a]		0,60	0,06	0,06	0,07	0,13	0,15
After Exposure[a]		0,66	0,23	0,14	0,10	0,20	0,21
450	0	0,50	0,10	0,04	0,08	0,12	0,12
450	20	0,75	0,15	0,07	0,08	0,16	0,16
450	58	0,80	0,17	0,08	0,08	0,18	0,18
450	106	0,84	0,23	0,09	0,09	0,18	0,20
450	154	0,85	0,23	0,10	0,10	0,19	0,20
450	226	0,91	0,23	0,12	0,10	0,20	0,22
450	274	0,90	0,23	0,11	0,11	0,21	0,22
450	322	0,94	0,29	0,10	0,11	0,21	0,24
450	394	0,95	0,27	0,10	0,11	0,20	0,24
450	488	0,87	0,28	0,13	0,11	0,22	0,24
450	560	0,87	0,24	0,14	0,12	0,20	0,23
450	608	0,85	0,30	0,14	0,13	0,22	0,24
450	656	0,88	0,28	0,18	0,13	0,22	0,24
450	728	0,85	0,31	0,16	0,13	0,24	0,26
450	776	0,80	0,31	0,16	0,14	0,25	0,25
450	824	0,75	0,35	0,20	0,14	0,25	0,26

T [K]	t [h]	**α for Xenon Lamp**					α_s
		Range of λ x 10^7 [m]					
		2-4,1	**4,1-6**	**6-8,5**	**8,5-**	**Total**	
450	896	0,80	0,30	0,20	0,14	0,25	0,26
450	944	0,80	0,30	0,19	0,14	0,25	0,25
450	1004	0,85	0,30	0,20	0,14	0,25	0,26
Before Exposure[a]		0,60	0,05	0,05	0,07	0,12	0,14
After Exposure[a]		0,90	0,25	0,15	0,10	0,21	0,23
534	0	-	-	-	-	0,11	-
534	0	0,60	0,03	0,05	0,08	0,11	0,12
534	12	0,55	0,20	0,08	0,09	0,16	0,16
534	60	0,55	0,27	0,10	0,12	0,20	0,20
534	140	0,55	0,28	0,13	0,16	0,21	0,22
534	181	0,55	0,27	0,15	0,17	0,22	0,23
534	256	0,55	0,25	0,20	0,16	0,23	0,24
534	304	0,55	0,25	0,20	0,18	0,23	0,24
534	356	0,50	0,25	0,20	0,18	0,23	0,24
534	404	0,50	0,25	0,23	0,19	0,24	0,25
534	426	0,55	0,26	0,22	0,19	0,24	0,25
534	502	0,55	0,26	0,23	0,19	0,24	0,25
Before Exposure[a]		0,64	0,05	0,05	0,07	0,13	0,14
After Exposure[a]		0,70	0,28	0,19	0,16	0,25	0,26

[a] Values deduced from spectral reflectance data.

Degrading Source: 2x10^{-7} to 4x10^{-7} m Xenon Lamp, 1 Sun level

Method of obtaining data: Calorimetric in situ absorptance. Chamber pressure: 1,33x10^{-5} Pa.

From Cunnington, Grammer & Smith (1969) [33].

Table 5-4: Ultra-Violet Radiation Effects on Solar Absorptance of Zinc Oxide-Potassium Silicate Paint

T [K]	Intensity Suns	Exp. Time ESH	$\Delta\alpha_s$	Comments
258-280		0	0,003	Calculated from sample temperature; flight data of Lunar Orbiter I. Data from smooth curve.
		310	0,022	
		444	0,029	
		661	0,038	
		881	0,047	
		1194	0,058	
		1629	0,071	
		1995	0,081	
278	3,9	1020	0,010	Sample No. 1 of Table 5-2
279	10	2160	0,006	Sample No. 3
279	10	2160	0,006	Sample No. 4
279	10	2160	0,004	Sample No. 5
279	4,8	300	0,003	Sample No. 6
279	6,1	4500	0,024	Sample No. 7
279	5,8	7900	0,049	Sample No. 8
279	4,8	300	0,005	Sample No. 10
279	6,1	4500	0,026	Sample No. 12
279	5,8	7900	0,053	Sample No. 14
279	4,8	300	0,005	Sample No. 15
279	6,1	4500	0,024	Sample No. 16
279	5,8	7900	-0,004	Sample No. 17
293	11,7	1000	0,006	Sample No. 32
298	6	800	0,010	UV from a G.E.AH-6 lamp in vacuum. Absorptance calculated from reflectance measured in situ.
~ 298		100	0,000	UV from a AH-6 lamp in vacuum; property measured in situ. Data from smooth curve.
		500	0,005	
		1000	0,009	
		3000	0,019	
~ 298	1	100	0,083	UV from Xenon lamp in vacuum at 460 K, property measured in situ. Data from smooth curve.
		500	0,129	
		1000	0,152	
		1800	0,155	
~ 298	1	100	0,000	UV from Xenon lamp in vacuum; property measured in situ. Data from smooth curve.
		500	0,012	
		1000	0,024	
		2100	0,041	
unknown		100	0,010	Calculated from flight data of Mariner IV.
		500	0,046	

T [K]	Intensity Suns	Exp. Time ESH	$\Delta\alpha_s$	Comments
		650	0,050	
		1000	0,068	
		2650	0,118	
unknown		0,46	0,002	Calculated from temperature of substrate from flight data of OSO III.
		1,1	-0,001	
		3,9	-0,004	
		4,0	-0,001	
		4,3	-0,001	
		4,9	-0,001	
		5,2	0,002	
		7,1	-0,003	
		7,4	0,001	
		7,7	-0,001	
		8,1	0,000	
		8,5	-0,004	
		8,7	0,001	
		721	-0,004	
		717	0,000	
		727	0,002	
		751	0,000	
		1336	-0,004	
		1336	-0,001	
		1336	0,000	
		1336	0,003	
		1513	0,005	
		1577	0,002	
		1577	0,003	
		1577	0,005	
unknown		0,1	0,000	Calculated from temperature of substrate from flight data of Pegasus II. Data from smooth curve.
		1,0	0,000	
		10	0,000	
		100	0,000	
		1000	0,000	
		2500	0,000	
unknown		0,1	0,000	Calculated from temperature of substrate from flight data of OSO III. Data from smooth curve.
		1,0	0,000	
		10	0,000	
		100	0,000	
		1000	0,000	
		2500	0,000	

NOTE From Touloukian, DeWitt & Hernincz (1972) [126].

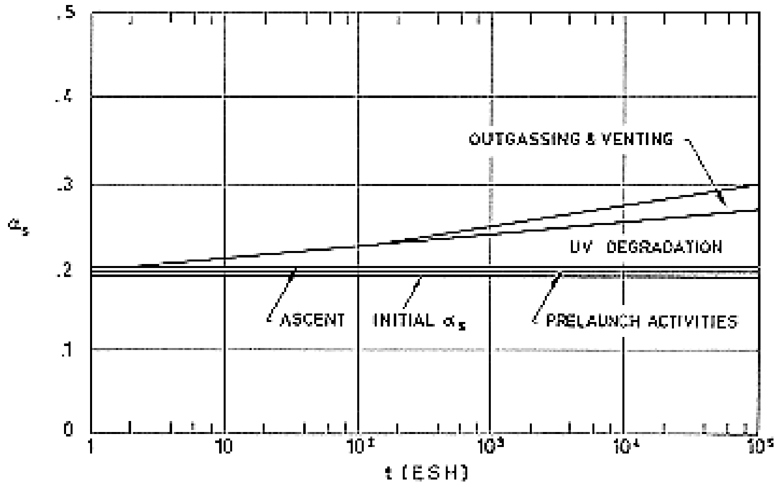

Note: non-si units are used in this figure

Figure 5-6: Estimated changes in the solar absorptance, α_s, of Z-93 during the total mission profile for a near-Earth orbit. From McCargo, Spradley, Greenberg & McDonald (1971) [82].

7.3.2.5.3. Protons only exposure. The available data are given in the following table.

Radiation Exposure		α_{so} Initial	$\Delta\alpha_s$	Comments
Intensity [keV]	Integrated Flux [protons.m^{-2}]			
150	$1x10^{18}$	0,17	0,02	Protons in situ
20	$1x10^{20}$	0,17	0,13	Solar wind protons
2	$5x10^{20}$	0,15	0,26	Solar wind protons
1	$4,2x10^{21}$	0,15	0,35	
1	$1,9x10^{22}$		0,67	

NOTE From Rittenhouse & Singletary (1969) [105].

7.3.2.5.4. Electrons only exposure.

Radiation Exposure		α_{so} Initial	$\Delta\alpha_s$	Comments
Intensity [keV]	Integrated Flux [protons.m^{-2}]			
$2x10^3$	$1x10^{20}$	0,17	0,03	

NOTE From Rittenhouse & Singletary (1969) [105].

7.3.2.5.6. Combined exposure.

Near UV ESH	Lyman ESH	Protons		*T* [K]	α_{so} Initial	$\Delta\alpha_s$
		[keV]	[protons.m^{-2}]			
375-450	750	10	$1{,}4\times10^{19}$	304	0,139	0,019
375-450	750	-	-	304	0,139	0,004
-	-	-	-	304	0,139	0,002
375-450	750	10	1×10^{19}	301	0,143	0,023
375-450	750	-	-	301	0,144	0,005
-	-	10	1×10^{19}	290	0,147	0,020
-	-	10	1×10^{19}	291	0,142	0,026
750	750	10	2×10^{19}	300	0,145	0,030
750	750	-	-	300	0,145	0,007
-	-	-	-	300	0,148	0,001
750	750	10	2×10^{19}	304	0,144	0,035
750	750	-	-	304	0,146	0,014
750	750	10	2×10^{19}	295	0,144	0,029
750	750	-	-	295	0,144	0,011

NOTE From Stevens (1971) [120].

7.3.2.6. Effects of the Space Environment on solar absorptance to emittance ratio.

T [K]	ESH	α_s/ε	Comments
~ 298	1160	0,183	Data taken from flight of Pegasus II. Values deduced from the temperature of the substrate.
	1169	0,226	
	1178	0,199	
	1198	0,231	
	1258	0,212	
	1291	0,240	
	1308	0,208	
	1537	0,259	
	2048	0,188	
	2070	0,200	
	2089	0,221	
	2100	0,200	
	2110	0,173	
	2133	0,254	
	2141	0,282	
	2243	0,245	
	2246	0,229	
	2260	0,243	
	2291	0,173	
	2300	0,234	

T [K]	ESH	α_s/ε	Comments
	2300 2423 2431 2431 2442	0,279 0,173 0,240 0,270 0,216	
258-280	0 54 120 214 346 783 2038	0,185 0,226 0,251 0,285 0,309 0,336 0,416	Data taken from flight of Lunar Orbiter V. Values deduced from the temperature of the substrate. Data stracted from smooth curve.

NOTE From Touloukian, DeWitt & Hernicz (1972) [126].

7.3.3. Reflectance.

7.3.3.1. Normal-hemispherical spectral reflectance: Figure 5-7.

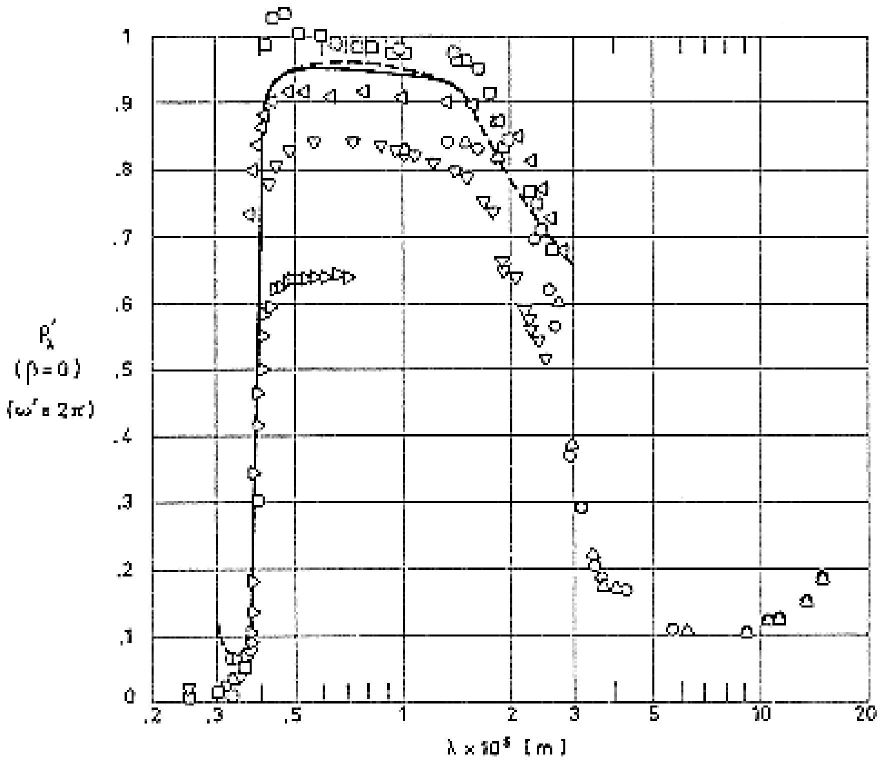

Note: non-si units are used in this figure

Figure 5-7: Normal-hemispherical spectral reflectance, ρ_λ', of Z-93 vs. wavelength, λ. All data are from Touloukian, DeWitt & Hernicz (1972) [126] except solid and dashed lines which are from Cunnington, Grammer & Smith (1969) [33].

Explanation

Key	Description	Comments
○	Sprayed onto 1,27x10^{-3} m thick aluminium substrate.	$T \sim 300$ K. Measured in vacuum (1,33x10^{-4} Pa). Data from smooth curve.
□	Sprayed on an aluminium substrate.	$T \sim 298$ K. Measured relative to MgO. Data from smooth curve.
△	Same as □ .	Same as □ .> Not referenced to MgO.
▽		$T \sim 298$ K. Data from smooth curve.
▷		$T \sim 298$ K. Measured in vacuum. data from smooth curve.
◁		$T \sim 298$ K. Exposed to vacuum. Measured in situ.
▬▬	Applied to disc substrates of 6061-T6 Aluminium. The discs, 2,54x10^{-2} m diameter by 1,27x10^{-3} m thick, were polished on one side and the edge. The surface to be coated was machined to a (30± 3)x10^{-6} m RMS finish.	$T \sim 298$ K. Measured in vacuum (1,33x10^{-5} Pa) by using an integrating sphere attached to a Cary Model 14 Spectrophotometer. Reported error 2%.
▬ ▬	Same as ▬▬ .	Same as ▬▬ except measured using a Gier-Dunkle reflectometer. Reported error ± 1%.

7.3.3.2. Effects of Space Environment on reflectance.

7.3.3.2.1. Ultra-Violet Radiation: Figure 5-8.

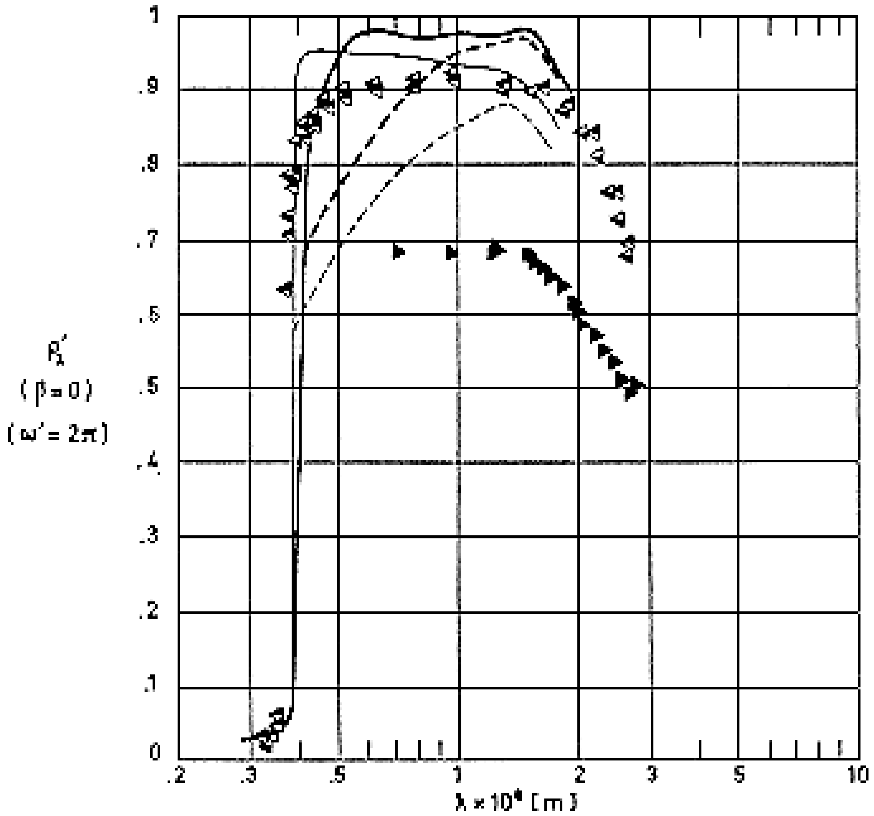

Note: non-si units are used in this figure

Figure 5-8: Effect of Ultra-Violet Radiation on normal-hemispherical spectral reflectance, ρ_λ', of Z-93 vs. wavelength, λ. Data points are from Touloukian, DeWitt & Hernicz (1972) [126], while smooth curves are from Cunnington, Grammer & Smith (1969) [33].

Explanation

Key	Description	Comments
▶		$T \sim 298$ K. Exposed in vacuum to 200 ESH. Measured in situ. Data from smooth curve.
◁		$T \sim 298$ K. Exposed to UV radiation (from a GE AH-6 lamp) in vacuum. ESH 800. Measured in situ.
◁		Same as ◁ except measured in air after UV exposure.
━	Applied to disc substrates of 6061-T6 Aluminium. The discs, $2{,}54 \times 10^{-2}$ m	$T \sim 422$ K. Measured in vacuum (1,33x10-5 Pa) by

Key	Description	Comments
	diameter by 1,27x10^{-3} m thick, were polished on one side and the edge. The surface to be coated was machined to a (30± 3)x10^{-6} m RMS finish.	using an integrating sphere attached to a Cary Model 14 spectrophotometer. Reported error 2% (Calibration made using a Gier-Dunkle reflectometer)
▬ ▬	Same as ▬▬▬.	Same as ▬▬▬ except exposed to UV radiation (from a 900 W Hanovia xenon lamp, 1 Sun level). ESH 10014.
―――	Same as ▬▬▬.	Same as ▬▬▬ except T~534 K.
— —	Same as ▬▬▬.	Same as ――― except exposed to UV radiation (from a 900 W Hanovia xenon lamp, 1 Sun level). ESH 502.

7.3.3.2.3. Protons only exposure: Figure 5-9.

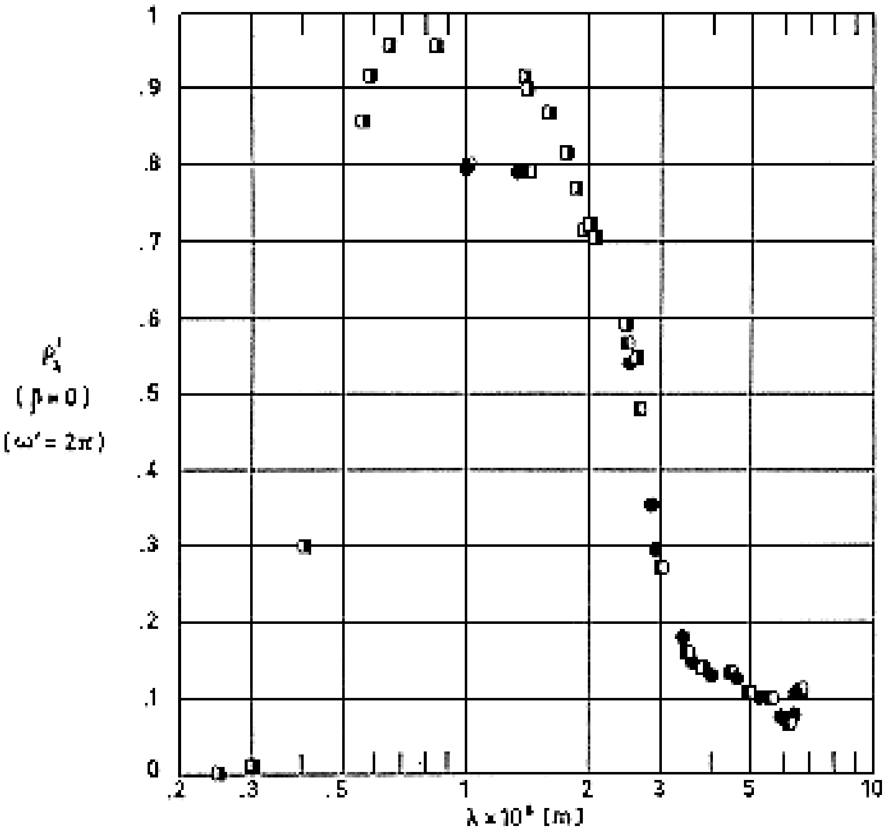

Note: non-si units are used in this figure

Figure 5-9: Effect of Proton Radiation on normal-hemispherical spectral reflectance, ρ_λ', of Z-93 vs. wavelength, λ. From Touloukian, DeWitt & Hernicz (1972) [126].

Explanation

Key	Description	Comments
●	Sprayed onto a 1,27x10^{-3} m thick aluminium substrate.	$T \sim 298$ K. Exposed to 10^{20} p.m^{-2}.
◨	Sprayed on an aluminium substrate.	$T \sim 298$ K. Irradiated in vacuum at 300 K with 7,7x10^{3} eV protons to a total dose of 10^{20} p.m^{-2}. Measured in vacuum (1,33x10^{-4} Pa). Measured relative to MgO. Data from smooth curve.
◧	Same as ◨ .	Same as ◨ except not referenced to MgO.

8. ENVIRONMENTAL BEHAVIOR

8.1. Prelaunch. The coating is brittle, hard to apply and maintain (Scollon & Carpitella (1970) [113]).

8.2. Postlaunch. Blistering during ascent heating can be avoided by curing appropriately the paint (Stevens (1971) [120]).

8.2.1. Ascent. Ascent heating histories with peak temperature below 645 K do not cause increase in α_s and ε (Rittenhouse & Singletary (1969) [105]).

8.2.2. Orbital. The primary source of degradation appears to be the near ultraviolet portion of incident solar and albedo radiation.

The presence of impurities can greatly decrease the stability to the space environment of this coating (Cunnington, Grammer & Smith (1969) [33]).

9. THERMAL CYCLING

The maximum and minimum temperatures at which the paint has been tested without major changes in properties were:

$T_{min} = 211$ K

$T_{max} = 366$ K

(Rittenhouse & Singletary (1969) [105]).

10. SOURCE

IIT Research Institute. 10 West 35 Street, Chicago, Illinois 60616.

11. COST

Pigment: 165 US \$.kg^{-1} (Minimum order 2 lb).

Potassium Silicate: 22 US \$.kg^{-1}.

These prices are FOB Chicago. 35 US $ per shipment for prepaid should be added.

Effective July 1, 1974

(IITRI 1974) [63].

12. PAST SPATIAL USE

This coating has been widely tested and used in spacecraft. The table below gives several precedents.

Spacecraft	Launching Date	Used or Tested	References
Mariner IV	Nov. 28, 1964	Tested	Lewis & Thostesen (1965) [79].
Pegasus II	May 25, 1965	Tested	Schafer & Bannister (1967) [110].
Pegasus III	July 30, 1965		
Lunar Orbiter V	Aug. 1, 1967	Tested	Caldwell & Nelson (1968) [26].
SERT II (Space Electric Rocket Test)	Feb. 3, 1970	Used	Stevens (1971) [120], Stevens & Smolak (1971) [121].
OSO III (Orbiting Solar Observatory)	March 8, 1967	Tested	Millard & Pearson (1973) [85].

5.2.3 Zinc Orthotitanate-Potassium Silicate

1. COMPOSITION

Pigment: IIT Research Institute, Zn_2TiO_4.

Binder: GTE Sylvania Incorporated, PS7 potassium silicate. Distilled water.

From Harada & Wilkes (1979) [58].

Details on pigment preparation are given in the following. These details, which are not very relevant to the user of the coating, could be essential to the proper understanding of this data item.

2. FORMULATION

As given in the following table, PBR is the pigment to binder ratio by weight.

PBR	Components		
	Zn_2TiO_4 [kg]	PS7 [m^3]	H_2O [m^3]
4,3	0,1	$50x10^{-6}$	$30x10^{-6}$
5,3	0,1	$40x10^{-6}$	$35x10^{-6}$
6,1	0,1	$35x10^{-6}$	$40x10^{-6}$
7,1	0,1	$30x10^{-6}$	$45x10^{-6}$

PBR	Components		
	Zn_2TiO_4 [kg]	PS7 [m^3]	H_2O [m^3]
8,5	0,1	$25\text{x}10^{-6}$	$50\text{x}10^{-6}$
10,6	0,1	$20\text{x}10^{-6}$	$55\text{x}10^{-6}$

NOTE From Harada & Wilkes (1979) [58].

High PBR values provide both higher reflectance and greater stability.

PREPARATION OF THE PIGMENT

Three processes have been considered at IITRI for the synthesis of Zn_2TiO_4. All of them involve calcination and reaction of zinc and titanium precursors.

Solid State Reaction (SSR)

New Jersey Zinc Co., SP500 zinc oxide, ZnO, and E.I. DuPont de Nemours Co., R900 anatase, TiO_2, are grinded and mixed at low temperature, for a total of 4 h of wet grinding and 0,5 h of dry grinding. The aim of these grinding and mixing operations is to assure good particle to particle contact, and hence, reactivity of the two oxides.

Zn_2TiO_4 pigment is formed by firing at 1200 K for 18 h, additional 12 h to 24 h of grinding followed by reactive encapsulation and/or induction plasma calcining to obtain a stable product.

Reactive encapsulation aims at stabilizing pigments against ultra-violet space damage. Encapsulating a pigment also avoids the possibility of a radiation-induced change in surface state. A number of reactive encapsulants can be used as, sodium acid phosphate, potassium hexafluorosilicate, ferro-ferricyanide, PS7 potassium silicate,... The last is the most widely used. Plasma heat treatment basically consists in passing an Ar/O_2 aerosol of the pigment through a plasma reactor with temperature jumps across the boundary layer close to 2000 K. This annealing of the reactively encapsulated pigment results in enhanced ultra-violet behavior of both pigment alone and coating.

The solid state reaction process is time consuming, presents the danger of introducing degradable contaminants and does not allow an appropriate control of the pigment size. Because of these limitations, studies on the use of salt precursors for Zn and Ti were conducted in order to improve the pigment.

Coprecipitation (COP)

A mixed solution of zinc and titanium chlorides is added to a solution of oxalic acid. The resulting solution is then heated to 873 K and held at this temperature during 2 h, being continuously stirred while the Zn_2TiO_4 precipitate is formed.

Calcination and firing at 1473 K are performed in standard atmospheric Globar furnaces (bonded silicon carbide resistance elements).

No grinding is required for obtaining pigment particles amenable to incorporation to a paint. Ultra-violet irradiation in vacuum of these powders resulted in minimal change in reflectance after 1000 ESH, although damage resulted when the powders, incorporated in a silicone binder, were irradiated as coating. The particles showed a tendency toward agglomeration which can be avoided by use of the third process, below.

Mixed Oxalate Process (MOX)

Zinc and titanium oxalates are produced from the corresponding chlorides through two independent steps which can be separately established and controlled to produce an optimum precipitated product.

The resulting titanium and zinc oxalates are mixed and ball milled for 4 h, pre-calcined at 873 K for 2 h and, finally, calcined at 1173 K for 4 h.

Fine particle size zinc orthotitanate is achieved using very fine precursors.

The product obtained by this method a be utilized as a pigment with no grinding.

This is the most current state of the art pigment preparation process. Most of the information given below refers to a coating based on MOX prepared pigment.

FIGURA SIN NUMERO, pag. H1-30

References: Zerlaut, Gilligan & Ashford (1972) [141], Gilligan & Zerlaut (1973) [47], Gilligan, Harada & Gates (1974) [45], Harada & Wilkes (1979) [58].

3. USUAL DESIGNATION

Zinc Orthotitanate (ZOT). IIT Research Institute.

Coating corresponding to PBR = 7,1, which is the most current, is known as YB-71 (Harada (1981) [57]).

4. SUBSTRATE

Most surfaces (IITRI (1974) [63]).

5. METHOD OF APPLICATION

5.1. Preparation of paint for application. The components are mixed in a porcelain ball mill with porcelain balls for 4 h.

5.2. Preparation of surfaces for painting. The surface should be chemically etched or abraded and then cleaned with an alkaline detergent and rinsed with distilled water.

The complete surface should be water-break free after the abrasion and cleaning process. By observing the above practices, excellent adhesion on metal surfaces is achieved.

5.3. Application of paint. By spray-painting, using standard paint spray guns. The coating is applied as a continuous, wet film. This film is permitted to dry until the gloss has almost disappeared and then the next coat is sprayed on. The process is repeated until the desired thickness is achieved.

5.4. Coating thickness. A thickness of 0,004" to 0,006" (10^{-4} m to $1{,}5\times10^{-4}$ m) is recommended by the supplier (IITRI (1974) [63]), which concerns a silicone binded coating). Minimum solar absorptance is achieved with a coating thickness close to 0,010" ($2{,}5\times10^{-4}$ m), Figure 5-11.

5.5. Curing process. According to Harada & Wilkes (1979) [58] the YB-71 coating can be air-dried, or can be backed at 390 k for complete water removal.

The curing process indicated in IITRI (1974) [63], also given in Gilligan, Harada & Gates (9174) [45], is for a silicone binded coating.

6. SOLVENTS RESISTANCE

Not attacked by the solvents.

7. PHYSICAL PROPERTIES

7.1. Density. 2460 kg.m^{-3} for the YB-71 formulation. This value has been deduced by Harada & Wilkes (1979) [58] from a plot of coating mass vs. coating thickness for several samples.

7.2. Outgassing. No data available. Water is the only volatile component of these inorganic coatings.

7.3. Thermal radiation properties. The optical properties of these coatings depend upon pigment purity, stoichiometry, particle size and ZnO content. Stability also relates to the last three mentioned variables. In addition, the influence of the binder on the ultra-violet damage of the coating has been noted by Zerlaut, Gilligan & Ashford (1972) [141], Gilligan & Zerlaut (1973) [47], and Gilligan, Harada & Gates (1974) [45]. Since these coatings are evolving from many years of research effort and apparently conflicting data have been reported, emphasis should be placed on the correct identification of both

pigment preparation process and binder used. Table 5-5 has been devised to this aim.

Table 5-5: Literature Search for Thermal radiation Properties of ZOT Coatin

Reference	**Pigment**		**Binder**	**Available Data**	**Data in this Item**
	Process	**Encapsulation**			
Zerlaut, Giligan & Harada (1964) [141] quoted by Touloukian, DeWitt & Hernicz (1972) [126]	Solid State Reaction (SSR).	Not given. Pigment calcined at 973 K for 16 h.	PS7 Potassium Silicate. Silvania, Inc.	α_s and $\Delta\alpha_s$ after 690 ESH, UV radiation.	Table 5-6 and Table 5-7.
		Not given.			
		Not given. Pigment calcined at 973 K for 4 h.		α_s	
		Not given.		α_s and $\Delta\alpha_s$ after 170 ESH, UV radiation.	
Zerlaut, Noble & Rogers (1968) [143].	SSR.	None. Phosphated. Phosphated and reclacined at 925 K for 18 h. None but recalcined at 925 K for 18 h.	OI-650 Polymonomethyl-siloxane, Owens Illinois Inc.	α_s and $\Delta\alpha_s$ after 300, 550, 1200 ESH, UV radiation and after Air exposure. ρ'_λ vs. λ before and after the above exposures.	Not given.
Gilligan & Zerlaut (1971) [46]	SSR.	None. Plasma calcined.	None	ρ'_λ vs. λ before and after proton exposure.	Not given.
		Ferro-ferricyanide treated.	OI-650	ρ'_λ vs. λ before and after the following exposures: proton, UV radiation (600, 1300 ESH), combined UV and proton (1300 ESH	

Reference	Pigment		Binder	Available Data	Data in this Item
	Process	Encapsulation			
				+ 972 EWH) and O_2 bleach. $\Delta\alpha_s$ after the above exposures.	
		Phosphated.	PS7.	ρ'_λ vs. λ before and after 1300 ESH and O_2 bleach.	Figure 5-15.
				ρ'_λ vs. λ before and after proton exposure.	Figure 5-16.
				$\Delta\alpha_s$ after UV radiation (600, 1300 ESH), combined UV and proton (1300 ESH + 972 EWH) and O_2 bleach.	Paragraph 6.3.2.5.3 of this clause.
Zerlaut, Gilligan & Ashford (1972) [141].	SSR.	Several treatments with soluble alkali salts were tested, among them: Potassium silicate, Lithium silicofluoride, Potassium silicofluoride.	None	UV effect on ρ'_λ after 970 or 1010 ESH (depending on the case) at selected values of λ. ρ'_λ vs. λ for the mentioned encapsulants, before and after 970 or 1010 ESH (depending on the case), UV radiation.	Not given.
		Untreated, plasma calcined (several plasma temperatures).	None.	UV effect on ρ'_λ after 1010 or 2500 ESH (depending on the case) at selected values of λ. α_s and $\Delta\alpha_s$ after 1010 of 2500 ESH (depending on the	

Reference	Pigment		Binder	Available Data	Data in this Item
	Process	Encapsulation			
				case) UV radiation. ρ'_λ vs. λ before and after 2500 ESH, UV radiation. $\Delta\alpha_s$ after proton exposure.	
		Phosphated and silicated, plasma calcined (several plasma temperatures).	None	UV effect on ρ'_λ after 2500 ESH, UV radiation at selected values of λ. α_s and $\Delta\alpha_s$ after 2500 ESH, UV radiation. ρ'_λ vs. λ before and after 2500 ESH, UV radiation.	
		Potassium silicated. Phosphated. Ferro-ferricyanide treated. Potassium hexafluorosilicate treated.	PS7 Potassium Silicate.	UV effect on ρ'_λ after 1200, 2000 or 2400 ESH (depending on the case) at selected values of λ.	Paragraph 5.3.3.2.1 of this clause
				α_s and $\Delta\alpha_s$ after 1200, 2000 or 2400 ESH (depending on the case), UV radiation.	Table 5-6 and Table 5-7.
		Potassium hexafluorosilicate treated.	PS7.	ρ'_λ vs. λ before and after 1200 ESH, UV radiation.	Figure 5-15.
		Phosphated.	PS7.	$\Delta\alpha_s$ after proton exposure.	Paragraph 7.3.2.5.3 of this clause
		Untreated.	OI-650.	UV effect on ρ'_λ	Not

Reference	**Pigment**		**Binder**	**Available Data**	**Data in this Item**
	Process	**Encapsulation**			
		Phosphated and silicated. Ferro-ferricyanide treated. Potassium hexafluorosilicate treated.		after 970, 1000, 1200 or 2000 ESH (depending on the case) at selected values of λ. α_s and $\Delta\alpha_s$ after 1200 or 2000 ESH (depending on the case), UV radiation. ρ'_λ vs. λ before and after 970 or 2000 ESH (depending on the case), UV radiation (Phosphated and Silicated). $\Delta\alpha_s$ after proton exposure (Ferro-ferricyanide treated).	given.
		Untreated.	RTV-602 Silicone General Electric Co.		
Triolo (1973) [128].	SSR.	Phosphated (Zerlaut et al. (1972) [141]), plasma calcined.	PS7.	α_s/ε initial and after 20, 780 and 8225 OSO-H orbits (~ 8000 ESH).	OSO-H in paragraph 5.3.2.5.1 of this clause.
			OI-650.	ε. α_s initial. $\Delta\alpha_s$ vs. ESH, UV radiation.	Not given.
Triolo, Heaney & Hass (1978) [129].	SSR.	Phosphated (Zerlaut et al. (1972) [141]), plasma calcined.	PS7.	α_s/ε initial and after 20, 780 and 8225 OSO-H orbits (~ 8000 ESH).	OSO-H in paragraph 5.3.2.5.1 of this clause.
Keyte (1975) [70].	SSR.	Phosphated.	PS7.	ε at room temperature.	Figure 5-10.
				ρ'_λ vs. λ.	Figure 5-14.

Reference	Pigment		Binder	Available Data	Data in this Item
	Process	Encapsulation			
				α_s and $\Delta\alpha_s$ after 700 ESH, UV radiation.	Table 5-6 and Table 5-7.
				$\alpha_s$vs. incidence angle, β.	Figure 5-12.
				$\Delta\alpha_s$after 15 and 330 d, Prospero satellite.	PROSPERO in paragraph 5.3.2.5.1 of this clause.
Gilligan & Zerlaut (1973) [47].	Co precipitation (COP).	None.	None.	ρ'_λ vs. λ before and after 100 ESH, UV radiation.	Not given.
Gilligan, Harada & Gates (1974) [45].	COP.	None	None	ρ'_λ vs. λ before and after 1650 ESH, UV radiation. O_2 bleach effect also considered.	Not given.
		None.	OI-650.		
		Potassium silicated.	OI-650 G (modified by IITRI).		
Harada & Wilkes (1979) [58].	Mixed Oxalate (MOX).	None.	PS7.	ε vs. T.	Figure 5-10.
				ρ'_λ vs. λ for different values of t_c.	Figure 5-14.
				α_s and $\Delta\alpha_s$ after 1000 ESH, UV radiation, several PBRs.	Table 5-6 and Table 5-7.
				α_s vs. t_c.	Figure 5-11 & Figure 5-14 (Caption)

7.3.1. Emittance.

7.3.1.1. Hemispherical total emittance. Figure 5-10.

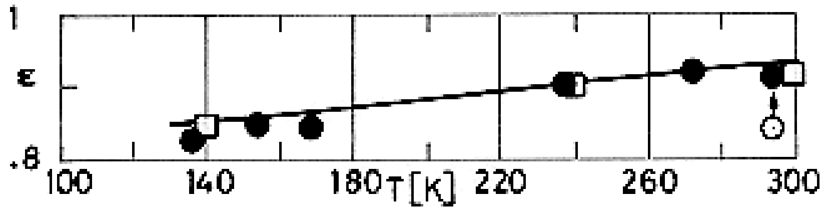

Note: non-si units are used in this figure

Figure 5-10: Hemispherical total emittance, ε, of Zinc Orthotitanate-Potassium Silicate Coatings vs. temperature, T.
○: SSR pigment,> phosphated. From Keyte (1975) [70].
●: MOX pigment,> YB-71. From Harada & Wilkes (1979) [58].
□: YB-71.> AESC. From Ahern & Karperos (1983) [4].

7.3.2. Absorptance.

7.3.2.1. Solar absorptance. Table 5-6. See also Figure 5-13 below.

7.3.2.2. Variation of solar absorptance with coating thickness.

Figure 5-11. Differently prepared coatings. Partial removal of ZnO from the pigment decreases α_s.

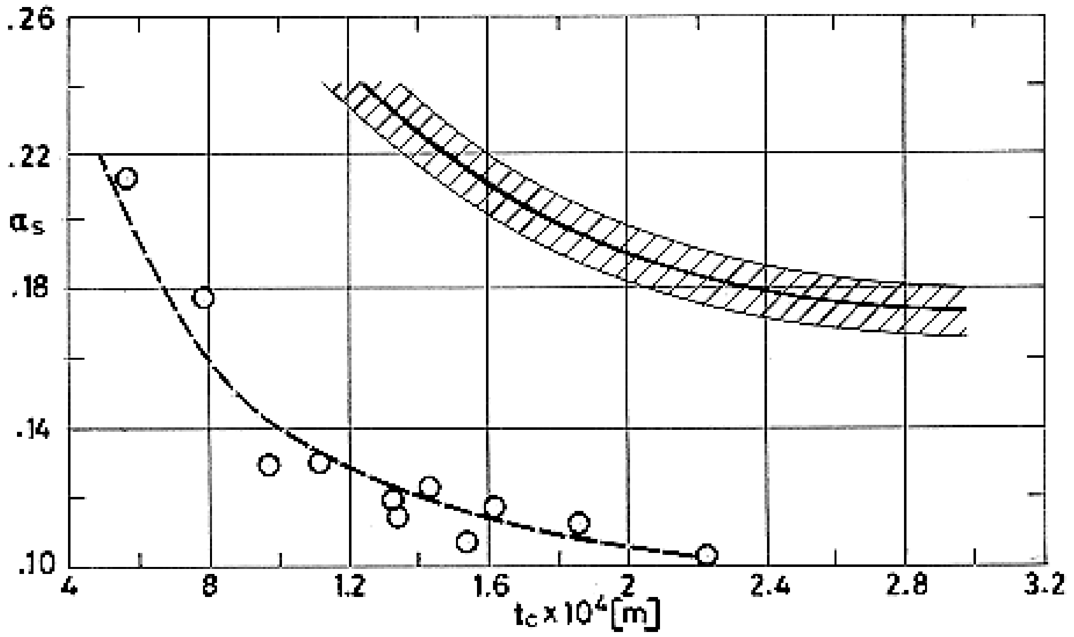

Note: non-si units are used in this figure

Figure 5-11: Solar absorptance, α_s, of YB-71 vs. thickness, t_c.
○: From Harada & Wilkes (1979) [58].
▨: From measurements on 16 panels by AESC. Scatter is due to t_c variation. From Ahern & Karperos (1983) [4].

Table 5-6: Solar Absorptance of Zinc Orthotitanate-Potassium Silicate Coatings[a]

SAMPLE									TEST CONDITIONS	α_s	Ref.
No.	PIGMENT					PBR	Coating Curing Process	Author's Designation	Temp. [K]. Pressure [Pa]. Incidence [degrees]		
	Process	Zn/Ti Stoichiometric Ratio	Encapsulation	Calcination							
				Temp. [K]	Time [h]						
1	Solid State Reaction (SSR).			973	16	4,30	Air dried	Sample No. 7008	T~ 298 K β~ 0°	0,122	Zerlaut, Gilligan & Harada (1964), quoted by Touloukian, DeWitt & Hernicz (1972) [126].
2				773	2			Sample No. 7009		0,118	
3				973	4		Air dried	Sample No. H-19-53		0,139	
4				773	2					0,128	
5			Silicated					Batch No. B-419	p = $1,3x10^{-4}$–$1,3x10^{-5}$Pa β = 7°	0,136	Zerlaut, Gilligan & Ashford (1972) [141]. Test Conditions, Zerlaut & Courtney (1967) [140]
6			Phosphated					Batch No. B-421		0,122	
7			Ferro-ferricyanide treated.					Batch No. B-424		0,154	
8			Potassium hexafluorosilicate treated.	773	7			Batch No. B-563		0,120	
9			Phosphated					Surface No. 9 white paint B-	p=10^5 Pa β = 0°	0,109	Keyte (1975) [70].

SAMPLE									TEST CONDITIONS	α_s	Ref.
No.	PIGMENT					PBR	Coating Curing Process	Author's Designation	Temp. [K]. Pressure [Pa]. Incidence [degrees]		
	Process	Zn/Ti Stoichiometric Ratio	Encapsulation	Calcination							
				Temp. [K]	Time [h]						
								303			
10	Mixed Oxalate (MOX).	1,95		1173		4,26				0,192	Harada & Wilkes (1979) [58].
11						5,32				0,169	
12						7,09				0,153	
13				1323		4,26				0,228	
14						5,32				0,203	
15						7,09				0,205	
16		2,00		1173		4,26				0,190	
17						5,32				0,183	
18						7,09				0,154	
19				1323		4,26				0,230	
20						5,32				0,225	
21						7,09				0,198	

[a] Values deduced from spectral reflectance data.

7.3.2.3. Variation of solar absorptance with incidence angle.

Figure 5-12 Solar absorptance deduced from spectral reflectance measured in air. Two different sample sizes were used to assure full sample illumination at all incidence angles. Thence, a discontinuity appears in the curve plotted in Figure 5-12 at $\beta = 60°$.

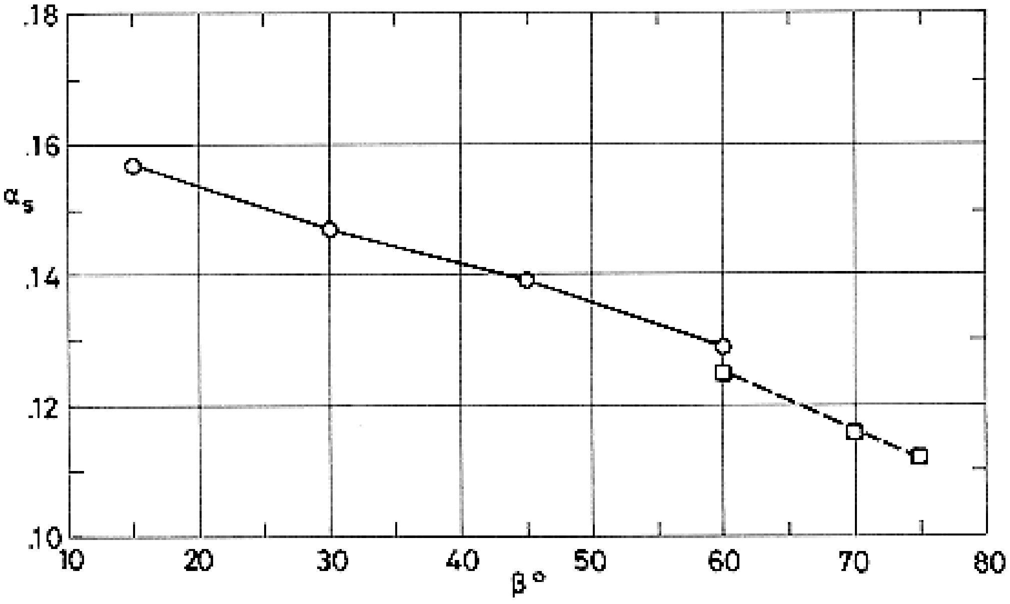

Note: non-si units are used in this figure

Figure 5-12: Solar absorptance, α_s, of Zinc Orthotitanate-Potassium Silicate coating vs. incidence angle, β. SSR pigment, phosphated. From Keyte (1975) [70].

7.3.2.5. Effects of the Space Environment on absorptance.

7.3.2.5.1. Ultra-Violet Radiation. Table 5-7.

Low-orbit (UV-only environment) data appear in OSO-H and PROSPERO of this clause. UV, protons and electrons are present in geosynchronous orbit (Table 5-19, paragraph 5.3.3.2.6 in clause 5.2.4, or Table 5-29, same paragraph of clause 5.2.6). See Spacecraft in Geosynchronous Orbit, paragraph 5.3.2.5.1 of this clause, for several experiments.

Table 5-7: Ultra-Violet Radiation Effects on Solar Absorptance of Zinc Orthotitanate-Potassium Silicate Coatings[a]

Sample[b] No.	Exposure Time [ESH]	Test Conditions	$\Delta\alpha_s$	References
1	690	Irradiated in vacuum.	0,019	Zerlaut, Gilligan & Harada (1964), quoted by Touloukian, DeWitt & Hernicz
2			0,032	
4	170	Irradiated in vacuum (below $1,3\text{x}10^{-3}$Pa).	0,031	

Sample[b] No.	Exposure Time [ESH]	Test Conditions	$\Delta\alpha_s$	References
		Intensity 3,5 Suns.		(1972) [126].
5	2400	Irradiated in vacuum ($1,3x10^{-4}$Pa–$1,3x10^{-5}$ Pa) with 1 kw General Electric AH-6 Mercury-Argon lamp. Spectral reflectance measured in situ.	0,020	Zerlaut, Gilligan & Ashford (1972) [141]. Test Conditions, Zerlaut & Courtney (1967) [140]. Keyte (1975) [70].
6	2000		0,010	
7			0,011	
8	1200		0,002	
9	700	Irradiated in vacuum (below $1,3x10^{-5}$ Pa) with 1 kw Thorn Mercury discharge lamp (type LRD 94-0151). Intensity 3,5 Suns. Measured in situ.	0,026 to 0,040	
	700+10min in Air	Same as above except measured after 10 min exposure in Air.	0,038 to 0,061	
10	1000		0,006	Harad & Wilkes (1979) [58].
11				
12			0,004	
13				
14			0,003	
15			0,005	
16			0,006	
17			0,003	
18				
19			0,008	
20			0,004	
21			0,006	

[a] Values deduces from spectral reflectance data.

[b] Sample numbers in this Table correspond to those in Table 5-6.

OSO-H

TEST CONDITIONS

Spacecraft & Programme

Orbiting Solar Observatory (OSO-H)

Thermal Control Coating Experiments (TCCE).

Orbit

Launched on September 29, 1971 into a 327 km by 560 km near to Earth elliptical orbit with a 33° inclination angle.

Configuration

OSO satellite have two main parts: a lower section, consisting of a nine-sided wheel, which rotates to provide gyroscopic stabilization, and a stabilized semicircular upper section, or sail, aimed at the Sun.

Thermal Test

Twelve samples (Triolo (1973) [128]) were placed in the Sun-oriented, non-spinning sail. Data up to 8225 orbits for eight of these samples are given by Triolo, Heaney & Hass (1978) [129].

SAMPLE

Sample Description

SSR-processed Zn_2TiO_4 pigment, plasma calcined. PS7 binder.

Sample Mounting

The sample is mounted on a disc $2x10^{-2}$ m diameter. The disc is supported by a Kapton film cylinder fastened to both the disc and an inner cup. The thermistor and its leads were attached to the underside of the sample disc with conductive silver epoxy. Another Kapton film cylinder was used for attaching the inner cup to the outer cup. The two Kapton cylinders and the film covering the thermistor network were vapor-aluminized during assembly. Dimpled Mylar sheets were placed inside each cylinder for the reduction of radiative losses.

Holes were cut in the cylinders and the bases of both cups for venting when the assembly is exposed to a vacuum environment. In order to prevent contamination during cup fabrication, the coating was applied to the cup once assembled.

The aim of the inner cup is to act as a thermal guard for the back of the sample disc and thermistor leads. The inner cup flange has the same area and thermal coating as the sample disc. In addition, the thermal capacity of the disc and the inner cup are made as close as possible, thus the sample disc and the inner cup temperatures are maintained close to each other under both steady and transient conditions.

CALCULATION METHOD

α_s/ε is measured calorimetrically from the disc temperature, T. The terms which appear in the heat balance equation are: $c(T)dT/dt$, Sensible heat of the sample and substrate. This term disappears since the sample is in thermal equilibrium when readings are taken.

$\varepsilon A\sigma(T_s^4-T^4)$, Radiation to outer space. The hemispherical total emittance of the sample is measured before launch. The equivalent surrounding temperature, Ts, is assumed to be zero. $\alpha_s AS$, Radiation from the Sun. Recall that the sail, where the coating is located, remains Sun-oriented. Q, Heat transfer between the back of the sample and the outer cup. Measured before launch.

Albedo and Earth infrared radiations do not appear since reads where only taken at the Earth subsolar points. α_s/ε is deduced from the resulting simplified equation, assuming that Q/ε is equal to its prelaunch value.

RESULTS

$\alpha_s/\varepsilon = 0{,}17$ Measured in the laboratory.

$\alpha_s/\varepsilon = 0{,}21$ Deduced from flight data after 20, 780 and 8225 orbits.

COMMENTS

The first usable data point corresponded to the 20th orbit because of malfunction of the tape recorder.

Data on a "model coating" (Alzak), previously tested both in the laboratory and in orbit, were used to convert from orbital time to ESH. (1,5 orbital hours ≈ 1 ESH. 1 orbit takes 1,5 orbital hours).

The difference between the laboratory and the first in-flight data, (which is common to all the tested coatings) would have been caused by a systematic error in the measurements.

References: Triolo (1973) [128], Triolo, Heaney & Hass (1978) [129].

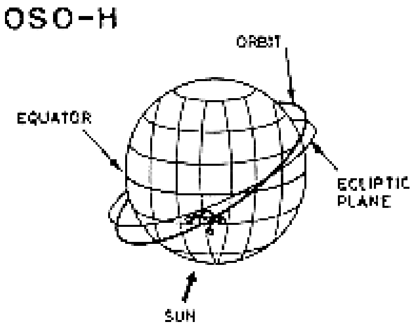
OSO-H
ORBIT
EQUATOR
ECLIPTIC PLANE
SUN

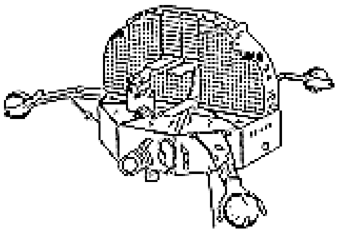

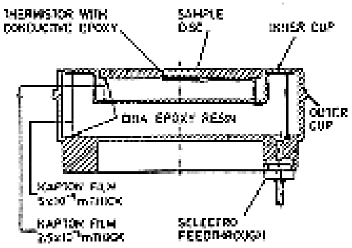
THERMISTOR WITH CONDUCTIVE EPOXY
SAMPLE DISC
INNER CUP
OUTER CUP
EPOXY RESIN
KAPTON FILM 5x10-5 m THICK
KAPTON FILM 2.5x10-5 m THICK
SELECTRO FEEDTHROUGH

PROSPERO

TEST CONDITIONS

Spacecraft & Programme

Thermal Control Surface Experiment (TCSE).

Orbit

Launched by the Black Arrow R3 launch vehicle on October 28, 1971.

The initial orbit parameters were: Apogee, 1580 km; Perigee, 547 km; Inclination, 82,06°; Period, 106,5 min (13,53 orbits per day).

Configuration

Prospero is a 26-faced polyhedron, 0,71 m height and 1,09 m in equatorial diameter. Mass, 65,8 kg. The satellite is spin stabilized and fitted with nutation dampers. The spin axis-Sun angle at launch was approximately 94°, providing roughly normal incidence of solar radiation on most of the coatings. Initial spin rate was 17,8 rad.s^{-1}.

Thermal Test

64 thermal control surfaces were flown, including 7 gold reference surfaces, 6 black gloss reference surfaces and 3 of each of 17 different coatings, among them 9 white paints. Two types of sample housing were used; 4 of rectangular shape each containing 12 samples and mounted in corner fillets parallel to the satellite spin axis, and 4 of triangular geometry, each containing 4 samples and also mounted in corner fillets, but at an angle of about 30° to the spin axis.

The 3 samples of this coating were placed in a rectangular housing.

SAMPLE

Sample Description

SSR-processed Zn_2TiO_4 pigment, phosphated. PS7 binder.

Sample Mounting

The coating was applied on an aluminium clad alloy (L72) substrate, goldized on the edges and on the rear side. The sample plate was mounted in a cup, machined in a magnesium alloy housing, by means of four fiber-glass Z pieces. The cup was goldized on both sides.

4 goldized radiation shields were placed between the substrate and the cup. The shields were mutually separated by small fiber-glass washers, and held in position by four bolts. Slots were cut in the radiation shields for passage of the above mentioned Z pieces.

The temperature was measured by a YSI precision thermistor attached with Araldite in the center of the rear face of the plate.

CALCULATION METHOD

α_s is measured calorimetrically from the temperature, T, of the plate. The terms which appear in the heat balance equation are:

$c(T)dT/dt$, Sensible heat of the sample plate. Since readings were only taken with the surface in thermal equilibrium, this term vanishes.

$\varepsilon A\sigma(T_s^4-T^4)$, Radiation to outer space. ε measured before launch ($\varepsilon = 0{,}91$).

The equivalent surrounding temperature, T_s, is assumed to be zero. Attempts were made to deduce ε from in-flight measurements during the eclipse part of the orbit. This effort was unsuccessful because of the many parameters involved.

$\alpha_s AS(t)$, Radiation from the Sun. S is the solar flux, a known function of the time, t.

$\alpha_s F_a AaS$, Albedo radiation. F_a view factor, a is the mean albedo of the Earth.

$\alpha_s F_{sp} AP$, Earth infrared radiation, F_{sp} is the view factor, and $F_{sp}P$ the flux of energy on the sample.

The last two terms were deduced from assumed values of α_s and ε for a reference surface (gold), using the balance equation for both the eclipse and the sunlit parts of the orbit.

$Q(T,T_c)$, Thermal coupling between the plate, at temperature T, and housing, at temperature T_c. Three methods for calculating Q were explored, none of them was completely successful. These methods were:

1. calibration in a solar simulation vacuum chamber. Attempts to remove the many sources of error failed.
2. Thermal modeling of the sensor-housing assembly by a six-node network. Heat input was that on an orbiting-spinning plate. Temperatures for a given α_s and ε were compared with in-flight data. Correlation was poor.
3. Calculation from in-flight data. ε was fixed for 4 samples. Only eclipse temperatures were used. Data of Q vs. T-T_c were arranged as $Q = k+w_1(T-T_c)+w_2(T-T_c)^2$ and values of k, w_1 and w_2 for an average housing, as well as values of $c(T)$ for each sample were deduced. The results for the 4 samples were fair, although discrepancies appeared.

Finally, a "best estimate" of Q vs. T-T_c was made by a critical analysis of the above methods.

RESULTS

α_s = 0,109, measured in the laboratory. α_s = 0,110, after 15 days in orbit. α_s = 0,141, after 330 days in orbit.

COMMENTS

Owing to the design of the sample mounting, Q was 10 times too large for reaching sufficient sensitivity.

Reference: Adams (1973) [3], Keyte (1975) [70].

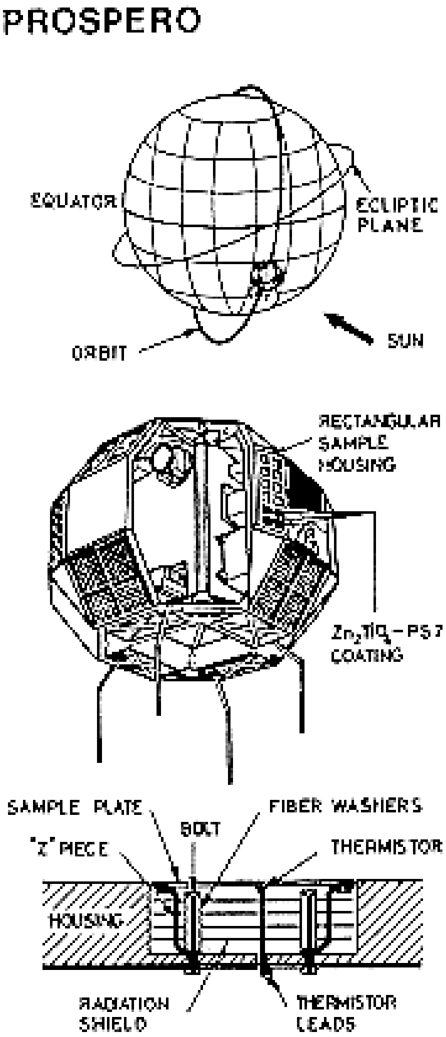
PROSPERO
EQUATOR
ECLIPTIC PLANE
ORBIT
SUN
RECTANGULAR SAMPLE HOUSING
Zn_2TiO_4 - PS7 COATING
SAMPLE PLATE
BOLT
FIBER WASHERS
"Z" PIECE
THERMISTOR
HOUSING
RADIATION SHIELD
THERMISTOR LEADS

SPACECRAFT IN GEOSYNCHRONOUS ORBIT

TEST CONDITIONS

Spacecraft & Programme

Different spacecraft in similar orbits.

Orbit

Geosynchronous.

Configuration

No data are given except that the calorimeters holding the samples were all installed in the same clean location (–T axis in the enclosed figure a) on several spacecraft. The calorimeter locations were so chosen as to minimize radiant heat exchange with spacecraft external surfaces. They were mounted in one of the main radiators of the satellite.

Thermal Test

Two set of data from calorimetric tests have been issued, Curran & Millard (1978) [34], Ahern & Karperos (1983) [4]. The last set includes, among others, five ZOT coating samples of various thicknesses on different substrates. Calorimeter sample areas were $76x10^{-3}$ m by $76x10^{-3}$ m. See figure b.

SAMPLE

Sample Description

YB-71. Coating characteristics are given in the following Table.

Sample Designation	Thickness t_cx10^4 [m]	Substrate
9	2,03 - 2,54	Al alloy 6061-T6
10		
14	2,54 - 3,05	
18		
20		Mg Alloy AZ31B

Sample Mounting (figures b and c)

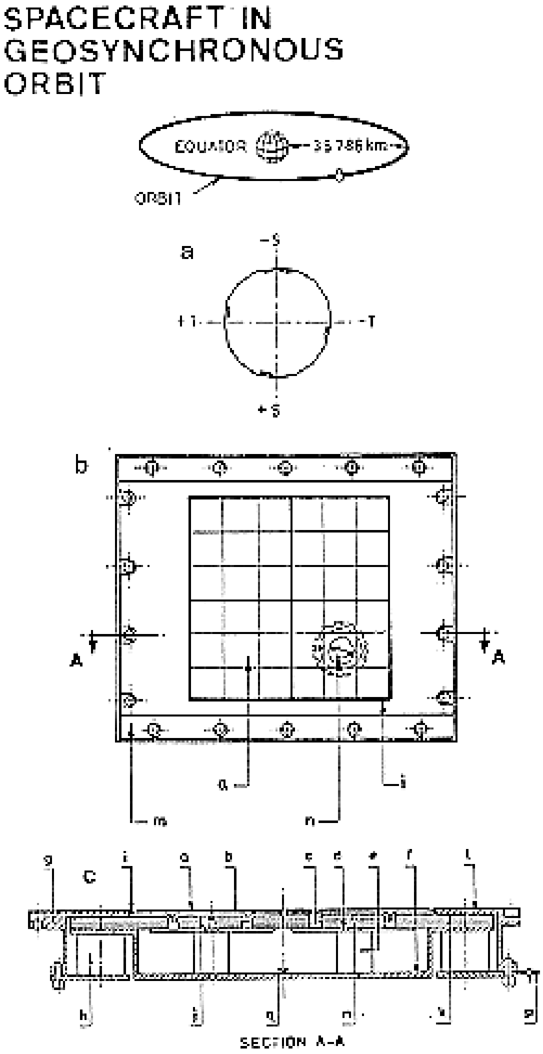

Each sample (a) is bonded to a magnesium mounting platform (b) bonded to a series of thin-walled (10^{-4} m to $1,5x10^{-4}$ m) fiber-glass support cylinders for improved thermal isolation. Shown in the figure are, upper cylinders (c), discs (d) and lower cylinders (e). The lower cylinders are mounted to a magnesium housing (f). The housing is attached to the radiator mounting frame (g) (and thermally isolated from it) by fiber-glass support cylinders (h). All of the fiber-glass support cylinders and discs along with the housing are coated on both sides with vacuum-deposited aluminium ($\varepsilon < 0,1$) to minimize radiation heat transfer between surfaces. Silvered teflon gap seals (i) close the space between samples so that solar energy cannot reach the housing enclosure. An MLI (j) is held in place between the support discs and the corresponding mounting platform to minimize heat transfer between samples and the housing enclosure. This MLI (see ESCC-E-31-01 Part 7 clause 4.10) is composed of several aluminized mylar sheets and has an aluminized side facing the housing enclosure. The MLI also extends outwards (k) and insulates the housing from the mounting frame, where it overlaps the housing adjacent to the samples. The top of the mounting frame in this overlapping region is covered with SSMs (see ECSS-E-HB-31-01 Part 6 clause 4.2.6 and 4.2.7) to minimize heat absorption adjacent to the samples ((1) in the figure). A strip of silvered teflon (m) serves the same purpose where the mounting frame bolts to the radiator.

Attached beneath each sample mounting platform is a thermal sensor (n), the leads of which travel through the fiber-glass cylinders to the terminal board (p). An additional thermal sensor (q) is mounted on the inside housing base plate to provide data for the heat leak calculations of each individual sample.

CALCULATION METHOD

One of the main aims of the configuration design was simplicity of the computer thermal model.

Basically the sample temperature provides α/ε, where ε, although temperature dependent (Figure 5-10), does not change with time. A typical thermal network for one specimen is shown in the enclosed figure. For the nodes corresponding to external spacecraft surfaces viewing the sample, an AESC-developed Monte Carlo view factor programme was used. The temperatures of these external surfaces were supplied to the programme.

Solar heating of the sample was introduced in the computer mode through a diurnal table automatically adjusted for solar angle and heat flux. The diurnal temperatures for the radiating spacecraft nodes (available at 15 min intervals) and the calorimeter base temperature, were introduced into the program. Temperatures are then calculated on the basis of an assumed α_s value (normally the previous one). The computer then adjusts α_s and iterates until the calculated temperatures match the flight data within 1° F (0,56 K) thus giving the α_s for the day. The analysis was repeated at varying intervals which generally were determined by the temperature rise rate. Usually large rises followed a roll-off trend and, thence, early data were obtained at time intervals of the order of one month, whereas at three years in orbit data were taken at approximately 3 moths interval.

The measurements of the absolute solar absorption involves the full calorimeter design errors, the thermal sensor calibration error and the telemetry quantization error. The estimated error in α_s is +0,009, −0,006.

RESULTS

Laboratory α_s data have been compared to initial flight measurements in the following Table. Laboratory measured hemispherical total emittance at 295 K was $\varepsilon = 0{,}91$ in any case (see also Figure 5-10).

Sample	**Laboratory α_s**	**Flight α_s**
9	0,194	0,197
10	0,181	0,185
14	0,167	0,177
18	0,167	0,190
20	0,167	0,199

Among the results for twenty samples reported by Aherns & Karperos (1983) [4], ZOT samples are those giving the worst agreement between laboratory and flight data. The reason for this apparent ground-handling or launching degradation has not been determined.

The flight evolution of α_s with time t is shown in Figure 5-13. An exponential expression in t has been fitted to these data as follows:

$$\alpha_s = \alpha_0 + (\alpha_m - \alpha_0)(1 - e^{-t/\tau})$$

Values of α_s, α_0 and τ, together with the time range of validity of the expression are given in the enclosed Table.

Sample	α_0	α_m	**τ ESH**	**t_{max} ESH**
9	0,198	0,301	2863	5800
10	0,185	0,314	2933	5800
14	0,188	0,358	5920	3400
18	$\alpha_s = 0{,}190+3{,}65\text{x}10^{-5}t$, preliminary			1100
20	$\alpha_s = 0{,}199+3{,}09\text{x}10^{-5}t$, preliminary			1100

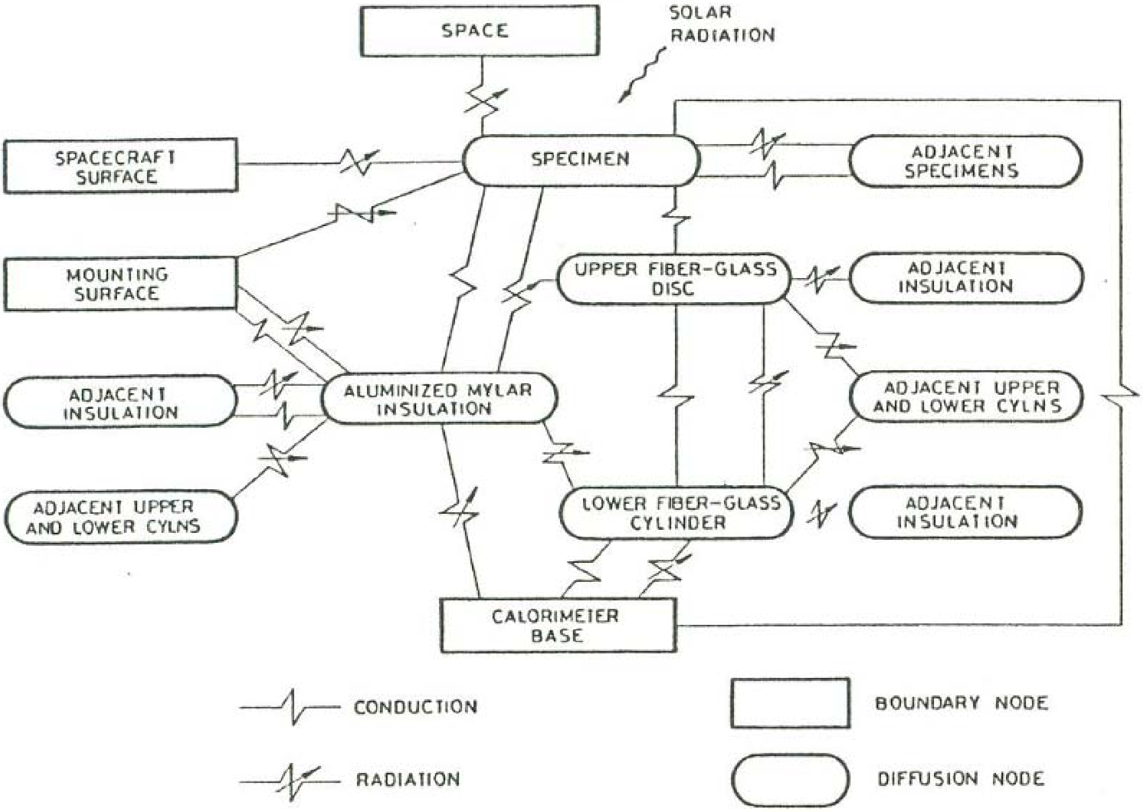
SPACE
SOLAR RADIATION
SPACECRAFT SURFACE
SPECIMEN
ADJACENT SPECIMENS
MOUNTING SURFACE
UPPER FIBER-GLASS DISC
ADJACENT INSULATION
ADJACENT INSULATION
ALUMINIZED MYLAR INSULATION
ADJACENT UPPER AND LOWER CYLNS
ADJACENT UPPER AND LOWER CYLNS
LOWER FIBER-GLASS CYLINDER
ADJACENT INSULATION
CALORIMETER BASE
CONDUCTION
RADIATION
BOUNDARY NODE
DIFFUSION NODE

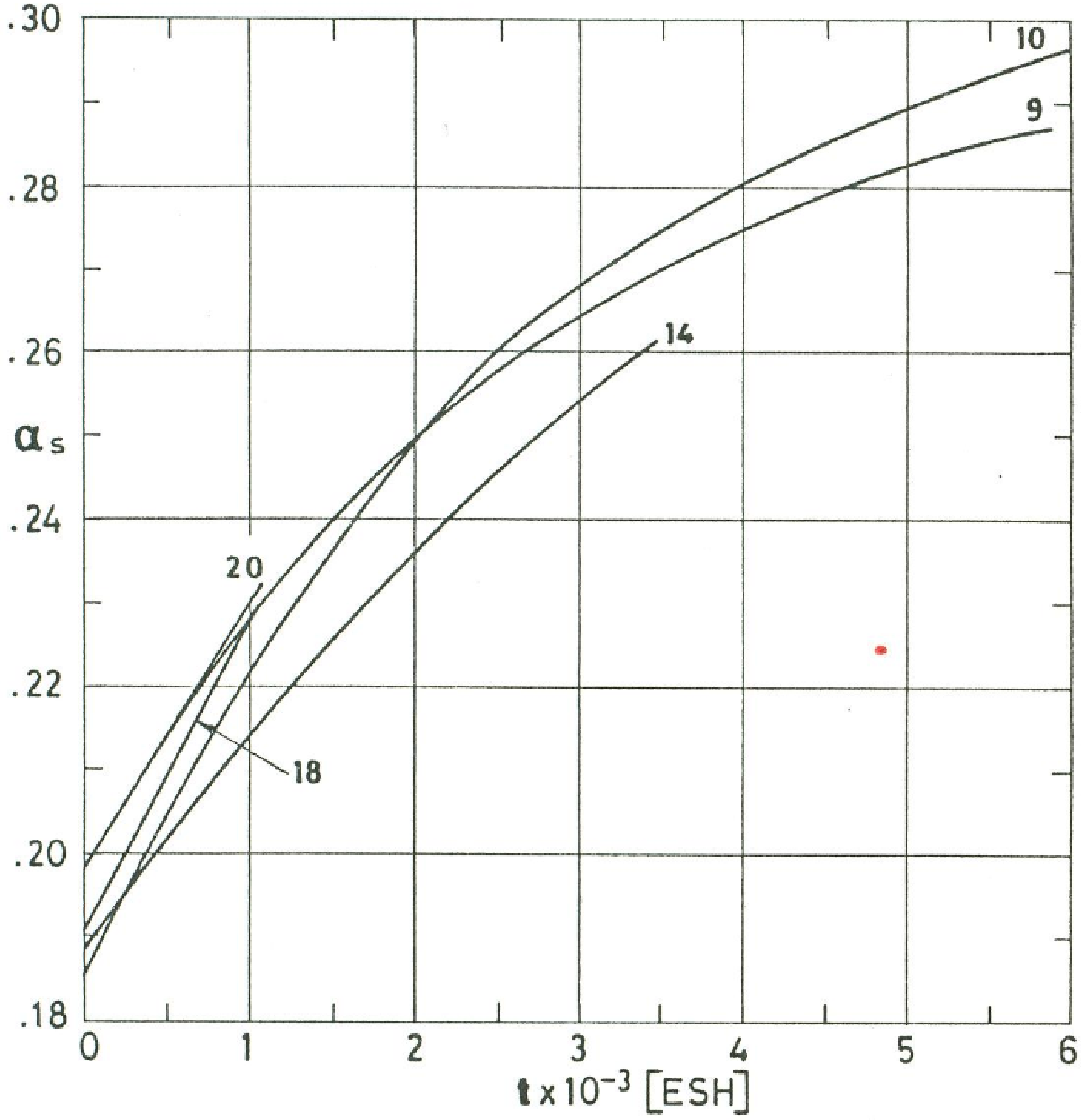

Note: non-si units are used in this figure

Figure 5-13: Solar absorptance, α_s, of several YB-71 coatings vs. exposure time, *t*, as deduced from data of various spacecraft in geosynchronous orbits. Numbers corresponds to sample designations.

COMMENTS

Solar absorptance, α_s, depends on coating thickness as shown in Figure 5-11. Samples 18 and 20 depart from this rule but the discrepancy are not clear since the results given are only preliminary. On the other hand the rate of degradation seems to be independent of the coating thickness. Samples14, 18 and 20 were tested in the same flight and that on magnesium substrate exhibits a slightly larger degradation rate.

References: Curran & Millard (1978) [34], Ahern & Karperos (1983) [4].

7.3.2.5.3. Protons only exposure. The data below refer to a SSR pigment, phosphated.

α_s deduced from spectral reflectance measured in situ.

Radiation Exposure			α_{s0} Initial	$\Delta\alpha_s$	Comments
Intensity [keV]	**Integrated Flux [protons.m^{-2}]**	**Flux [protons.m^{-2}.s^{-1}]**			
1,2	8,4 x 10^{19}	5,4x10^{13}	0,149	0,038	Irradiation performed at 1,3x10^{-5} Pa. Sample temperature, 285 K. Reflectance measured in situ (initially at 8x10^{-6} Pa).

NOTE From Zerlaut, Gilligan & Ashford (1972) [141]. For a description of the experimental set up see Gilligan & Zerlaut (1971) [46].

7.3.2.5.6. Combined exposure. α_s deduced from spectral reflectance measured in situ.

Chamber pressures and sample temperature as above.

Exposures in the order given from left to right, except those under Combined which are simultaneous.

UV Exposure Time [ESH]	Combined					$\Delta\alpha_s$	$\Delta\alpha_s$ after O_2 Bleach
	Protons				**UV Exposure Time [ESH]**		
	Intensity [keV]	**Integrated Flux [protons.m^{-2}]**	**Flux [protons.m^{-2}.s^{-1}]**	**Exposure [a] Time [EWH]**			
600						0,033	
600	1,2	8,3x10^{18}	1,21x10^{13}	927	700	0,074	0,053
600					700	0,019	0,010

[a] EWH: Equivalent Wind Hours.

NOTE From Gilligan & Zerlaut (1971) [46].

7.3.2.6. Effects of the Space Environment on solar absorptance to emittance ratio. See OSO-H and PROSPERO, paragraph 7.3.2.5.1 of this clause.

7.3.3. Reflectance.

7.3.3.1. Normal-hemispherical spectral reflectance. See Figure 5-14.

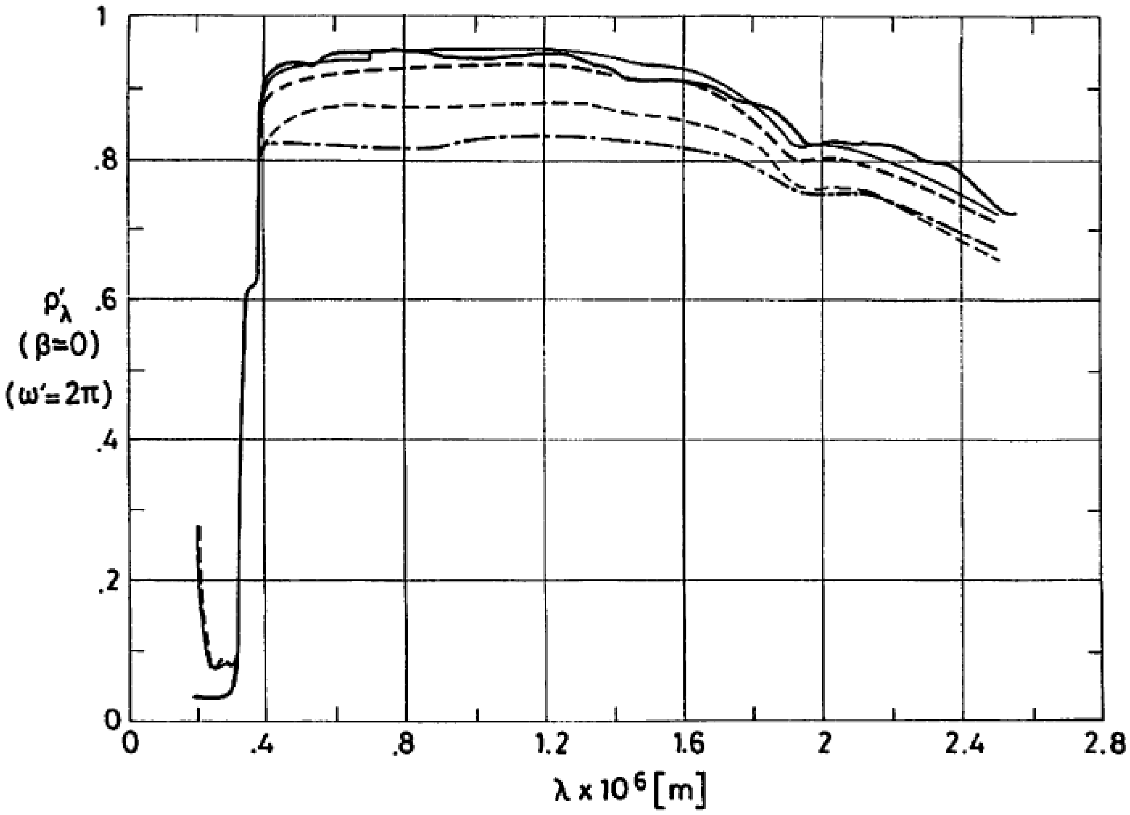

Note: non-si units are used in this figure

Figure 5-14: Normal-hemispherical spectral reflectance, ρ'_λ, of Zinc Orthotinanate-Potassium Silicate coatings vs. wavelength, λ.

Explanation

Key	**Description**			**Comments**	**References**
	Pigment Process and Encapsulation	**Coating Thicckness t_cx10^4 [m]**	**α_s**		
▬▬	SSR Phosphated		0,109	Measured in air with an integrating sphere attached to a Beckman DK2A reflectometer. β= 0°.	Keyte (1975) [70]
――	MOX	1,73	0,108	Measured in vacuum (1,3x10^{-5} Pa) with an integrating sphere attached to a Beckman DK2A reflectometer. β= 7°.	Harada & Wilkes (1979) [58]. Test Conditions Zerlaut & Courtney (1967) [140].
▬ ▬		1,45	0,125		
— —		0,79	0,178		
▬·▬		0,56	0,214		

7.3.3.2. Effects of the Space Environment on reflectance.

7.3.3.2.1. Ultra-Violet Radiation. The data below refer to coatings based on SSR processed pigments.

Sample [a] No.	**Exposure Time [ESH]**	**Spectral Reflectance Decrease, $10^2 x \Delta\rho'_\lambda/\rho'_\lambda$, at Wavelengths, λ, below**				
		$\lambda x10^7$ [m]				
		3,62	**4,25**	**7,00**	**9,25**	**24,0**
5	2400	4,0	7,0	1,0	1,0	–1,0
6	2000	7,0	5,5	0,2	–0,4	–2,2
7	2000	4,2	5,0	1,8	1,0	–2,2
8	1200	2,2	2,8	0	0	0,5

[a] Sample numbers in this Table correspond to those in Table 5-6 and Table 5-7.

Degrading Source: 1 kw General Electric AH-6 Mercury-Argon lamp, 6 Suns level.

Irradiated in vacuum ($1,3x10^{-4}$Pa - $1,3x10^{-5}$ Pa).

Measured in situ with an integrating sphere attached to a Beckman DK2A reflectometer.

From Zerlaut, Gilligan & Ashford (1972) [141]. For a description of the experimental set up see Gilligan & Zerlaut (1971) [46].

Additional information, in graphical form, is given in Figure 5-15.

7.3.3.2.3. Protons only exposure. See Figure 5-16, paragraph 7.3.3.2.3 of this clause.

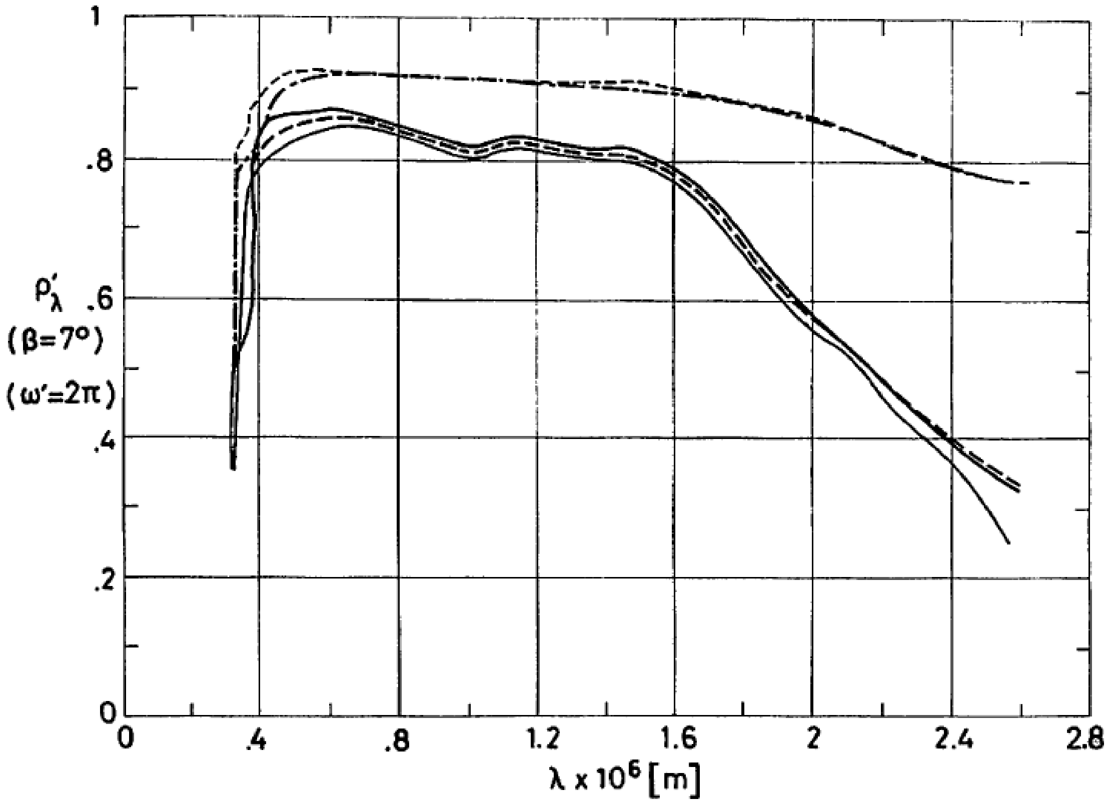

Note: non-si units are used in this figure

Figure 5-15: Effect of Ultra-Violet Radiation on normal-hemispherical spectral reflectance, ρ'_λ, of Zinc Orthotitanate- Potassium Silicate coatings vs. wavelength, λ.

Explanation

Key	Pigment Process and Encapsulation	Comments	References
━━━	SSR Phosphated.	Measured in vacuum (initially at 8x10^{-6} Pa). Sample temperature, 285 K.	Gilligan & Zerlaut (1971) [46].
───		Same as above bur irradiated in vacuum (1,3x10^{-5} Pa). 1300 ESH.	
━ ━		Same as above. O$_2$ bleached. This is the same sample as in the Table of paragraph 7.3.3.2.1.	
─ ─	SSR Potassium hexafluorosilicate treated.	Coating cured at 773 K for 7 h. Sample No. 8 in Table 5-6 and Table 5-7. Measured in vacuum (initially at 8x10^{-6}Pa).	Zerlaut, Gilligan & Ashford (1972) [141].
━·━		Same as above but irradiated in vacuum (1,3x10^{-5} Pa). 1200 ESH.	

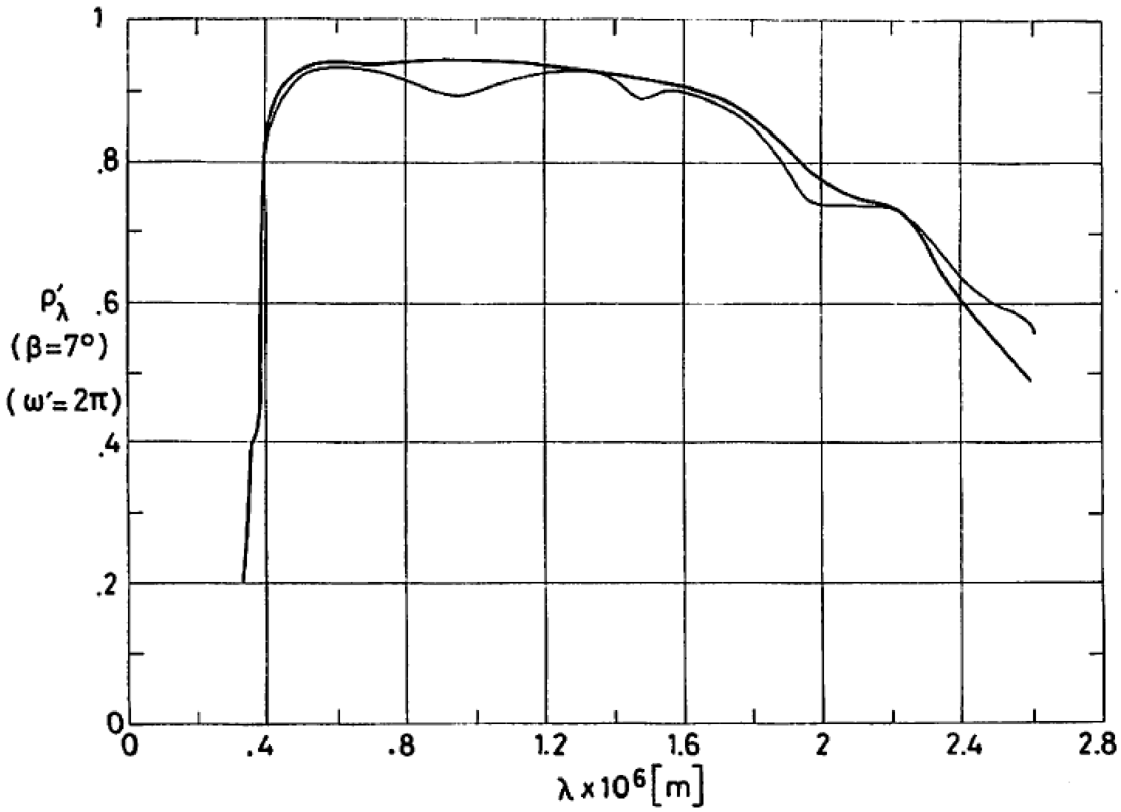

Note: non-si units are used in this figure

Figure 5-16: Effect of Protons Radiation on normal-hemispherical spectral reflectance, ρ'_λ, of Zinc Orthotitanate-Potassium Silicate coatings vs. wavelength, λ. From Gilligan & Zerlaut (1971) [46].

Explanation

Key	Pigment Process and Encapsulation	Protons Exposure			Comments
		Intensity [keV]	Integrated Flux [protons.m^{-2}]	Flux [protons.m^{-2}.s^{-1}]	
━━	SSR Phosphated.				Measured in vacuum (8×10^{-6} Pa). Sample temperature, 285 K.
──		1,2	$2,7\times10^{19}$	$5,4\times10^{13}$	Irradiated in vacuum ($1,3\times10^{-5}$ Pa). Measured in situ (initially at 8×10^{-6} Pa).

8. ENVIRONMENTAL BEHAVIOR

8.1. Prelaunch. The adhesion to 6061-T6 aluminium alloy and cohesion of YB-71 coating appears to be similar to that for Z-93 (see clause 5.2.2) which is a space-qualified paint. Scratching of the coating with a steel microspatula showed that the material is quite tough and could be removed only by applying strong pressure. Good adhesion as indicated in that after penetration to the substrate, complete removal of the coating at the coating-metal interface could not be effected. Initial conical mandrel bend tests have also revealed god adhesion (Harada & Wilkes (1979) [58]).

According to Keyte (1975) [70], who refers to a SSR pigment, phosphated, the coating is not as strong as Z-93 mechanically.

8.2. Postlaunched. Although this coating has been proposed for use in a number of satellites, actual in orbit performance data is very limited.

8.2.1. Ascent. The coating based on SSR processed pigment, phosphated, exhibits little tendency to change under vacuum (Keyte (1975) [70]).

8.2.2. Orbital. The coating based on SSR processed pigment, phosphated, degrades itself very slightly, by about $\Delta\alpha_s$ = 0,03, under ultra-violet radiation and near-to-Earth flight. (Keyte (1975) [70]).

The initial degradation shown by all coatings tested on OSO-H has not been explained satisfactorily.

9. THERMAL CYCLING

The maximum and minimum temperatures at which YB-71 has been tested, in a vacuum of $1,3\text{x}10^{-5}$ Pa, without any evidence of deterioration in adhesion were:

T_{min} = 116 K

T_{max} = 380 K.

Samples have been cooled to the range 33 K to 88 K for 45 min with no apparent loss in bond integrity.

(Harada & Wilkes (1979) [58]).

10. SOURCE

IIT Research Institute, 10 West 35 Street, Chicago, Illinois 60616. Contact person: Mr. Yoshiro Harada.

11. COST

12. PAST SPATIAL USE

No information other than that given in OSO-H and PROSPERO, paragraph 7.3.2.5.1 of this clause, has been found by the compiler.

Data on the performance of YB-71 coating samples in a geosynchronous orbit is now being collected (Harada (1981) [57]). A sample of this coating, on aluminium substrate, can be tested, among others, onboard Long Duration Exposure Facility (LDEF) 1st Mission (scheduled for early 1984), Experiment S0010. In this experiment the coating would be examined before flight and after retrieval (Clark (1981) [30]).

5.2.3.1 Zinc-Oxide Methylsilicone

Three slightly different coatings will be introduced in this data item. For the time being they will be designated a, b and c respectively.

1. COMPOSITION

(a) Pigment: New Jersey Zinc Co., SP500 zinc oxide
Binder: General Electric Co., RTV-602, methylsilicone
Solvent: Toluene

(b) Pigment: New Jersey Zinc Co., SP500 zinc oxide, PS7-treated

Binder: General Electric Co., RTV-602, methylsilicone

Solvent: Toluene, USP (US Pharm.)

The pigment is reactively encapsulated to enhance its stability against UV radiation. The zinc oxide (the unstable component) is reacted in slurry with PS7 potassium silicate (Sylvania Electric Products Co.) The details vary from reference to reference. "Sweating" involves sealing in aluminium foil the slurry resulting from hot treatment of a slurry containing 1,7 parts PS7 and 1 part SP500 letting it to stand during 6 h at least. Satisfactory softness, whiteness and protection against UV is achieved with sweating times above 6 h. Paints prepared from 24 h-sweated pigment have extended shelf lives without the use of retarders. Sweating times of 48 h result in paints which cannot be easily applied or cured (Zerlaut, Rogers, Noble (1969) [144]).

(c) Pigment and solvent as in b

Binder: stripped methylsilicone

Outgassing characteristics are enhanced by devolatilization of the binder at 423 K ± 3 K and a vacuum of the order of 7 x 10^{-4} Pa for 24 h (Seidenberg, Park & Clatterbuck (1972) [114]).

The properties (other than outgassing), application procedures and handling procedures are the same for both b and c coatings.

The silicones of General Electric were originally sold under the name of LTV (Low Temperature Vulcanizing). Sometime in the sixties the name LTV was changed into RTV (Room Temperature Vulcanizing) (Zwaal (1986) [145]). Here either LTV or RTV were used according to the corresponding source.

In 1982 General Electric Co. discontinued the manufacture of RTV-602. Since then IITRI, manufacturer of the coatings, is engaged in a program to find at least two new suitable replacement binders for RTV-602. See Cull et al (1984) [31] for preliminary results with 21 commercial silicone resins.

2. FORMULATION

(a) 2,4:1:1,7 by weight of pigment, binder and solvent

(b) 2,4:1:1,75 by weight of pigment, binder and solvent

From Cunnington, Grammer & Smith (1969) [33].

3. USUAL DESIGNATION

(a) S-13

(b) S-13 G

(c) S-13 G/LO

IIT Research Institute.

4. SUBSTRATE

Any substrate to which the primer (General Electric proprietary S-4044 silane) adheres to. This primer can be applied to either anodized or zinc-chromate-primed surfaces.

From Cunnington, Grammer & Smith (1969) [33].

5. METHOD OF APPLICATION

5.1. Preparation of paint for application

(a) S-13. The paint is furnished in 5 gal epoxy-lined metal pails. The paint should be thoroughly stirred before transfer to other containers or before additions of catalyst. The catalyst is SRC-05. The recommended concentration is 1 part SRC-05 in 20 parts of toluene to 670 parts of S-13 (by weight). This is equivalent to 0,76 atalyst based on polymer solids. Lower catalyst concentrations are recommended to ensure optimum stability to UV irradiation in vacuum. For example a concentration of 1 part SRC-05 in 20 parts of toluene to 1 275 parts of S-13 (which represents 0,4 % catalyst based on polymer solids) provides optimum stability to UV irradiation in vacuum without greatly sacrificing terminal-cure properties.

The catalyst solution is added only as the paint is used and only to the amount that can be applied in about 30 min. Allow the catalyst paint to set for 10 min before application to the primed surface.

(b) S-13 G and S-13 G/LO. As above but now the recommended concentration of catalyst is 1 part SRC-05 in 10 parts of toluene to 1 030 parts of S-13 G (by weight), which corresponds to 0,75 % SRC-05. A concentration of 0,4 % based upon RTV-602 provides optimum stability without sacrificing terminal-cure properties.

The undiluted catalyst has a shelf life of six months and the diluted a shelf life of thirty days (Cull, Stevenson, Harada & Mell (1984) [31]).

From Cunnington, Grammer & Smith (1969) [33] unless otherwise stated.

5.2. Preparation of surfaces for painting. Greasy surfaces should be cleaned with standard detergent and water, and thoroughly dry prior to priming. Primer is SS-4044.

From Cunnington, Grammer & Smith (1969) [33].

5.3. Application of paint. The primer can be spray-applied (Binks model 18 or comparable gun) at about 2 x 10^5 Pa. Only about 12,7 x 10^{-6} m thick primer is required. Allow primer to air dry for 1 h before application of the paint. Paint can be spray-applied (Binks model 18 or comparable gun) at about 4 x 10^5 Pa. Unless clean dry air is available prepurified nitrogen or prepurified air should be used. Paint viscosity is rated at 25 s to 31 s with a No. 4 Ford cup. It can be used until the viscosity exceeds 100 s No. 4 Ford. Paint should be thinned to 17 s - 23 s No. 4 Ford with X-99 thinner (Cull, Stevenson, Harada & Mell (1984) [31]).

From Cunnington, Grammer & Smith (1969) [33] unless otherwise stated.

5.3.1. Pot life. Pot life of S-13 G/LO is one hour for the catalyzed paint.

From Cull, Stevenson, Harada & Mell (1984) [31].

5.3.2. Shelf life. Shelf life of S-13 G/LO is guaranteed for 30 d after purchase, providing that paint is stored at 280 K.

From Cull, Stevenson, Harada & Mell (1984) [31].

5.4. Coating thickness

(a) S-13. 89 x 10^{-6} m to 140 x 10^{-6} m.
From Cunnington, Gramer & Smith (1969) [33].

(b) S-13 G. 127 x 10^{-6} m to 203 x 10^{-6} m.
From Breuch (1967) [22].

(c) S-13 G/LO. 17 x 10^{-6} m to 50 x 10^{-6} m per coat. Nominal total, 203 x 10^{-6} m (+ 50 x 10^{-6} m or -25 x 10^{-6} m) thick.
From Cull, Stevenson, Harada & Mell (1984) [31].

5.5. Curing process. Air drying cure for 16 h at room temperature, optionally 16 h at 394 K. Dust and debris should be kept off the surface during the curing process.

From Gilligan, Harada & Gates (1974) [45].

There is a minimum time of 10 minutes required between coats and 50 h required before handling.

For the qualification testing, S-13 G/LO is allowed to cure for 7 days prior to testing.

5.6. Reapplication. Soiled or damaged areas can be recoated. Soiled areas should be cleaned thoroughly with detergent and water, and dried before application of additional paint.

Damaged or gouged areas can be recoated by making a paste of paint in which the bulk of solvent is omitted. Such a material can be troweled or brushed over the damaged areas and cures can be tack free within a few hours.

From Cunnington, Grammer & Smith (1969) [33].

6. SOLVENTS RESISTANCE

See a typical list of solvents in clause 5.2.1.

Optimum solvent composition based on Toluene.

7. PHYSICAL PROPERTIES

7.1. Density

(a) S-13 G. Coating surface density is 0,03 kg.m^{-2} as measured from test specimens (Breuch (1967) [22]).

(b) Paint density is between 1 425 kg.m^{-3} and 1 475 kg.m^{-3} (Cull, Stevenson, Harada & Gates (1984) [31]).

(c) Paint density as in b).

7.2. Outgassing. See table below.

Coating	**% TML [a]**	**% VCM [b]**	**Cure Time [h]**	**Cure Temp. [K]**	**Vacuum Conditions [Pa]**	**References**
S-13 G	0,42	0,09	48 16	298 [c] 394	10^5 $13x10^{-5}$	Campbell, Marriott & Park (1978) [28]
	0,26	0,03				
	0,82	0,16	24	298	10^5	
S-13 G/LO	0,56	0,13	48 24	298 [c] 366	10^5 10^5	
A/B as 100/1 [d]	0,54	0,10	168	298	10^5	
	0,40	0,01	1	394	10^5	
No primer	0,50	0,12				
A/B as 100/1 [d]	0,59	0,11	168	298	10^5	
S-13 G/LO	0,40 [e]	0,05				INTA (1976) [65]

[a] TML: Total Mass Loss.

[b] VCM: (Collected) Volatile Condensable Material

[c] Each one of these cures was used in the order given.

[d] A refers to S-13 G/LO and B to SRC-05 catalyst in toluene. See b) in paragraph 5.1 above.

[e] Data for this sample have been obtained per Specification ESA PSS-09/QRM-02T. %RML = 0,25.

7.3. Thermal radiation properties

7.3.1. Emittance

7.3.1.1. Hemispherical total emittance. The data in the Table 5-8 below have been taken from several sources. They correspond to samples under different conditions and have been determined by different procedures

Table 5-8: Hemispherical Total Emittance of S-13 and S-13 G Coating

Coating	T [K]	$t_c x10^3$ [m]	ε [a]	ε [b]	References
S-13	294			0,87 [b1]	Cunnington, Grammer & Smith (1969) [33]
	395	0,090-0,140	0,87±0,02 [a1]	0,84 [b1]	
	300	0,127		0,81 [b2]	Millard & Pearson (1973) [85]
S-13 G	294			0,84 [b1]	Cunnington, Grammer & Smith (1969) [33]
	395	0,090-0,140	0,89±0,02 [a1]	0,85 [b1]	
	300	0,127		0,81 [b2]	Millard & Pearson (1973) [85]

[a] Determined calorimetrically.

[a1] 6061-T6 Al alloy disc substrate. $25,4 \times 10^{-3}$ m diameter, $1,27 \times 10^{-3}$ m thick. Chamber pressure $1,33 \times 10^{-5}$ Pa.

[b] From spectral reflectance data and the blackbody function for the quoted temperature.

[b1] λ range 2×10^{-6} m to $2,5 \times 10^{-5}$ m.

[b2] OSO III preparation. Substrate primed with G.E. SS-4044.

Hemispherical total emittance vs. temperature is given in Figure 5-17. The coating is S-13 G, 2×10^{-4} m thick, on molybdenum substrate. Hemispherical total emittance, absorptance and specific heat of the coating have been measured by a calorimetric cyclic radiation method (Spisz & Jack (1971) [119]).

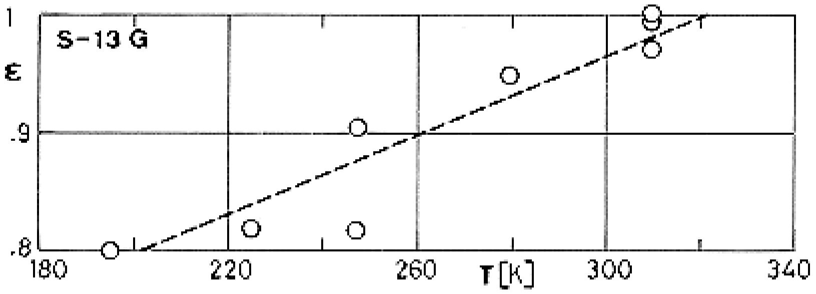

Note: non-si units are used in this figure

Figure 5-17: Hemispherical total emittance, *ε*, of S-13 G coating vs. temperature, *T*. 2×10^{-4} m thick coating on molybdenum substrate. From Spisz & Jack (1971) [119].

The method consists basically in the following: First the substrate is irradiated in vacuum. After thermal equilibrium is reached, the radiant intensity is varied sinusoidally and the substrate temperature is measured as a function of time. From the temperature variation the properties of the substrate are deduced. The coating is then applied to the bottom side of the substrate and the process is repeated by irradiating the top side. Now the average hemispherical total emittance of both sides, the absorptance of the substrate, and the specific heat of coating plus substrate are deduced. The process is repeated again, irradiating the bottom side. The measurements indicate that the solar absorptance of this coating is practically temperature independent.

7.3.1.3. Effects of the Space Environment on hemispherical total emittance

7.3.1.3.1. Ultra-Violet Radiation. Table 5-9 below has been prepared using data from Cunnington, Grammer & Smith (1969) [33].

Table 5-9: Ultra-Violet Radiation Effects on Hemispherical Total Emittance of S-13 and S-13 G Coating

Coating	Sample	T [K]	t [h]	n	ε_o	ε_f		σ
S-13	27	395	500	12	0,86	0,86	0,862	0,006
	28	395	636 [a]	14	0,85	0,87	0,867	0,005
S-13 G	43	395	500	10	0,90	0,91	0,914	0,008
	44	395	520	11	0,91	0,91	0,911	0,005

Degrading Source: 2×10^{-7} m to 4×10^{-7} m Xenon Lamp, 1 Sun level.

Method of obtaining data: Calorimetric. Chamber pressure: $1{,}33 \times 10^{-5}$ Pa. 6061-T6 Al disk, $25{,}4\times10^{-3}$ m diameter, $1{,}27\times10^{-3}$ m thick.

t, total exposure time. [h]

n, number of data points given in the source at the quoted temperature.

ε_o, ε_f, initial and after-exposure values of the hemispherical total emittance.

$\bar{\varepsilon}$, mean value,

$$\bar{\varepsilon} = \frac{\sum_{1}^{n} \varepsilon_i \Delta t_i}{t} \qquad [5\text{-}3]$$

σ, standard deviation,

$$\sigma = \sqrt{\frac{\sum_{1}^{n} \left(\varepsilon_i - \bar{\varepsilon}\right)^2 \Delta t_i}{t-1}} \qquad [5\text{-}4]$$

[a] Failure during test (electronic pump off, pressure increase to > 6,65 Pa (50×10^{-3} mm Hg) for 2 h).

Test data have been represented in Figure 5-18 below.

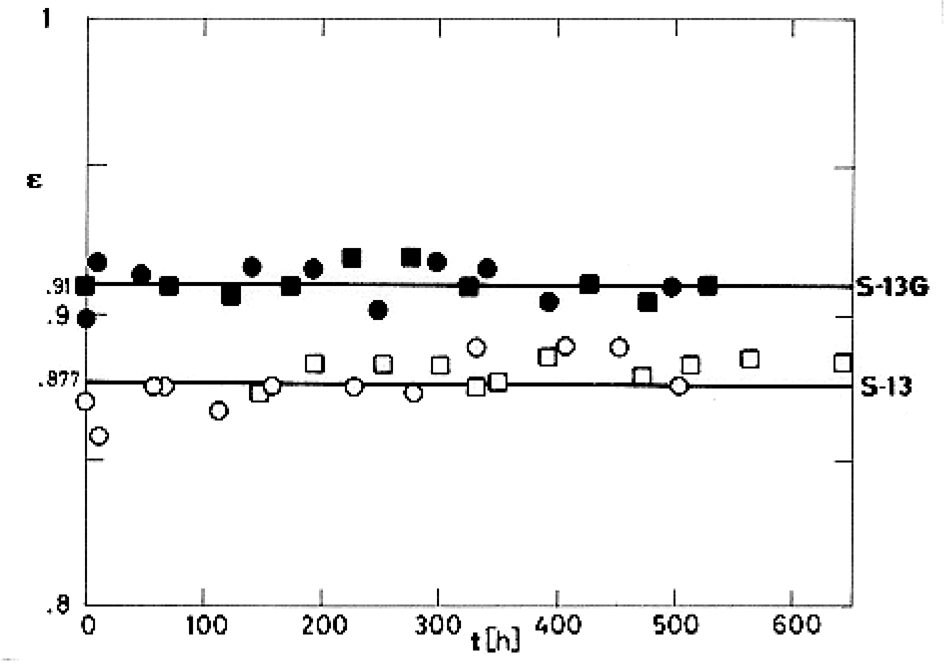

Note: non-si units are used in this figure

Figure 5-18: Hemispherical total emittance, *ε*, of S-13 and S-13 G coatings vs. exposure time, *t*, at 1-Sun level and 395 K. From Cunnington, Grammer & Smith (1969) [33]. Equal symbols correspond to the same sample. ○ :> Sample 27; ● :> Sample 43; □ :> Sample 28; ■ :> Sample 44.

7.3.1.4. Normal total emittance.

See Table 5-10 below.

Room-temperature emittance measurements were performed in the past using an infrared spectrophotometer with an attached heated cavity. The spectral reflectance data were then used to calculate the emittance. More recent data are being obtained with a Gier-Dunkle portable emissometer, model DB-100 (Henninger (1984) [60]).

Table 5-10: Normal Total Emittance of S-13 G and S-13 G-LO Coatings

T [K]	Coating Description	ε'	References
311	S-13 G over B-1056 ZnO in methyl silicone binder (0,0508x10^{-3} m thick), over ZnO in RTV-602 silicone resin binder substrate (0,254x10^{-3} m thick). Property calculated from reflectance. Laboratory data taken on sample to be tested on LO IV.	0,860	Touloukian DeWitt & Hernicz (1972) [126]
	Similar to above specimen and conditions except sample to be tested on LO V.	0,860	
	S-13 G, ZnO in methyl silicone binder (0,254x10^{-3} m thick). Calculated from reflectance. Laboratory data taken on sample to be tested on LO IV.	0,879	
	B-1060; SP-500 ZnO in silicone binder (0,264x10^{-3} m thick). ZnO silicated. Property calculated from reflectance. Laboratory data taken on sample to be tested on LO IV.	0,880	
300	S-13 G. Measured with a Gier-Dunkle portable emissometer. NASA specifications.	0,90±0,05	Henninger (1984) [60]
	S-13 G/LO. As above.	0,90±0,05	Cull et al (1984) [31]

7.3.2. Absorptance

7.3.2.1. Solar absorptance

a. S-13. Near normal solar absorptance. Coating thickness, t_c = 0,127 x 10^{-3} m substrate primed with G.E. S-4044.

α_s = 0,19, T = 300 K.

From spectral reflectance data.

From Millard (1969) [83].

b. S-13 G. Near normal solar absorptance.

t_c = 0,127 x 10^{-3} m substrate primed with G.E. S-4044.

α_s = 0,23, T = 300 K.

From spectral reflectance data.

From Millard (1969) [83].

A recent value for S-13 G is

α_s = 0,20, T = 300 K.

From spectral reflectance.

Data on absolute reflectance, absorptance and transmittance are presently taken at NASA Goddard with a Beckman DK-2A spectrophotometer with a Gier-Dunkle absolute integrating sphere. The instrument covers the wavelength region from 0,3 x 10^{-6} m to 2,4 x 10^{-6} m. It is coupled to a microcomputer for data reduction. The manufacturer of the instrument lists an accuracy of α_s ± 0,015 units over the total measurement range. From Henninger (1984) [60].

7.3.2.2. Variation of solar absorptance with coating thickness.

Data in Figure 5-19 are for S-13 coating.

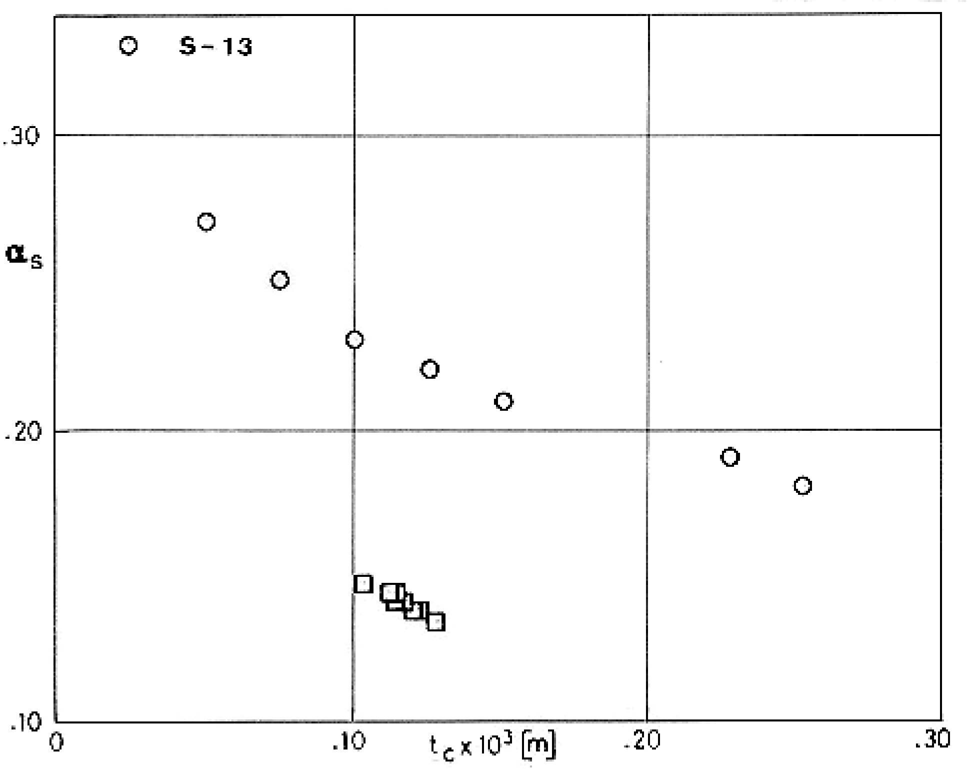

Note: non-si units are used in this figure

Figure 5-19: Variation of solar absorptance, α_s, of S-13 coating with coating thickness, t_c . ○ :> Nominal composition. Sprayed on primed surface. Air dryed. T = 298 K. (Designation in the ref.: 119 to 127). ☐ :> ZnO in silicone binder. T = 298 K. (Designation in the ref.: 29, 30). From Touloukian, DeWitt & Hernicz (1972) [126].

7.3.2.3. Variation of solar absorptance with incidence angle.

Figure 5-20. Solar absorptance deduced from spectral reflectance measured in air. Two different sample sizes were used to assure full sample illumination at all incidence angles. S-13 coating, silicated pigment in silicone binder applied to aluminium substrate. Sample to be tested on PROSPERO.

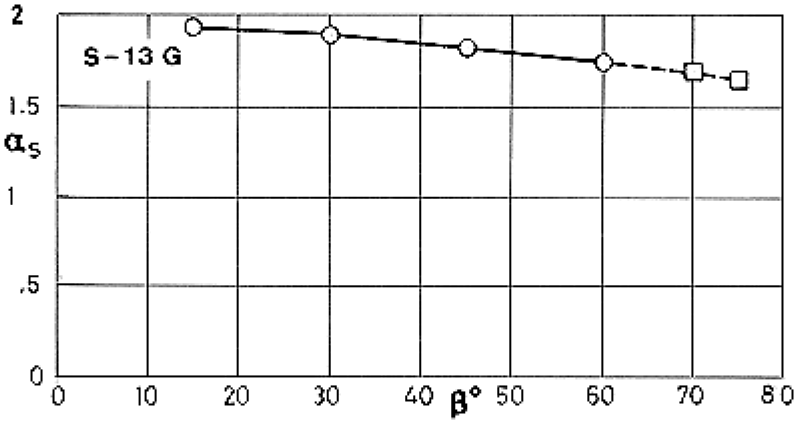

Note: non-si units are used in this figure

Figure 5-20: Solar absorptance, α_s, of S-13 G coating vs. incidence angle, β. From Keyte (1975) [70].

7.3.2.5. Effects of Space Environment on absorptance

7.3.2.5.1. Ultra-Violet Radiation. Detailed laboratory data on the effects of UV radiation on spectral absorptance are given in Table 5-11.

Table 5-11: Ultra-violet radiation effects on spectral absorptance of S-13 coating (samples 27 & 28)

T [K]	t [h]	α for Xenon Lamp Range of λ x 10^7 [m]					α_s
		2-4,1	4,1-6	6-8,5	8,5-	Total	
294	0	--	--	--	--	0,21	--
339	0	--	--	--	--	0,21	--
395	0	--	--	--	--	0,21	--
395	4	0,65	0,08	0,06	0,24	0,21	0,21
395	53	0,65	0,10	0,06	0,27	0,23	0,23
395	61	0,65	0,15	0,06	0,28	0,24	0,24
395	113	0,70	0,15	0,08	0,30	0,27	0,26
395	158	0,70	0,19	0,08	0,28	0,26	0,26
395	230	0,75	0,21	0,09	0,28	0,27	0,27
395	280	0,75	0,25	0,08	0,29	0,27	0,28
395	330	0,70	0,26	0,10	0,28	0,26	0,28
395	402	0,65	0,26	0,08	0,28	0,27	0,28
395	450	0,65	0,27	0,08	0,30	0,27	0,28
395	500	0,70	0,27	0,10	0,28	0,27	0,28
Before Exposure [a]		0,65	0,08	0,10	0,14	0,18	0,18
After exposure [a]		0,76	0,31	0,15	0,17	0,26	0,28

T [K]	t [h]	α for Xenon Lamp					α_s
		Range of λ x 10^7 [m]					
		2-4,1	4,1-6	6-8,5	8,5-	Total	
290	0	--	--	--	--	0,21	--
342	0	--	--	--	--	0,20	--
395	0	0,70	0,10	0,10	0,19	0,21	0,20
395	4	0,70	0,10	0,10	0,23	0,22	0,21
395	50	0,65	0,12	0,10	0,26	0,23	0,23
395	146	0,65	0,18	0,10	0,28	0,26	0,26
395	196	0,65	0,23	0,08	0,32	0,27	0,28
395	246	0,70	0,28	0,08	0,32	0,30	0,30
395	296	0,70	0,26	0,09	0,31	0,29	0,30
395	328 [b]	0,70	0,21	0,10	0,26	0,25	0,26
395	346	0,70	0,22	0,10	0,29	0,27	0,27
395	396	0,70	0,22	0,10	0,31	0,28	0,28
395	468	0,70	0,24	0,11	0,30	0,27	0,28
395	516	0,70	0,23	0,14	0,30	0,27	0,28
395	564	0,70	0,24	0,14	0,30	0,27	0,28
395	636	0,70	0,24	0,14	0,30	0,27	0,28
Before exposure [a]		0,65	0,08	0,10	0,14	0,19	0,19
After exposure [a]		0,78	0,32	0,17	0,21	0,28	0,31
294	0	--	--	--	--	0,23	--
339	0	--	--	--	--	0,21	--
395	0	--	--	--	--	0,21	--
395	0	0,85	0,12	0,05	0,15	0,20	0,20
395	4	0,90	0,12	0,05	0,16	0,21	0,21
395	51	0,90	0,17	0,08	0,17	0,23	0,24
395	149	0,90	0,21	0,09	0,17	0,24	0,25
395	195	0,92	0,27	0,10	0,17	0,26	0,27
395	248	0,90	0,28	0,10	0,17	0,26	0,27
395	296	0,90	0,32	0,09	0,17	0,26	0,28
395	344	0,85	0,35	0,11	0,17	0,26	0,28
395	392	0,85	0,35	0,11	0,17	0,26	0,28
395	500	0,85	0,35	0,10	0,18	0,26	0,28
Before exposure [a]		0,70	0,10	0,10	0,13	0,19	0,19
After exposure [a]		0,82	0,37	0,20	0,15	0,28	0,31
294	0	--	--	--	--	0,24	--
339	0	--	--	--	--	0,22	--
395	0	0,80	0,10	0,08	0,14	0,19	0,19
395	5	0,80	0,10	0,08	0,14	0,20	0,20
395	75	0,80	0,16	0,09	0,15	0,20	0,21

T [K]	**t [h]**	**α for Xenon Lamp**					**α_s**
		Range of λ x 10^7 [m]					
		2-4,1	**4,1-6**	**6-8,5**	**8,5-**	**Total**	
395	123	0,80	0,16	0,08	0,16	0,21	0,22
395	172	0,80	0,21	0,08	0,16	0,21	0,22
395	227	0,75	0,27	0,08	0,16	0,22	0,23
395	274	0,75	0,27	0,08	0,16	0,22	0,23
395	327	0,75	0,27	0,10	0,16	0,22	0,24
395	423	0,75	0,27	0,10	0,17	0,22	0,24
395	471	0,75	0,27	0,10	0,17	0,22	0,24
395	520	0,75	0,28	0,10	0,18	0,22	0,25
Before exposure [a]		0,65	0,10	0,10	0,13	0,18	0,20
After exposure [a]		0,75	0,29	0,12	0,15	0,23	0,27

[a] Values from Cary room temperature reflectance measurements.

[b] Electronic pump off, pressure increase to > 6,65 Pa (50 μm Hg). Ultraviolet source is a 900 W

Hanovia Xenon Lamp, Model 538-CL. Method of obtaining data: calorimetric in situ absorptance. Chamber pressure: 1,33 x 10^{-5} Pa.

From Cunnington, Grammer & Smith (1969) [33].

The UV radiation induced absorption of zinc oxide pigments is based on a photochemical evolution of oxygen. UV degraded zinc oxide rapidly recovers its initial optical properties upon re exposure to air. Table 5-12 below lists results obtained under varied experimental conditions, and deduced from spectral reflectance given in Figure 5-35 to Figure 5-40.

Data from flight experiments have been grouped in paragraph 7.3.2.5.6 under Combined exposure. Reported measurements correspond to widely different orbits. Effects on solar absorptance of UV exposure and thermal cycling at cryogenic and room temperatures have been reported by Breuch (1967) [22] and are given below. Coating is S-13.

Table 5-12: Ultra-Violet Radiation Effects on Solar Absorptance of S-13 and S-13 G Coatings

Coating	Spectral Reflectance Data		t [ESH]	α_s	$\Delta\alpha_s$
S-13	Figure 5-34	Solid lines	800	0,21	0,08
S-13 G	Figure 5-35 & Figure 5-36	Solid lines	600	0,21	0,01
	Figure 5-35	Dashed lines	600	0,22	0,03
	Figure 5-36	Dashed lines	800	0,20	0,03
	Figure 5-37	Solid lines	600	0,22	0,06
		Dashed lines	600	0,22	0,02
	Figure 5-38 & Figure 5-39	Solid lines	1400	0,24	0,01
	Figure 5-39	Dashed lines	1400	0,22	0,02
		Dashed-dotted lines	1400	0,22	0,03
		Dotte lines	1400	0,26	0,05
		Dashed-double dotted lines	1400	0,23	0,06
	Figure 5-40	Thick solid and thick dashed lines	600+700		0,039
		Solid lines	600+700+O_2 bleaching		0,013

Data obtained by Cary Reflectometer

Chamber pressure:

For T = 136 K, $p = 8 \times 10^{-6}$ Pa to $13{,}3 \times 10^{-6}$ Pa.

For T = 133-297 K, $p = 4 \times 10^{-6}$ Pa to 8×10^{-6} Pa

T [K]	t [ESH]	UV [Suns]	α_s	$\Delta\alpha_s$
136	2790	14	0,18	0,01
133-297 (275 cycles)	2560	12	0,20	0,03

NOTE From Beruch (1967) [22].

7.3.2.5.3. Protons only exposure. Data for coatings S-13 and S-13 G are given in Figure 5-21. Data for S-13 have been measured in air after exposure and those for S-13 G in situ (see comments in paragraph 7.3.3.2.1).

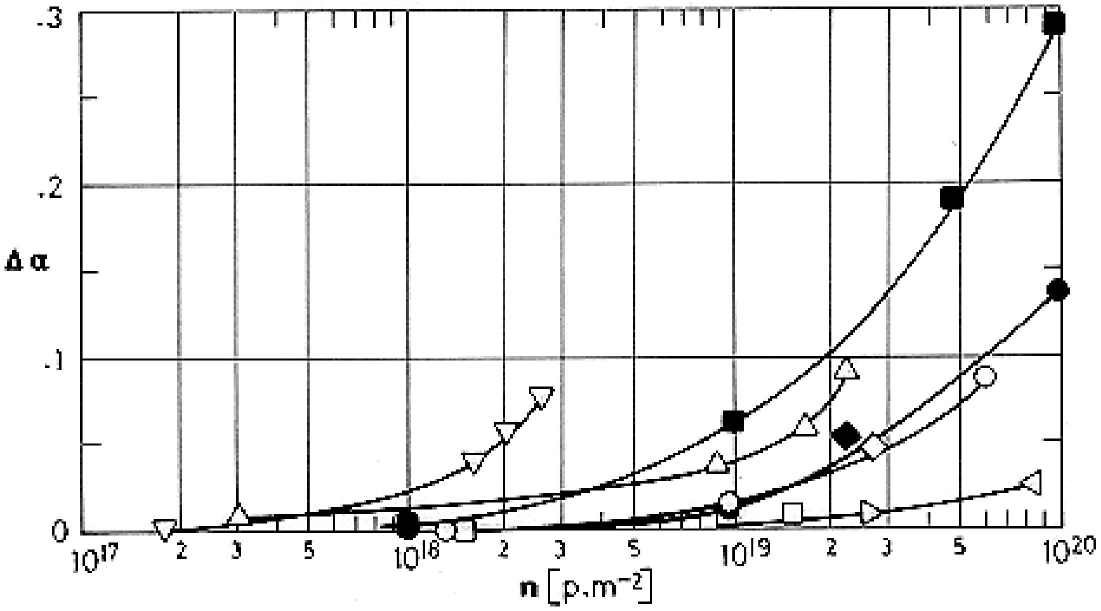

Note: non-si units are used in this figure

Figure 5-21: Change in solar absorptance, $\Delta\alpha_s$, of S-13 and S-13 G coatings due to Protons and Alpha Particles Radiation vs. integrated flux, n.

Explanation

Key	Coating	Intensity [keV]	Comments	References
○	S-13	8 p	p 10^{-4} Pa, T=303 K ± 5 K. Irradiated in vacuum by a low energy particle accelerator and a Dynamitron. From spectral reflectance measured in air (20 h-40 h delay). Cracking observed.	Gillette, Brown, Seiler & Sheldon (1966) [54]
□		8 p		
△		$2{,}5 \times 10^3$ p		
▽		5×10^3		
▷	S-13 G	1,2 p	$4{,}9 \times 10^{13}$ p.m^{-2}.s^{-1}. T=285 K	Compiled by Bourrieau, Paillous & Romero (1967) [21]
◁		1,2 p	5×10^{13} p.m^{-2}.s^{-1}	
◇		2 & 10 p		
◆		10 & 20 p	$7{,}3 \times 10^{13}$ p.m^{-2}.s^{-1}. T=288 K	
●		40 p	T=293 K	
■		40 p	10^{14}-5×10^{14} p.m^{-2}.s^{-1}. T=291 K	

Data for Protons Radiation up to 400 keV intensity are also given by Miller & Campbell (1966) [87]. The coating binder is Dow Corning Q 90016 methyl silicone. Reflectance data are presumably taken ex situ.

7.3.2.5.4. Electrons only exposure. Coating in the table below is GSFC, 101-7 (similar to S-13 G) on Al substrate. Absorptance deduced from spectral reflectance. See paragraph 7.3.2.5.1. in clause 5.2.4.

Intensity [keV]	Cumulative Integrated Flux [e.m^{-2}]	Measured in	α_s
20		Air T = 298 K	0,22
	10^{17}	Vacuum T = 298 K $1{,}33 \times 10^{-6}$ Pa	0,22
	5×10^{17}		0,23
	10^{1}		0,23
	3×10^{18}		0,24
	10^{19}		0,26
	10^{20}		0,29

Intensity [keV]	Cumulative Integrated Flux [e.m^{-2}]	Measured in	α_s
80		Air T = 298 K	0,22
	10^{17}	Vacuum T = 298 K 1,33 x 10^{-6} Pa	0,23
	5 x 10^{17}		0,24
	10^{18}		0,26
	3 x 10^{18}		0,32
	10^{19}		0,37
	10^{20}		0,41

NOTE From Fogdall, Cannaday & Brown (1970) [43]. Data from several sources are shown in Figure 5-22.

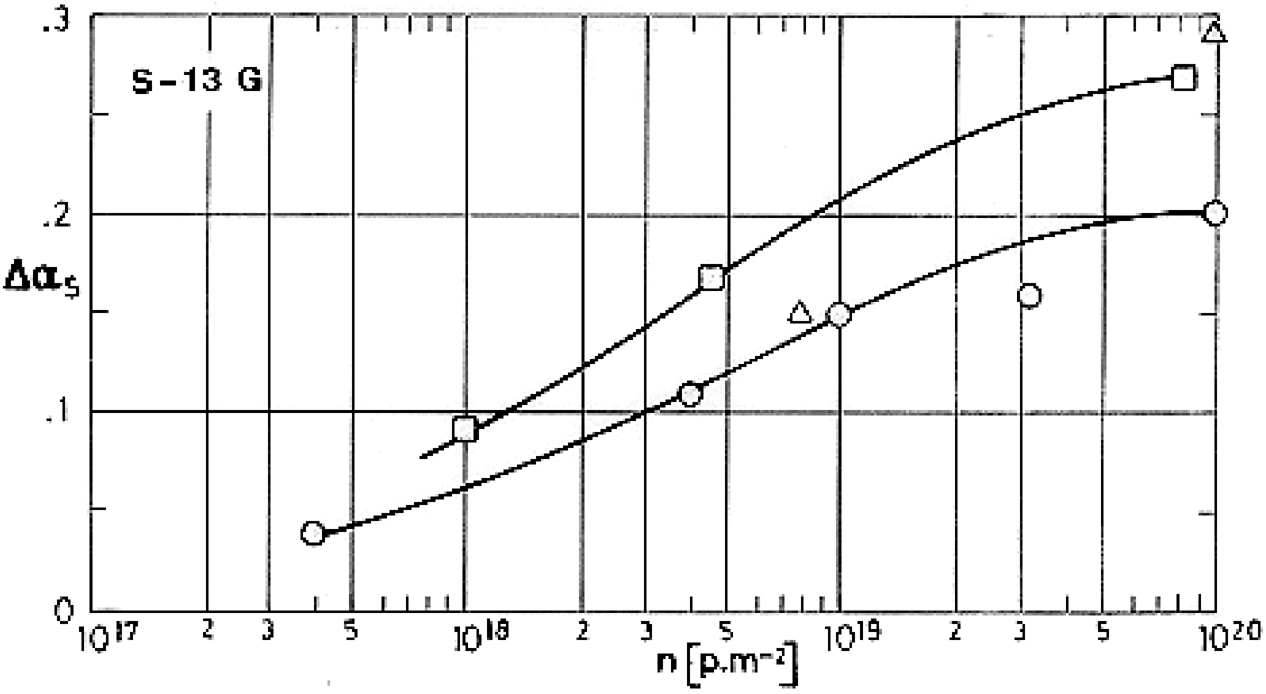

Note: non-si units are used in this figure

Figure 5-22: Change in solar absorptance, $\Delta\alpha_s$, of S-13 G coating due to Electrons Radiation vs. integrated flux, n. Data taken in situ. Compiled by Bourrieau, Paillous & Romer (1976) [21].

Explanation

Key	Intensity [keV]	Flux [e.m^{-2}.s^{-1}]	T [K]
○	35	10^{14} - 7 x 10^{14}	291
□	50	2 x 10^{14} - 5 x 10^{15}	295
△	80		281

7.3.2.5.5. Contamination. Changes in α_s and ε of S-13 G coating due to rocket exhaust impingement have been given by McCargo et al. (1971) [82]. The results are hardly useful due to their very limited scope (they depend on the motor generating the exhaust products) and to the inability to reproduce the space environment on a laboratory scale. The main phenomena inducing contamination and (or) degradation are heating, chemical reactions, deposition of solid particles and liquids, and erosion.

No change in emittance was observed, but the change in solar absorptance was appreciable.

Exhausts from non-chemical thrusters also affect the optical properties of the coating.

Results are summarized in the table below.

t [h]	ε	α_s	α_s/ε
0	0,880	0,163	0,185
0,167	0,872	0,309	0,354
0,667	0,877	0,344	0,392
3,25	0,876	0,338	0,386

NOTE From McCargo, Spradley, Greenberg & McDonald (1971) [82].

7.3.2.5.6. Combined exposure

The available information regarding in flight measurements of solar absorptance is summarized in the following.

The experiments performed both before and during OSO III flight are described in Millard & Pearson (1973) [85]. An incertitude analysis is given in Millard (1968) [83].

a. Laboratory tests. The coatings were bombarded with Ultra-violet radiation, 2 and 10 keV protons, and both UV and protons.

UV irradiations were made with a Xenon lamp and a mercury arc lamp at one Sun level up to 265 h, and with mercury arc lamps at 10 Suns intensity for the remaining ESH. Mercury arc irradiation at one Sun level seems to match the flight data to about 1000 ESH.

Data were taken in situ.

Coating	UV [ESH]	p [p.m^{-2}]	UV+p [ESH+p.m^{-2}]	$\Delta\alpha_s$ UV	$\Delta\alpha_s$ p	$\Delta\alpha_s$ UV+p
S-13	90	0,43 x 10^{19}	90 (0,28 x 10^{20})	0,08	0,01	0,06
	432	1,3 x 10^{19}	432 (1,1 x 10^{20})	0,10	0,02	0,09
	1098	3 x 10^{20}	1098 (2,8 x 10^{20})	0,11	0,10	0,19
S-13 G	750	2 x 10^{19}	750 (2 x 10^{19})	0,01	0,05	0,08

NOTE From Millard (1969) [84].

b. Flight Experiments. OSO III was launched on March 8, 1967 in a near circular orbit (of about 550 km) with a 33° angle of inclination relative to the Equator. The zone of the spacecraft on which the experiment was mounted continually spun at a rate of about 37 rpm. The plane of spin contained the satellite-Sun line. Thus the sensors alternatively viewed Sun and Earth without being affected by this spin because of their relatively large thermal mass. Upper and lower temperatures for each orbit were 255 K and 210 K respectively.

Data from OSO III coatings experiment up to four years are given by Millard & Pearson (1973) [85].

Unfortunately, in the case of S-13, data are only available up to 2400 ESH, afterward the temperature of the calorimeter exceeded the instrumentation range. On the other hand figures for S-13 and S-13 G in the mentioned reference are the same as those in 1969 Millard's paper.

The results, see Figure 5-23, do not compare well with previous tests. It seems that the degradation of S-13 G coating depends on the exact method of preparation (see, however, comments in p. 5-48.36).

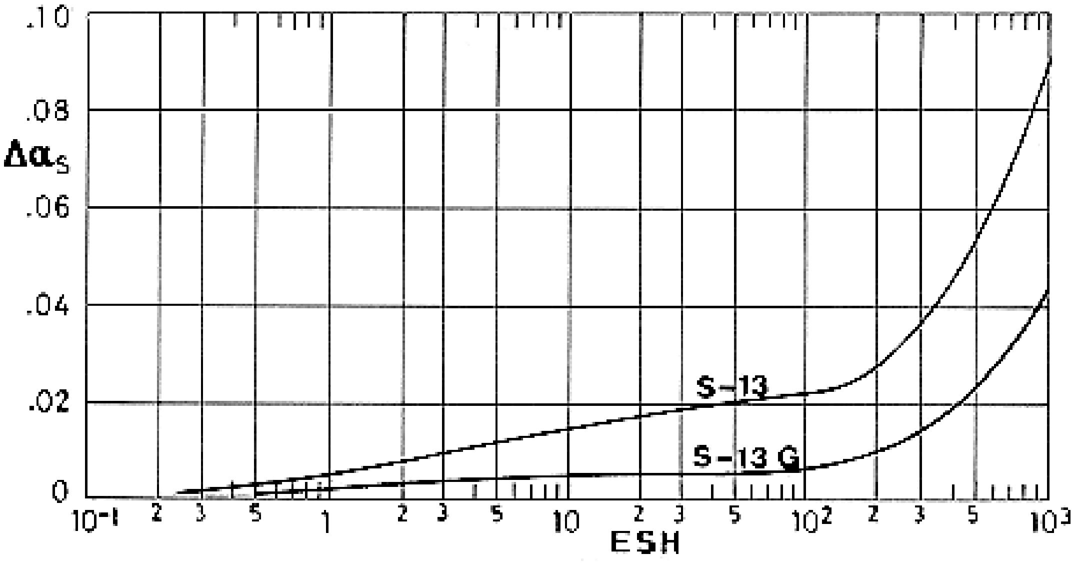

Note: non-si units are used in this figure

Figure 5-23: Changes in solar absorptance of S-13 and S-13 G coatings. OSO III experiment. From Millard (1969) [84].

Figure 5-24 and Figure 5-25 show data from several coatings experiments as compiled from Touloukian, DeWitt &Hernicz (1972) [126]. Agreement for the Pegasus I and II, OSO II and III is excellent. In flight contamination looks negligible for all four flights. Data for Mariner V and ATS-1 exhibit increased damage due to the particulate environment in deep space.

Comparison of the S-13 and S-13 G data confirms the increased protection in the later due to the silicate treated binder. This is now generally accepted, nevertheless, information on the contrary from the early seventies can be found (see f.e. Keyte (1972) [70], p. 38). Although the reasons for the discrepancies remain unclear, they could be due to an un appropriate manipulation of the coating.

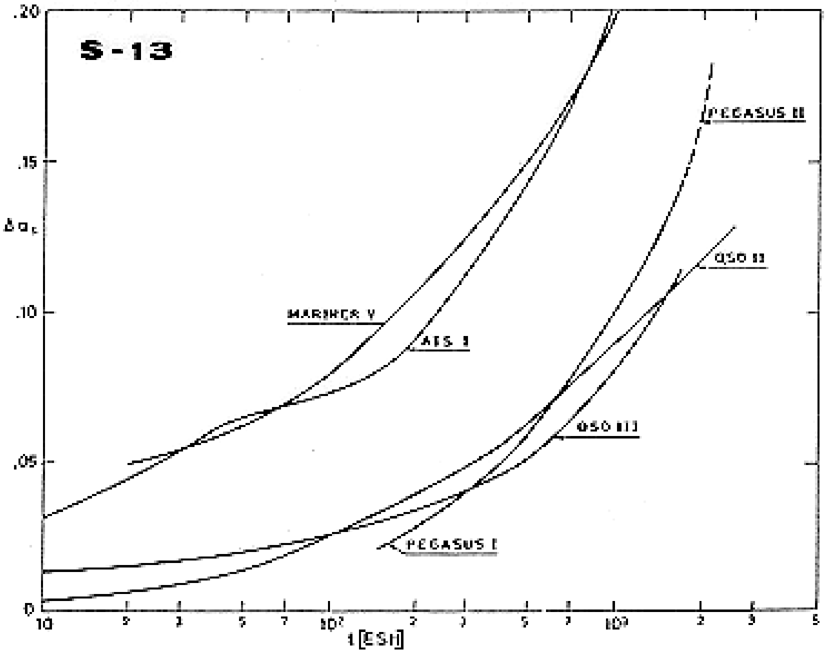

Note: non-si units are used in this figure

Figure 5-24: Change in solar absorptance, $\Delta\alpha_s$, of S-13 coatings vs. flight time in ESH as measured in orbital flight. Prepared by the compiler after Touloukian, DeWitt & Hernicz (1972) [126].

Explanation

Satellite	Orbit Altitude [km]	Inclination [deg]	Duration of Data Acquisition [mo]
OSO II	550-630	33	16
OSO III	540-560	33	< 1
Pegasus I	500-740	32	< 26
Pegasus II	510-750	32	< 23
ATS I	35-790	0	< 4
Mariner V	Deep Space Venus probe	-	-

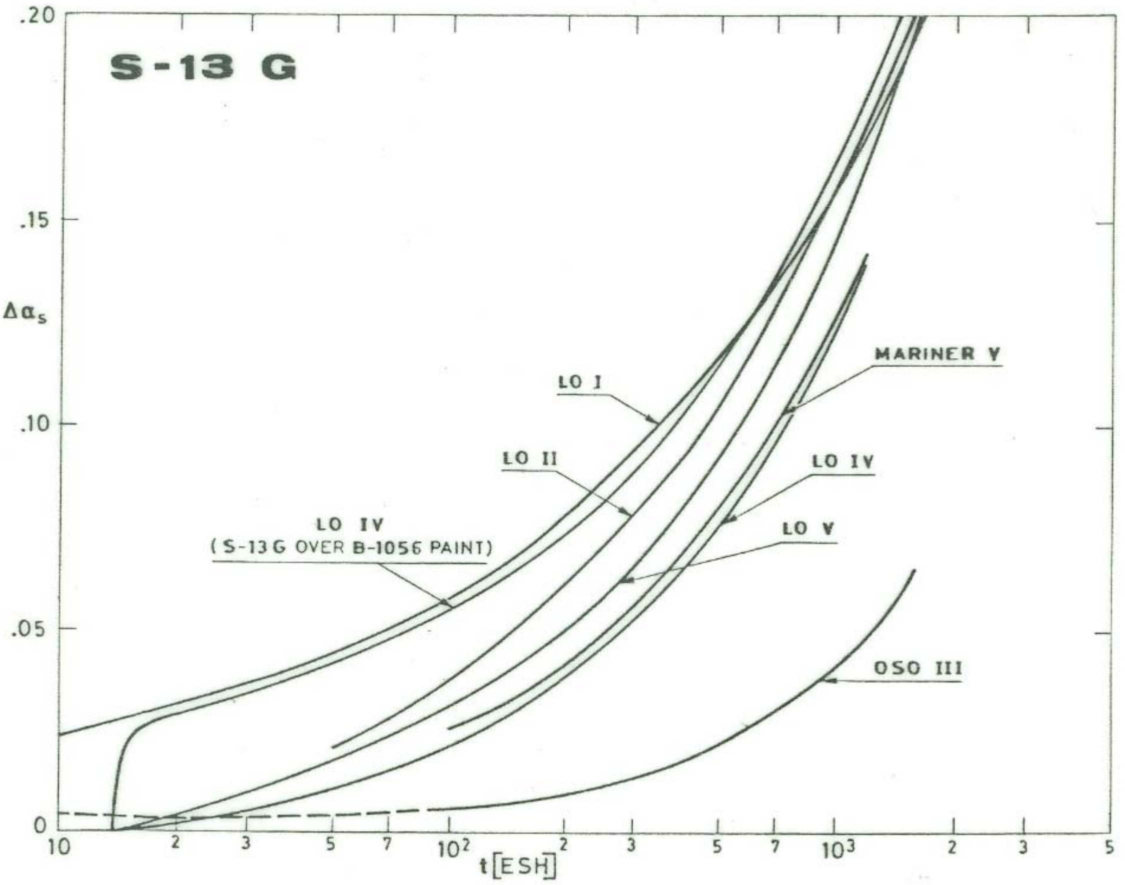

Note: non-si units are used in this figure

Figure 5-25: Change in solar absorptance, $\Delta\alpha_s$, of S-13 G coating vs. flight time in ESH as measured in orbital flight. Prepared by the compiler after Touloukian, DeWitt & Hernicz (1972) [126].

Explanation

Satellite	Orbit Altitude [km]	Inclination [deg]	Duration of Data Acquisition [mo]
OSO III	540-560	33	< 1
Mariner V	Deep Space Venus Probe	-	-
Lunar Orbiter I			
Lunar Orbiter II	-	-	-
Lunar Orbiter IV			
Lunar Orbiter V			

More recent experimental data on S-13 G, plasma annealed and potassium silicate treated binder, are given in the table below. Measurements have been performed in situ. Spectral reflectance curves and additional information are given in Figure 5-49. Experimental data for S-13 G/LO on Al substrate are summarized in Table 5-13, after DERTS.

Exposure	$\Delta\alpha_s$
600 ESH + 668 EWH	0,044
Above plus 700 ESH	0,065
Above plus O_2 bleaching	0,032

Table 5-13: Combined Exposure Effects on Solar Absorptance of S-13 G/LO Coating

Test Conditions	Sample 1						Sample 2					
	Measured in situ			Corrected [a]			Measured in situ			Corrected [a]		
	α_s	$\Delta\alpha_s$	$\Delta\alpha_s/\alpha_s$	α_s	$\Delta\alpha_s$	$\Delta\alpha_s/\alpha_s$	α_s	$\Delta\alpha_s$	$\Delta\alpha_s/\alpha_s$	α_s	$\Delta\alpha_s$	$\Delta\alpha_s/\alpha_s$
BEFORE IRRADIATION	0,336			0,180			0,343			0,180		
AFTER A UNDER VACUUM [b]	0,456	0,120	0,358	0,329	0,149	0,828	0,471	0,128	0,373	0,339	0,159	0,883
BEFORE B	0,395	0,059	0,176	0,253	0,073	0,406	0,400	0,057	0,167	0,251	0,071	0,394
AFTER B [b]	0,517	0,181	0,539	0,405	0,225	1,250	0,531	0,188	0,547	0,414	0,234	1,300
AFTER PUMP DAMAGE [c]	0,384	0,049	0,146	0,241	0,061	0,339	0,391	0,048	0,139	0,240	0,060	0,333
BEFORE C	0,419	0,083	0,248	0,283	0,103	0,572	0,423	0,080	0,233	0,279	0,099	0,550
AFTER C [b]	0,537	0,201	0,600	0,430	0,250	1,388	0,545	0,202	0,589	0,413	0,251	1,394
BEFORE D	0,513	0,177	0,528	0,400	0,220	1,222	0,519	0,176	0,514	0,399	0,219	1,217
AFTER D UNDER VACUUM [b]	0,594	0,258	0,770	0,501	0,321	1,783	0,599	0,256	0,746	0,498	0,318	1,767
AFTER D AND AIR EXPOSURE	0,530	0,194	0,577	0,421	0,241	1,339	0,541	0,198	0,577	0,426	0,246	1,367

[a] The correction has been made by the compiler as follows:

1) Value before irradiation, $\alpha_{so} = 0{,}18$

2) $\Delta\alpha_{s\ corrected}/\Delta\alpha_{s\ in\ situ} = (1-\alpha_{so})/(1-\alpha_{so\ in\ situ}) = 0{,}82/0{,}66$

where α_{so} has been measured (in air) with an integrating sphere attached to a Beckman DK2A reflectometer. $\alpha_{so\ in\ situ}$ is the value measured, before irradiation, as indicated in 7.3.3.2.3.

[b] Steps A to D correspond, respectively, to the following times in geosynchronous orbit.

A: 0,18 yr = 508 ESH

B: 0,94 yr = 2443 ESH

C: 2,11 yr = 5604 ESH

D: 3 yr = 7949 ESH

[c] See 7.3.3.2.6 for further details.

NOTE From Paillous (1976) [96].

Now the initial value of the solar absorptance is $\alpha_{so} = 0,18$.

The tests simulate geosynchronous orbit exposure of the OTS equatorial faces. See ECSS-E-HB-31-01 Part 15, clause 5.

Solar absorptance deduced from spectral reflectance (see Figure 5-50 to Figure 5-52).

Two samples (here labeled Sample 1 and Sample 2) were tested among several others. Figure 5-26 shows the location of the different samples during the irradiation.

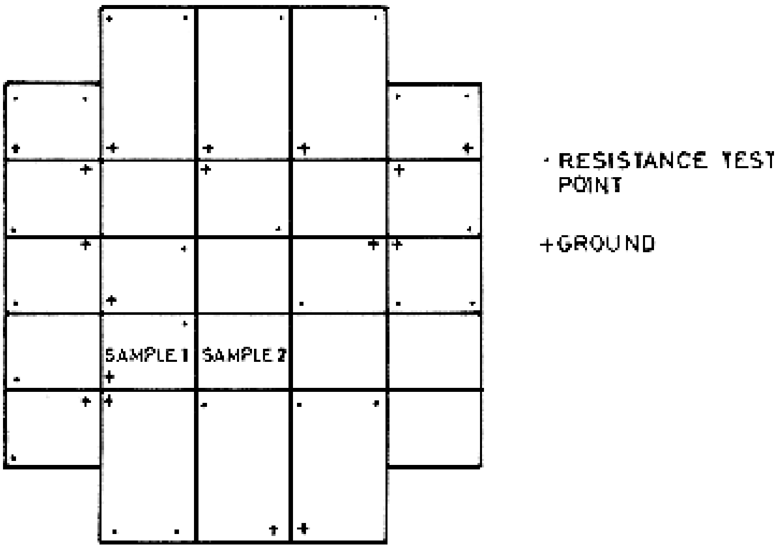

Figure 5-26: Position on the sample holder of the samples 1 and 2, for irradiation and measurement. From Paillous (1976) [96].

Test conditions are the same as in Table 5-19, paragraph 7.3.3.2.6 of clause 5.2.4. Irradiation and measurement procedures are explained in paragraph 7.3.3.2.6 of clause 5.2.4.

The "Corrected" values in Table 5-13 were used to estimate the degradation of the coating up to 3 years in orbit. Results are represented in Figure 5-27. Incidents during testing, see paragraph 7.3.3.2.6 of clause 5.2.4, could cast some doubts on the validity of the data beyond 1 year in orbit. Nevertheless, the comparison with OTS measurements, up to three years, is excellent, as can be seen in the figure.

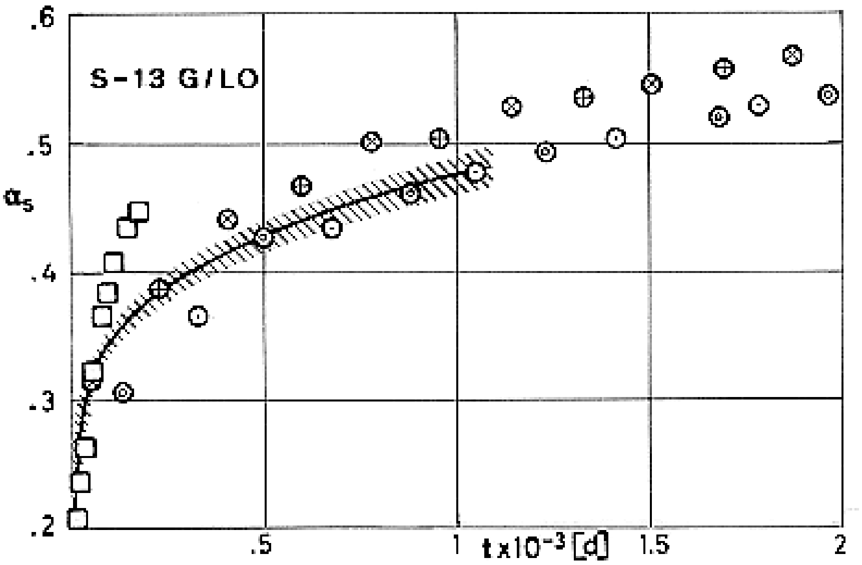

Note: non-si units are used in this figure

Figure 5-27: Solar absorptance, α_s, of S-13 G/LO coating vs. flight time,

t. White circle: OTS, see ECSS-E-HB-31-01 Part 15, clause 5.10. Cross in circle: SS; Plus in circle: WS; Point in circle: VE; Circle in circle: AE
From Chalmers, Konzok, Bouchez & Howle (1983) [29].
Shadowed line: Prediction, up to three years in orbit by Paillous (1976) [96]. See Table 5-13, above.
White square: Navstar 6
From Pence & Grant (1981) [99].
OTS was launched in May 11, 1978 in a geostationary orbit 35779 km- 35072 km. Navstar 6 was launched in April 26, 1980. Orbit altitude 170 km - 20288 km. Inclination 63,02°. The reasons for the severe degradation of the coatings tested onboard Navstar series are unclear. See paragraph 7.3.2.5.6 in clause 5.2.6 and paragraph 7.3.2.5.1 of clause 5.2.3.

Data in Figure 5-27 are recent in orbit measurements. They correspond to OTS and Navstar 6, respectively. The coating is S-13 G/LO.

7.3.2.6. Effects of the Space Environment on solar absorptance to emittance ratio. Results from several flight experiments are given in Figure 5-28 and Figure 5-29.

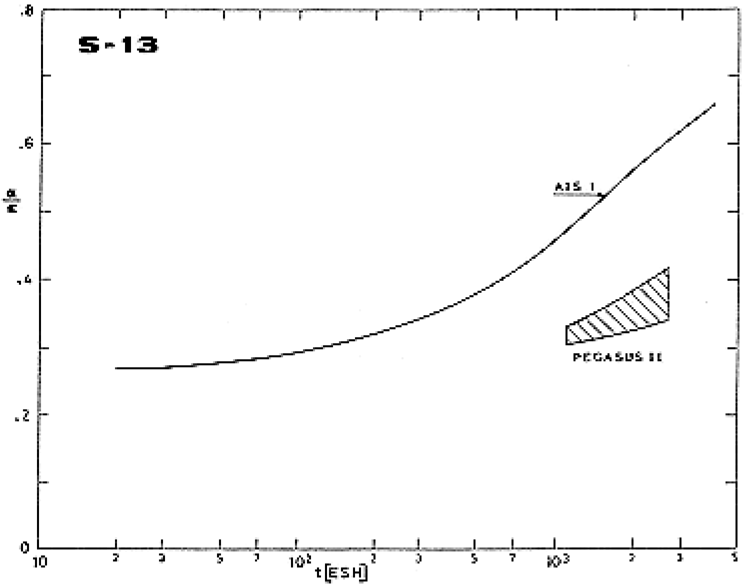

Note: non-si units are used in this figure

Figure 5-28: Variation of absorptance to emittance ratio, *α/ε*, of S-13 coating vs. flight time. Prepared by the compiler after Touloukian, DeWitt & Hernicz (1972) and Triolo (1973) [126]

Explanation

Satellite	Orbit Altitude [km]	Inclination [deg]	Duration of Data Acquisition [mo]
Pegasus II	510-570	32	< 23
ATS I	35790	0	< 36

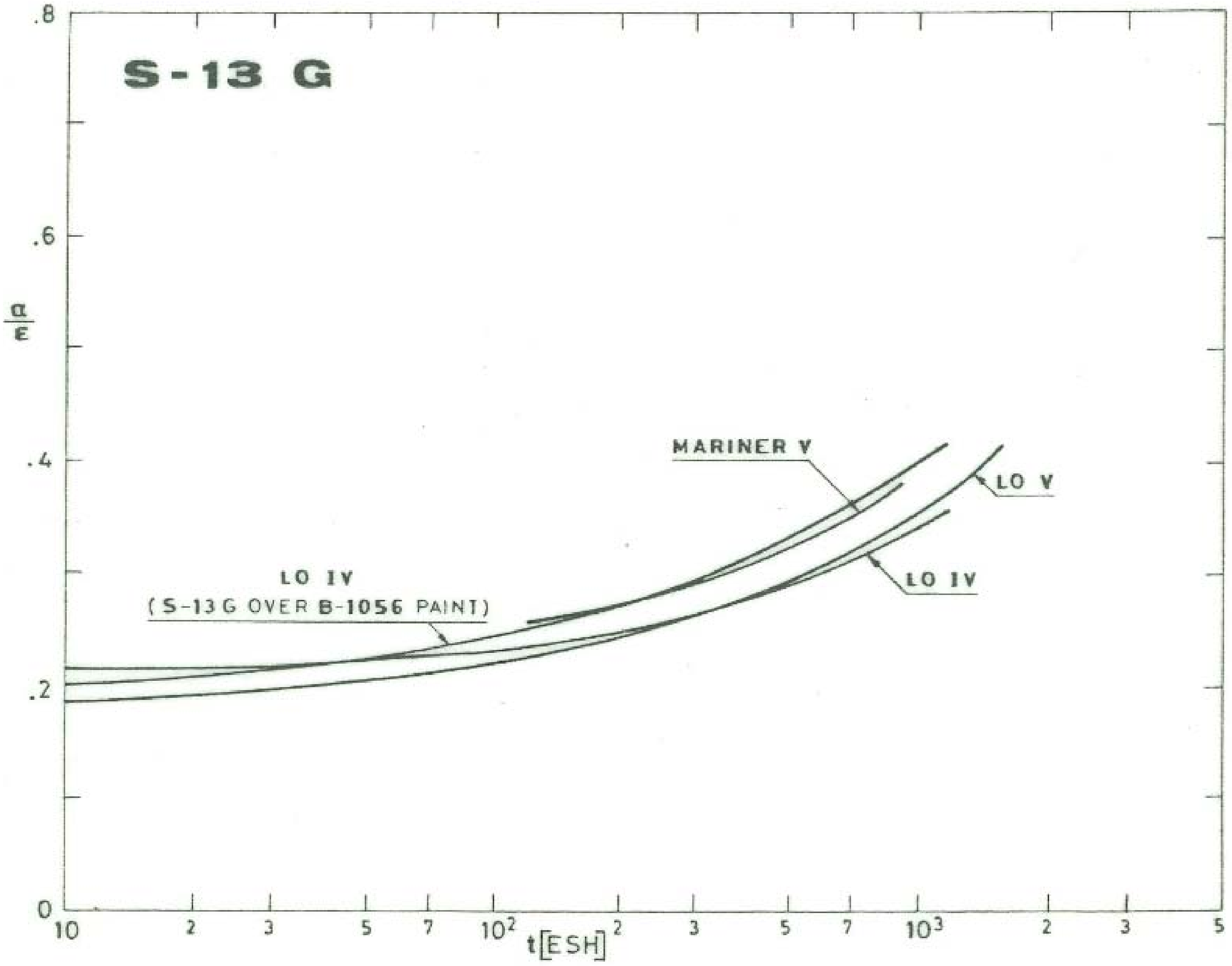

Note: non-si units are used in this figure

Figure 5-29: Variation of absorptance to emittance ratio, α/ε, of S-13 G coating vs. flight time. Prepared by the compiler after Touloukian, DeWitt & Hernicz (1972) [126].

Explanation

Satellite	Orbit Altitude [km]	Inclination [deg]	Duration of Data Acquisition [mo]
Mariner V	Deep Space Venus Probe		
Lunar Orbiter IV			
Lunar Orbiter V			

7.3.3. Reflectance.

7.3.3.1. Normal-hemispherical spectral reflectance. The available information regarding slightly different coating preparations is abundant. As an example Figure 5-30 shows the influence of pigment volume concentration (P-VC) on spectral reflectance.

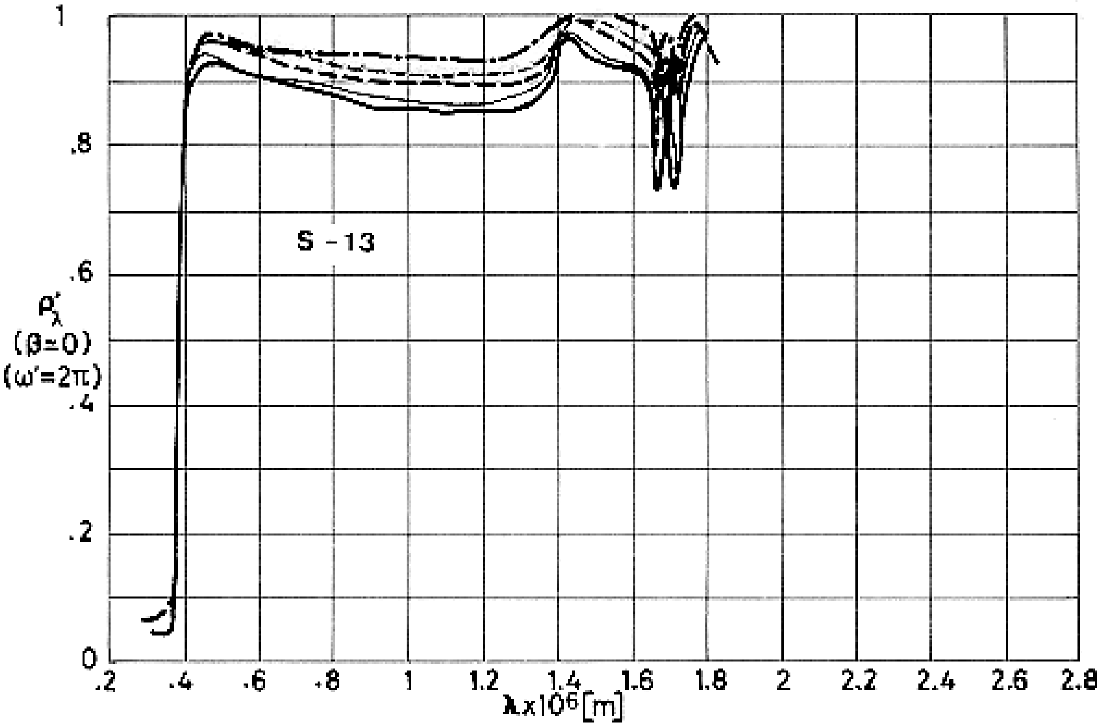

Note: non-si units are used in this figure

Figure 5-30: Normal-hemispherical spectral reflectance, ρ'_λ, of S-13 coating vs. wavelength, l, for five different values of P-VC. G.E. LTV-602 binder. From Touloukian, DeWitt & Hernicz (1972) [126].

Explanation

Key	P-VC	Comments
▬▬▬	15	0,17 x 10^{-3} m thick 6061 Al substrate. T ≈ 298 K. Measured relative to magnesium carbonate. P-VC is the pigment volume concentration, percent.
―――	20	
▬ ▬	25	
— —	35	
▬•▬	40	

7.3.3.2. Effects of the Space Environment on reflectance

7.3.3.2.1. Ultra-Violet Radiation. We will mention two points:

1st. Stability of these coatings to UV radiation strongly depends on their composition. The optimum composition has been obtained after a lengthy process and data exist to evaluate the sensibility of the coatings to small changes in composition.

2nd. Ex situ vs. in situ measurements. Up to 1965, the standard practice for space simulation was to irradiate the coatings with UV under vacuum, performing the measurements ex situ. Since a recovery exists after breaking vacuum, early flight tests showed an extreme degradation not foreseen at the light of the space simulation tests.

Figure 5-31 and Figure 5-32 show the influence of pigment-binder ratio (PBR) on the stability against UV radiation. Data after irradiation have been obtained from ex situ measurements.

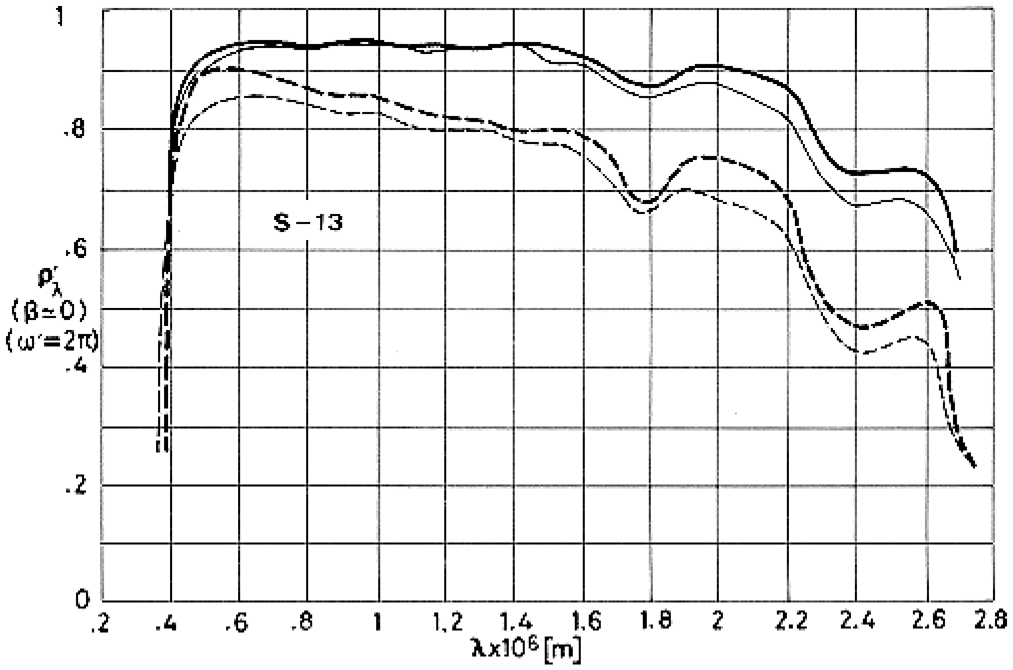

Note: non-si units are used in this figure

Figure 5-31: Effect of Ultra-violet Radiation on normal-hemispherical spectral reflectance, ρ'_λ, of S-13 coating vs. wavelength, λ. LTV-602 silicone binder. Two different pigment-binder ratios (PBR). From Touloukian, DeWitt & Hernicz (1972) [126].

Explanation

Key	PBR	P-VC	Exposure	Comments
▬	3,73	40	In vacuum before irradiation	Sample on Al substrate. Airbrush application. T ≈ 298 K. Exposed in

━━━			UV. 1200 ESH	vacuum p ≈ 1,33 x 10^{-3} Pa. Measured ex-situ.
▬ ▬	1,40	20	In vacuum before irradiation	Above specimen and conditions except Catalyst G.E. SRC-04 and toluene as solvent.
— —			UV. 1460 ESH	

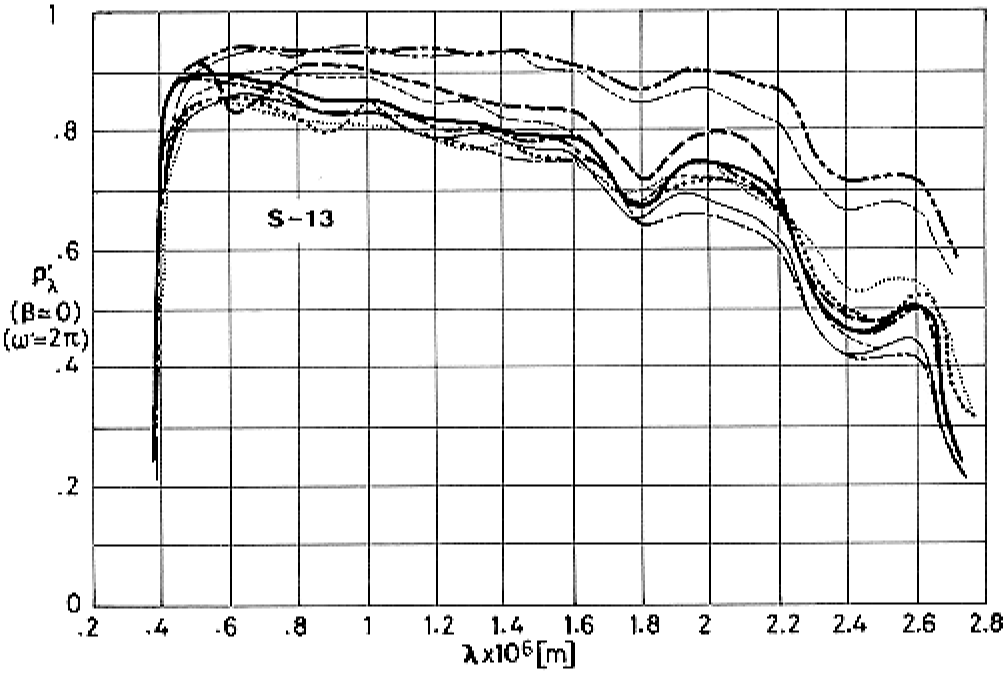

Note: non-si units are used in this figure

Figure 5-32: Effect of Ultra-Violet Radiation on normal-hemispherical spectral reflectance, ρ'_λ, of S-13 coating vs. wavelength, λ. Several binders and PBRs. From Touloukian, DeWitt & Hernicz (1972) [126].

Explanation

Key	Blinder	Me-Si Ratio	PBR	P-VC	Exposure	Comments
━━━	LTV-602		1,40	20	In vacuum before irradiation	Catalyst, G.E. SRC-04; solvent, toluene. Sample on Al substrate. Airbrish application. T ≈ 298 K. Exposed in vacuum
───					UV. 1460 ESH	
▬ ▬	R-2	1,46	1,70	25	In vacuum before irradiation	

— —					UV. 1460 ESH	$p \approx 1{,}33 \times 10^{-5}$ Pa. Measured ex-situ.
▬•▬	R-5	1,38	1,63	25	In vacuum before irradiation	
—·—					UV. 1460 ESH	
••••••••	R-7	1,33	1,64	25	In vacuum before irradiation	
....					UV. 1600 ESH	
▬••▬	LTV-602		3,73	40	In vacuum before irradiation	
—··—					UV. 1200 ESH	

Figure 5-33 and Figure 5-34, on the other hand, compare in situ with ex situ measurements.

Figure 5-34,indicates that S-13 exhibits a reflectance decrease of about 35% at $\lambda = 2 \times 10^{-6}$ m after approximately 800 ESH of UV radiation in vacuum and an almost instantaneous increase when the irradiated specimen is admitted to the atmosphere.

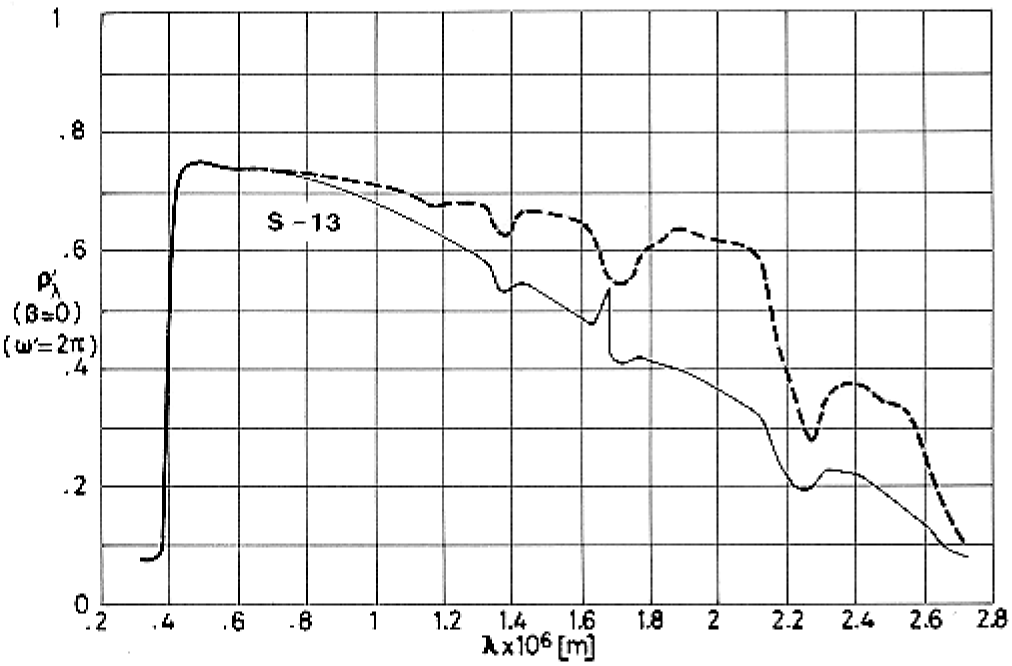

Note: non-si units are used in this figure

Figure 5-33: Effect of Ultra-Violet Radiation on normal-hemispherical spectral reflectance, ρ'_λ, of S-13 coating vs. wavelength, λ. From Touloukian, DeWitt & Hernicz (1972) [126].

Explanation

Key	Exposure	Comments
▬▬▬	In vacuum before irradiation	T ≈ 298 K. Measured and exposed in situ.
———	UV. 1200 ESH	
▬ ▬	Above after breaking vacuum	Recovery is complete

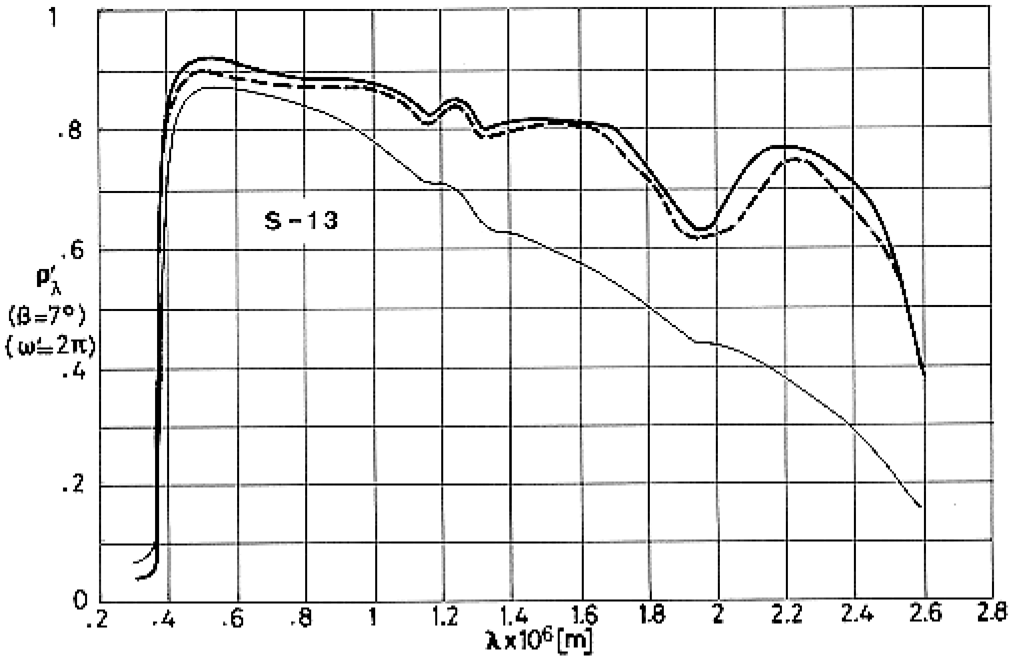

Note: non-si units are used in this figure

Figure 5-34: Effect of Ultra-Violet Radiation on normal-hemispherical spectral reflectance, ρ'_λ, of S-13 coating vs. wavelength, λ. From Zerlaut, Rogers & Noble (1969) [144]. Drawn from Touloukian, DeWitt & Hernicz (1972) [126].

Explanation

Key	Exposure	Comments
▬▬▬	In vacuum before irradiation	T ≈ 298 K. p ≈ 1,33 x 10^{-5} Pa. Measured and exposed in situ. UV source G.E. AH-6 lamp. IITRI test facility (In situ Reflectometer Irradiation Facility, see Zerlaut & Courtney (1967) [140]). α_s and $\Delta\alpha_s$ in Table 5-12
———	UV. 800 ESH	
▬ ▬	Above after breaking vacuum	

Figure 5-35 to Figure 5-40 present data taken when optimizing the composition of S-13 G.

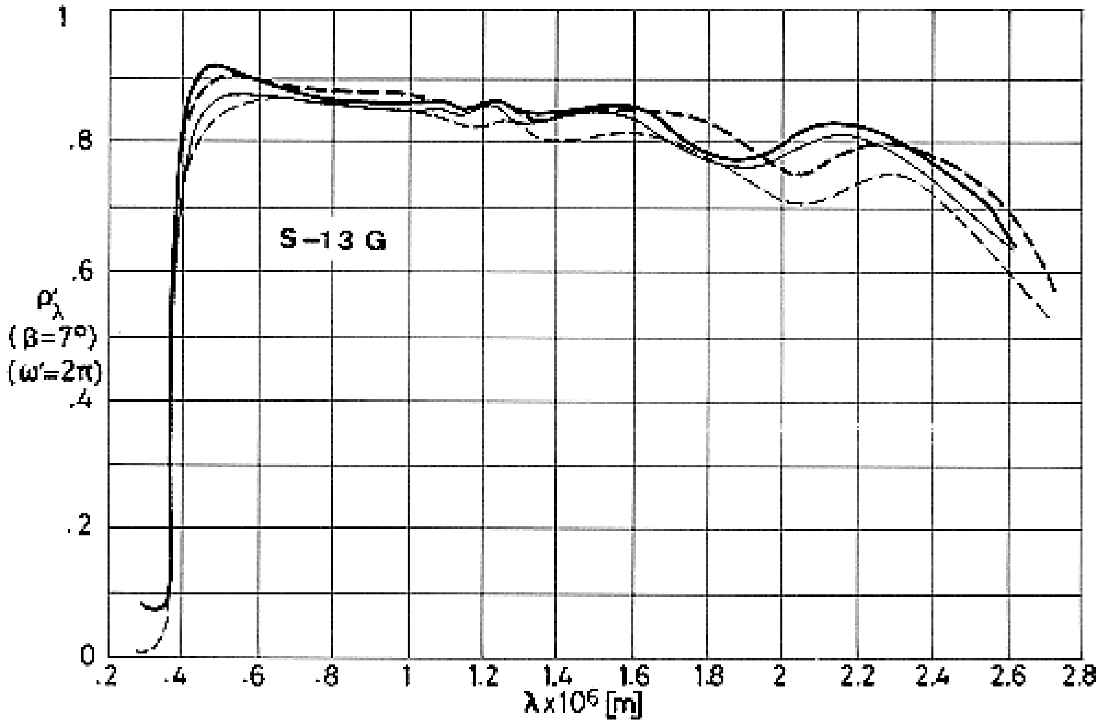

Note: non-si units are used in this figure

Figure 5-35: Effect of Ultra-Violet Radiation on normal-hemispherical spectral reflectance, ρ'_λ, of S-13 G coating vs. wavelength, λ. Two different pigment treatment processes. From Zerlaut, Rogers & Noble (1969) [144]. Drawn from Touloukian, DeWitt & Hernicz (1972) [126].

Explanation

Key	Pigment Treatment	Exposure	Comments
━━━	16 h. sweating. Solvent toluene	In vacuum before irradiation	T ≈ 298 K. p ≈ 1,33 x 10^{-5} Pa. Measured and exposed in situ. UV source G.E. AH-6 lamp. IITRI test facility (In situ Reflectometer Irradiation Facility, see Zerlaut & Courtney (1967) [140]). α_s and $\Delta\alpha_s$ in Table 5-12
───		UV. 600 ESH	
━ ━	Sweating, calcining for 16 h at 293 K	In vacuum before irradiation	
─ ─		UV. 600 ESH	

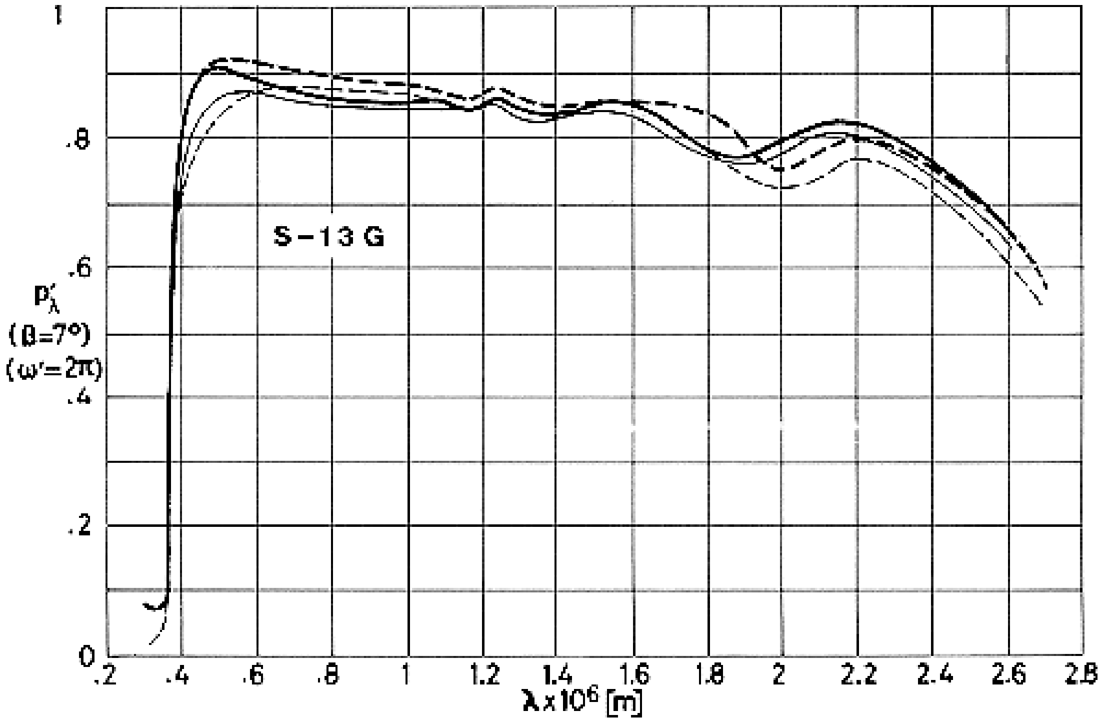

Note: non-si units are used in this figure

Figure 5-36: Effect of Ultra-Violet Radiation on normal-hemispherical spectral reflectance, ρ'_λ, of S-13 G coating vs. wavelength, λ. Sweated pigment. Two different solvent systems. From Zerlaut, Rogers & Noble (1969) [144]. Drawn from Touloukian, DeWitt & Hernicz (1972) [126].

Explanation

Key	Solvent	Exposure	Comments
▬▬▬	Toluene	In vacuum before irradiation	T ≈ 298 K. p ≈ 1,33 x 10^{-5} Pa. Measured and exposed in situ. UV source G.E. AH-6 lamp. IITRI test facility (In situ Reflectometer Irradiation Facility, see Zerlaut & Courtney (1967) [140]). α_s and $\Delta\alpha_s$ in Table 5-12.
———		UV. 600 ESH	
▬ ▬	Toluene and petroleum ether	In vacuum before irradiation	
— —		UV. 800 ESH	

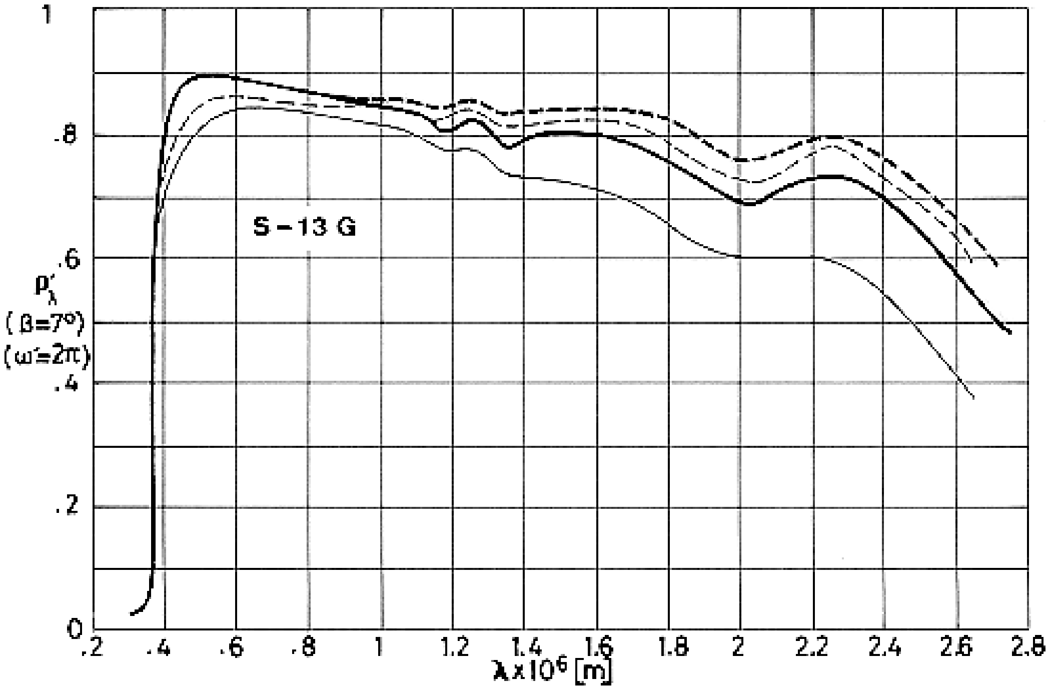

Note: non-si units are used in this figure

Figure 5-37: Effect of Ultra-Violet Radiation on normal-hemispherical spectral reflectance, ρ'_λ, of S-13 G coating vs. wavelength, λ. Two different pigment treatment processes. Owens-Illinois 650 binder. From Zerlaut, Rogers & Noble (1969) [144]. Drawn from Touloukian, DeWitt & Hernicz (1972) [126].

Explanation

Key	Pigment Treatment	Exposure	Comments
▬▬▬	Sweated, neutralized with formic acid and calcined for 16 h at 932 K.	In vacuum before irradiation	T ≈ 298 K. p ≈ 1,33 x 10^{-5} Pa. Measured and exposed in situ. UV source G.E. AH-6 lamp. IITRI test facility (In situ Reflectometer Irradiation Facility, see Zerlaut & Courtney (1967) [140]). α_s and $\Delta\alpha_s$ in Table 5-12.
———		UV. 600 ESH	
▬ ▬	Sweated, neutralized with sodium acid phosphate and calcined for 16 h at 923 K.	In vacuum before irradiation	
— —		UV. 600 ESH	

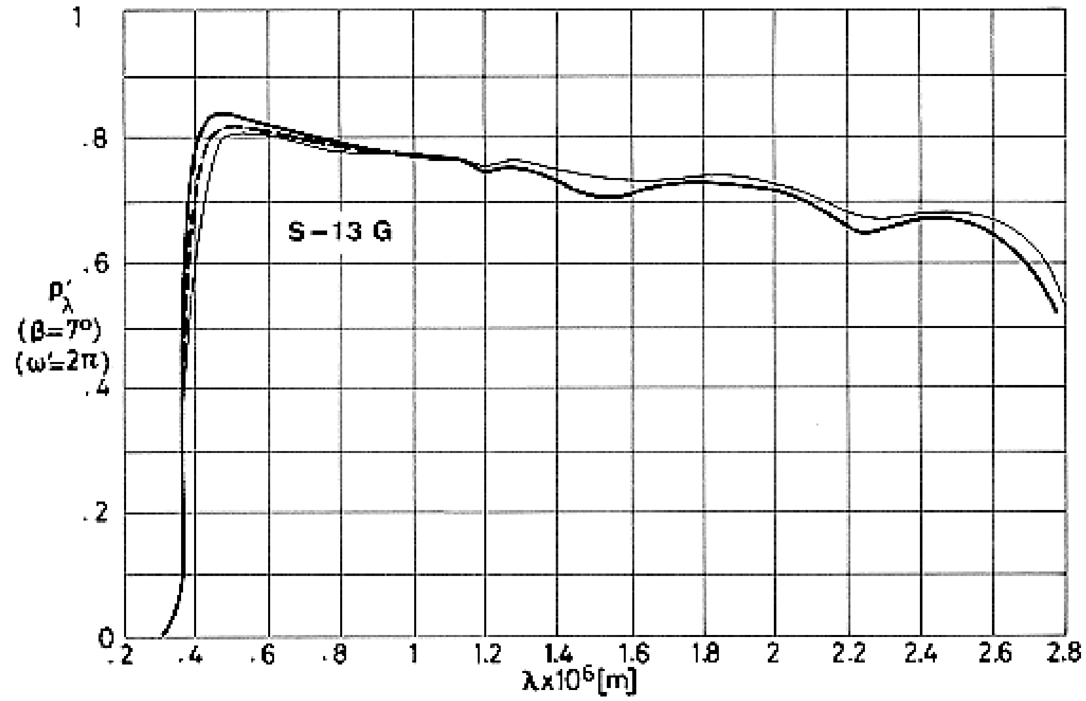

Note: non-si units are used in this figure

Figure 5-38: Effect of Ultra-Violet Radiation on normal-hemispherical spectral reflectance, ρ'_λ, of S-13 G coating vs. wavelength, λ. Pigment was sifted prior to wet grinding. Paint grind time 3 h. From Zerlaut, Rogers & Noble (1969) [144]. Drawn from Touloukian, DeWitt & Hernicz (1972) [126].

Explanation

Key	Exposure	Comments
▬▬▬	In vacuum before irradiation	T ≈ 298 K. p ≈ 1,33 x 10^{-5} Pa. Measured and exposed in situ. UV source G.E. AH-6 lamp. IITRI test facility (In situ Reflectometer Irradiation Facility, see Zerlaut & Courtney (1967) [140]). α_s and $\Delta\alpha_s$ in Table 5-12.
―――	UV. 1400 ESH	
▬ ▬	Above after breaking vacuum	

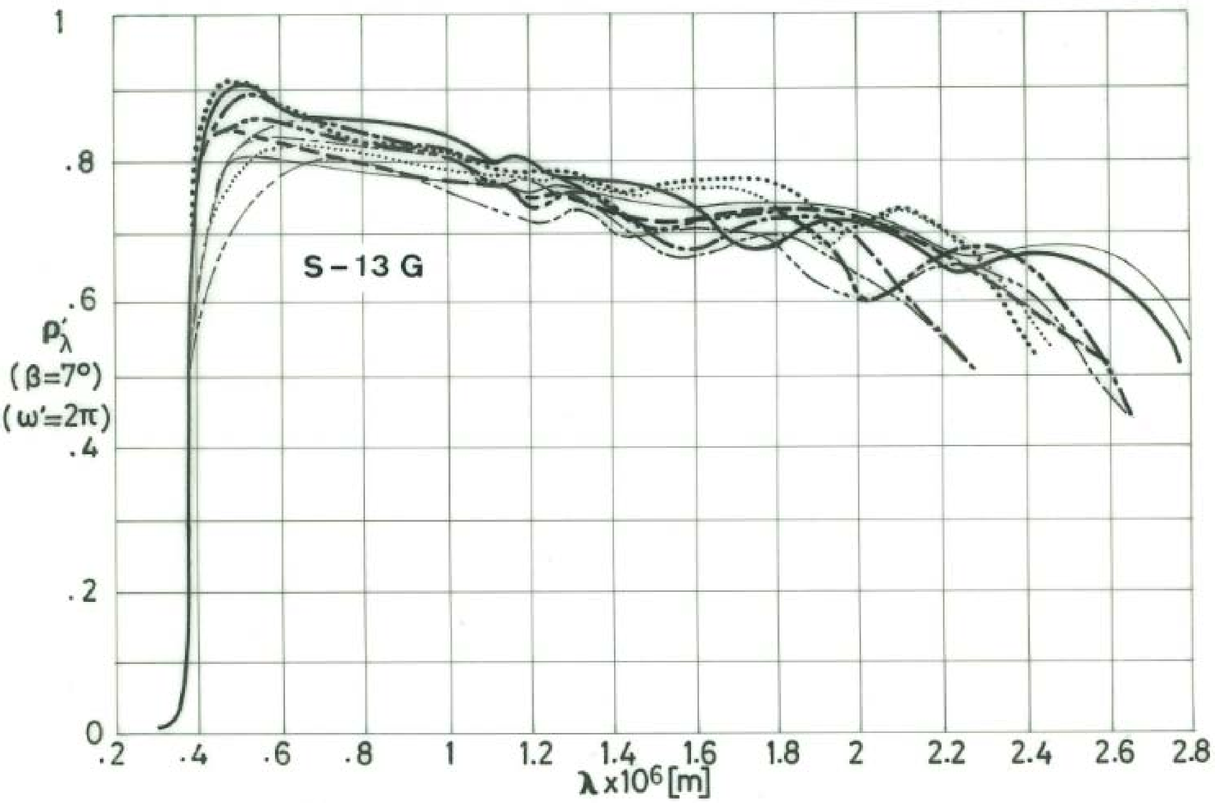

Note: non-si units are used in this figure

Figure 5-39: Effect of Ultra-Violet Radiation on normal-hemispherical spectral reflectance, ρ'_λ, of S-13 G coating vs. wavelength, λ. Silicated pigment with five mechanical perturbations. From Zerlaut, Rogers & Noble (1969) [144]. Drawn from Touloukian, DeWitt & Hernicz (1972) [126].

Explanation

Key	Pigment Mechanical Perturbation	Exposure	Comments
▬▬▬	Shifting prior to wet-grinding. Grind time 3 h	In vacuum before irradiation	T ≈ 298 K. p ≈ 1,33 x 10^{-5} Pa. Measured and exposed in situ. UV source G.E. AH-6 lamp. IITRI test facility (In situ Reflectometer Irradiation Facility,
———		UV. 1400 ESH	
▬ ▬	Unshifted and unground prior to wet-grinding. Grind time 4 h	In vacuum before irradiation	
— —		UV. 1400 ESH	
▬·▬	Dry-ground 30 min. Grind time 3 h	In vacuum before irradiation	
—·—		UV. 1400 ESH	

••••••••	Hand-mulling prior to wet grinding. Grind time 3 h	In vacuum before irradiation	see Zerlaut & Courtney (1967) [140]). α_s and $\Delta\alpha_s$ in Table 5-12
- - - - - - - -		UV. 1400 ESH	
▬••▬	Remulled from first-hand mulling. Grind time 5 h	In vacuum before irradiation	
—··—		UV. 1400 ESH	

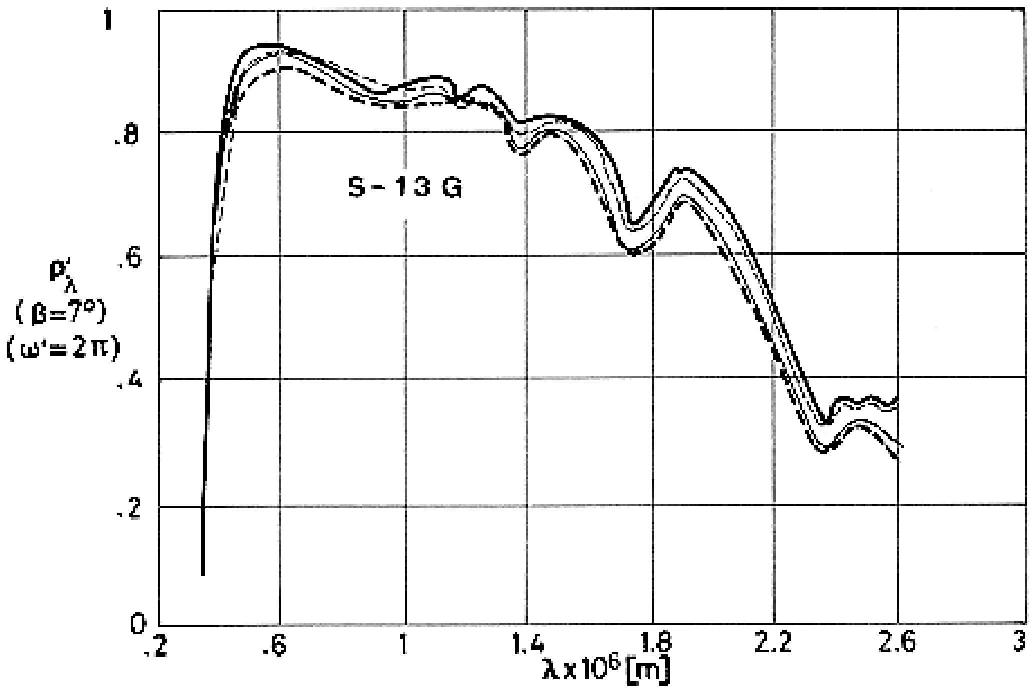

Note: non-si units are used in this figure

Figure 5-40: Effect of Ultra-Violet Radiation on normal-hemispherical spectral reflectance, ρ'_λ, of S-13 G coating vs. wavelength, λ. Plasma annealed and potassium silicate treated pigment. From Gilligan & Zerlaut (1971) [46].

Explanation

Key	Exposure	Comments
▬▬▬	In vacuum before irradiation	T ≈ 285 K. Measured in situ. Initially at 8 x 10^{-6} Pa pressure. Irradiation performed at 1,33 x 10^{-5} Pa. IITRI test facility (Combined Environment Radiation Facility). $\Delta\alpha_s$ in Table 5-12.
———	UV. 600 ESH. First part of exposure.	
▬ ▬	Above plus UV. 700 ESH. Second part of exposure.	
— —	Above plus O_2 bleaching.	

Figure 5-35 compares sweating (see clause 5.2.3.1) versus sweating and calcining. Calcination of the sweated pigment decreases the stability in the infrared. This could be due to the greater grinding required to reduce the calcined pigment which yields ZnO surfaces devoided of barriers to photo desorption. Figure 5-36 shows partial results in the process of solvent optimization. Originally toluene was used as the sole solvent. This resulted in excessive spray dust, in very poor shelf life, and in the production of ""range peel""inRTV-602 films (a pock marked appearance due to film failure to flow out to a level surface).

Films from solutions containing petroleum ether showed inferior stability. Paints prepared from sweated pigment are less sensitive to solvent composition. The optimum composition resulted to be

Toluene	40% by weight
Xilene	20% by weight
n-Butanol	15% by weight
Isopropanol	20% by weight
Butyl acetate	5% by weight

This composition provides: 2 weeks shelf life, good spray flow-out, and good cure characteristics.

Figure 5-37 shows results of two attempts made to neutralize the sweated pigment prior to manufacture. The specimen prepared from the sodium acid phosphate neutralized pigment exhibited the greatest UV stability that has been observed for S-13 G prepared from calcinedpigment. On the other hand, most wavelengths was destroyed by neutralization with formic acid.

Neutralization was required because in this case Owens-Illinois 650 resin was used. This resin is high stable against UV irradiation and can be thermally cured at low temperatures without using catalysts. Unfortunately this causes nearly instantaneous gellation when mixed with silicate-treated zinc oxide. Gelled coatings exhibit a jelly-like condition.

Figure 5-38 and Figure 5-39 show additional effects of different pigment treatment processes. In Figure 5-38 pigment was shifted before wet-grinding, a technique which is no longer used.

Reaction of ZnO with potassium silicate provides an effective barrier to photo desorption reactions on the surface of ZnO which the binder does not.

The idea behind this treatment was put forward in the Z-93 coating (see clause 5.2.2) where the reactivity of ZnO with potassium silicate precluded the bleachable infrared degradation exhibited by ZnO powder and ZnO-silicone coatings.

Figure 5-39 deals with silicate treated pigments under different mechanical processes. The only difference between the different coatings was the manner in which the dried, treated ZnO powder was conditioned for grinding into the paint.

The data show that the stability to UV radiation in vacuum is an inverse function of the shear stress applied to the dry pigment prior to wet-grinding. A fivefold increase in damage, as measured by $\Delta\alpha_s$, was observed between the paint prepared from only shifted pigment and the hand-mulled prior to wet-grinding specimen (recall comment regarding Figure 5-35). Hand-mulling is no longer used after these studies.

Shifting out the millable pigment is a highly inefficient and costly technique, even though it permits shorter wet-grinding times and greater stability. At present only wet-grinding is used.

Figure 5-40 corresponds to the state of the art S-13 G coating.

From Zerlaut, Rogers & Noble (1969) [144], Gilligan & Zerlaut (1971) [46].

7.3.3.2.3. Protons only exposure. Figure 5-41 refers to S-13 and Figure 5-42 to S-13 G coating.

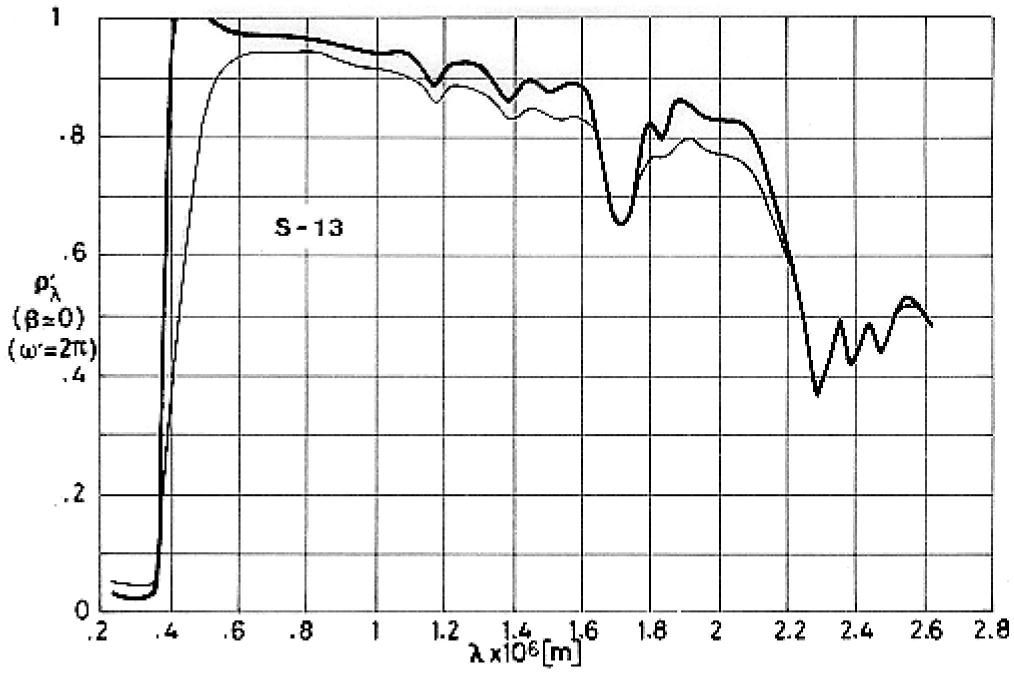

Note: non-si units are used in this figure

Figure 5-41: Protons exposure effects on normal-hemispherical spectral reflectance, ρ'_{λ}, of S-13 coating vs. wavelength, λ. LTV-602 silicone binder. From Gillette, Brown, Seiler & Sheldon (1966) [54]. Drawn from Touloukian, DeWitt & Hernicz (1972) [126].

Explanation

Key	Exposure	Comments
▬	In vacuum before irradiation	Sprayed on aluminium substrate. T = 300 K. Measured in air, exposed in vacuum (1,33 x 10^{-4} Pa). Measurement relative to MgO. Boeing low-energy particle accelerator.
—	Protons. 8,2 keV, 6,1 x 10^{19} p.m^{-2}, integrated flux. In air 20 h – 40 h after irradiation.	

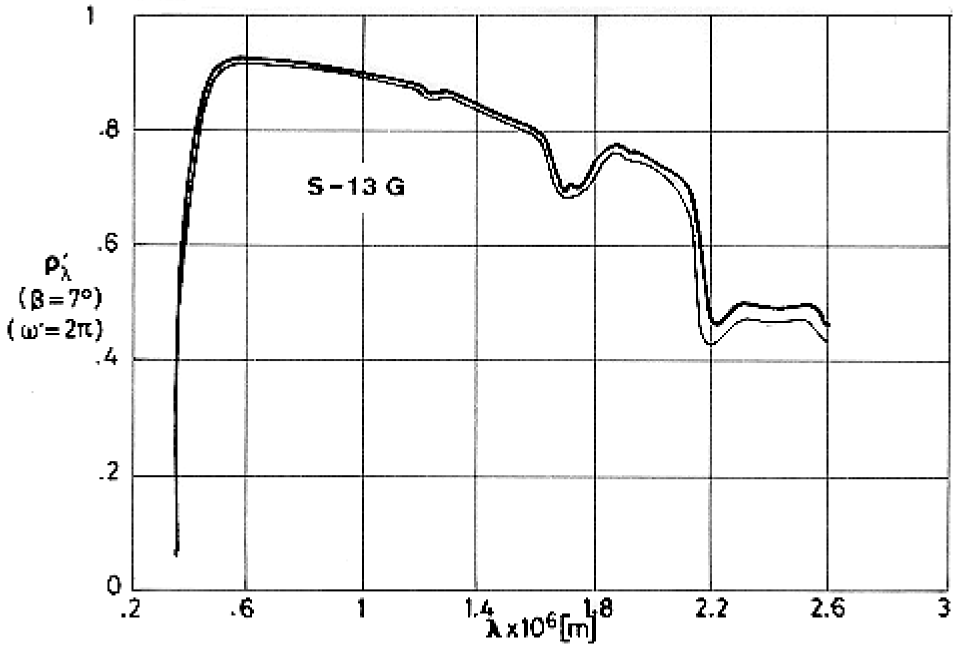

Note: non-si units are used in this figure

Figure 5-42: Protons exposure effects on normal-hemispherical spectral reflectance, ρ'_λ, of S-13 G coating vs. wavelength, λ. Plasma annealed and potassium silicate treated pigment. From Gilligan & Zerlaut (1971) [46].

Explanation

Key	Exposure	Comments
━━━	In vacuum before irradiation	T ≈ 285 K. Measured in situ. Initially at 8 x 10^{-6} Pa pressure. Irradiation performed at 1,33 x 10^{-5} Pa. IITRI facility (In situ Reflectance Irradiation Facility - IRIF).
───	Protons. 1,2 keV, 4,9 x 10^{13} p.m^{-2}.s^{-1} flux. 2,5 x 10^{19} p.m^{-2} integrated flux.	

Unfortunately both the exposure conditions and the measuring method widely differ in either case. In Figure 5-41 an Earth to Mars Mission has been simulated whereas Figure 5-42 seems to represent the conditions of a high altitude (200,000km to 250,000 km) nearly circular orbit.

After exposure data in Figure 5-41, which were taken in the early sixties, were measured in air and those in Figure 5-42, from the seventies, in situ.

Figure 5-40 shows that changes in reflectance include a slight increase in the UV region (λ< 0,35 x 10^{-6} m) a shift in the Ultra-Violet absorption cut off, and a general increase in the infrared wavelength region.

The reflectance of a typical exposed sample was measured at time intervals of 14 h to 2070 h after irradiation. No annealing of damage was observed between reflectance measurements at 14 h and 2 070 h after exposure.

Changes in solar absorptance of similar samples are given in Figure 5-21. From Gillette, Brown, Seiler & Sheldon (1966) [54].

7.3.3.2.4. Electrons only exposure. Figure 5-43 and Figure 5-44 concern S-13 G coating, whereas Figure 5-45 to Figure 5-48 are related to GSFC, 101-7, a similar coating developed by NASA Goddard.

Both coatings exhibit a slow improvement in reflectance with time after exposure, even when the samples remain in the dark in a 1,33 x 10^{-6}Pa vacuum. The mechanisms of recovery are not quite understood. They probably depend on time, temperature, chamber residual atmosphere species, sample composition, radiation particle type, flux and integrated flux. Recovery occurs after exposure whether the impinging particle is stopped in the sample or passes through to its substrate.

Recovery proceeds to a greater extent and at a faster rate after 20 keV exposure than after 80 keV exposure and is probably reduced at improved vacuum conditions. Compared to S-13 G, series 101-7 recovers more slowly and to a smaller fraction of original degradation.

From Fogdall, Cannaday & Brown (1970) [43].

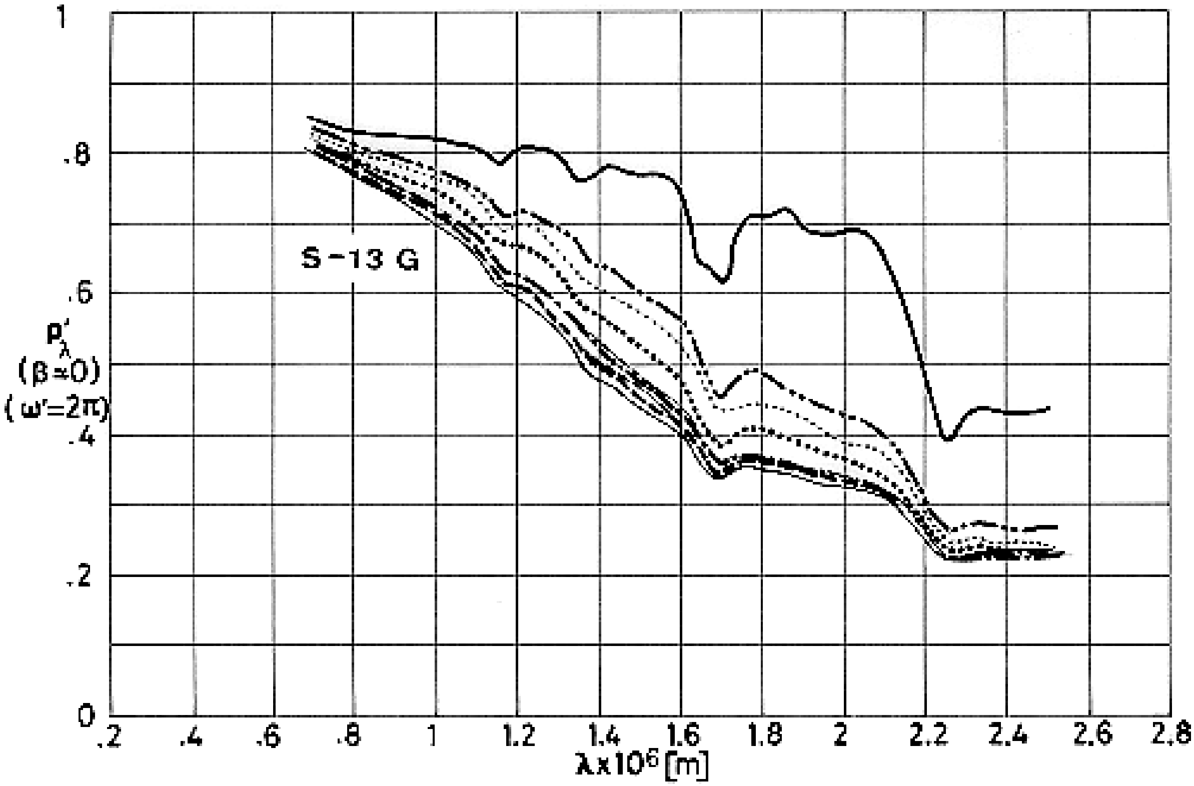

Note: non-si units are used in this figure

Figure 5-43: Electrons exposure effects on normal-hemispherical spectral reflectance, ρ'_λ, of S-13 G coating vs. wavelength, λ. Radiation intensity 20 keV. Recovery after exposure. From Fogdall, Cannaday & Brown (1970) [43]. Drawn from Touloukian, DeWitt & Hernicz (1972) [126].

Explanation

Key	Intensity [keV]	Cumulative Integrated Flux [e.m^{-2}]	Time after Exposure [h]	Comments
━━━━━	In air before irradiation.			Sample on Al substrate. T = 298 K
─────	20	10^{19} (10^{14} to 5 x 10^{15} e.m^{-2}.s^{-1})	0,066	Sample on Al substrate. T = 281 K. 1,33 x 10^{-6} Pa vacuum maintained by ion pump. Measured in situ after exposure. Boeing test facility (Radiation Effects Laboratory) see Brown, Fogdall & Cannaday (1969) [24].
━━ ━━			0,82	
── ──			1,65	
━━·━━			4,12	
──·──			6,92	
••••••••			23,07	
········			53,68	
━━··━━			122,87	

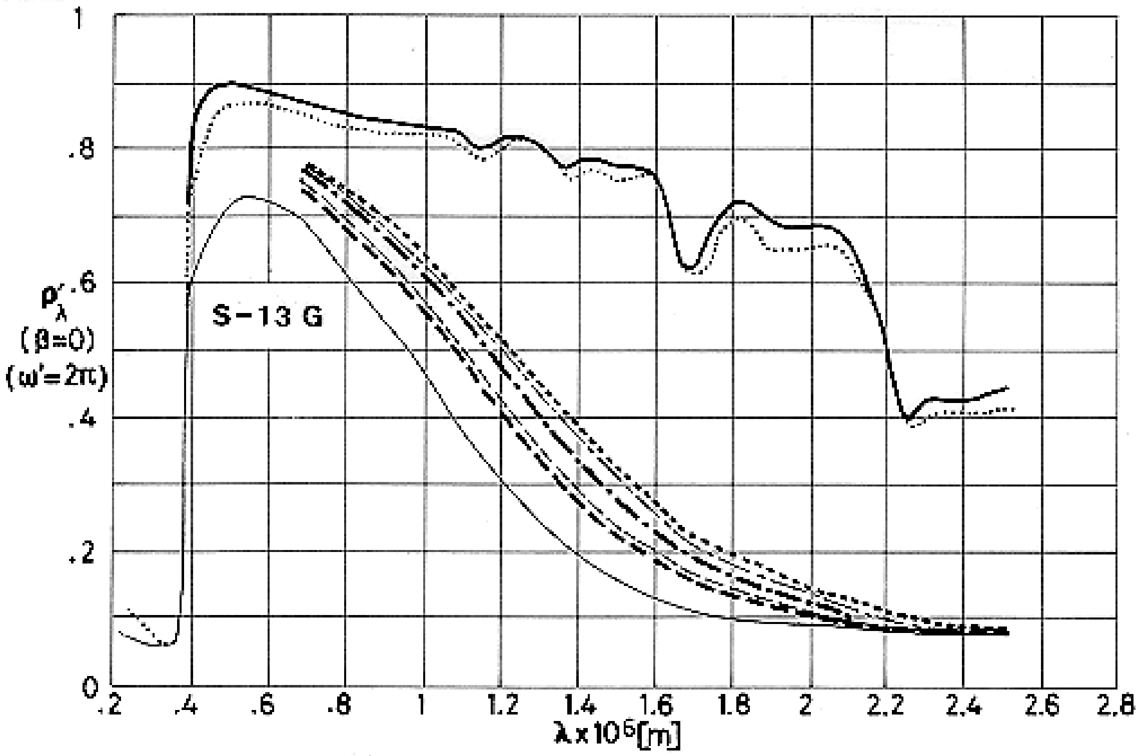

Note: non-si units are used in this figure

Figure 5-44: Electrons exposure effects on normal-hemispherical spectral reflectance, ρ'_λ, of S-13 G coating vs. wavelength, λ. Radiation intensity 80 keV. Recovery after exposure. From Fogdall, Cannaday & Brown (1970) [43]. Drawn from Touloukian, DeWitt & Hernicz (1972) [126].

Explanation

Key	Intensity [keV]	Cumulative Integrated Flux [e.m^{-2}]	Time after Exposure [h]	Comments
━━━	In air before irradiation.			Sample on Al substrate. T = 298 K
───	80	10^{20} (10^{14} to 5 x 10^{15} e.m^{-2}.s^{-1})	0	Sample on Al substrate. T = 281 K. 1,33 x 10^{-6} Pa vacuum maintained by ion pump. Measured in situ after exposure. Boeing test facility (Radiation Effects Laboratory) see Brown, Fogdall & Cannaday (1969) [24].
▬ ▬			48	
— —			72	
▬•▬			96	
—·—			168	
••••••••			432	
········			Measured in air after the above tests had been made. T = 298 K.	

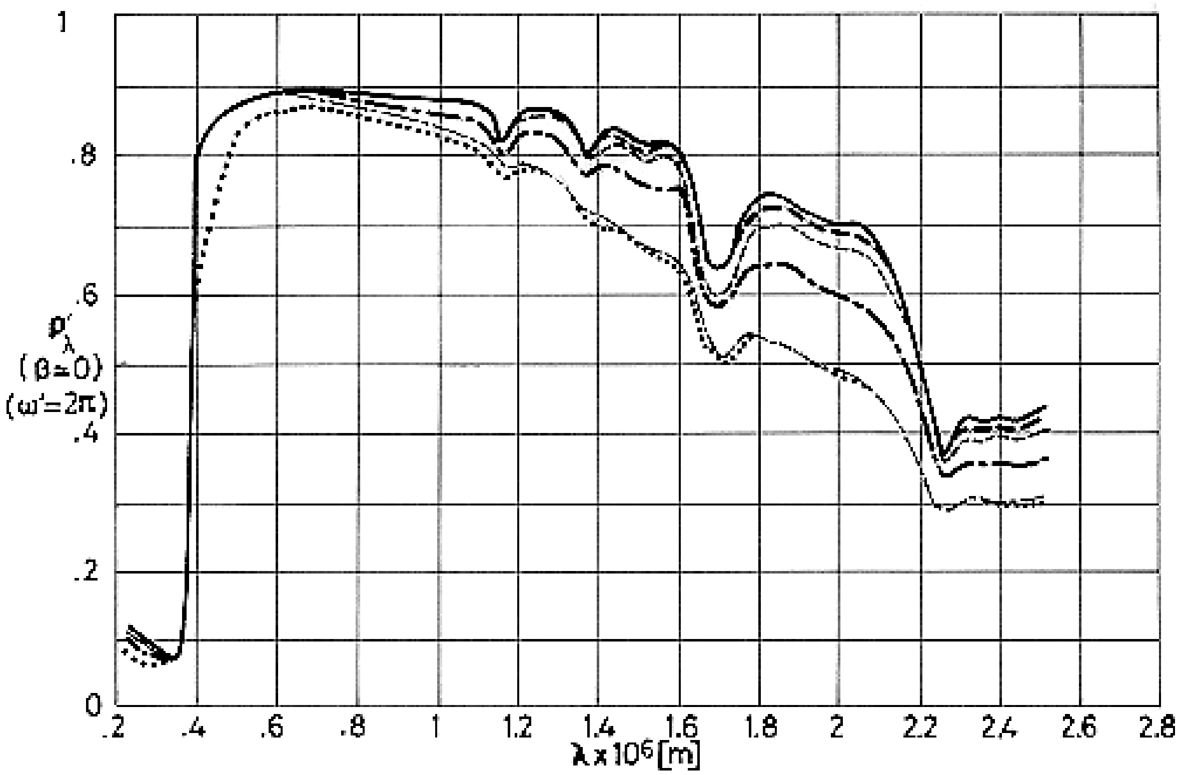

Note: non-si units are used in this figure

Figure 5-45: Electrons exposure effects on normal-hemispherical spectral reflectance, ρ'_{λ}, of GSFC, 101-7 coating vs. wavelength, λ. Radiation intensity 20 keV. Different integrated fluxes. 101-7 is a coating, similar to S-13 G, developed by NASA Goddard. From Fogdall, Cannaday Brown (1970) [43]. Drawn from Touloukian, DeWitt & Hernicz (1972) [126].

Explanation

Key	Intensity [keV]	Flux [e.m^{-2}.s^{-1}]	Cumulative Integrated Flux [e.m^{-2}]	Comments
▬▬▬	In air before irradiation.			Sample on Al substrate. T = 298 K
———	20	10^{14} to 5 x 10^{15}	10^{17}	Sample on Al substrate. T = 281 K. 1,33 x 10^{-6} Pa vacuum maintained by ion pump. Measured in situ after exposure. Boeing test facility (Radiation Effects Laboratory) see Brown, Fogdall & Cannaday (1969) [24]. α_s in paragraph 7.3.2.5.4.
▬ ▬			5 x 10^{17}	
— —			10^{18}	
▬·▬			3 x 10^{18}	
—·—			10^{19}	
••••••••			10^{20}	

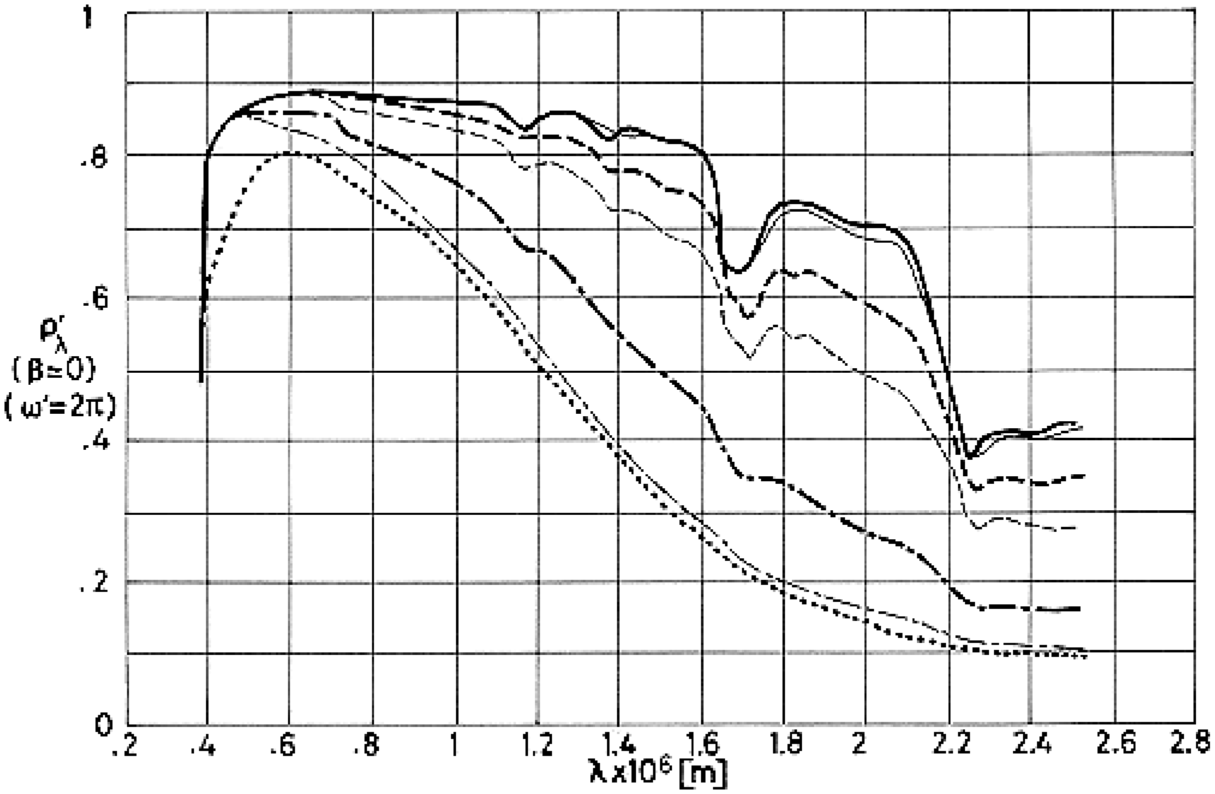

Note: non-si units are used in this figure

Figure 5-46: Electrons exposure effects on normal-hemispherical spectral reflectance, ρ'_λ, of GSFC, 101-7 coating vs. wavelength, λ. Radiation intensity 80 keV. Different integrated fluxes. 101-7 is a coating, similar to S-13 G, developed by NASA Goddard. From Fogdall, Cannaday & Brown (1970) [43]. Drawn from Touloukian, DeWitt & Hernicz (1972) [126].

Explanation

Key	Intensity [keV]	Flux [e.m^{-2}.s^{-1}]	Cumulative Integrated Flux [e.m^{-2}]	Comments
━━━	In air before irradiation.			Sample on Al substrate. T = 298 K
───	80	10^{14} to 5 x 10^{15}	10^{17}	Sample on Al substrate. T = 281 K. 1,33 x 10^{-6} Pa vacuum maintained by ion pump. Measured in situ after exposure. Boeing test facility (Radiation Effects Laboratory) see Brown, Fogdall & Cannaday (1969) [24]. α_s in paragraph 7.3.2.5.4.
▬ ▬			5 x 10^{17}	
— —			10^{18}	
▬·▬			3 x 10^{18}	
—·—			10^{19}	
••••••••			10^{20}	

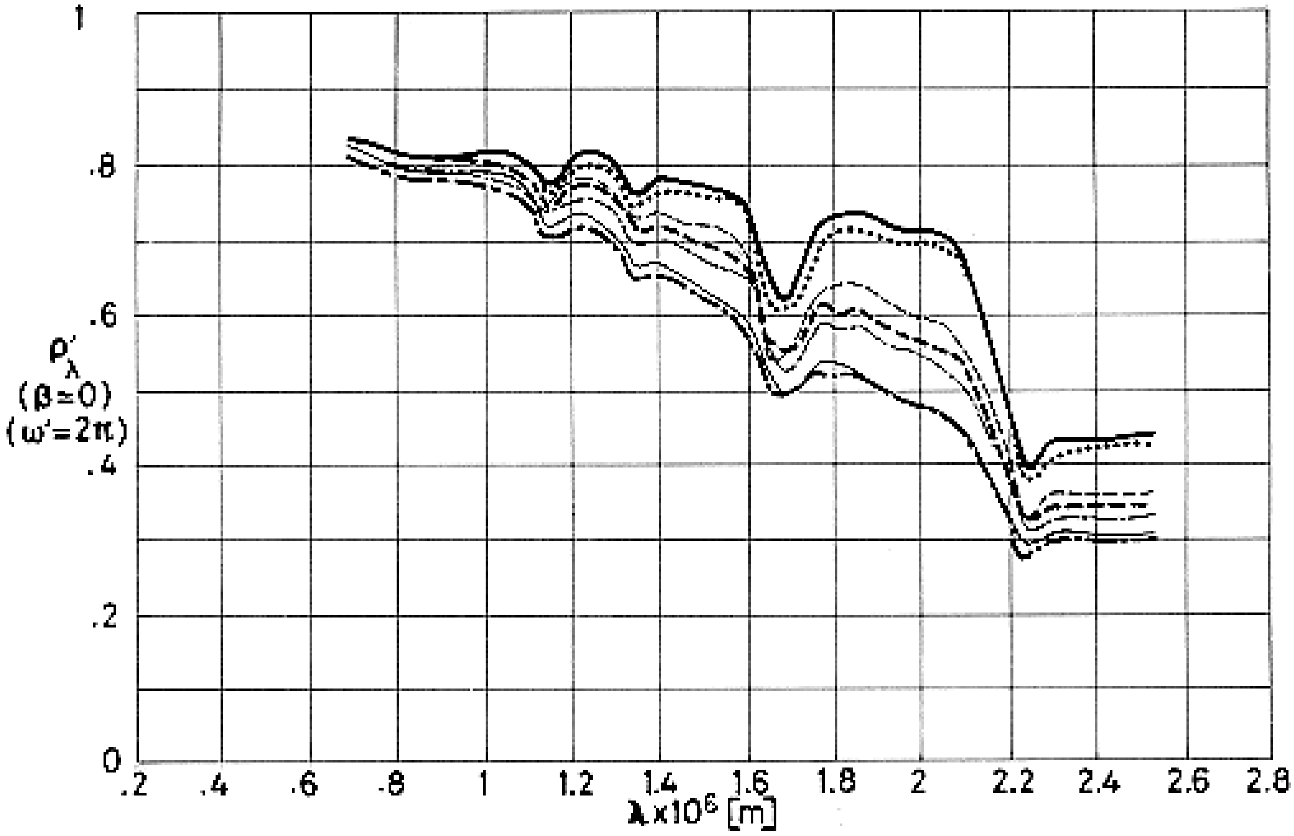

Note: non-si units are used in this figure

Figure 5-47: Electrons exposure effects on normal-hemispherical spectral reflectance, ρ'_λ, of GSFC, 101-7 coating vs. wavelength, λ. Radiation intensity 20 keV. Recovery after exposure. 101-7 is a coating, similar to S-13 G, developed by NASA Goddard. From Fogdall, Cannaday & Brown (1970) [43]. Drawn from Touloukian, DeWitt & Hernicz (1972) [126].

Explanation

Key	Intensity [keV]	Cumulative Integrated Flux [e.m^{-2}]	Time after Exposure [h]	Comments
━━━━	In air before irradiation.			Sample on Al substrate. T = 298 K
────	20	10^{19}	3,87	Sample on Al substrate. T = 281 K. 1,33 x 10^{-6} Pa vacuum maintained by ion pump. Measured in situ after exposure. Boeing test facility (Radiation
━ ━			54	
— —			123	
━•━		10^{20}	1,08	

Key	Intensity [keV]	Cumulative Integrated Flux [e.m^{-2}]	Time after Exposure [h]	Comments
—·—			50	Effects Laboratory) see Brown, Fogdall & Cannaday (1969) [24].
••••••••			168	120 h after dry air back fill. T = 298 K

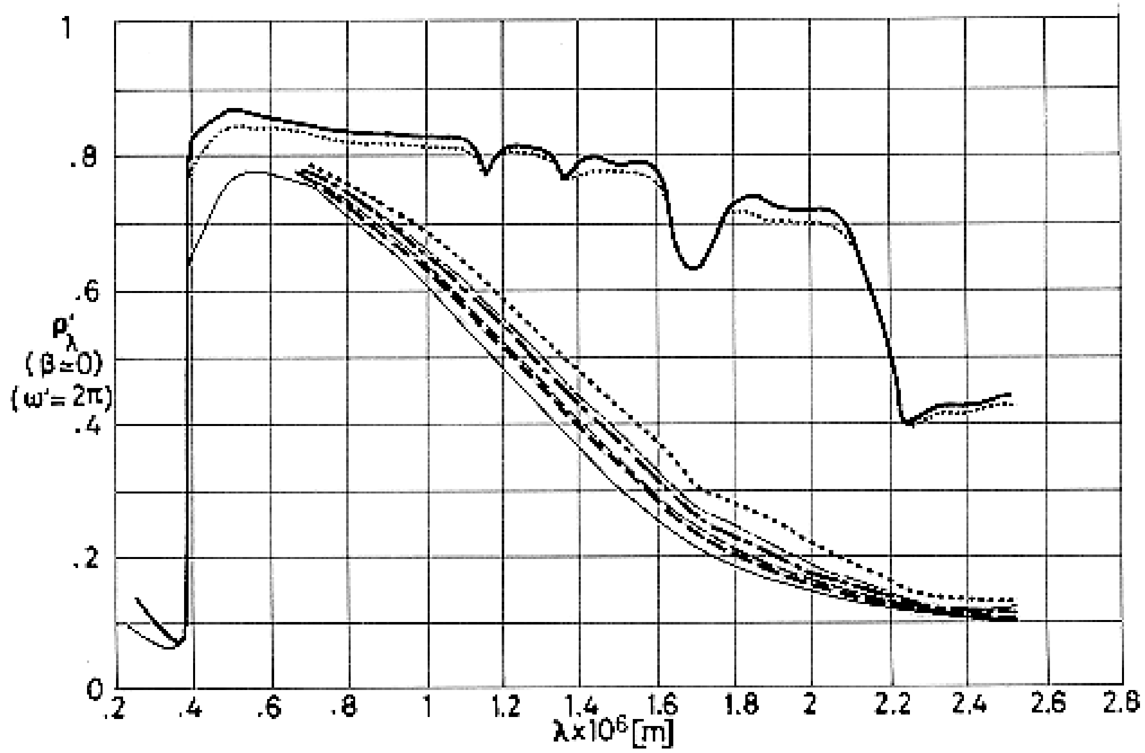

Note: non-si units are used in this figure

Figure 5-48: Electrons exposure effects on normal-hemispherical spectral reflectance, ρ'_{λ}, of GSFC, 101-7 coating vs. wavelength, λ. Radiation intensity 80 keV. Recovery after exposure. 101-7 is a coating, similar to S-13 G, developed by NASA Goddard. From Fogdall, Cannaday Brown (1970) [43]. Drawn from Touloukian, DeWitt & Hernicz (1972) [126].

Explanation

Key	Intensity [keV]	Cumulative Integrated Flux [e.m^{-2}]	Time after Exposure [h]	Comments
▬	In air before irradiation.			Sample on Al substrate. T = 298 K

Key	**Intensity [keV]**	**Cumulative Integrated Flux [e.m^{-2}]**	**Time after Exposure [h]**	**Comments**
———	80	10^{20} (10^{14} to 5 x 10^{15} e.m^{-2}.s^{-1})	0	Sample on Al substrate. T = 281 K. 1,33 x 10^{-6} Pa vacuum maintained by ion pump. Measured in situ after exposure. Boeing test facility (Radiation Effects Laboratory) see Brown, Fogdall & Cannaday (1969) [24].
▬ ▬			48	
— —			72	
▬·▬			96	
—·—			168	
••••••••			432	
········			Measured in air after the above tests had been made. T = 298 K.	

7.3.3.2.6. Combined exposure. Two different set of data are presented here.

Figure 5-49 shows the effect of Ultra-Violet and Protons exposure on S-13 G coating.

The damage in the visible spectrum (λ = 0,4 x 10^{-6} m to 0,7 x 10^{-6} m) is fairly slight and bleachable. The exposure produces displacement of atoms, ionization and excitations. After exposure most of the atoms return to the previous or similar equilibrium positions and a recovery process follows, in which X ray and Ultra-Violet radiations are emitted. When long wavelength radiation is not present the damage is not bleached.

Charged particle damage produces effects which Ultra-Violet produces, as well as others which result from massive interactions. In combined exposures radiative bleaching will produce "synergism" and invalidate any reciprocity which might have existed in single environment testing.

$\Delta\alpha_s$ is given in the table from Filligan and Zerlaut of paragraph 7.3.2.5.6.

From Gilligan & Zerlaut (1971) [46].

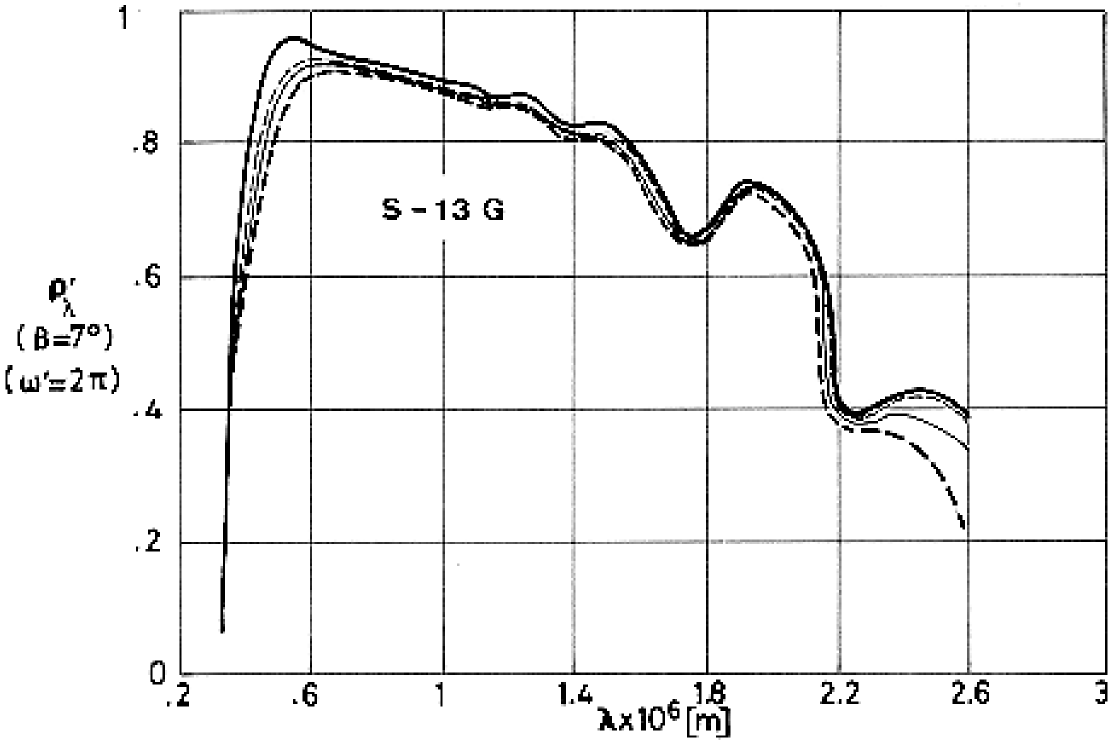

Note: non-si units are used in this figure

Figure 5-49: Effect of Combined Exposure on normal-hemispherical spectral reflectance, ρ'_λ, of S-13 G coating vs. wavelength, λ. Plasma annealed and potassium silicate treated pigment. From Gilligan & Zerlaut (1971) [46].

Explanation

Key	Exposure	Comments
▬▬▬	In vacuum before irradiation	T ≈ 285 K. Measured in situ. Initially at 8 x 10^{-6} Pa pressure. Irradiation performed at 1,33 x 10^{-5} Pa. IITRI test facility (In situ Reflectance Irradiation Facility – IRIF). $\Delta\alpha_s$ in the table from Filligan and Zerlaut of paragraph 7.3.2.5.6
———	UV. 600 ESH. Protons. 668 EWH 1,05 x 10^{13} p.m^{-2}.s^{-1} Flux ≈ 6 x 10^{18} p.m^{-2} Integrated Flux First part of exposure	
▬ ▬	Above plus UV. 700 ESH. Second part of exposure.	
— —	Above plus O_2 bleaching.	

The other set of data, Figure 5-50 to Figure 5-52, are for S-13 G/LO on Al substrate and are intended to represent up to three years exposure in geosynchronous orbit of the Orbital Test Satellite (OTS) equatorial faces. Solar absorptance data have been presented and evaluated in paragraph 7.3.2.5.6.

Figure 5-50 indicates that in the visible range (λ = 0,4 x10^{-6} m to 0,7 x 10^{-6} m) the reflectance decreases regularly with the exposure time; whereas the decrease in the infrared (λ > 0,8 x 10^{-6} m) rapidly reaches a saturation.

Figure 5-51 shows the influence of air exposure after irradiation. To this aim the upper and lower reflectance curves in Figure 5-50 have been compared with that resulting from air exposure.

Figure 5-52 indicates that bleaching appears after pump damage but an increased reflectance also results when an irradiation with Ultra-Violet and particles is followed by an irradiation with particles only. Again the infrared part of the spectrum (λ> 0,8x10^{-6} m) is the most affected, as can be seen by comparing the curves corresponding to data taken after step C and before step D.

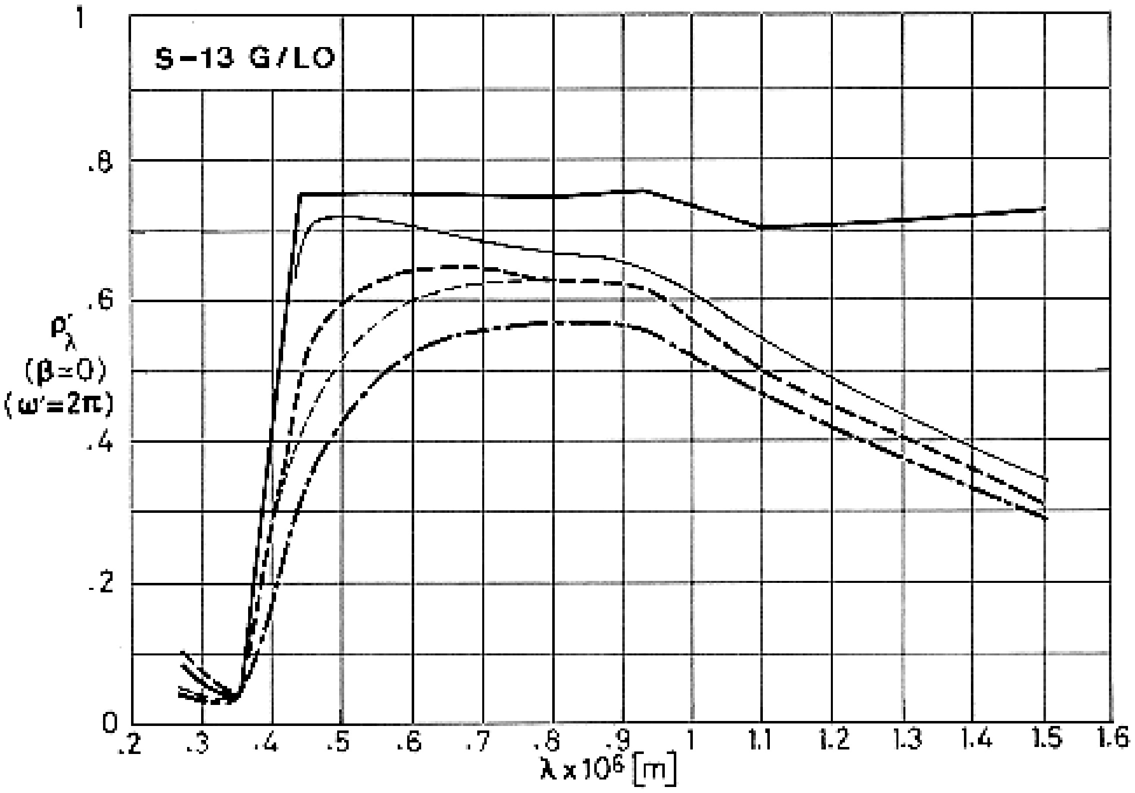

Note: non-si units are used in this figure

Figure 5-50: Effect of Combined Exposure, simulating up to three years in geosynchronous orbit, on normal- hemispherical spectral reflectance, ρ'_λ, of S-13 G/LO coating vs. wavelength, λ. From Paillous (1976) [96].

Explanation

Key	Description	Comments
━━━	After 125 h below 1,3 x 10^{-4} Pa pressure. T = 363 K.	Test conditions: See Table 5-19
───	After Step A (0,18 yr in orbit). T = 363 K.	

Key	Description	Comments
▬ ▬	After Step B (0,94 yr in orbit). T = 363 K.	
— —	After Step C (2,11 yr in orbit). T = 363 K.	After unintentional O_2 bleaching
▬•▬	After Step D (3 yr in orbit). T = 363 K	

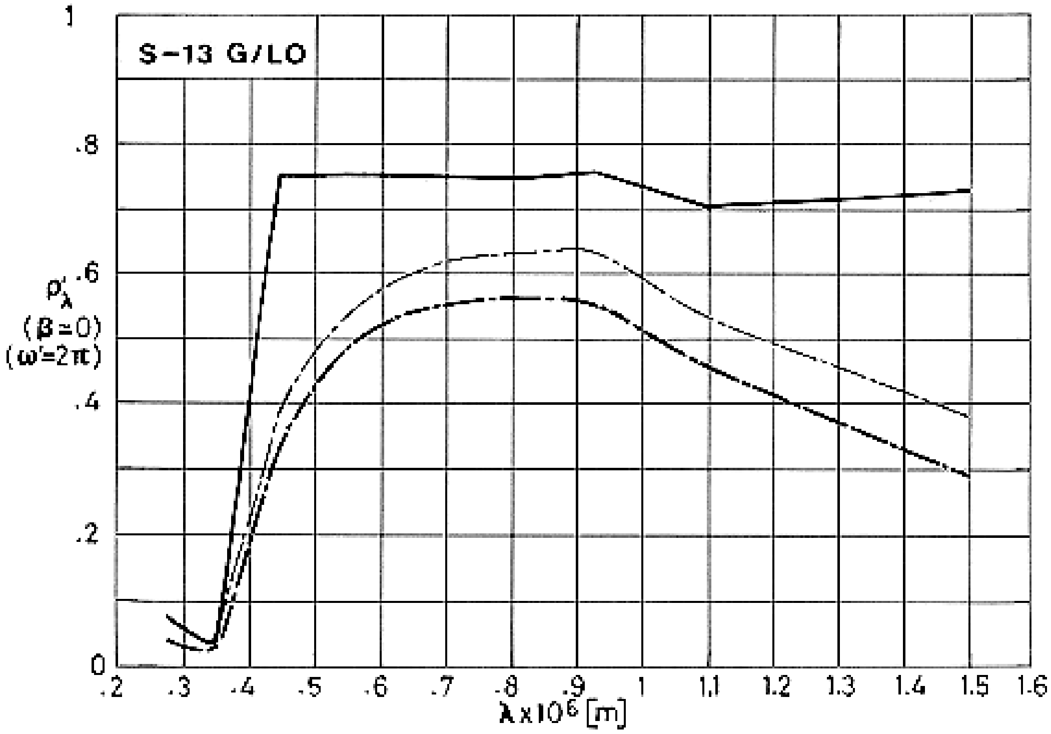

Note: non-si units are used in this figure

Figure 5-51: Effect of O_2 bleaching, after Combined Exposure, on normal-hemispherical spectral reflectance, ρ'_λ, of S-13 G/LO coating vs. wavelength, λ. Curves of ▬▬ and ▬•▬ are those shown in Figure 5-19. From Paillous (1976) [96].

Explanation

Key	Description	Comments
▬▬	After 125 h below 1,3 x 10^{-4} Pa pressure. T = 363 K.	Test conditions: See Table 5-19
▬•▬	After Step D (3 yr in orbit). T = 363 K	After unintentional O_2 bleaching
—•—	After Step D and air exposure. T = 293 K	

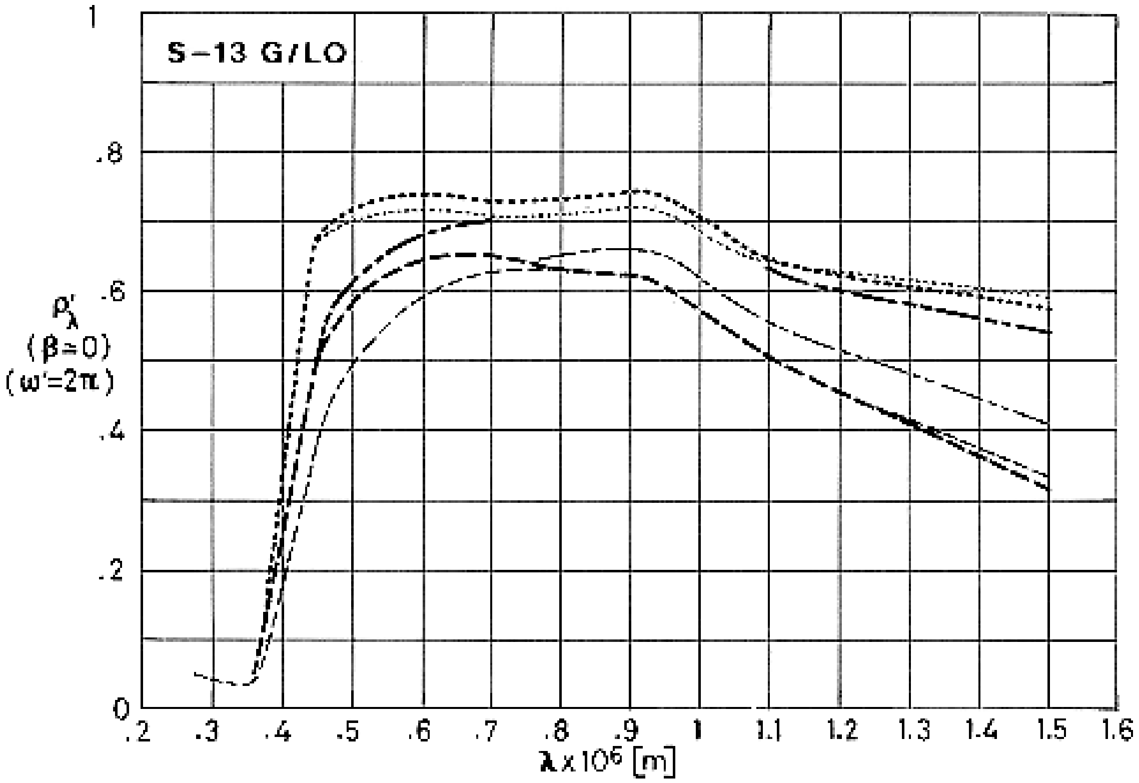

Note: non-si units are used in this figure

Figure 5-52: Effect of Combined Exposure, simulating up to three years in geosynchronous orbit, on normal- hemispherical spectral reflectance, ρ'_λ, of S-13 G/LO coating vs. wavelength, λ. Curves of ▬ ▬ and — — are those shown in Figure 5-50. From Paillous (1976) [96].

Explanation

Key	Description	Comments
••••••••	Before Step B. T = 363 K.	Test conditions: See Table 5-19
▬ ▬	After Step B (0,94 yr in orbit). T = 363 K.	
....	After pump damage. T = 363 K.	After unintentional O_2 bleaching
▬••▬	Before Step C. T = 363 K.	
— —	After Step C (2,11 yr in orbit). T = 363 K.	
—··—	Before Step D. T = 363 K	

7.4. Electrical resistance.

These coatings are non conductive.

A slight conductivity has been observed in S-13 G/LO by Paillous (1976) [96] under two experimental conditions:

1. For the sample in air. Conductivity vanished to zero after exposure in vacuum. This was attributed to sample moisture.
2. When the sample was UV irradiated. Now the effect was attributed to photo-emission on the electrodes attached to the sample.

8. ENVIRONMENTAL BEHAVIOR

8.1. Prelaunch. These paragraphs concern S-13 G and S-13 G/LO coatings. Early information on S-13 can be found in Breuch (1967) [22].

Two NASA Specifications cover the properties, qualification test and preparation of S-13 G and S-13 G/LO coatings. These are NASA Specification 10M01835, entitled "Paint, S-13 G, Temperature Control, Specification For" and 10M01836, entitled "Paint, S-13 G, Temperature Control, Application of, Specification For". Although these specifications are for S-13 G, they apply to S-13 G/LO since the only difference between them is that S-13 G/LO uses a stripped binder (see paragraph 1).

These coatings are easy to apply, flexible, cleanable and reparable. The surface is soft, rubbery and should be protected from sand, dust, salt, smog and human sebum with appropriate plastic coverings. No ill effects were evident when exposed to UV and vacuum after 14 months in storage under Mylar, H-polymer, Lexan, Teflon A or Tedlar films.

8.2. Postlaunch. These coatings have an accepted low α_s ($\alpha_s \leq 0{,}22$) high emittance ($\varepsilon \approx 0{,}90$) and a low outgassing (the LO version).

8.2.1. Ascent. These coatings are thermal shock resistant when cured as indicated in paragraph 5,5, provided that the primer is not too thick.

8.2.2. Orbital. UV and vacuum degradation are fair (UV degradation is due to damage in the binder).

These coatings have been often used on short flights at low altitudes.

From Cull, Stevenson, Mell & Harada (1984) [31].

9. THERMAL CYCLING

The maximum and minimum temperatures at which these coatings have been tested with no cracking or spalling evident to the unaided eye or at 100x magnification were

T min = 83 K

T max = 395 K

Chamber pressure below 0,7 x 10^{-3} Pa.

(Cunnington, Grammer & Smith (1969) [33]).

10. SOURCE

IIT Research Institute. 10 West 35 Street, Chicago, Illinois 60616.

11. COST

Quotations in the early eighties were of the order of 350 US $/pint (FOB, Chicago) for 1-7 pints and 300 US$/pint for 8 or more pints of S-13 G. (1 US pint = 473,2x10^{-6} m^2). Quotations for S-13 G/LO were 30 % higher.

12. PAST SPATIAL USE

Spacecraft or Programme	Launching Date	Used or Tested	References
OSO-II	Feb. 3, 1965	Tested	McCargo, Spradley, Greenberg & McDonald (1971) [82]
Pegasus I	Feb. 16, 1965	Tested	Touloukian, DeWitt & Hernicz (1972) [126]
Pegasus II	May 25, 1965	Tested	McCargo, Spradley, Greenberg & McDonald (1971) [82]
Pegasus III	July 30, 1965	Tested	
Lunar Orbiter I	Aug. 10, 1966	Tested	Touloukian, DeWitt & Hernicz (1972) [126]
Lunar Orbiter II	Nov. 6, 1966	Tested	
ATS-I	Dec. 7, 1966	Tested	Reichard & Triolo (1967) [103]; Triolo (1973) [128]; Triolo, Heaney & Hass (1978) [129]
OSO-III	March 8, 1967	Tested	Millard (1969) [86]
ATS-II	Apr. 5, 1967	Tested	McCargo, Spradley, Greenberg & McDonald (1971) [82]
Lunar Orbiter IV	May 4, 1967		Touloukian, DeWitt & Hernicz (1972) [126]
Mariner V	June 14, 1967	Tested	
Lunar Orbiter V	Aug. 1, 1967	Tested	McCargo, Spradley, Greenberg & McDonald (1971) [82]
Prospero	Oct. 28, 1971	Tested	Keyte (1975) [70]
OTS	May 11, 1978	Used on the antenna dishes. See ECSS-E-HB-31-01 Part 15, clause 5.9.	Chalmers, Konzok, Bouchez & Howle (1983) [29]
NAVSTAR	Apr. 26, 1980	Tested	Pence & Grant (1981) [99]
LANDSAT D	July 16, 1982	Used on antennae. See ECSS-E-HB-31-01 Part 15, clause 5.7.	Bachofer (1979) [10]
LDEF	Apr. 6, 1984	Tested	Clark (1981) [30].

5.2.4 Zinc Oxide-Methylsilicone

1. COMPOSITION

Pigment: New Jersey Zinc Co., SP500 zinc oxide.

Binder: RTV 121 silicone elastomer.

From Guillaumon & Guillin (1979, 1981) [52] & [53].

RHODORSIL RTV 121 is a bicomponent liquid silicone elastomer. This liquid, once mixed with catalyst 10028 and vulcanized at room temperature, yields a transparent material which is used as a potting and encapsulating compound.

From RHONE-POULENC (1978) [104]

2. FORMULATION

Not given by the producer.

3. USUAL DESIGNATION

PSG 120. ASTRAL.

PSG 120 FD CNES has the same composition as above, but with the RTV 121 binder purified by CNES (Toulouse).

From Guillaumon & Guillin (1979, 1981) [52] & [53].

4. SUBSTRATE

Practically any metallic substrate. Fiber-glass also quoted.

See Preparation of surfaces for painting.

5. METHOD OF APPLICATION

5.1. Preparation of paint for application. PSG 120 is delivered as a system consisting of:

Base PSG 120: 1 kg,

Hardener CT 122: 0,2 kg,

Thinner S 105: 10^{-3} m^3,

to mix when using it.

Shelf life, in the temperature range 288K-298K, between 10 h and 12 h.

Storage time of the unmixed components, held in closed containers, in the above temperature range, is 6 months.

From ASTRAL (1976)a [6].

5.2. Preparation of surfaces for painting. Excellent adhesion is obtained on metallic substrates such as: ferrous metals, steels and light alloys, as well as on fiber-glass composites, by use of P 128 primer which can be applied either by hand-rubbing or by spray painting.

Adhesion to electrolytic gold is excellent provided that the substrate is primed either with P 123 or with P 131, using P 128 as post-primer.

5.2.1. Use of P 123 primer. The surface should be cleaned from any trace of oxide or die lubricant and degreased with a rag soaked with toluene, trichloroethylene, acetone or ether.

The primer consists of three components which should be mixed as follow:

Base P 123: 4 parts by volume,

Hardener CX 124: 1 part by volume,

Thinner S 125: 2 parts by volume,

The mixing should be filtered through a nylon net, mesh size 5x10^{-5} m.

Shelf life in the temperature range 288 K-298 K is 8 h. The primer can be spray-applied. Use Kremlin model Junior or comparable gun, at about 2x10^{5} Pa air pressure. Also recommended, Blinks model Wren B or comparable 2,4x10^{5} Pa air pressure. In the last case, an additional thinning of 1 part by volume of S 125 should be used.

A single crosswise layer should be applied in an environment at 288 K to 298 K temperature.

Polymerization times at 293 K are:

Dust off: 30 min,

Dry to be handled: 4 h,

Final polymerization: 8 d.

The primer should be allowed to air-dry for 8 h at 293 K before application of the finishing coat.

Use paint remover D 165 for cleaning.

From ASTRAL (1976)b [7].

5.2.2. Use of P 128 primer. Ferrous metals, steels, light alloys and fiber-glass composites should be cleaned as above. In the case of electrolytic gold, the surface should be degreased before application of a thin layer of primer P 123 or P 131, using P 128 as post-primer after at least 8 h drying at 293 K.

Primer P 128 is delivered ready for use. It can be applied as a thin and uniform single crosswise layer, rather by hand rubbing or by spray painting. Application temperature in the range 288 K-298 K.

Polymerization times at 293 K are:

Dust off: 15 min,

Dry to be handled: 30 min,

Final polymerization: 3 h.

The primer should be allowed to air-dry for 30 min at 293 K before application of the finishing coat.

From ASTRAL (1976)c [8].

5.3. Application of the paint. By spray gun.

Yield (five layers): 1 kg.m^{-2}.

From ASTRAL (1976)a [6].

5.4. Coating thickness. Measured on A-U4G T4 aluminium alloy substrate, primed with P 128. t_c = 0,9x10^{-4} m to 1,1x10^{-4} m.

From ASTRAL (1976)a [6].

5.5. Curing process. On the above substrate and primer, the polymerization times at 293 K are:

Dust off: 3 h,

Dry to be handled: 24 h,

Final polymerization: 5 d.

Once cured, the coating appears as a glossless white surface.

From ASTRAL (1976)a [6].

CAUTIONS

Flammability. Primers P 123, P 128 and P 131, and coating PSG 120 should be handled far from any flame and in properly ventilated rooms.

Flash points of coating components, per NP M 07-019, are:

PSG 120: 278 K,

CT 122: 278 K,

S 105: 290 K.

Toxicity. Avoid breathing vapors during application.

Avoid frequent and lasting contacts on the skin, particularly while hardeners CT 122 and CX 124.

From ASTRAL (1976)a [6].

6. SOLVENTS RESISTANCE

A list of solvents of silicone elastomers is given in clause 5.2.1. RHODORSIL HUILE 47 V 50 can be used for decreasing the viscosity of RTV 121.

From RHONE-POULENC (1978) [104].

7. PHYSICAL PROPERTIES

7.1. Density. On A-U4G T4 aluminium alloy, primed with P 128, the surface density is: 0,26 kg.m^{-2} to 0,30 kg.m^{-2}.

These values, together with the above quoted coating thicknesses yield a density close to 2800 kg.m^{-3}.

The densities of the wet components are:

Base PSG 120: 1380 kg.m^{-3},

Hardener CT 122: 860 kg.m^{-3},

Thinner S 105: 910 kg.m^{-3}.

From ASTRAL (1976)a [6].

7,2. Outgassing. See Table 5-14. Outgassing characteristics given in that Table have been measured per Specification ESA PSS-09/QRM-02T. According to this specification, the sample is heated at 398 K, below 1,3x10^{-4} Pa pressure, during 24 h. The condensing plate is held at 298 K.

Table 5-14: Outgassing Characteristics of PSG 120 Coating

Coating	% TML [a]	% CVCM [b]	Cure Time [h]	Cure Temp. [K]	References
PSG 120 FD (binder purified by CNES). On aluminium substrate. Primer P 128.	0,70	0,03	120	298	Guillaumon & Guillin (1979, 1981) [52] & [53].
	0,79	0,05	120	298	
	0,80	0,03	120	298	
	0,43	0,03	120 24 [c]	298 333	
	0,49	0,03	120	298	

			24 [c]	333	
	0,24	0,02	120 24 [c]	298 373	
	0,24	0,03	120 24 [c]	298 373	
PSG 120 FD (binder purified by CNES). Primer P 128.	0,63 % RML: 0,61 [d]	0,04			ESTEC (1980) [39].
PSG 120 FD (binder purified by CNES). Primer P 128.	0,65 % RML: 0,62 [d]	0,03		298	ESTEC (1980) [39].

[a] TML : Total mass Loss.

[b] CVCM: Collected Volatile Condensable Materials.

[c] Each one of these cures was used in the order given.

[d] RML: Remainder Mass Loss.

7.3. Thermal radiation properties.

7.3.1. Emittance.

7.3.1.1. Hemispherical total emittance.

$\varepsilon = 0,87 \pm 0,02$.

From ASTRAL (1976)a [6].

The following value refers to PSG 120 FD.

$\varepsilon = 0,88$.

From Guillaumon & Guillin (1979, 1981) [52] & [53].

7.3.1.3. Effects of the Space Environment on hemispherical total emittance.

7.3.1.3.1. Ultra-Violet radiation.

$\Delta\varepsilon < 0,01$

Chamber pressure below $1,3x10^{-3}$ Pa.

Sample temperature: 353 K.

Exposure time: 120 ESH.

From ASTRAL (1976)a [6].

7.3.2. Absorptance.

7.3.2.1. Solar absorptance.

$\alpha_s = 0,17 \pm 0,02$

From ASTRAL (1976)a [6], Guillaumon & Guillin (1979, 1981) [52] & [53].

7.3.2.5. Effects of the Space Environment on absorptance.

7.3.2.5.1. Ultra-Violet Radiation. Figure 5-53 to Figure 5-55, from CNES.

Data measured in vacuum (below 1,3x10^{-5}Pa), several sample temperatures, with an integrating sphere attached to a Beckman DK2A reflectometer, $\beta = 0°$.

Aluminium used as standard.

Irradiated in vacuum.

Degrading source: OSRAM type XBO 900 W, Arc Xenon lamp, quartz Suprasil envelope. Around 1 Sun level.

From Simon (1973) [117].

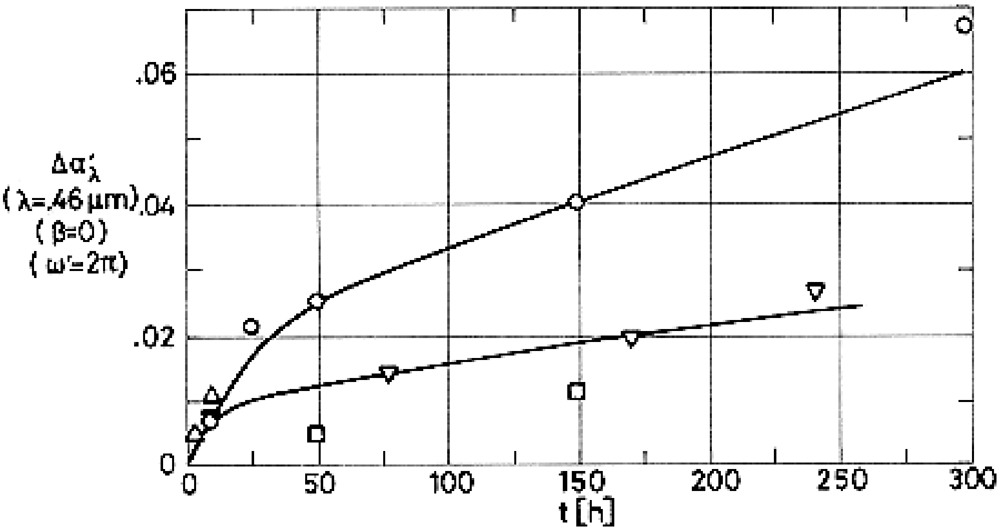

Note: non-si units are used in this figure

Figure 5-53: Change in normal-hemispherical spectral absorptance, $\Delta\alpha'_\lambda$, of PSG 120 coating, due to Ultra-Violet Radiation, vs. exposure time, t. Wavelength, λ = 0,46x10^{-6} m. From Simon (1974) [118].

Explanation

Key	T [K]	λx10^6 [m]	Comments
○	393	0,46 (Figure 5-53) 2,5 (Figure 5-54)	
□	353		
△	283		
▽	283		After 9 h of UV radiation plus 25 h in nitrogen (bleaching).

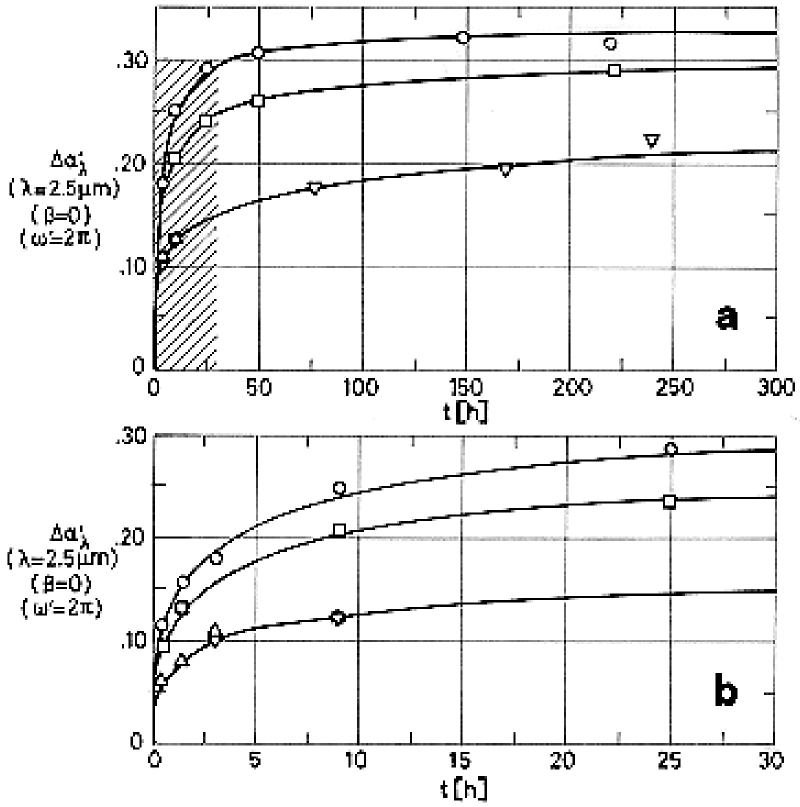

Note: non-si units are used in this figure

Figure 5-54: Change in normal-hemispherical spectral absorptance, $\Delta\alpha'_{\lambda}$, of PSG 120 coating, due to Ultra-Violet Radiation, vs. exposure time, t. Wavelength, λ = 2,5x10^{-6} m.

Shaded zone in *a* is enlarged in *b*.

See Explanation in the caption of Figure 5-53.

From Simon (1974) [118].

Data concerning the effect of ultra-violet radiation on solar absorptance are given in Figure 5-55. α_s deduced from spectral reflectance measured as above.

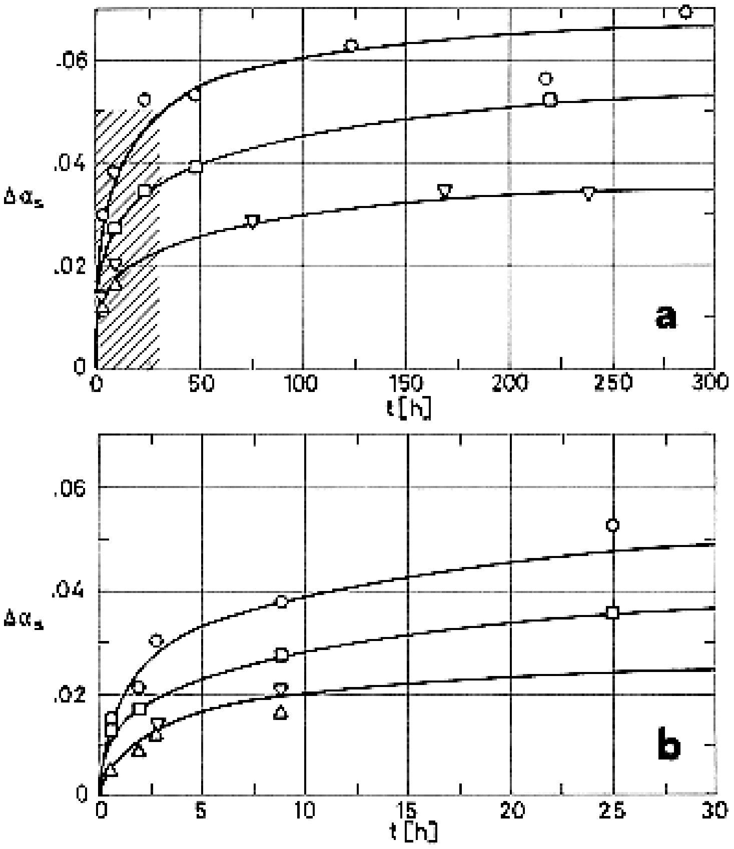

Note: non-si units are used in this figure

Figure 5-55: Change in solar absorptance, $\Delta\alpha_s$, of PSG 120 coating, due to UV radiation, vs. exposure time, *t*. Shaded zone in *a* is enlarged in *b*. From Simon (1974) [118].

Explanation

Key	T [K]	Comments
○	393	
□	353	
△	283	
▽	283	After 9 h of UV radiation plus 25 h in nitrogen (bleaching).

7.3.2.5.3. Protons only exposure. Table 5-15 has been prepared after results reported by DERTS (Toulouse).

Solar absorptance is deduced from the spectral reflectance data given in paragraph 7.3.3.2.3.

CAUTION

Solar absorptance values of white paints deduced from spectral reflectance data by DERTS group, are larger, by a factor close to 2, than other widely accepted values.

The following table has been prepared by the compiler. Values of α_s before irradiation.

Solar Absorptance, α_s, of Four White Paints

Coating	**S 13 IITRI**	**PSG 120 ASTRAL**	**Z 93 IITRI**	**PSZ 184 ASTRAL**
DERTS	0,37± 0,03	0,38± 0,02	0,33± 0,02	0,36± 0,03
Other	0,19± 0,04	0,17± 0,02	0,15± 0,02	0,14± 0,02

Sources of data

S 13 DERTS, 6 values from Paillous (1976) [96].

Other, 42 values from Touloukian, DeWitt & Hernicz (1972) [126].

PSG 120 DERTS, 9 values from Paillous (1976) [96] and Paillous, Amat, Marco & Panabiere (1977) [97].

Other, paragraph 7.3.2.1, clause 5.2.4.

Z 93 DERTS, 6 values as for S 13.

Others, paragraph 7.3.2.1, clause 5.2.2 (soiled specimen has been excluded).

PSZ 184 DERTS, 9 values as for PSG 120.

Other, paragraph 7.3.2.1, clause 5.2.5.

Spectral reflectance is measured in situ by DERTS group using a movable integrating sphere one of whose apertures faces successively each one of the samples in the sample holder, and the standard coating. See for further details paragraph 7.3.3.2.3, clause 5.2.4.

A distance of the order of $3x10^{-3}$ m (not the same for all samples) exists between the sample and the sphere during reflectance measurements. This results in a loss of reflected light for diffusely reflecting coatings which affects ALL THE DATA regarding protons, electrons and combined exposure effect on reflectance (and absorptance) of PSG 120 coating.

Integrated values of solar absorptance from DERTS in Table 5-17 have been corrected, according to Paillous (1976) [96], as follows:

1. The initial value for PSG 120 has been assumed to be,

   $\alpha_{so} = 0{,}20$,

   measured (in air) by ESTEC and by CNES using an integrating sphere attached to a Beckman DK2A reflectometer.

2. $\Delta\alpha_{s\ corrected}$ has been related to $\Delta\alpha_{s\ in\ situ}$ as follows,

   $(\Delta\alpha_{s\ corrected})/(\Delta\alpha_{s\ in\ situ}) = (\Delta\rho_{s\ corrected})/(\Delta\rho_{s\ in\ situ}) = 0{,}80/(1-\alpha_{so\ in\ situ})$

   α_s variations in the different sub ranges of the spectrum (ultra-violet, visible, infrared) are given by Paillous, Amat, Marco & Panabiere (1977) [97] regarding protons and electrons, and by Paillous (1976) [96] regarding combined exposure. These data have not been compiled here.

Table 5-15: Protons Radiation Effects Solar Absorptance of PSG 120 Coating

Intensity [keV]	45			75			150		
Integrated Flux [p.m^{-2}]	α_s	$\Delta\alpha_s$	$\Delta\alpha_s/\alpha_s$	α_s	$\Delta\alpha_s$	$\Delta\alpha_s/\alpha_s$	α_s	$\Delta\alpha_s$	$\Delta\alpha_s/\alpha_s$
Before (in air)	0,293			0,353			0,348		
Before (in vacuum)	0,326			0,384			0,383		
10^{17}	0,325	–0,001	–0,004	0,397	0,013	0,033	0,385	0,002	0,005
10^{18}	0,333	0,007	0,020	0,401	0,017	0,043	0,397	0,014	0,036
10^{19}	0,383	0,057	0,148	0,459	0,075	0,164	0,495	0,112	0,226
2,1x10^{19} for 45 keV 2,8x10^{19} otherwise	0,456	0,130	0,285	0,528	0,144	0,273	0,582	0,199	0,342
After (in air)	0,390			0,438			0,458		

NOTE From Paillous, Amat, Marco & Panabiere (1977) [97].

7.3.2.5.4. Electrons only exposure. Table 5-16 after results from DERTS.

Solar absorptance is deduced from the spectral reflectance data given in paragraph 7.3.3.2.4, clause 5.2.4.

Table 5-16: Electrons Radiation Effects on Solar Absorptance of PSG 120 Coating

Intensity [keV]	40			80			210		
Integrated Flux [e.m^{-2}]	α_s	$\Delta\alpha_s$	$\Delta\alpha_s/\alpha_s$	α_s	$\Delta\alpha_s$	$\Delta\alpha_s/\alpha_s$	α_s	$\Delta\alpha_s$	$\Delta\alpha_s/\alpha_s$
Before (in air)	0,333			0,335					
Before (in vacuum)	0,341			0,366			0,346		
2x10^{14}	0,354	0,013	0,035	0,392	0,026	0,066	0,412	0,066	0,160
5x10^{14}	0,356	0,015	0,043	0,403	0,037	0,091	0,411	0,065	0,158
10^{15}	0,365	0,024	0,067	0,416	0,049	0,119	0,426	0,080	0,189
2x10^{15}	0,375	0,034	0,091						
After (in air)	0,334			0,363			0,355		

NOTE From Paillous, Amat, Marco & Panabiere (1977) [97].

7.3.2.5.6. Combined exposure. Table 5-17 after DERTS.

Solar absorptance from spectral reflectance data.

The tests simulate geosynchronous orbit exposure of the Orbital Test Satellite (OTS) equatorial faces.

"Corrected" values in Table 5-17 were used to estimate coating degradation up to 3 years in orbit, Figure 5-56. Also shown data from Guillaumon & Guillin (1981) [53], CNES. Incidents during testing, see paragraph 7.3.3.2.6, clause 5.2.4, cast doubts on the validity of the data beyond 1 year in orbit.

Table 5-17: Combined Exposure Effects on Solar Absorptance of PSG120 Coating

Test Conditions	Sample 1						Sample 2					
	Measured in situ			Corrected [a]			Measured in situ			Corrected [a]		
	α_s	$\Delta\alpha_s$	$\Delta\alpha_s/\alpha_s$	α_s	$\Delta\alpha_s$	$\Delta\alpha_s/\alpha_s$	α_s	$\Delta\alpha_s$	$\Delta\alpha_s/\alpha_s$	α_s	$\Delta\alpha_s$	$\Delta\alpha_s/\alpha_s$
BEFORE IRRADIATION	0,358			0,200			0,367			0,200		
AFTER *A* UNDER VACUUM [b]	0,422	0,063	0,177	0,279	0,079	0,395	0,440	0,073	0,199	0,291	0,091	0,455
BEFORE *B*	0,388	0,029	0,082	0,236	0,036	0,180	0,402	0,035	0,096	0,244	0,044	0,220
AFTER *B* [b]	0,410	0,051	0,144	0,264	0,064	0,320	0,451	0,084	0,230	0,305	0,105	0,525
AFTER PUMP DAMAGE [c]	0,378	0,020	0,055	0,225	0,025	0,125	0,390	0,023	0,062	0,229	0,029	0,145
BEFORE *C*	0,425	0,067	0,188	0,284	0,084	0,420	0,440	0,073	0,200	0,291	0,091	0,455
AFTER *C* [b]	0,485	0,127	0,354	0,359	0,159	0,795	0,502	0,135	0,369	0,369	0,169	0,845
BEFORE *D*	0,474	0,116	0,323	0,345	0,145	0,725	0,487	0,120	0,327	0,350	0,150	0,750
AFTER *D* UNDER VACUUM [b]	0,505	0,147	0,410	0,384	0,184	0,920	0,516	0,149	0,405	0,386	0,186	0,930
AFTER *D* AND AIR EXPOSURE	0,430	0,072	0,201	0,290	0,090	0,450	0,557	0,190	0,518	0,438	0,238	1,19

[a] The correction has been made by the compiler as follows:

1) Value before irradiation, $\alpha_{s0} = 0{,}20$.

2) $\Delta\alpha_{s\ corrected}/\Delta\alpha_{s\ in\ situ} = (1-\alpha_{s0})/(1-\alpha_{s0\ in\ situ}) = 0{,}80/0{,}64$

where α_{s0} has been measured (in air) with an integrating sphere attached to a Beckman DK2A reflectometer. $\alpha_{s0in\ situ}$ is the value measured before irradiation as indicated in paragraph 7.3.3.2.3, clause 5.2.4.

[b] Steps *A* to *D* correspond, respectively, to the following times in geosynchronous orbit.

A: 0,18 yr = 508 ESH.

B: 0,94 yr = 2443 ESH.

C: 2,11 yr = 5604 ESH.

D: 3 yr = 7949 ESH.

[c] See paragraph 7.3.3.2.6, clause 5.2.4, for further details.

NOTE From Paillous (1976) [96].

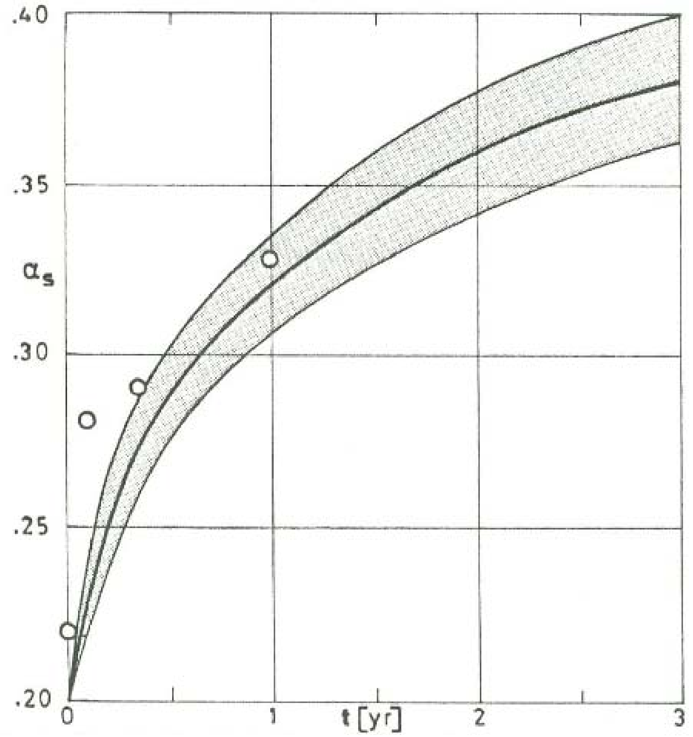

Note: non-si units are used in this figure

Figure 5-56: Estimated change in solar absorptance, α_s, of PSG 120 vs. time, t. From Paillous (1976) [96].
○: From Guillaumon & Guillin (1981) [52].

7.3.3. Reflectance. Data related with bidirectional total reflectance are given in Figure 5-57.

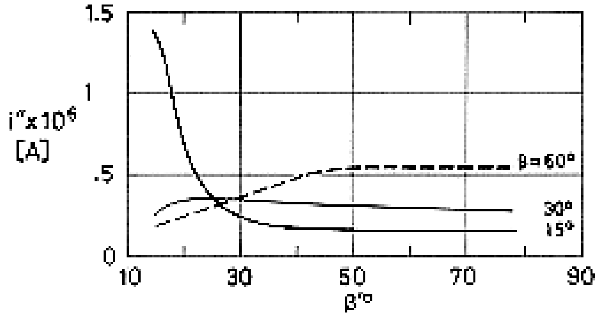

Note: non-si units are used in this figure

Figure 5-57: Bidirectional total radiation intensity of reflected flux, i'', vs. cone angle, β', for several values of the cone angle of the incident flux, β. PSG 120 coating. Incident and reflected fluxes are coplanar. i'' is measured by the response of a photocell attached to a photogoniometer. From ASTRAL (1976)a [6].

7.3.3.1. Normal-hemispherical spectral reflectance. Figure 5-58 from CNES.

Chamber pressure below 1,3x10^{-5} Pa.

Sample temperature: 348 K.

Spectral reflectance measured in situ with an integrating sphere, operating in the direct mode, attached to a Beckman DK2A reflectometer.

Aluminium used as standard. Sample and standard are alternatively illuminated.

See Simon (1973) [117] for further details on the measurement procedure.

7.3.3.2. Effects of the Space Environment on reflectance.

7.3.3.2.1. Ultra-Violet Radiation. Figure 5-58.

Sample conditions and spectral reflectance measurements as above.

Sample irradiated in vacuum.

Degrading source: OSRAM type XBO 900 W, Arc Xenon lamp, quartz Suprasilenvelope.

Radiation flux density at the sample level: ~1 Sun.

Exposure time: 212 ESH.

See Figure 5-53 and ff. where similar data from CNES are presented.

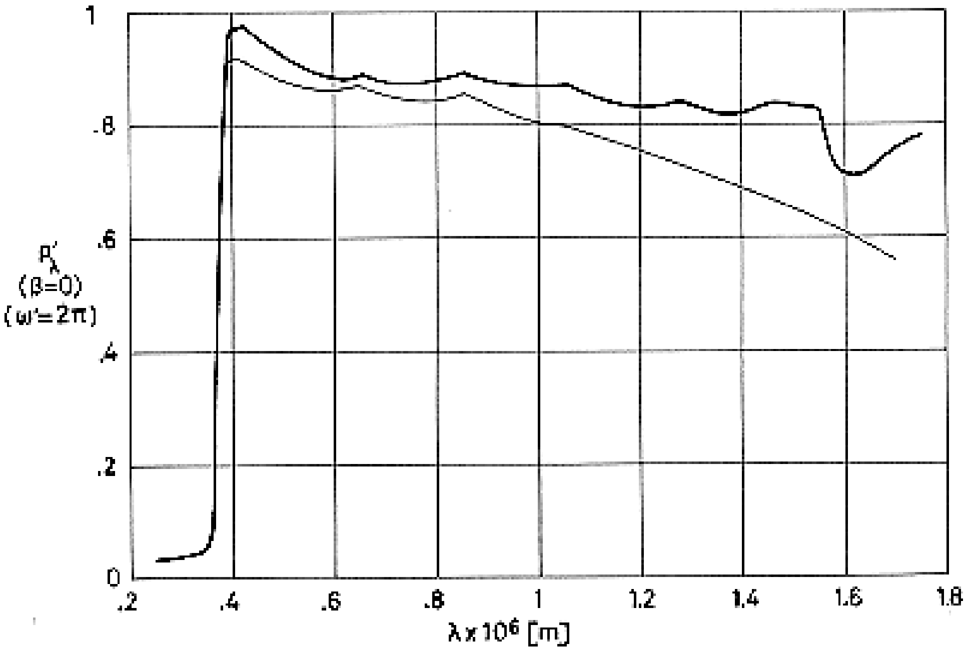

Note: non-si units are used in this figure

Figure 5-58: Effect of Ultra-Violet Radiation on normal-hemispherical spectral reflectance, ρ'_λ, of PSG 120 coating vs. wavelength, λ. Thick line: Before irradiation. p<1,3x10^{-5} Pa. T = 348 K. Thin line: After irradiation. p<1,3x10^{-5} Pa. T = 348 K. A Sun level. t = 212 ESH. From Simon (1973) [117].

7.3.3.2.3. protons only exposure. Figure 5-59 and ff., from DERTS.

Sample on aluminium substrate.

A SAMES proton accelerator has been used. The proton beam impinges normally on the sample.

Tests were performed in four successive steps. Data, which were taken before 3 h from the end of each step, are for cumulative damage.

Chamber pressure in the range 6,7x10^{-5} Pa to 10^{-4} Pa.

Sample temperature: 303 K ± 0,5 K.

Spectral reflectance measured in situ with an integrating sphere, operating in the direct mode, and appropriate detectors (depending on the λ range) viewing an area of the sphere inner wall.

A Zeiss monochromator can be displaced, together with the sphere, to successively illuminate the sample (2x10^{-2} m square) and a vacuum deposited aluminium standard (not exposed to the damaging irradiation). Readings for the sample and for the standard provide the directional-hemispherical reflectance factor, given in the following figures as directional-hemispherical spectral reflectance.

The experimental set-up is basically that described by Paillous (1975) [95], except for minor improvements in the optical detector system.

Neither the incidence angle, β, nor a schematic of the sphere are given in the source.

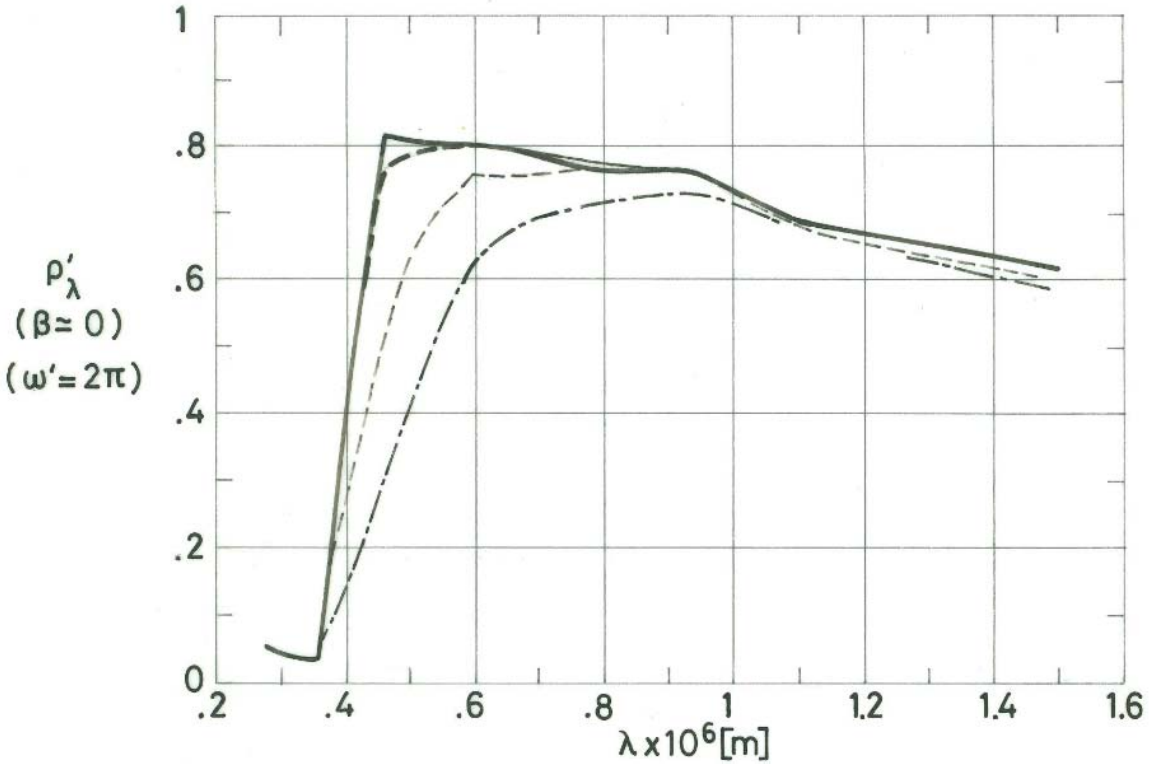

Note: non-si units are used in this figure

Figure 5-59: Effect of Protons radiation on normal-hemispherical spectral reflectance, ρ'_λ, of PSG 120 coating vs. wavelength, λ. Radiation intensity ≅ 45 keV. See Explanation in the caption of Figure 5-61. From Paillous, Amat, Marco & Panabiere (1977) [97].

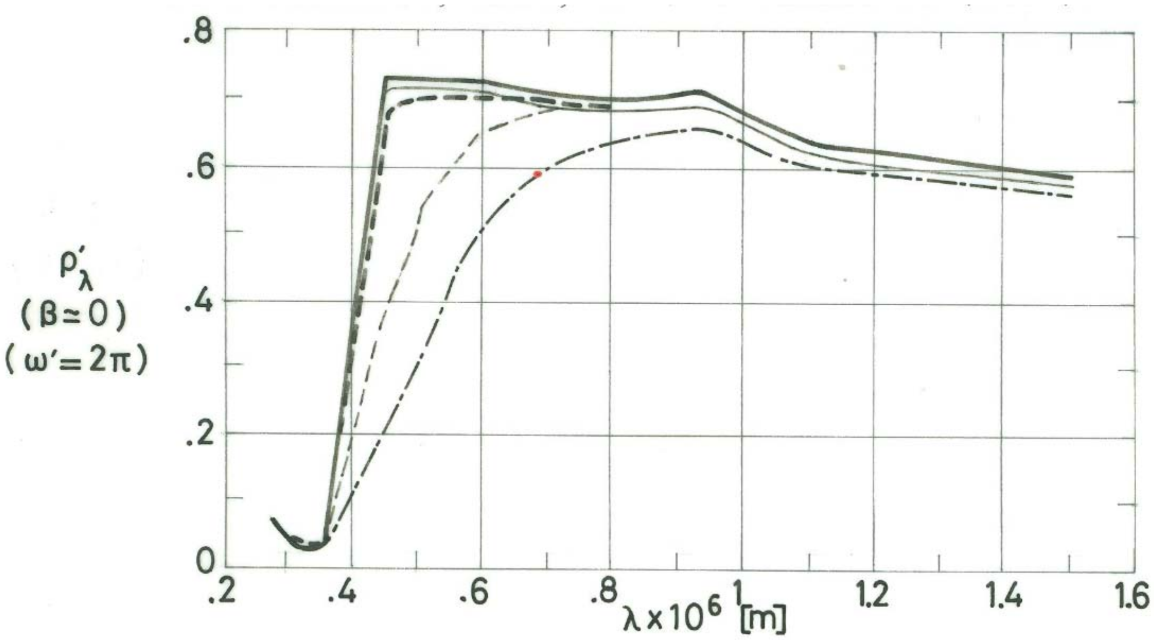

Note: non-si units are used in this figure

Figure 5-60: Effect of Protons radiation on normal-hemispherical spectral reflectance, ρ'_λ, of PSG 120 coating vs. wavelength, λ. Radiation intensity ≅ 75 keV. See Explanation in the caption of Figure 5-61. From Paillous, Amat, Marco & Panabiere (1977) [97].

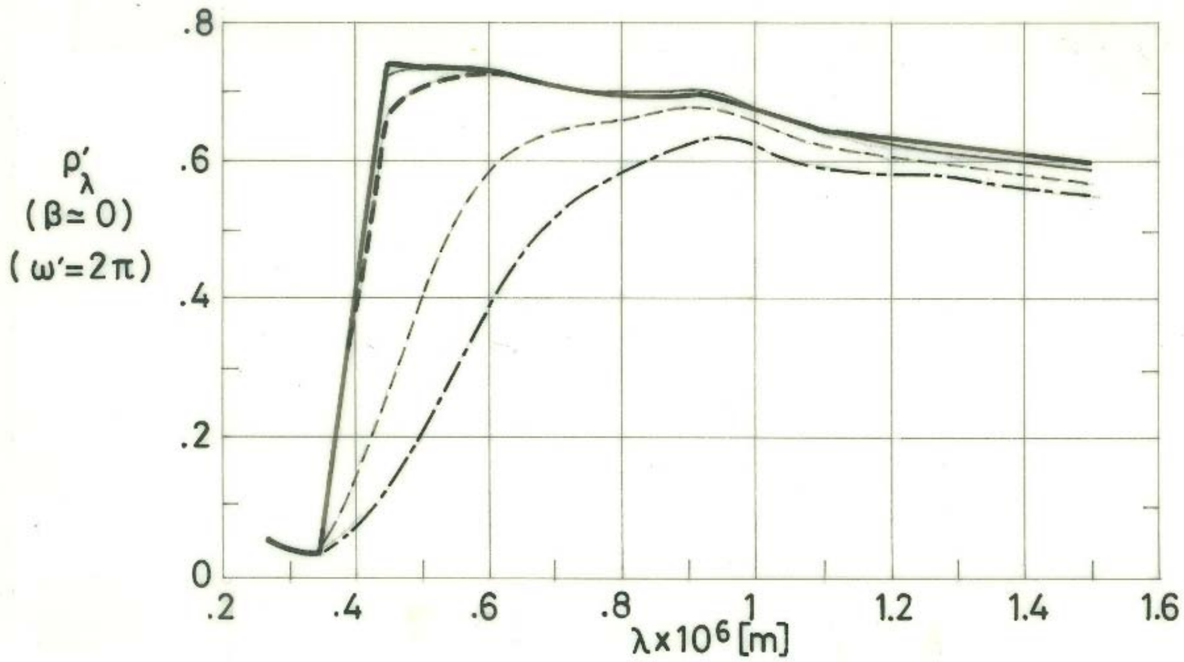

Note: non-si units are used in this figure

Figure 5-61: Effect of Protons radiation on normal-hemispherical spectral reflectance, ρ'_λ, of PSG 120 coating vs. wavelength, λ. Radiation intensity ≅ 150 keV. From Paillous, Amat, Marco & Panabiere (1977) [97].

Explanation

Key	Intensity [keV]	Flux [p.m^{-2}.s^{-1}]	Integrated Flux [p.m^{-2}]	Cumulative Integrated Flux [p.m^{-2}]	Comments
━━━━	45 keV in Figure 5-59. 75 keV in Figure 5-60. 150 keV in Figure 5-61.				Sample on aluminium substrate. $p = 1{,}3 \times 10^{-4}$ Pa. $T = 303$ K ± 0,5 K. Incidence of the protons beam: 0°.
────		1,3x10^{14}	10^{17}	10^{17}	
━ ━		2,5x10^{14}	9x10^{17}	10^{18}	
— —		2,5x10^{14} (Figure 5-59). 6,2x10^{14} (Figure 5-60 & Figure 5-61)	9x10^{18}	10^{19}	
━·━		6,2x10^{14}	1,1x10^{19} (Figure 5-59). 1,8x10^{19} (Figure 5-60 & Figure 5-61)	2,1x10^{19} (Figure 5-59). 2,8x10^{19} (Figure 5-60 & Figure 5-61)	

7.3.3.2.4. Electrons only exposure. Figure 5-62 and ff., from DERTS.

Sample on aluminium substrate.

A SAMES electron accelerator has been used. The electron beam impinges on the sample at 45°, but this has been taken into account for estimating the mean flux and the deviation from the mean. This is kept within ± 35% for the 25 samples being irradiated all at once. The achievable electrons energy at the sample is of the order of 200 keV.

See Paillous (1975) [95] for further details.

The tests were performed in four successive steps, and readings were taken at the end of each step. Sample conditions and reflectance measurements as in paragraph 7.3.3.2.3, clause 5.2.4.

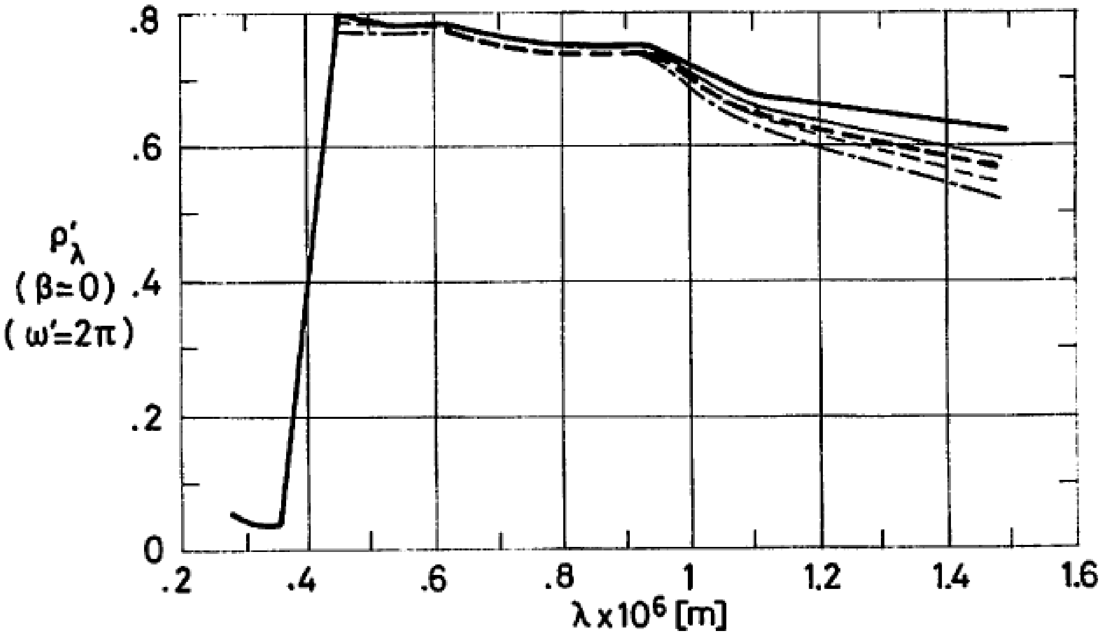

Note: non-si units are used in this figure

Figure 5-62: Effect of Electrons Radiation on normal-hemispherical spectral reflectance, ρ'_λ, of PSG 120 coating vs. wavelength, λ. Radiation intensity ≅ 40 keV. See Explanation in the caption of Figure 5-63. From Paillous, Amat, Marco & Panabiere (1977) [97].

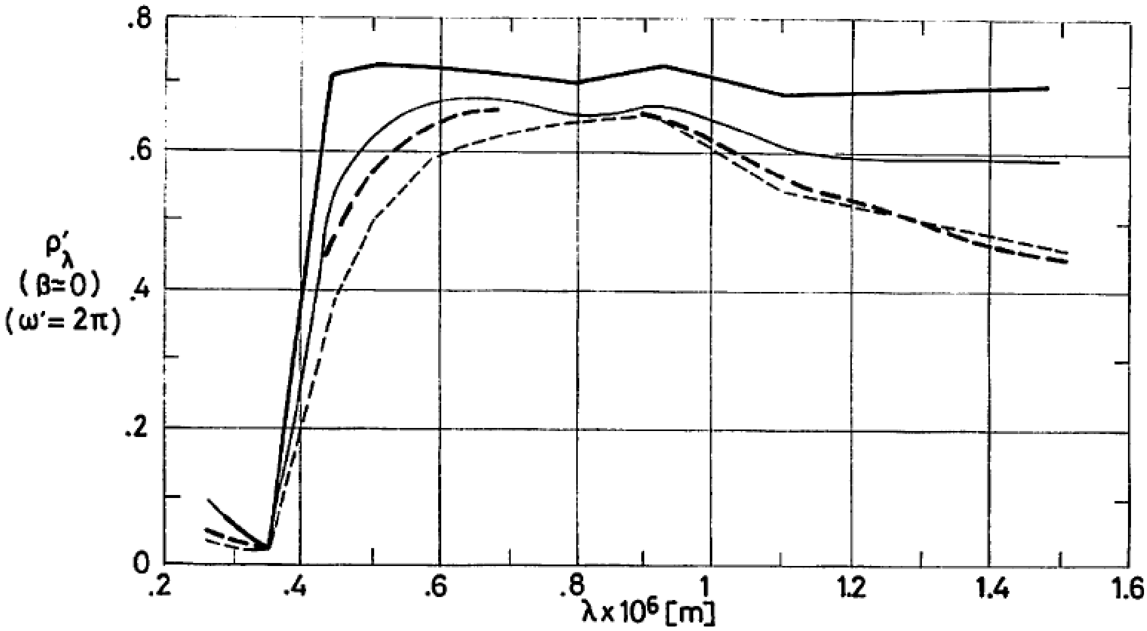

Note: non-si units are used in this figure

Figure 5-63: Effect of Electrons Radiation on normal-hemispherical spectral reflectance, ρ'_λ, of PSG 120 coating vs. wavelength, λ. Radiation intensity ≅ 80 keV. From Paillous, Amat, Marco & Panabiere (1977) [97].

Explanation

Key	Intensity [keV]	Flux [p.m^{-2}.s^{-1}]	Integrated Flux [p.m^{-2}]	Cumulative Integrated Flux [p.m^{-2}]	Comments
▬▬▬	40 keV in Figure 5-62. 80 keV in Figure 5-63.				Sample on aluminium substrate. *p* = 1,3x10^{-4} Pa. *T* = 303 K ± 0,5 K. Incidence of the electrons beam: 45°.
———		2,7x10^{14} (Figure 5-62). 2,9x10^{14} (Figure 5-63).	2x10^{18}	2x10^{18}	
▬ ▬		4x10^{14} (Figure 5-62). 2,8x10^{14} (Figure 5-63).	3x10^{18}	5x10^{18}	
— —		4x10^{14} (Figure 5-62). 5,3x10^{14} (Figure 5-63).	5x10^{18}	10^{19}	
▬·▬		5,4x10^{14} (Figure 5-62)	10^{19} (Figure 5-62)	2x10^{19} (Figure 5-62)	

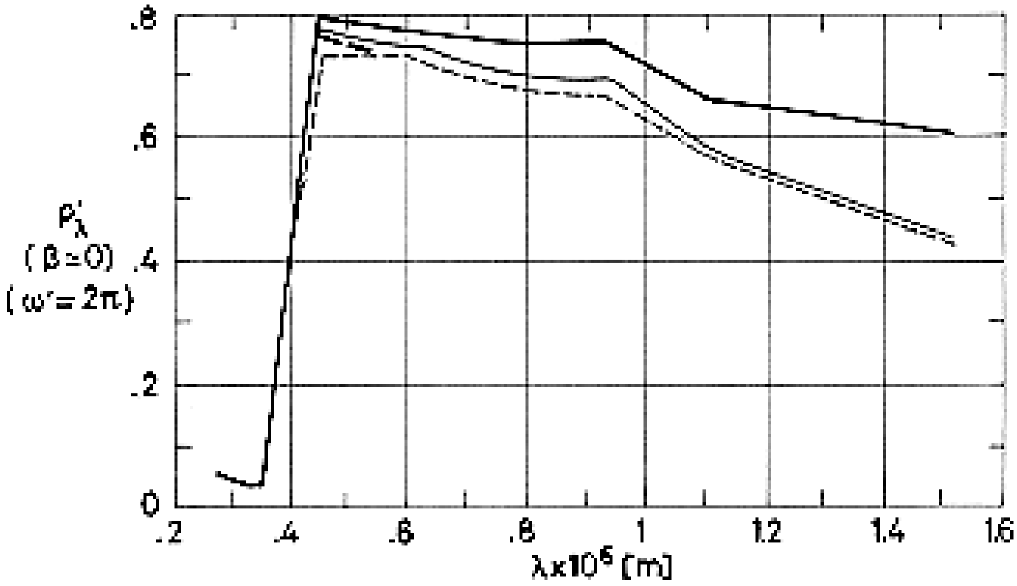

Note: non-si units are used in this figure

Figure 5-64: Effect of Electrons Radiation on normal-hemispherical spectral reflectance, ρ'_{λ}, of PSG 120 coating vs. wavelength, λ. Radiation intensity ≅ 210 keV. From Paillous, Amat, Marco & Panabiere (1977) [97].

Explanation

Key	**Intensity [keV]**	**Flux [p.m^{-2}.s^{-1}]**	**Integrated Flux [p.m^{-2}]**	**Cumulative Integrated Flux [p.m^{-2}]**	**Comments**
━━━	210				Sample on aluminium substrate. p = 1,3x10^{-4} Pa. T = 303 K ± 0,5 K. Incidence of the electrons beam: 45°.
───		3,0x10^{14}	2x10^{18}	2x10^{18}	
━ ━		3,1x10^{14}	3x10^{18}	5x10^{18}	
— —		6,3x10^{14}	5x10^{18}	10^{19}	

An analytical model of the solar absorptance degradation because of the irradiation of protons and electrons, with application to white paints, has been set forth by Bourrieau (1978) [19], Bourrieau & Paillous (1979) [20].

The model ascribes the changes in solar absorptance to the creation within the coating of defect centers, the concentration of which depends only on the local absorbed dose.

The defect density produces an absorption band which results in the optical degradation of the coating. The intensity of that absorption band is assumed to depend only on the defect density.

The absorption bands become apparent when the spectral reflectance curves before and after irradiation are compared to each other.

The distribution of absorbed dose in the coating can be calculated by use of available computational techniques (Bourrieau (1978) [19]). In practice a mean dose, $\overline{D}$, is> assumed to be uniformly distributed throughout a disturbed layer, the thickness of which, X_d, is called the penetration range.

The analytical model shows that:

1. When the disturbed layer is much thicker than the layer of photon absorption and scattering (optical range, X_u), the change in spectral reflectance does not depend on X_d. This occurs for high energy particles or very large irradiation doses.
2. On the other hand, when $X_d \ll X_u$ the changes in spectral reflectance are proportional to the penetration range, X_d.

In the case of PSG 120 coating two absorption bands are present, probably at $\lambda = 0{,}41\text{x}10^{-6}$ m and $\lambda = 2{,}1\text{x}10^{-6}$ m. None of them was clearly detected, since measurements of spectral reflectance were made at discrete values of λ, and the nearest values were, respectively, $\lambda = 0{,}45\text{x}10^{-6}$ m and $\lambda = 2{,}5\text{x}10^{-6}$ m.

The experimental results for $\lambda = 2{,}05\text{x}10^{-6}$ m have been used to test the applicability of the analytical model to PSG 120 coating degradation.

The relevant irradiation parameters are summarized in Table 5-18.

Table 5-18: Application of the Degradation Model to PSG 120 Coating

Type of Particle	**Protons**			**Electrons**		
Intensity [keV]	45	75	150	40	80	210
Flux [particles.m^{-2}.s^{-1}]	$1,3x10^{14}$ to $6,2x10^{14}$			$2,7x10^{14}$ to $5,4x10^{14}$	$2,9x10^{14}$ to $5,3x10^{14}$	$3,0x10^{14}$ to $6,3x10^{14}$
Cumulative Integrated Flux [particles.m^{-2}]	10^{17} to $2,8x10^{19}$			$2x10^{18}$ to $2x10^{19}$	$2x10^{18}$ to 10^{19}	
Regeneration Range, X_d [kg.m^{-2}]	$2,4x10^{-3}$	$3,4x10^{-3}$	$5,6x10^{-3}$	$2,5x10^{-2}$	$9,0x10^{-2}$	$5,0x10^{-1}$
Mean Dose, $\overline{D}$ GY/Particle [a]	$3,0x10^{-8}$	$3,6x10^{-8}$	$4,3x10^{-8}$	$1,7x10^{-9}$	10^{-9}	$5,8x10^{-10}$
Related Figure	Figure 5-59	Figure 5-60	Figure 5-61	Figure 5-62	Figure 5-63	Figure 5-64

[a] 1 GY (Gray) = 1 J.kg^{-1}.

NOTE From Bourrieu (1978) [19].

Experimental have been compared to theoretical as can be seen in Figure 5-65. Data from protons irradiation at 75 keV, not deemed to be reliable, are not shown. Agreement is fair, even though the assumption of an uniformly-distributed mean dose (throughout the disturbed layer) cannot be justified for high energy electron irradiations.

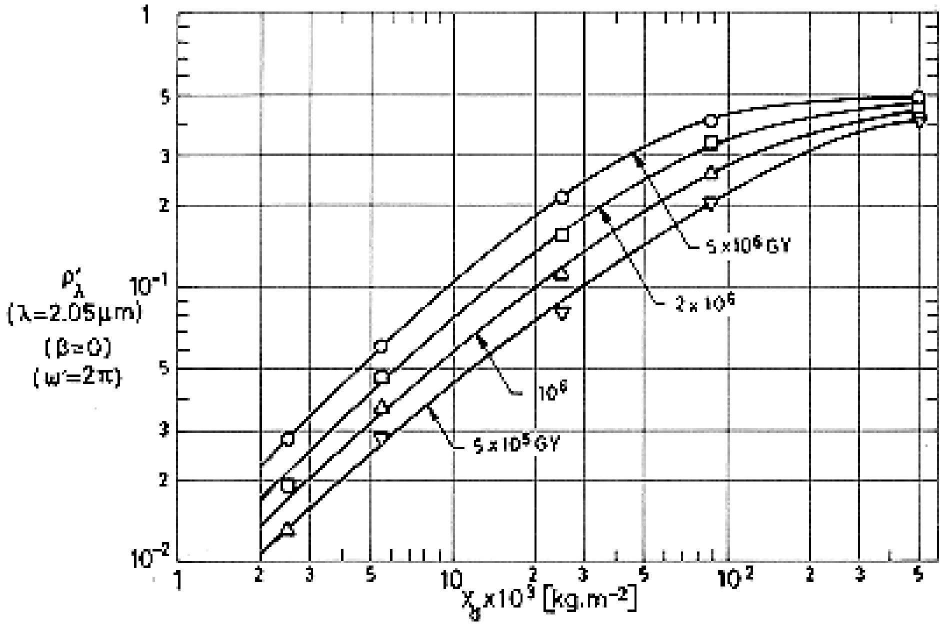

Note: non-si units are used in this figure

Figure 5-65: Change in normal-hemispherical spectral reflectance, ρ'_λ, of PSG 120 coating, due to particulate irradiation, vs. penetration range, X_d. Wavelength, λ = 2,05x10^{-6} m. From Bourrieau (1978) [19].

7.3.3.2.6. Combined exposure. Figure 5-66 and Figure 5-67 from DERTS.

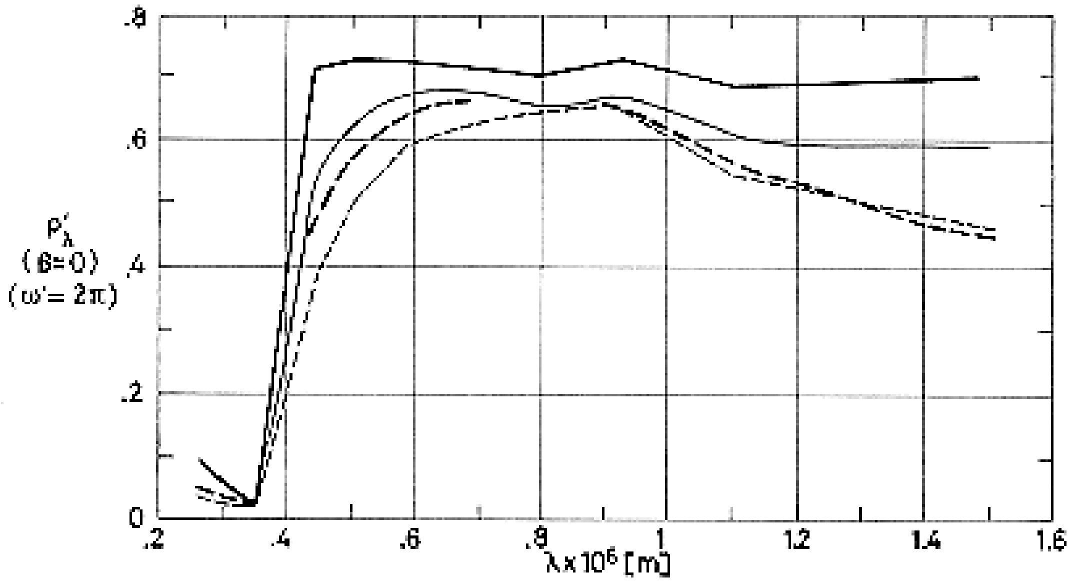

Note: non-si units are used in this figure

Figure 5-66: Effect of Combined Exposure, simulating up to three years in geosyncronous orbit, on normal-hemispherical spectral reflectance, ρ'_λ, of PSG 120 coating vs. wavelength, λ. From Paillous (1976) [96].

Explanation

Key	Description	Comments
━━━	After 125 h below 1,3x10^{-4} Pa pressure. T = 363 K.	
───	After step B (0,94 years in orbit). T = 363 K.	
━ ━	After step C (2,11 years in orbit). T = 363 K.	After unintentional O_2 bleaching.
— —	After step D (3 years in orbit). T = 363 K.	

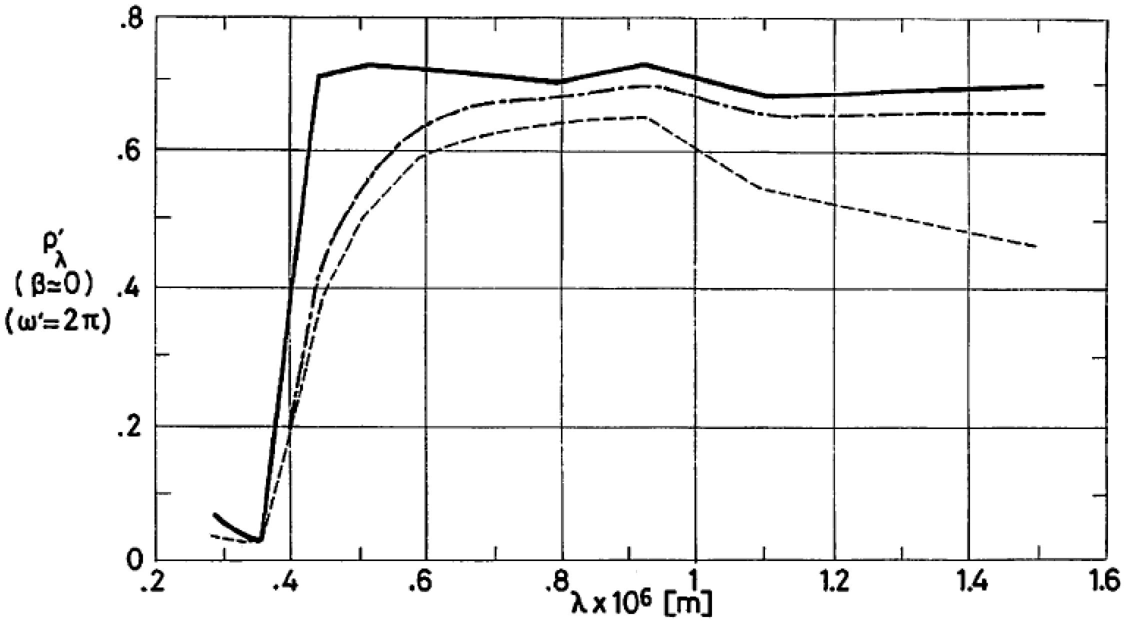

Note: non-si units are used in this figure

Figure 5-67: Effect of O_2 bleaching, after Combined Exposure, on normal-hemispherical spectral reflectance, ρ'_λ, of PSG 120 coating vs. wavelength, λ. Curves ━━━ and — — are those shown in Figure 5-66. From Paillous (1976) [96].

Explanation

Key	Description	Comments
━━━	After 125 h below 1,3x10^{-4} Pa pressure. T = 363 K.	
— —	After step D (3 years in orbit). T = 363 K.	After unintentional O_2 bleaching.
━·━	After step D and Air exposure. T = 293 K.	

Sample on aluminium substrate.

Irradiations were performed under the following conditions:

Chamber pressure below 1,3x10^{-4} Pa.

Sample temperature: 363 K.

Reflectance measured in situ without breaking vacuum, unless otherwise stated.

The exposure is intended to simulate 3 years in geosynchronous orbit of the three-axis stabilized Orbital Test Satellite (OTS) equatorial faces. The tests reproduced the simultaneous action of vacuum and temperature, and of ultra-violet, protons and electrons irradiations.

Ultra-violet irradiation was only possible at or below 3 Suns. Because of this limited capability, particle irradiations were performed intermittently, within the constraint of a correct simulation on the integrated fluxes at the end of the four main steps of the test (Table 5-19). Ultra-violet irradiation, on the contrary, was performed continuously.

Table 5-19: Test Conditions Simulating up to Three Years in Geosynchronous Orbit

		Step A	**Step B**	**Step C**	**Step D**
Years in Orbit		0,18	0,94	2,11	3
Simulation Test Time [h]		160	883	1868	2650
ESH		508	2443	5604	7949
Protons Exposure 40 keV	Starting Time, First Run [h]	90	790	1850	2630
	Stopping Time, Last Run [h]	169	831	1868	2650
	Net Running Time [h]	16	32	16	12
	Flux [Protons.m^{-2}.s^{-1}]	1,33x10^{13}	3,04x10^{13}	8,33x10^{13}	8,80x10^{13}
	Integrated Flux [Protons.m^{-2}]	0,77x10^{18}	0,35x10^{19}	0,48x10^{19}	0,39x10^{19}
	Cumulative Integrated Flux [Protons.m^{-2}]	0,77x10^{18}	0,43x10^{19}	0,91x10^{19}	1,30x10^{19}
Protons Exposure	Starting Time, First Run [h]	0	548	1700	2615

		Step A	**Step B**	**Step C**	**Step D**
150 keV	Stopping Time, Last Run [h]	90	790	1850	2630
	Net Running Time [h]	16	32	16	12
	Flux [Protons.m^{-2}.s^{-1}]	4,51x10^{11}	9,98x10^{11}	2,73x10^{12}	2,92x10^{12}
	Integrated Flux [Protons.m^{-2}]	0,27x10^{17}	1,17x10^{17}	1,58x10^{17}	1,27x10^{17}
	Cumulative Integrated Flux [Protons.m^{-2}]	0,27x10^{17}	1,44x10^{17}	3,02x10^{17}	4,29x10^{17}
Electrons Exposure **200 keV**	Starting Time, First Run [h]	0	548	1700	2615
	Stopping Time, Last Run [h]	169	831	1868	2650
	Net Running Time [h]	32	64	32	24
	Flux [Electrons.m^{-2}.s^{-1}]	1,34x10^{13}	3,08x10^{13}	8,23x10^{13}	8,80x10^{13}
	Integrated Flux [Electrons.m^{-2}]	0,15x10^{19}	0,71x10^{19}	0,95x10^{19}	0,76x10^{19}
	Cumulative Integrated Flux [Electrons.m^{-2}]	0,15x10^{19}	0,86x10^{19}	1,81x10^{19}	2,57x10^{19}

NOTE From Paillous (1976) [96]

For the ultra-violet exposure, the samples were irradiated at 45° incidence, through a Suprasil ultra-pure silica window. Two different high pressure Xenon lamps were needed to reproduce the full ultra-violet spectrum. Uniformity of illumination was within ± 17 % for the whole ensemble of 25 samples in the sample holder. Particulate irradiations and in situ reflectance measurements were achieved as in paragraphs 7.3.3.2.3 and 7.3.3.2.4 .of clause 5.2.4.

The following measurements were performed:

1. Solar reflectance (in air) before and after irradiation was measured, by ESTEC and by CNES, with an integrating sphere attached to a Beckman DK2A reflectometer. Standards of polished aluminium. The resulting α_s before irradiation has been given in Table 5-15.

2. In situ measurements of global reflectance. A solar-simulating high pressureXenon-lamp, 75 W was used. The lamp was attached to the integrating sphere via a glass and quartz fiber optical tube. The resulting data have not been compiled here.

3. In situ spectral reflectance, as in paragraph 7.3.3.2.3, clause 5.2.4. A limited amount of data are given in Figure 5-66 and Figure 5-67. An incident occurred during ultra-violet only irradiation between steps B and C. The chamber pressure rose up to1,3 Pa because of some damage in the secondary vacuum pump. This incident resulted in an increase in the reflectance, which was measured and reported. Since test were resumed after repairing the pump and some bleaching occurred, the data for steps C and D should be looked at cautiously.

7.4. Electrical resistance. According to Paillous (1976) [96] this coating exhibited a small electrical conductivity during particulate irradiation. After air exposure the electrical conductivity vanished to zero. The reason for this effect remains unclear.

8. ENVIRONMENTAL BEHAVIOR

PSG 120 has been space-qualified by CNES. The qualification tests include:

8.1. Prelaunch. Moisture resistance test.

Relative humidity: above 90%.

Temperature: 363 K.

Duration: 5 d.

The coating showed no failures, not even tiny unstuck spots. From Guillaumon & Guillin (1979) [52]. ASTRAL (1976)a [6] quotes a duration of 7 d.

8.2. Postlaunch. Cure time for minimizing outgassing, in Table 5-14. The coating withstood vibrations per D2 Spacecraft Specification with no apparent change in adhesion.

8.2.1. Ascent. Thermal soak at normal pressure.

Temperature: 523 K.

Duration: 100 h.

Thermal soak under vacuum.

Pressure: below 1,3x10^{-5} Pa.

Temperature: 523 K.

Duration: 100 h.

From ASTRAL (1976)a [6].

8.2.2. Orbital. Data on Ultra-violet and particulate irradiation damage of this coating show a moderate increase in the solar absorptance which ceases before long. Compare, for example, the values of α_s after 2 and 3 years in orbit, as given in Figure 5-56.

9. THERMAL CYCLING

No cracking of the surface was observed after the following tests:

Pressure: below 1,3x10^{-4} Pa.

Temperature:

T_{min} = 173 K

T_{max} = 373 K.

Number of cycles: 200.

Cycle time: 1,5 h.

From ASTRAL (1976)a [6], Guillaumon & Guillin (1979) [53].

10. SOURCE

ASTRAL, Peintures et Vernis, 164 rue Ambroise Croizat, boîte postale 140.

93024 Saint-Denis. Cédex 1, France.

Contact Person: Mr. B. Dumont. Département Aéronautique.

11. COST

P 123 primer

One kit consists of:

1 liter Base P 123

2,5 liters Hardener CX 124

1 liter Thinner S 125

Cost: 1550 FF.

P 128 primer

One kit consists of:

0,25 liters P 128

Cost: 230 FF.

PSG 120 FD

One kit consists of:

1 kg Base PSG 120 FD

0,2 kg Hardener CT 122

1 kg Thinner S 105

Cost: 3300 FF.

These costs are FOB, factory of Montataire, Oise-France.

From a quotation dated Aug. 1984.

12. PAST SPATIAL USE

This coating has been used in several satellites, and considered for use in some other cases. Several examples of spatial use are given in the following Table.

Spacecraft or Programme	Launching Date	Used or Tested	References
D2A (Tuornesol) D2B (Aura)	April 15, 1971 Sept. 27, 1975	Used	ASTRAL (1976)a [6]
SRET 2 (MAS 2)	June 5, 1975	Tested in two different experiments.	ASTRAL (1976)a [6] Rolfo (1976) [106].
Meteosat 1 Meteosat 2	Nov. 23, 1977 June 19, 1981	Used in SRET 2-tested radiant cooler. (See L, clause 6.6.3).	Rolfo (1976) [106].
LDEF	April 6, 1984. Launched from Challenger	Experimented A0138-6 by A. Paillous & J.C. Guillaumon.	Clark (1981) [30].
Olympus	Scheduled for early 1988.	Used in the Propagation Antenna Package.	Domingo (1987) [36]

5.2.5 Zinc Oxide-Potassium Silicate

1. COMPOSITION

Pigment: New Jersey Zinc Co., SP500 zinc oxide.

Binder: Potassium silicate.

Filler: Chopped glass fibers (Triton).

From Simon (1974) [118] and ASTRAL (1981) [9].

2. FORMULATION

Not given by the producer.

3. USUAL DESIGNATION

PSZ 184. ASTRAL.

4. SUBSTRATE

Any clean substrate, particularly aluminium alloys, stainless steel, copper alloys. See Preparation of surfaces for painting.

5. METHOD OF APPLICATION

5.1. Preparation of paint for application. PSZ 184 is delivered as a system consisting of:

Pigment.

Binder.

Chopped glass fibers (Triton).

Glass balls.

Distilled water (as much as required for grinding).

In order to prepare the paint:

1. Mix Triton, glass balls and distilled water.
2. Grind the resulting mixing for 30 min by use of a "Red Devil" stirrer.
3. Add to above mixing the pigment and the binder.
4. Grind the solution for 30 min by use of a "Red Devil" stirrer.
5. Add $8x10^{-2}$ kg of distilled water.
6. Filter through a nylon 30 mesh ($6,3x10^{-4}$ m mesh size) in order to separate the glass balls.
7. Add 20% by weight of distilled water.
8. Filter through a nylon 300 mesh ($5x10^{-5}$ m mesh size).

Shelf life of the paint: 24 h.

From ASTRAL (1981) [9].

5.2. Preparation of surfaces for painting.

1. For aluminium alloys, stainless steel, copper alloys.

   The substrate should be thoroughly degreased with trichloroethylene, then scraped with an alkaline paint remover (steel wool and commercial detergent type VIM), or sandblasted, and copiously rinsed with water.

   When the above preparation becomes unfeasible, a satisfactory result is achieved by use of the procedure given below, which can be applied to other substrates.

2. For other substrates.

   Careful degreasing with trichloroethylene followed by a final cleaning with Freon TF or ethyl ether and a spray coat of P 131 primer.

From ASTRAL (1981) [9].

5.3. Application of paint. By spray techniques using a Kremlin model Junior or comparable gun at about $2,8x10^5$ Pa air or nitrogen pressure.

Compulsory conditions for application are:

Ambient temperature in the range 291 K - 298 K.

Relative humidity above 65%.

3 very thin layers should be applied to start with. Then 8 or 9 crosswise layers are sprayed on. The last layers show a glossy appearance during application. The successive layer should be allowed to dry slowly and uniformly until the gloss has disappeared (30 min - 35 min) before spraying on the next layer.

After curing the surface can be rinsed with soapy water.

Areas to be retouched should be slightly polished with steel wool and water. Then, a thin layer is applied. After around 5 min drying, one or two crosswise layers can be sprayed on.

From ASTRAL (1981) [9].

5.4. Coating thickness. Between 10^{-4} m and $1,2x10^{-4}$ m.

From ASTRAL (1981) [9].

5.5. Curing process. At 293 K.

Dust off: 3 h,

Deep dry: 24 h.

From ASTRAL (1981) [9].

6. SOLVENTS RESISTANCE

Not attacked by solvents.

The paint can be removed mechanically.

7. PHYSICAL PROPERTIES

7.1. Density. Not given by the producer.

7.2. Outgassing. Sample at 398 K to 423 K, below $1,3x10^{-3}$ Pa pressure, during 24 h. Condensing plate held at 298 K.

Total mass loss, % TML: 2,26.

Collected volatile condensable materials, % CVCM: 0,01.

Water is the only volatile component of this inorganic coating.

From ASTRAL (1981) [9].

7.3. Thermal radiation properties.

7.3.1. Emittance.

7.3.1.1. Hemispherical total emittance. See Table 5-20, which also gives information on solar absorptance, α_s.

Table 5-20: Hemispherical Total Emittance, ε, and Solar Absorptance, α_s, of PSZ 184

Description	Comments	ε	α_s
As received. Initial value.		0,94± 0,02	0,14± 0,02
After moisture resistance test. Relative humidity: 90%. Temperature: 363 K. During 7 d.	Emittance measured by use of a portable emissometer.	0,93± 0,04	0,14± 0,02
After thermal cycling under vacuum. 200 cycles. Temperature range: 173 K - 373 K.		0,94± 0,04	0,14± 0,02

Description	Comments	ε	α_s
Pressure: 1,3x10^{-3} Pa.			
After cumulative tests, moisture resistance plus thermal cycling, both as above.		0,90± 0,04	0,14± 0,02

NOTE From ASTRAL (1981) [9].

7.3.2. Absorptance.

7.3.2.1. Solar absorptance. See Table 5-20 above.

7.3.2.5. Effects of the Space Environment on absorptance.

7.3.2.5.1. Ultra-Violet Radiation. Figure 5-68 to Figure 5-70, from CNES.

Data measured as in paragraph 7.3.1.3.1, clause 5.2.4.

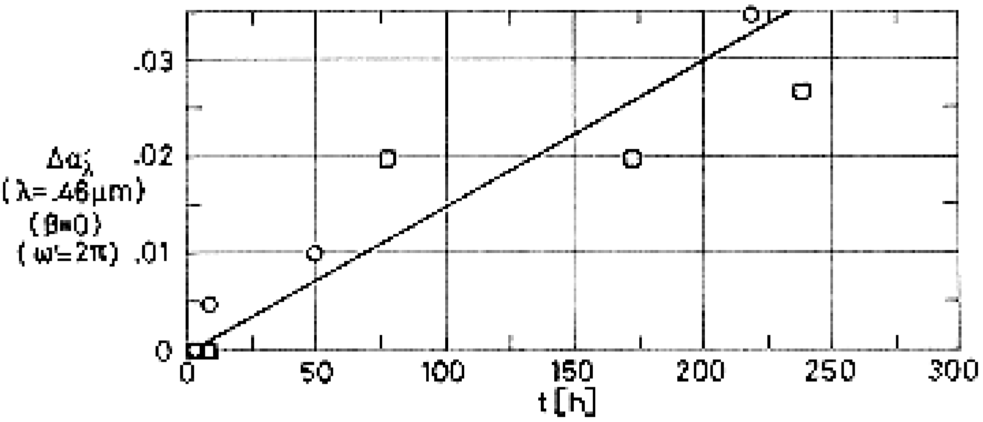

Note: non-si units are used in this figure

Figure 5-68: Change in normal-hemispherical spectral absorptance, $\Delta\alpha'_\lambda$, of PSZ 184 coating, due to UV Radiation, vs. exposure time, *t*. Wavelength, λ = 0,46x10^{-6} m. See Explanation in the caption of Figure 5-69. From Simon (1974) [118].

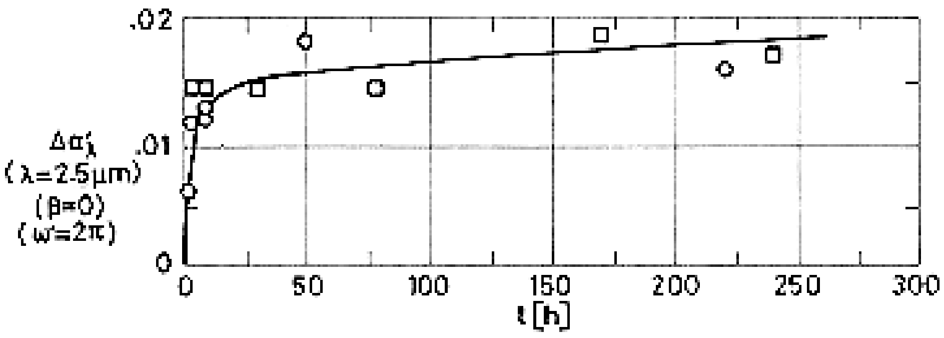

Note: non-si units are used in this figure

Figure 5-69: Change in normal-hemispherical spectral absorptance, $\Delta\alpha'_\lambda$, of PSZ 184 coating, due to UV Radiation, vs. exposure time, t. Wavelength, $\lambda = 2{,}5\mathrm{x}10^{-6}$ m. From Simon (1974) [118].

Explanation

Key	Sample Temperature [K]	Comments
○	353	
□	283	After 9 h of UV radiation plus 25 h in nitrogen (bleaching).

Data concerning the effects of ultra-violet radiation on solar absorptance are given in Figure 5-70. α_s deduced from spectral reflectance measured as above.

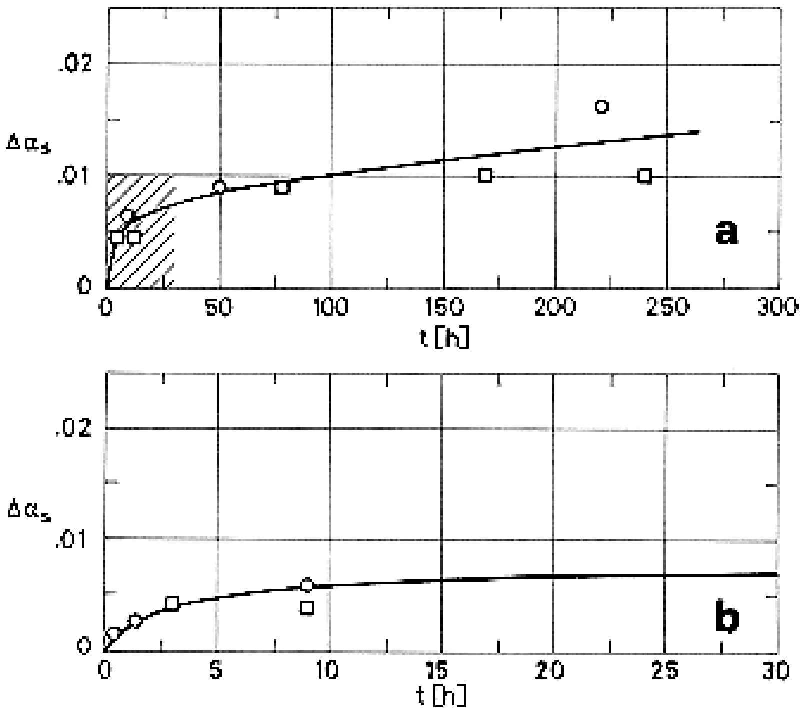

Note: non-si units are used in this figure

Figure 5-70: Change in solar absorptance, *Δα*$_s$, of PSZ 184 coating, due to UV Radiation, vs. exposure time, *t*. Shaded zone in *a* is enlarged in *b*. From Simon (1974) [118].

Explanation

Key	Sample Temperature [K]	Comments
○	353	
□	283	After 9 h of UV radiation plus 25 h in nitrogen (bleaching).

7.3.2.5.3. Protons only exposure. Table 5-21 after DERTS.

Solar absorptance from spectral reflectance data given in paragraph 7.3.3.2.3, clause 5.2.5.

Comments in paragraph 7.3.2.5.3 of clause 5.2.4 are relevant here. Now the initial value is α_{so} = 0,16.

Table 5-21: Protons Radiation Effects on Solar Absorptance of PSZ 184 Coating

Intensity [keV]	45			75			150		
Integrated Flux [p.m^{-2}]	α_s	$\Delta\alpha_s$	$\Delta\alpha_s/\alpha_s$	α_s [b]	$\Delta\alpha_s$	$\Delta\alpha_s/\alpha_s$	α_s	$\Delta\alpha_s$	$\Delta\alpha_s/\alpha_s$
Before (in air)	0,307								
Before (in vacuum)	0,349								
10^{17}	0,348	–0,001	–0,002						
10^{18} [a]	0,348	–0,001	–0,002						
10^{19}	0,376	0,027	0,071						
2,1x10^{19}	0,407	0,058	0,142						
After (in air)	0,386								
Before (in air)	0,279			0,328			0,332		
Before (in vacuum)	0,318			0,375			0,383		
10^{17}	0,323	0,005	0,015	0,384	0,009	0,024	0,396	0,013	0,033
10^{18}	0,334	0,016	0,047	0,394	0,019	0,049	0,411	0,028	0,068
10^{19}	0,362	0,044	0,122	0,420	0,045	0,107	0,442	0,059	0,134
2,1x10^{19}	0,396	0,078	0,196	0,443	0,068	0,154	0,471	0,088	0,187
After (in air)	0,358			0,392			0,405		
Comments (for silicated primer only).	Small cracks appeared after tests.		Severe cracking, particularly in the lower part of the sample (held up-right). Substrate badly primed.						

[a] On P 131 primer. [b] On silicated primer.

NOTE From Paillous, Amat, Marco & Panabiere (1977) [97].

7.3.2.5.4. Electrons only exposure. Table 5-22 after DERTS.

Solar absorptance from the spectral reflectance data given in paragraph 7.3.3.2.4 of clause 5.2.5. Sample on silicated primer.

Table 5-22: Electrons Radiation Effects on Solar Absorptance of PSZ 184 Coating

Intensity [keV]	40			80			210		
Integrated Flux [e.m^{-2}]	α_s	$\Delta\alpha_s$	$\Delta\alpha_s/\alpha_s$	α_s	$\Delta\alpha_s$	$\Delta\alpha_s/\alpha_s$	α_s	$\Delta\alpha_s$	$\Delta\alpha_s/\alpha_s$
Before (in air)	0,344			0,330					
Before (in vacuum)	0,351			0,360			0,341		
2x10^{14}	0,422	0,071	0,168	0,450	0,090	0,199	0,471	0,130	0,277
5x10^{14}	0,457	0,106	0,232	0,486	0,126	0,259	0,523	0,182	0,348
10^{15}	0,480	0,129	0,269	0,517	0,157	0,304	0,533	0,192	0,361
2x10^{15}	0,493	0,142	0,288						
After (in air)	0,326			0,360			0,359		
Comments	Very severe cracking. The paint becomes almost scaled off.			Small cracks away from the center of the sample.			Small cracks. Substrate badly primed.		

NOTE From Paillous, Amat, Marco & Panabiere (1977) [97].

7.3.2.5.6. Combined exposure. Table 5-23 after DERTS.

Solar absorptance from spectral reflectance data.

The test simulate geosynchronous orbit exposure of the Orbital Test Satellite (OTS) equatorial faces.

The "Corrected" values in Table 5-23 were used to estimate coating degradation up to 3 years in orbit, Figure 5-71.

Incidents during testing, see paragraph 7.3.3.2.6 of clause 5.2.4, cast doubts on the validity of the data beyond 1 year in orbit.

Table 5-23: Combined Exposure Effects on Solar Absorptance of PSZ 184 Coating

Test Conditions	Sample 1						Sample 2					
	Measured in situ			Corrected [a]			Measured in situ			Corrected [a]		
	α_s	$\Delta\alpha_s$	$\Delta\alpha_s/\alpha_s$	α_s	$\Delta\alpha_s$	$\Delta\alpha_s/\alpha_s$	α_s	$\Delta\alpha_s$	$\Delta\alpha_s/\alpha_s$	α_s	$\Delta\alpha_s$	$\Delta\alpha_s/\alpha_s$
BEFORE IRRADIATION	0,319			0,160			0,349			0,160		
AFTER *A* UNDER VACUUM [b]	0,332	0,013	0,041	0,176	0,016	0,100	0,372	0,023	0,066	0,189	0,029	0,181
BEFORE *B*	0,347	0,028	0,089	0,195	0,035	0,219	0,356	0,008	0,022	0,170	0,010	0,062
AFTER *B* [b]	0,390	0,071	0,225	0,249	0,089	0,556	0,405	0,056	0,161	0,230	0,070	0,437
AFTER PUMP DAMAGE [c]	0,373	0,055	0,080	0,229	0,069	0,431	0,386	0,037	0,107	0,206	0,046	0,287
BEFORE *C*	0,396	0,078	0,243	0,258	0,098	0,612	0,417	0,069	0,197	0,247	0,087	0,544
AFTER *C* [b]	0,421	0,103	0,322	0,289	0,129	0,806	0,438	0,089	0,256	0,272	0,112	0,700
BEFORE *D*	0,415	0,097	0,304	0,282	0,122	0,762	0,435	0,086	0,247	0,268	0,108	0,675
AFTER *D* UNDER VACUUM [b]	0,425	0,107	0,335	0,294	0,134	0,838	0,438	0,089	0,257	0,272	0,112	0,700
AFTER *D* AND AIR EXPOSURE	0,395	0,076	0,238	0,255	0,095	0,594	0,415	0,066	0,189	0,243	0,083	0,519

[a] The correction has been made by the compiler as follows:

1) Value before irradiation, $\alpha_{s0} = 0{,}16$.

2) $\Delta\alpha_{s\ corrected}/\Delta\alpha_{s\ in\ situ} = (1-\alpha_{s0})/(1-\alpha_{s0\ in\ situ}) = 0{,}84/0{,}67$

where α_{s0} has been measured (in air) with an integrating sphere attached to a Beckman DK2A reflectometer. $\alpha_{s0in\ situ}$ is the value measured before irradiation as indicated in paragraph 7.3.3.2.6 of clause 5.2.4.

[b] Steps *A* to *D* correspond, respectively, to the following times in geosynchronous orbit.

A: 0,18 yr = 508 ESH. *B*: 0,94 yr = 2443 ESH. *C*: 2,11 yr = 5604 ESH. *D*: 3 yr = 7949 ESH.

[c] See paragraph 7.3.3.2.6 of clause 5.2.4 for further details.

NOTE From Paillous (1976) [96].

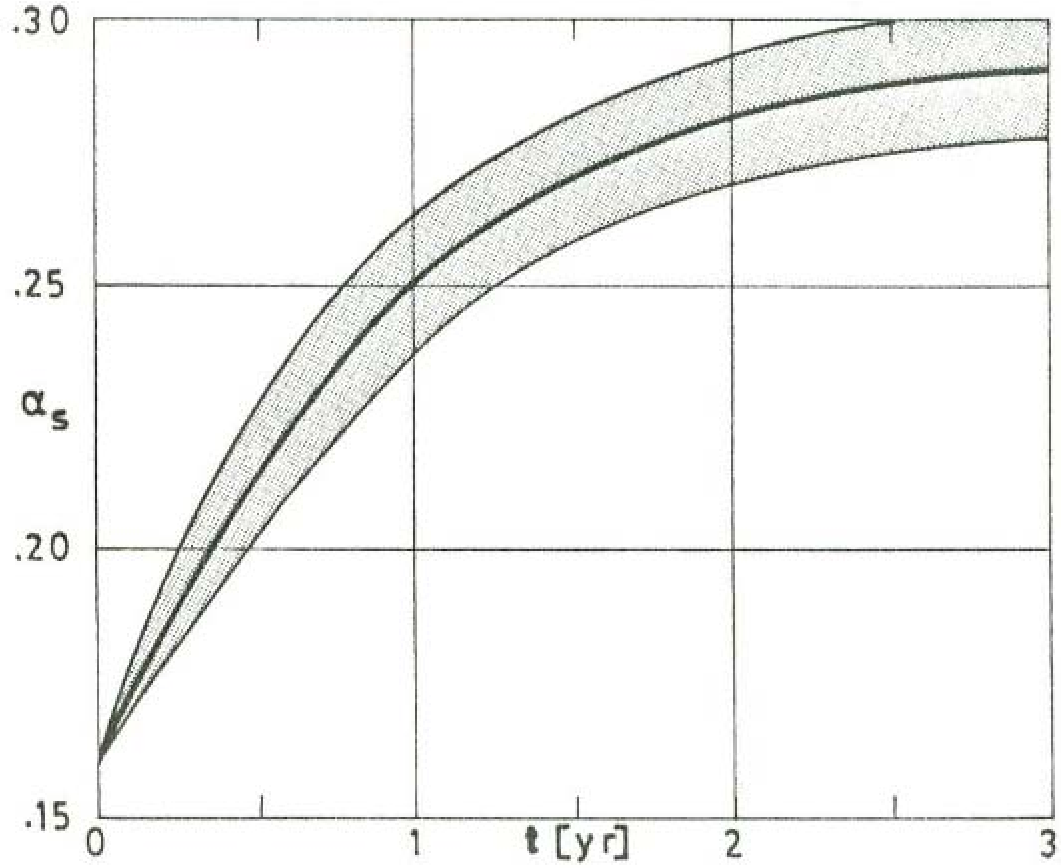

Note: non-si units are used in this figure

Figure 5-71: Estimated change in solar absorptance, α_s, of PSZ 184 vs. time, t. From Paillous (1976) [96].

7.3.3. Reflectance.

7.3.3.1. Normal-hemispherical spectral reflectance. Figure 5-72 from CNES.

Chamber pressure below 1,3x10^{-5} Pa.

Sample temperature not given.

Spectral reflectance measured in situ as indicated in paragraph 7.3.3.2.3 of clause 5.2.4.

7.3.3.2. Effects of the Space Environment on reflectance.

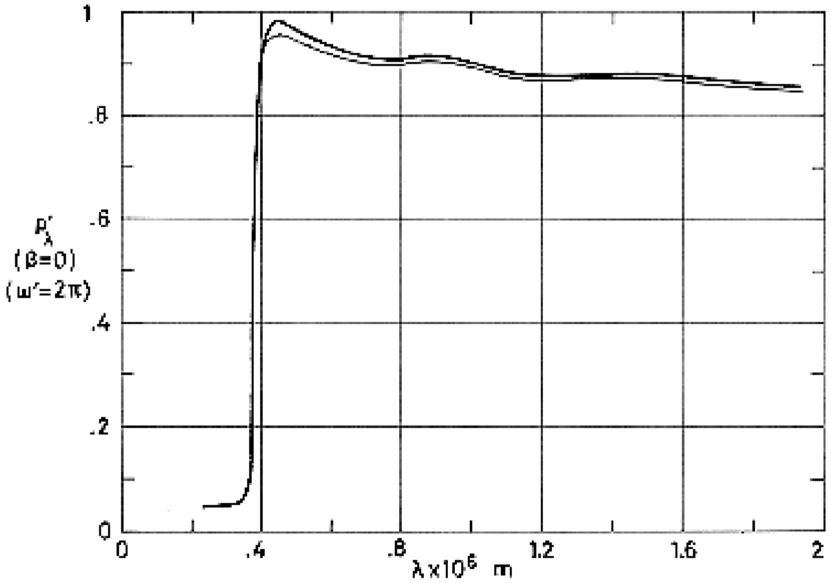

Note: non-si units are used in this figure

Figure 5-72: Effect of Ultra-Violet Radiation on normal-hemispherical spectral reflectance, ρ'_λ, of PSZ 184 coating vs. wavelength, λ.
Thick line: Before irradiation. $p<1{,}3x10^{-5}$ Pa.
Thin line: After irradiation. $p<1{,}3x10^{-5}$ Pa. 1 Sun level.
Neither sample temperature nor exposure time are given. From Simon (1974) [118].

7.3.3.2.1. Ultra-Violet radiation. Figure 5-72.

Sample conditions and spectral reflectance measurements as above.

Sample irradiated in vacuum as in paragraph 7.3.3.2.1 of clause 5.2.4.

Radiation flux density at the sample level: ~1 Sun.

Exposure time not given.

See Figure 5-68 and ff. where similar data from CNES have been also presented.

Figure 5-72 is interesting from a qualitative point of view when compared with Figure 5-58. In particular, the decreased reflectance in the infrared (λ $0{,}7x10^{-6}$ m) resulting from ultra-violet radiation, which is characteristic of silicone-binded white paints such as PSG 120, does not appear in this case where the binder is potassium silicate.

7.3.3.2.3. Protons only exposure. Figure 5-73 and ff., from DERTS.

Sample on aluminium substrate.

Irradiation and measurements as for PSG 120, paragraph 7.3.3.2.3 of clause 5.2.4.

One of the samples (that on silicated primer) exhibited severe cracks after exposure. These cracks have been attributed to bad priming of the substrate as it was made clear by the fact that a specimen using PSZ 184 on P 131 primer did not crack after a 45 keV proton irradiation. See Figure 5-73, and also Table 5-21.

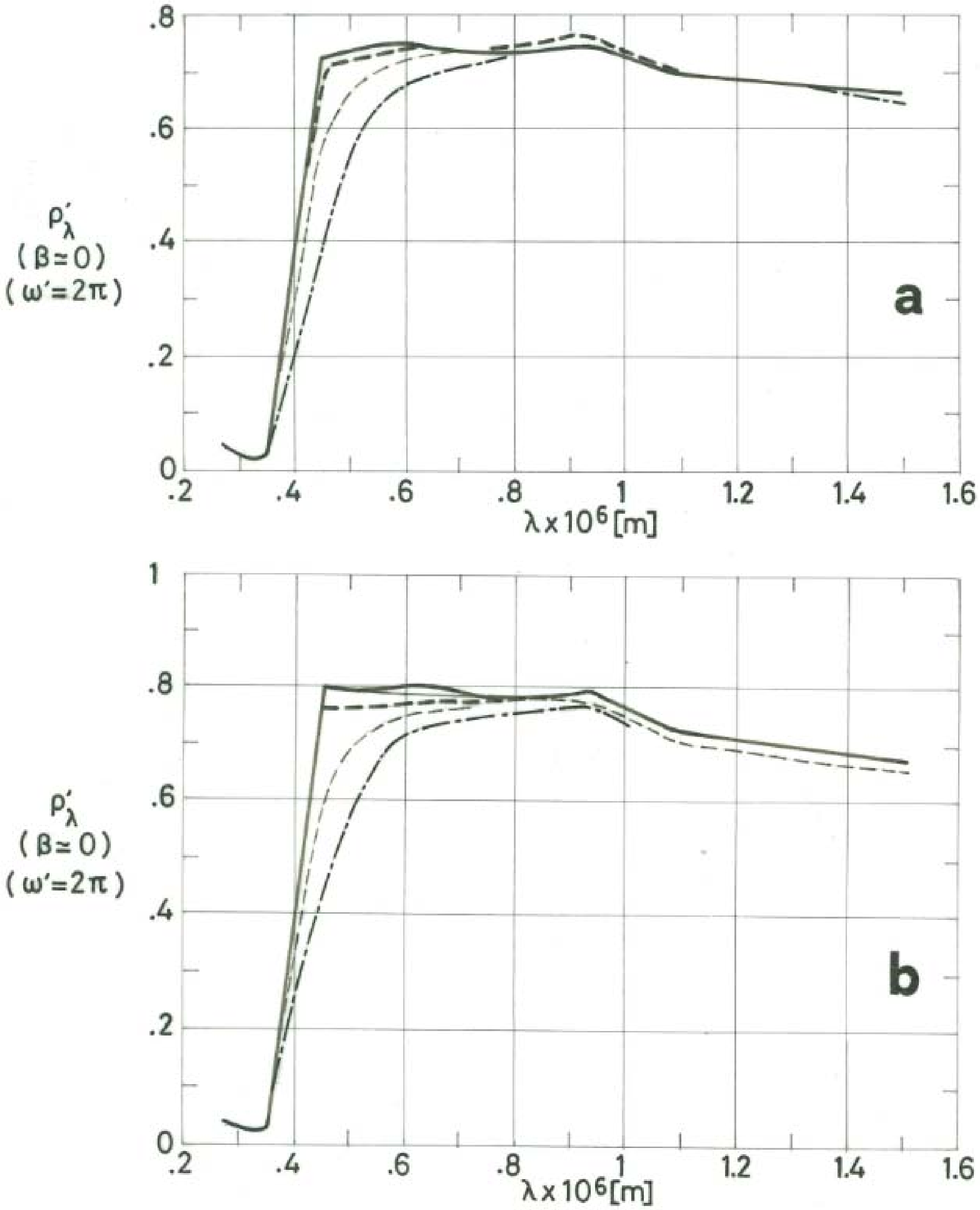

Note: non-si units are used in this figure

Figure 5-73: Effect of Protons Radiation on normal-hemispherical spectral reflectance, ρ'_λ, of PSZ 184 coating vs. wavelength, λ. *a* Coating on P 131 primer. *b* Coating on silicated primer. Radiation intensity ≅ 45 keV. See Explanation in the caption of Figure 5-74. From Paillous, Amat, Marco & Panabiere (1977) [97].

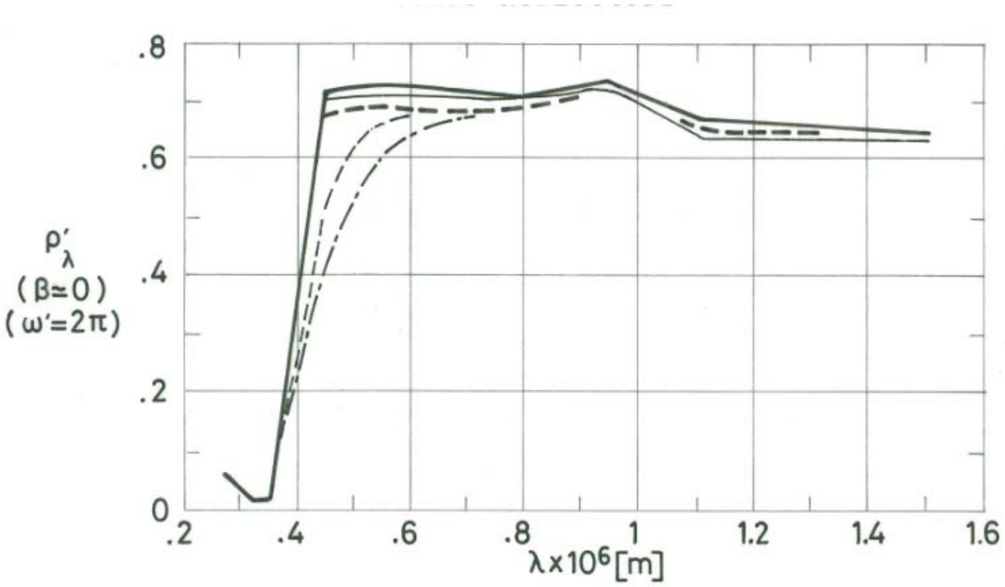

Note: non-si units are used in this figure

Figure 5-74: Effect of Protons Radiation on normal-hemispherical spectral reflectance, ρ'_λ, of PSZ 184 coating, on silicated primer, vs. wavelength, λ. Radiation intensity ≅ 75 keV. From Paillous, Amat, Marco & Panabiere (1977) [97].

Explanation

Key	Intensity [keV]	Flux [p.m^{-2}.s^{-1}]	Integrated Flux [p.m^{-2}]	Cumulative Integrated Flux [p.m^{-2}]	Comments
▬▬▬	45 keV in Figure 5-73. 75 keV in Figure 5-74.				Sample on aluminium substrate. $p = 1{,}3\text{x}10^{-4}$ Pa. $T = 303$ K ± 0,5 K. Incidence of the protons beam: 0°. Small cracks appeared after tests in the case of Figure 5-73b. Cracking was severest in the case of Figure 5-74. Cracks attributed to bad priming of the substrate.
———		1,3x10^{14}	10^{17}	10^{17}	
▬ ▬		2,5x10^{14}	9x10^{17}	10^{18}	
— —		2,5x10^{14} (Figure 5-73). 6,2x10^{14} (Figure 5-74).	9x10^{18}	10^{19}	
▬·▬		6,2x10^{14}	1,1x10^{19} (Figure 5-73). 1,8x10^{19} (Figure 5-74).	2,1x10^{19} (Figure 5-73). 2,8x10^{19} (Figure 5-74).	

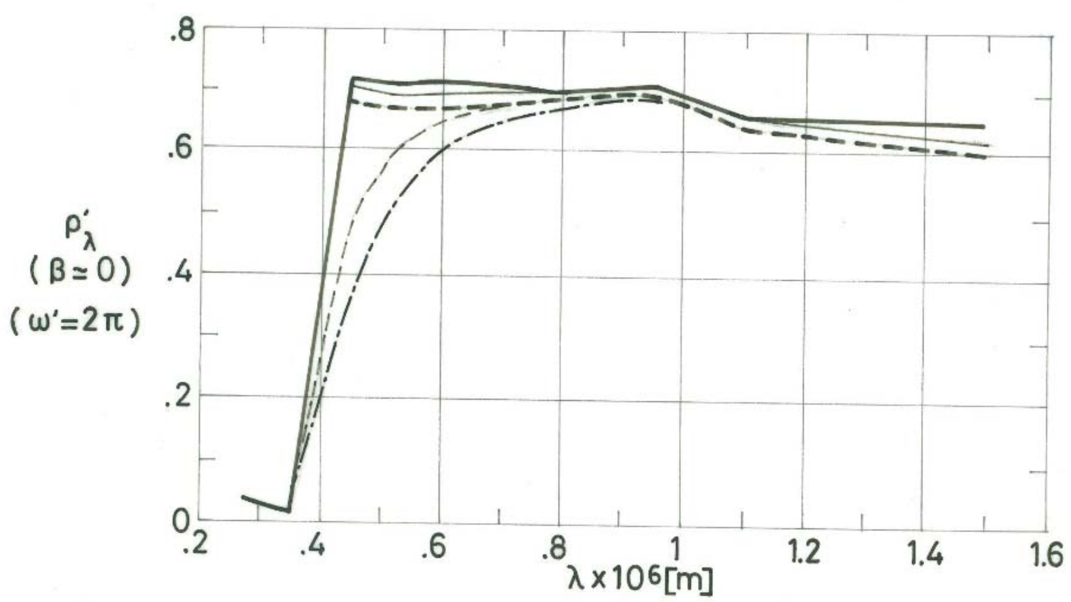

Note: non-si units are used in this figure

Figure 5-75: Effect of Protons Radiation on normal-hemispherical spectral reflectance, ρ'_{λ}, of PSZ 184 coating, on silicated primer, vs. wavelength, λ. Radiation intensity ≅ 150 keV. From Paillous, Amat, Marco & Panabiere (1977) [97].

Explanation

Key	Intensity [keV]	Flux [p.m^{-2}.s^{-1}]	Integrated Flux [p.m^{-2}]	Cumulative Integrated Flux [p.m^{-2}]	Comments
━━━━	150				Sample on aluminium substrate. Silicated primer p = 1,3x10^{-4} Pa. T = 303 K ± 0,5 K. Incidence of the protons beam: 0°. Severe cracking appeared after tests, particularly in the lower part of the sample (held upright). Substrate badly primed.
────		1,3x10^{14}	10^{17}	10^{17}	
━━ ━━		2,5x10^{14}	9x10^{17}	10^{18}	
── ──		6,2x10^{14}	9x10^{18}	10^{19}	
━━·━━		6,2x10^{14}	1,8x10^{19}	2,8x10^{19}	

7.3.3.2.4. Electrons only exposure. Figure 5-76 and ff., from DERTS.

Sample on aluminium substrate. Silicated primer.

Irradiation as for PSG 120, p. 1-68.

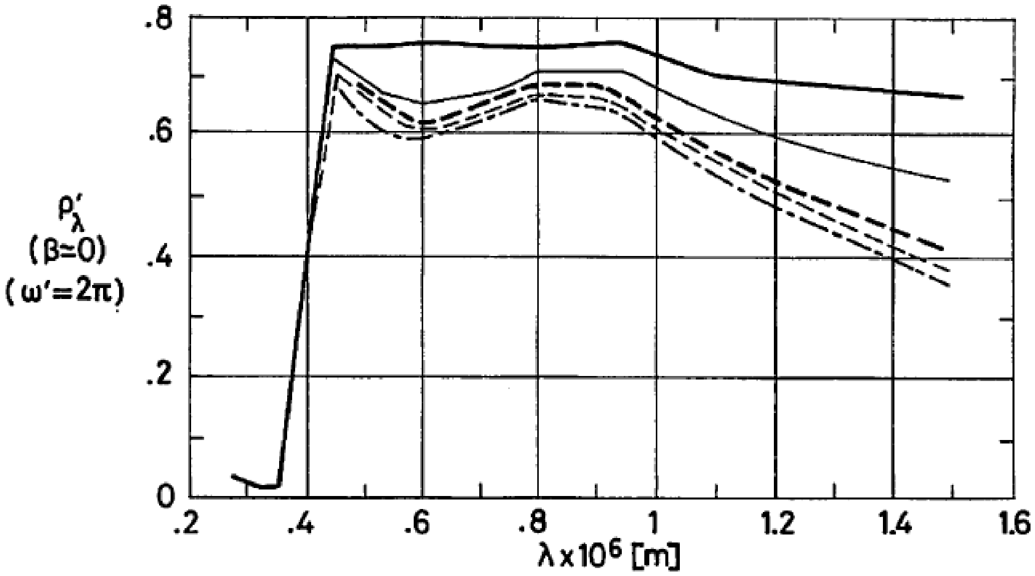

Note: non-si units are used in this figure

Figure 5-76: Effect of Electrons Radiation on normal-hemispherical spectral reflectance, ρ'_λ, of PSZ 184 coating, on silicated primer, vs. wavelength, λ. Radiation intensity ≅ 40 keV. From Paillous, Amat, Marco & Panabiere (1977) [97].

Explanation

Key	Intensity [keV]	Flux [$e.m^{-2}.s^{-1}$]	Integrated Flux [$e.m^{-2}$]	Cumulative Integrated Flux [$e.m^{-2}$]	Comments
▬▬▬	40				Sample on aluminium substrate. Silicated primer $p = 1{,}3\text{x}10^{-4}$ Pa. $T = 303$ K ± 0,5 K. Incidence of the electrons beam: 0°. Very severe cracking. The paint becomes almost scaled off. Substrate badly primed.
———		2,7x10^{14}	2x10^{18}	2x10^{18}	
▬ ▬		4x10^{14}	3x10^{18}	5x10^{18}	
— —		4x10^{14}	5x10^{18}	10^{19}	
▬·▬		5,4x10^{14}	10^{19}	2x10^{19}	

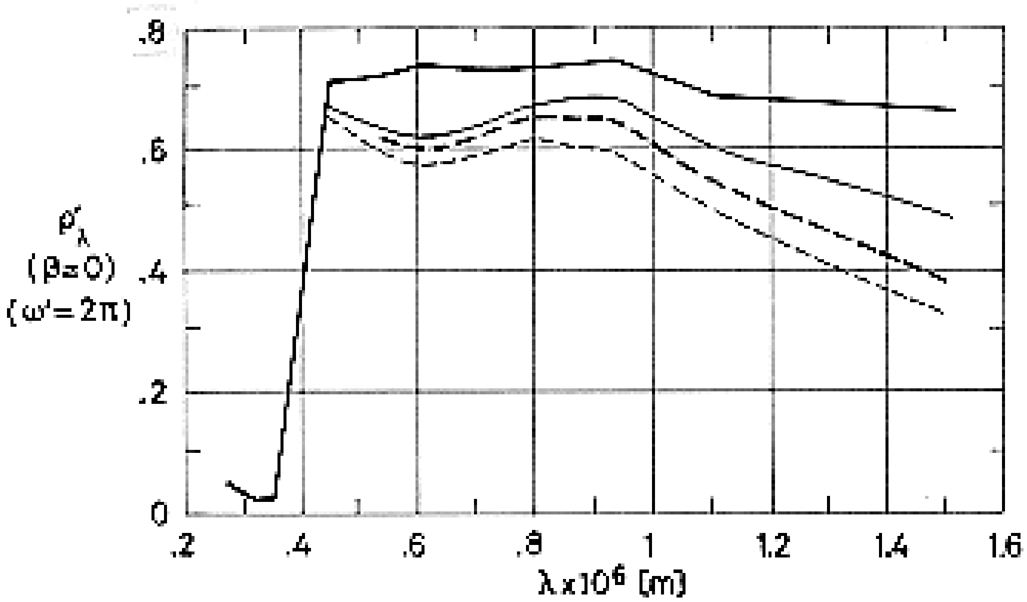

Note: non-si units are used in this figure

Figure 5-77: Effect of Electrons Radiation on normal-hemispherical spectral reflectance, ρ'_λ, of PSZ 184 coating, on silicated primer, vs. wavelength, λ. Radiation intensity ≅ 80 keV. From Paillous, Amat, Marco & Panabiere (1977) [97].

Explanation

Key	Intensity [keV]	Flux $[e.m^{-2}.s^{-1}]$	Integrated Flux $[e.m^{-2}]$	Cumulative Integrated Flux $[e.m^{-2}]$	Comments
━━━	80				Sample on aluminium substrate. Silicated primer p = 1,3x10^{-4} Pa. T = 303 K ± 0,5 K. Incidence of the electrons beam: 0°. Small cracks away from the center of the sample. Substrate badly primed.
———		2,9x10^{14}	2x10^{18}	2x10^{18}	
▬ ▬		2,8x10^{14}	3x10^{18}	5x10^{18}	
— —		5,3x10^{14}	5x10^{18}	10^{19}	

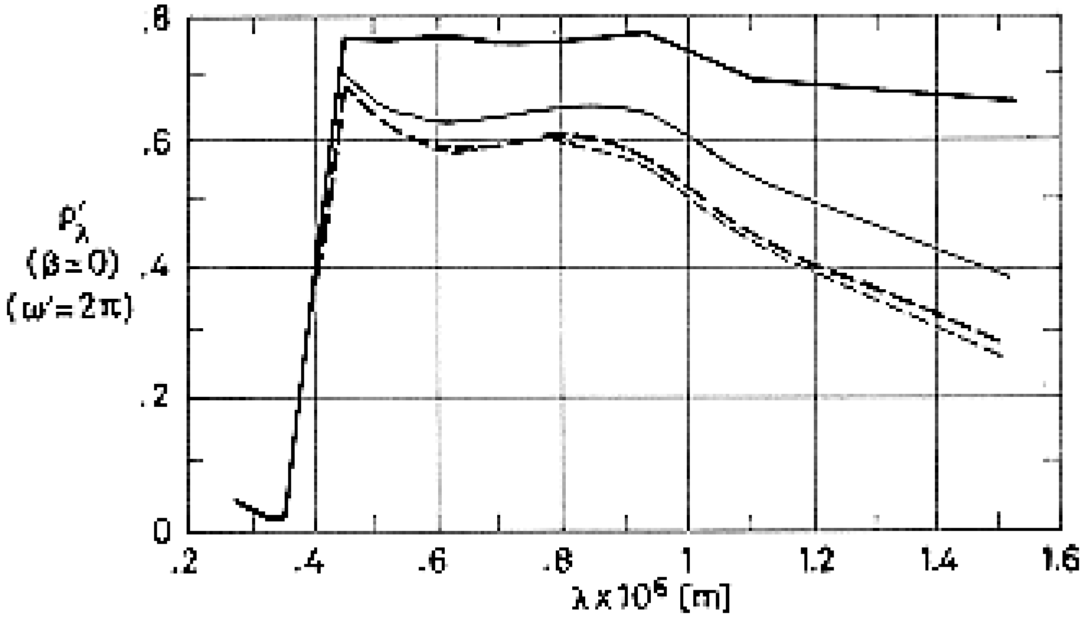

Note: non-si units are used in this figure

Figure 5-78: Effect of Electrons Radiation on normal-hemispherical spectral reflectance, ρ'_λ, of PSZ 184 coating, on silicated primer, vs. wavelength, λ. Radiation intensity ≅ 210 keV. From Paillous, Amat, Marco & Panabiere (1977) [97].

Explanation

Key	Intensity [keV]	Flux [e.m^{-2}.s^{-1}]	Integrated Flux [e.m^{-2}]	Cumulative Integrated Flux [e.m^{-2}]	Comments
━━━	210				Sample on aluminium substrate. Silicated primer $p = 1{,}3\text{x}10^{-4}$ Pa. $T = 303$ K ± 0,5 K. Incidence of the electrons beam: 45°. Small cracks. Substrate badly primed.
───		$3{,}0\text{x}10^{14}$	$2\text{x}10^{18}$	$2\text{x}10^{18}$	
━ ━		$3{,}1\text{x}10^{14}$	$3\text{x}10^{18}$	$5\text{x}10^{18}$	
─ ─		$6{,}3\text{x}10^{14}$	$5\text{x}10^{18}$	10^{19}	

An attempt has been made to check the validity of the analytical model of solar absorptance degradation, set forth by Bourrieau (1978) [19], against the experimental results which have been represented in paragraph 7.3.3.2.3 of clause 5.2.5.

For a description of the mentioned analytical model see paragraph 7.3.3.2.4 of clause 5.2.4.

The comparison was deceptive in the case of PSZ 184 because of the already mentioned cracks. Two absorption bands were detected, $\lambda = 0{,}61\text{x}10^{-6}$ m and $\lambda = 2{,}1\text{x}10^{-6}$ m, but only the last one was workable, the first being masked by a drift of the absorption threshold of the paint. No definite results were obtained.

7.3.3.2.6. Combined exposure. Figure 5-79 and Figure 5-80 from DERTS.

Sample on aluminium substrate.

Irradiation and measurements as for PSG 120, paragraph 7.3.3.2.6 of clause 5.2.4.

Data presented are:

1. Solar reflectance (in air) before irradiation, α_{s0} = 0,16, given in Table 5-23.
2. In situ spectral reflectance, Figure 5-79 and Figure 5-80

See also Table 5-23.

The chamber pressure rose up to 1,3 Pa because of some damage in the secondary vacuum pump. This incident resulted in an unintentional bleaching of the coating. Test were resumed after repairing the pump. Data beyond1 year in orbit should be used cautiously.

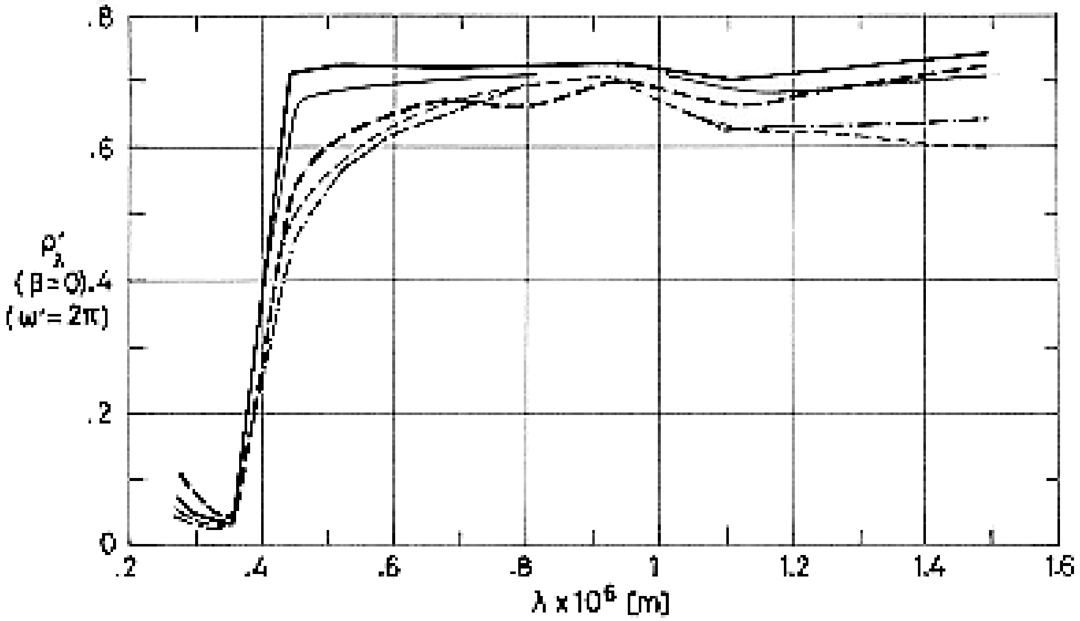

Note: non-si units are used in this figure

Figure 5-79: Effect of Combined Exposure, simulating up to three years in geosynchronous orbit, on normal-hemispherical spectral reflectance, ρ'_λ, of PSZ 184 coating, vs. wavelength, λ. From Paillous (1976) [96].

Explanation

Key	Description	Comments
━━━	After 125 h below $1{,}3 \times 10^{-4}$ Pa pressure. T = 363 K.	
───	After step A (0,19 years in orbit). T = 363 K.	

Key	Description	Comments
▬ ▬	After step *B* (0,94 years in orbit). $T = 363$ K.	
— —	After step *C* (2,11 years in orbit). $T = 363$ K.	After unintentional O_2 bleaching.
▬•▬	After step *D* (3 years in orbit). $T = 363$ K.	

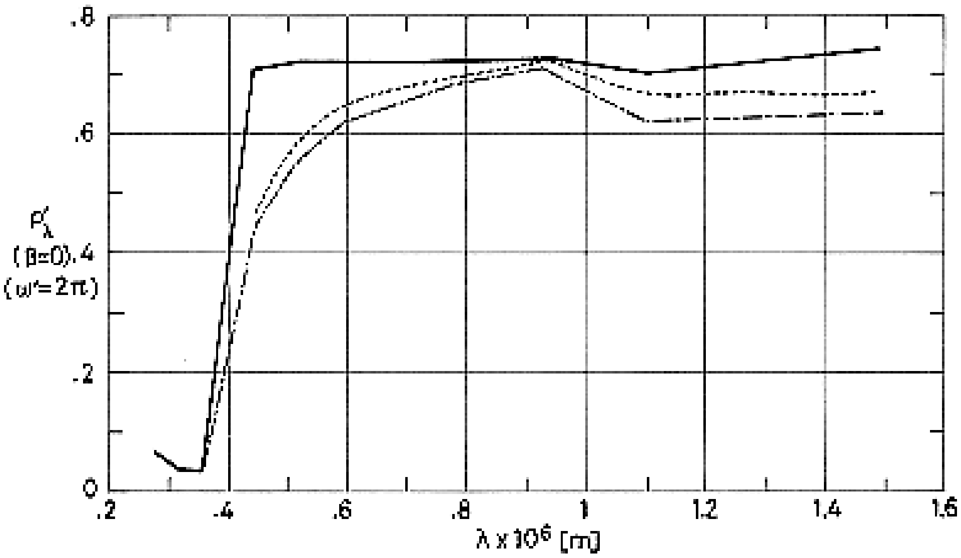

Note: non-si units are used in this figure

Figure 5-80: Effect of O_2 bleaching, after Combined Exposure, on normal-hemispherical spectral reflectance, ρ'_λ, of PSZ 184 coating, vs. wavelength, λ. Curves ▬▬▬ and — — are those shown in Figure 5-79. From Paillous (1976) [96].

Explanation

Key	Description	Comments
▬▬▬	After 125 h below $1{,}3 \times 10^{-4}$ Pa pressure. $T = 363$ K.	
— —	After step *D* (3 years in orbit). $T = 363$ K.	After unintentional O_2 bleaching.
••••••••	After step *D* and Air exposure. $T = 293$ K.	

7.4. Electrical resistance. PSZ 184 coating is nonconductive (Paillous (1976) [96]).

8. ENVIRONMENTAL BEHAVIOR

8.1. Prelaunch. The use of this coating in spacecraft demands great care. In addition to compulsory application conditions (preparation of the surface, humidity level, ambient temperature,...), it requires a particularly well trained applier. The coating withstood moisture resistance tests (Table 5-20). Neither degradation of its optical properties nor of its adhesion were observed.

8.2. Postlaunch. Outgassing characteristics are given in p. 1-86.

8.2.1. Ascent. See Table 5-20 for influence of thermal cycling under vacuum and moisture resistance plus thermal cycling. Changes look minimal. Nevertheless, some cracks and slight scalding off near the borders resulted from cumulative tests (moisture plus thermal cycling).

From ASTRAL (1981) [9].

8.2.2. Orbital. Data on ultra-violet and particulate irradiation damage of this coating compare favourably with those of other white paints which have been tested by Paillous (1976) [96].

9. THERMAL CYCLING

No cracking of the surface was observed after the following tests:

Pressure below $1{,}3\text{x}10^{-4}$ Pa.

Temperature:

T_{min} = 173 K

T_{max} = 373 K.

Number of cycles: 200.

Cycle time not given.

From ASTRAL (1981) [9].

10. SOURCE

ASTRAL, Peintures et Vernis, 164 rue Ambroise Croizat, boîte postale 140.

93204 Saint-Denis. Cédex 1, France.

Contact Person: Mr. B. Dumont. Département Aéronautique.

11. COST

12. PAST SPACIAL USE

No spacial use has been reported.

A sample of this coating, among others, are tested on board Long Duration Exposure Facility (LDEF) 1st Mission (scheduled for early 1984), Experiment A0138-6, by Paillous & Guillaumon. The sample are examined before flight and after retrieval. (Clark (1981) [30]).

5.2.5.1 Zinc Orthostannate-Methylsilicone

1. COMPOSITION

Pigment: Zinc Orthostannate (Zn_2SnO_4).

Binder: RHODORSIL 10 336 purified by CNES method. This purification consists in a number of cures (usually three) which reduce outgassing without modifying the properties of the polymerized binder (see Guillaumon & Guillin (1979) [53]).

From Guillaumon & Blet (1982) [51].

RHODORSIL 10 336 is a methyl phenyl silicone used for the production of industrial coatings which will withstand temperatures up to 650 K - 700 K, and for producing fast-pressing and recooking insulation bricks.

Contains xilene.

Also commercialized as Silicex 717.

From Siliconas Hispania (1985) [116].

Preparation of the pigment: 162,8 g (2 moles) of SP500 ZnO, New Jersey Zinc Co., and 150,7 g (1 mol) of Sn_4O_2, Merck (quality PUR) are dispersed in deionized water (0,6 l and 1,2 l respectively) during 5 min. Both dispersions are mixed and thoroughly stirred for 15 min. The mixture is then al- lowed to stand during 3 h. Then it is transferred to a Buchner funnel and filtered at reduced pressure. The filter cake is removed from the funnel and dried for 16 h at 380 K. The resulting powder is calcined for 16 h at 1 220 K. In order to enhance the stability under UV radiation, mixtures with 0,5 % excess ZnO have been calcined at different temperatures (1200 K, 1270 K, 1320 K, 1370 K) and then treated with acetic acid.

From Guillaumon (1982) [48].

2. FORMULATION

Not given by the producer.

3. USUAL DESIGNATION PCBZ

Conductive White Paint.

4. SUBSTRATE

Any light alloy, also fiber-glass, Kevlar or carbon fiber laminates.

5. METHOD OF APPLICATION

5.1. Preparation of paint for application. (See also clause 5.2.2).

Add sufficient thinner to 100 kg of paint in order to reach a viscosity of 33 s - 34 s at 293 K per AFNOR No. 2,5 cup (≈ 30 g of thinner).

This viscosity should be closely kept.

From Guillaumon & Blet (1982) [51].

Cup type viscometers are widely employed in the paint industry (Demmler, Ford, Zahn, Gardner, ...). They consist of an orifice cup with a metal orifice and a receiver cup. The measured efflux time, t, in seconds, is related to the kinematic viscosity ($\nu = \mu/\rho$) through

$\nu = kt - K/t$

where k and K are empirical values for each instrument.

For a table with the most widely used viscometers see Van Wazer et al. (1963) [130].

An account of AFNOR cups and pertinent procedures can be found in NF T 30-014 (1983) [92].

The range of standard AFNOR cups is given in the following Table.

t vs. ν Range of Standard AFNOR Cups		
Cup	**t [sec]**	**$\nu \times 10^3$ [Pa.s]**
2,5	30 to 250	5 to 140
4	20 to 300	50 to 1100
6	30 to 300	510 to 5100

NOTE From NF T 30-014 (1983) [92].

Storage time in full, closed containers at 278 ± 2 K, is 4 months.

5.2. Preparation of surfaces for painting.

1. Metallic surfaces should be cleaned from any trace of oxide, grease or die lubricant by immersion or with a rag soaked with acetone and then with flugene 113 (or equivalent).

   From Guillaumon & Blet (1982) [51].

   Flugene 113: Trichloro 1,1,2-Trifluoro 1,2,2 Ethane, is a product from Rhone-Poulenc.

2. Fiber-glass, Kevlar or carbon-fiber epoxy laminates should be grinded with abrasive cloth no. 320 and cleaned with acetone and then flugene 113 (or equivalent).

From MASTER (1985) [81].

5.2.1. Application of primers. Two alternative types of primers are quoted:

1. Primer P 128 could be applied either by hand rubbing or sprayed with a type Kremlin "Junior" or J3 spray gun. A single crosswise layer should be applied. Layer thick ness, 5 x 10^{-6} m. Drying time, 30 min.

   From Guillaumon & Blet (1982) [51].

   Very similar properties as those of the nominal coating on this primer have been obtained on light alloys without using P 128 primer (Guillaumon (1983) [49]).

   In the case of epoxy substrates it is advisable to apply a crosswise layer of P 123 primer (see paragraph 5.2 of clause 5.2.4).

2. PCBZ Primer.

   Ambient temperature in the range 291 K to 298 K.

   Relative humidity above 40 %.

   Throughput: 0,150 ± 0,020 kg.m^{-2} (dry) which corresponds to around 0,230 kg.m^{-2} as delivered. Thickness (dry) around 45 x 10^{-2} m.

   (a) For small surfaces (less than 0,5 m^2).

      Thining: 20 to 25 % of PCBZ thinner.

      Viscosity at application: 16 s to 20 s at 293 K per AFNOR No. 4 cup.

Filtering: through nylon filter 300 μ.

Application with Kremlin "Junior" or equivalent spray gun. Nozzle 203.

Vector gas: air at 2,5 x 10^5 Pa. Suction feeding.

Needle valve aperture: 4,5 turns. Oval jet.

A slight wet plus 2 crosswise layers wet on wet in order to obtain a wet and uniform appearance. 2b) For large surfaces (beyond 0,5 m^2).

Thinning: 20 to 25 % of PCBZ thinner.

Viscosity at application: 18 s to 22 s at 293 K per AFNOR No. 4 cup.

Filtering: through nylon filter 300 μ.

Application with Kremlin type SKM17. Head H 10. Nozzle No. 16.

Pressure: 3 x 10^5 Pa. Aspiration can.

Needle valve aperture: 4,5 turns. Semi-oval jet.

Vent opening: 3/4 turn.

A slight wet plus 2 crosswise layers wet on wet in order to obtain a wet and uniform appearance. After the last layer of PCBZ primer, wait 3 min before applying the layers of white finishing.

From MASTER (1985) [81].

5.2.2. Application of white finishing layers.

Thinning: 40 to 50 % of PCBZ thinner.

Viscosity at application: 33 s to 35 s at 293 K per AFNOR No. 2,5 cup.

Filtering: through nylon filter 50 μ.

Throughput: 0,170 ± 0,010 kg.m^{-2} (dry) which corresponds to around 0,230 kg.m^{-2} as delivered. Thickness (dry) around 40 x 10^{-6} m.

1. For small surfaces (less than 0,5 m^2).

   Application with Kremlin "Junior" or equivalent spray gun. Nozzle 203.

   Vector gas: air at 1,8 x 10^5 Pa. Suction feeding.

   Needle valve aperture: 4 turns. Oval jet.

   2 to 5 crosswise layers depending on applicator.

   Delay between layers so as to reach a semi-matte appearance.

2. For large surfaces (beyond 0,5 m^2).

   Application with Kremlin type SKM17. Head H 10. Nozzle No. 14.

   Pressure: 2 x 10^5 Pa. Aspiration can.

   Needle valve aperture: 4,5 turns. Oval jet.

   2 to 5 crosswise layers depending on applicator.

   Delay between layers so as to reach a semi-matte appearance.

   From MASTER (1985) [81].

5.5. Curing process. The coating should be air-dry during 5 d, at 293 K and normal humidity.

Dust off: 1 to 2 h.

Dry to be handled: 24 h.

Final curing: 5 d.

From MASTER (1985) [81].

5.6. Appearance. White Matte.

6. CLEANING

Cleaning. Use ethyl alcohol. Chlorinated, fluorochlorinated or benzene solvents should be avoided.

Pickling. Use D165 Astral or chlorinated solvents like trichlorethylene, chloroform, etc.

CAUTIONS

This coating is flammable, noxious through breathing, swallowing and skin contact.

It should be handled far from any flame and applied only in properly ventilated rooms. If this is not the case a suitable mask should be used.

7. PHYSICAL PROPERTIES

7.1. Density.

Data below correspond to specific density of wet components in the coating system.

PCBZ primer, 1,73 ± 0,05

PCBZ finishing, 2,02 ± 0,05

PCBZ thinner, 0,93 ± 0,02

From MASTER (1985) [81].

Surface density, depending on the number of layers:

0,26 $kg.m^{-2}$ to 0,37 $kg.m^{-2}$ (see paragraph 7,4).

7,2. Outgassing.Sample heated at 398 K, below $1,3 \times 10^{-4}$ Pa pressure, during 24 h. Condensing plate held at 298 K. (Specification ESA PSS-09/QRM-02T) (see Table below).

Table 5-24: Outgassing Characteristics of PCB Z Coating

Coating	TWL [a] %	RWL [b] %	VCM [c] %	Cure Time [h]	Cure Temp. [K]	References
PCBZ on A-U4G substrate primed with P 128 [d]	0,65	0,64	0,12	120	293	Guillaumon & Blet (1982) [51]
PCBZ system (primer and finishing layers) on A-U4G substrate [d]	0,65	0,64	0,12	360	298	MASTER (1985) [81]
	0,53	0,40	0,08	144 [e] 24	298 323	
	0,26	0,13	0,07	120 [e] 24	298 373	

Coating	TWL [a] %	RWL [b] %	VCM [c] %	Cure Time [h]	Cure Temp. [K]	References
	0,11	0,01	0,02	96 [e] 26	298 423	
PCBZ	0,85	0,81	0,09			INTA (1984) [65]

[a] TWL: Total Weight Loss.

[b] RWL: Relative Weight Loss.

[c] VCM: Volatile Condensarle Materials.

[d] Al-4CuMgSi Alloy.

[e] Each one of these cures was used in the order given.

7.3. Thermal radiation properties.

7.3.1. Emittance

7.3.1.1. Hemispherical total emittance.

$\varepsilon_p = 0{,}80 \pm 0{,}04$

$\varepsilon_c = 0{,}83$

On A-U4G substrate. ε_p has been measured with a portable emissometer and ε_c by calorimetry. From Guillaumon & Blet (1982) [51], Guillaumon (1983) [49].

See Millard & Streed (1969) [86] for a comparison of portable emissometer vs. calorimetric values.

7.3.2. Absorptance

7.3.2.1. Solar Absorptance

$\alpha_s = 0{,}26 \pm 0{,}02$

On A-U4G substrate.

From Guillaumon & Blet (1982) [51], Guillaumon (1983) [49].

7.3.2.2. Variation of solar absorptance with coating thickness. See p. 1-104,16.

7.3.2.5. Effects of the Space Environment on absorptance

7.3.2.5.1. Ultra-Violet Radiation. After 1 045 ESH at 298 K

$\Delta\alpha_s = 0{,}03$

On A-U4G substrate with P 128 primer.

From Guillaumon & Blet (1982) [51].

See also Figure 5-81.

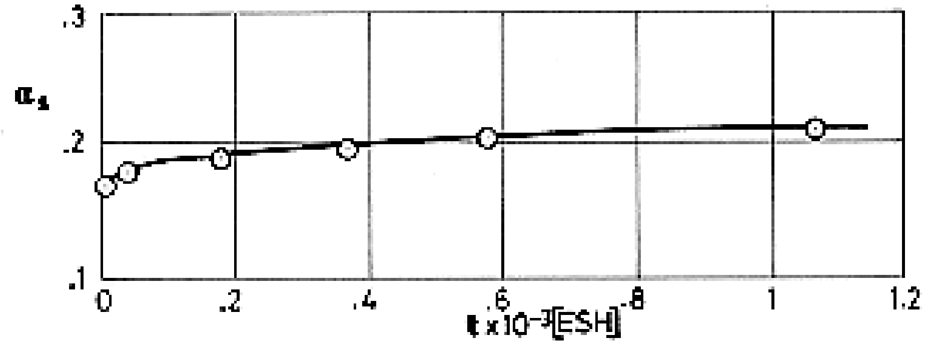

Note: non-si units are used in this figure

Figure 5-81: Solar absorptance, α_s, of PCBZ coating vs. UV Radiation exposure time, *t*. From Guillaumon (1982) [48].

From spectral reflectance data measured in the following pages.

Table 5-25: Ultra-Violet Radiation Effects on Solar Absorptance of PCBZ Coating

Test conditions	α_s TOTAL	α_s UV	α_s Visible	α_s Infrared
Sample A: PCBZ b4f5 four primer layers, five white finishing layers. Substrate not given.				
In air, Beckman	0,244	0,863	0,187	0,203
UV in vacuum 0 ESH	0,224	0,863	0,169	0,178
120 ESH	0,239	0,866	0,192	0,186
293 ESH	0,246	0,876	0,203	0,189
586 ESH	0,247	0,854	0,200	0,197
1 086 ESH	0,251	0,877	0,209	0,195
1 597 ESH	0,258	0,890	0,222	0,194
2 090 ESH	0,255	0,878	0,214	0,197
2 625 ESH	0,256	0,878	0,222	0,192
After breaking vacuum	0,240	0,874	0,199	0,180
In air, Beckman	0,262			
Sample C: PCBZ b4f8 four primer layers, eight white finishing layers. Substrate not given.				
In air, Beckman	0,230	0,864	0,178	0,181

Test conditions	α_s **TOTAL**	α_s **UV**	α_s **Visible**	α_s **Infrared**
UV in vacuum 0 ESH	0,210	0,860	0,156	0,161
110 ESH	0,217	0,864	0,175	0,157
268 ESH	0,230	0,868	0,187	0,172
536 ESH	0,233	0,861	0,193	0,174
994 ESH	0,241	0,881	0,204	0,176
1 459 ESH	0,237	0,881	0,204	0,167
1 910 ESH	0,241	0,883	0,206	0,174
2 400 ESH	0,243	0,884	0,217	0,166
After breaking vacuum	0,225	0,874	0,190	0,156
In air, Beckman	0,246			

UV degradation increases up to 1 000 ESH, becoming invariable beyond this time. Recovery after breaking the vacuum is noteworthy particularly in the infrared band. The number of white finishing layers (5 or 8) is immaterial except in the infrared.

From Paillous & Millan (1983) [98].

7.3.3.2. Effect of the Space Environment on reflectance.

7.3.3.2.1. Ultra-Violet Radiation.

Test performed at ONERA-CERT.

Two samples of PCBZ coating.

Author's designation: A: PCBZ b4f5; C: PCBZ b4f8

As in Table above.

Substrate not quoted.

Irradiation performed under a vacuum better than 1,3 x 10^{-4} Pa.

Sample temperature, T = 353 K ± 1 K controlled by a thermostatic bath.

Degrading source: Xenon lamp 2 500 W. Two independent filters are used, for the 0,2 x 10^{-6} m to 0,3 x 10^{-6} m band and for the 0,3 x 10^{-6} m to 0,38 x 10^{-6} m band respectively. Infrared and visible bands of lamp are thus suppressed.

The illumination from the lamp was independently measured on a standard target and on the sample position (four samples were irradiated simultaneously). Thus corrective factors, f_c, are asigned to each sample. f_c = 1,045 for sample A and f_c = 0,955 for sample C.

The solar radiant energy in ESH, received by each sample, is given by

$$t_s = f_c \frac{t_{s0,2} \times 16{,}2 + t_{s0,3} \times 78{,}4}{16{,}2 + 78{,}4} \qquad [5\text{-}5]$$

where $t_s = Q_s/\Phi_s$ (radiant energy over radiant flux) and $t_s0{,}2$ and $t_s0{,}3$ are radiant energies, in ESH, within each band. 16,2 W.m^{-2} is the mean intensity of the spectral irradiation (one Sun) in the 0,2 x 10^{-6} m to 0,3 x 10^{-6} m, and 78,4 W.m^{-2} that in the 0,3 x 10^{-6} m to 0,38 x 10^{-6} m band.

Spectral reflectance was measured as follows:

1. Before irradiation, measurements where performed in air using an integrating sphere attached to a Beckman DK 2A reflectometer. Once finished the run, the reflectance was measured as in 2) but breaking the vacuum.
2. During irradiation spectral reflectance was measured in situ by an integrating sphere operating in the direct mode. The sample is irradiated directly and the detector views an area on the sphere wall. A standard coating of known reflectance is then measured under the same conditions. The directional-hemispherical reflectance factor $R(\beta,2\pi)$ is the ratio of the sample reading to the standard reading times the known reflectance of the standard. According to the sketch in the reference report (Paillous & Millan (1983) [98]) $\beta \approx 0°$. In the following R, will be given as normal-hemispherical spectral reflectance.

Solar reflectance is calculated as

$$\rho_s = \frac{\int_{0,27\times10^{-6}}^{2,5\times10^{-6}} R(\lambda)E_s(\lambda)d\lambda}{\int_{0,27\times10^{-6}}^{2,5\times10^{-6}} E_s(\lambda)d\lambda} \qquad [5\text{-}6]$$

where $E_s(\lambda)$ is the solar irradiance.

For the numerical computation the integrals have been discretized taking 30 selected wavelengths. Solar reflectance was calculated in the whole band (total), in the UV, in the visible and in the infrared.

Since for each wavelength $\alpha(\lambda) = 1 - R(\lambda)$ it follows that $\alpha_s = 1 - \rho_s$.

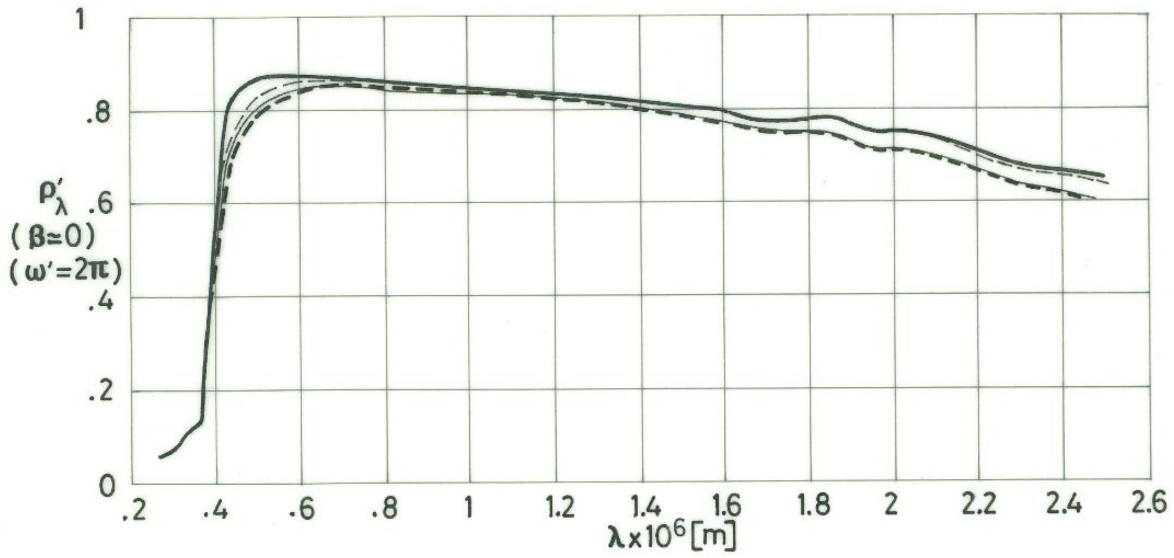

Note: non-si units are used in this figure

Figure 5-82: Normal-hemispherical spectral reflectance, ρ'_λ, of PCBZ coating, sample A, vs. wavelength, λ. Effect of Ultra-Violet radiation.

Explanation

T ≈ 353 K, $\beta \approx 0°$, $\omega' = 2\pi$, Vacuum less than 1,3 x 10^{-4} Pa

Zinc Orthostannate in Rhodorsil 10 336. Four primer layers, five white finishing layers.

Key	Test Conditions
━━━	UV in vacuum, 0 ESH
───	1086 ESH
━ ━	2625 ESH
─ ─	2625 ESH after breaking vacuum

NOTE From Paillous & Millan (1983) [98].

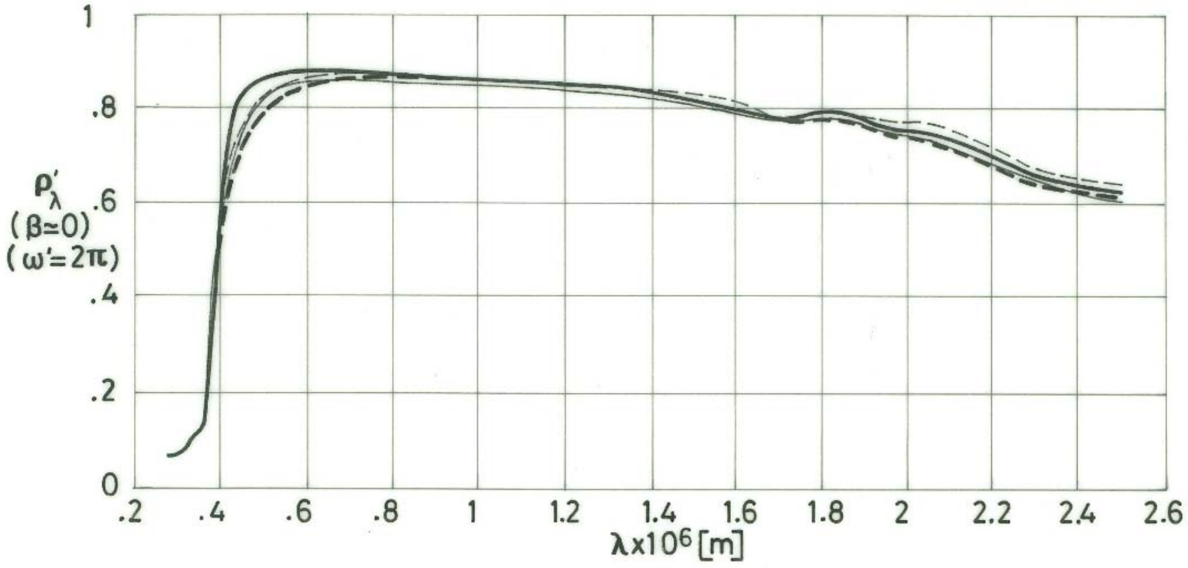

Note: non-si units are used in this figure

Figure 5-83: Normal-hemispherical spectral reflectance, ρ'_λ, of PCBZ coating, sample C, vs. wavelength, λ. Effect of Ultra-Violet radiation.

Explanation

$T \approx 353$ K, $\beta \approx 0°$, $\omega' = 2\pi$, Vacuum less than 1,3 x 10^{-4} Pa

Zinc Orthostannate in Rhodorsil 10 336. Four primer layers, eight white finishing layers.

Key	Test Conditions
▬▬▬	UV in vacuum, 0 ESH
———	994 ESH
▬ ▬	2400 ESH
— —	2400 ESH after breaking vacuum

NOTE From Paillous & Millan (1983) [98].

7.4. Electrical resistance.

Coating on glass substrate with P 128 primer.

0,260 kg.m^{-2} dry (≈ 4 layers, $\alpha_s = 0,35$) , R = 2 Ω/square[a]

0,310 kg.m^{-2} dry (≈ 5 layers, $\alpha_s = 0,29$) , R = 150 Ω/square

0,370 kg.m^{-2} dry (≈ 6 layers, $\alpha_s = 0,26$) , R = $10^4 \Omega$/square

From Guillaumon & Blet (1982) [51].

[a] From MASTER (1985) [81]. In this case primer is PCBZ primer. Measured per ASTM D 257-66.

The reason for the drastic increase in surface electrical resistance with thickness is twofold; 1) volume resistance of the semiconducting white layer increases with the number of layers, and 2) the diffusion of conducting particles through this white layer weakens when thickness increases (Guillaumon (1986) [50]).

7.4.3. Charging

The surface potential of PCBZ coating irradiated with electrons has been measured at DERTS. Coating on glass substrate with P 128 primer.

Although surface resistance was very high (of the order of $10^{10}\alpha$/square), surface potential was low in any case. Results are given in Table 5-26 for different impinging electron beam energies, in keV.

Beam current density, 10^{-2} A.m^{-2}.

Table 5-26: Charging Tests with PCBZ Coating

Exposure Time [h]	Surface Potential [V]			
	5 keV	10 keV	15 keV	20 keV
0	0	-	1	-
0,008	4	3	3	1
0,025	4	4	4	3
0,058	4	4	5	4
0,142	4	5	5	5
0,308	5	6	6,5	6

NOTE From Guillaumon & Blet (1982) [51].

8. ENVIRONMENTAL BEHAVIOR

PCBZ has been space-qualified by CNES. Results of the qualification tests are given in the following.

8.1. Prelaunch.

Moisture resistance test

Test conditions.

Relative humidity: 90 %

Temperature: 323 K

Duration: 7 d

Coating Behavior.

	Appearance	Adhesion to scotch adhesive	ε	α_s
Before test	Matte	4/5 good	0,80±0,04 [a] 0,83	0,26±0,02
After Test	No change	5/5 very good	0,80±0,04	0,29±0,04

[a] ε_p = 0,80 ± .04 (portable emissometer), ε_c = 0,83 (calorimetric)

NOTE From Guillaumon & Blet (1982) [51], Guillaumon (1983) [49].

Adhesion of a coating to the substrate is the subject of several standards (ISO 2409 - 1972; UNE 48032; ASTM-D-3359, method B; DIN 53151; INTA 160299, ...) All of them deal with the so called cross-cut test. A lattice pattern is cut into the coating, penetrating through it to the substrate, by use of a standard cutting tool. The resulting pattern is then visually examined and the coating classified by comparison with an illustrative figure (0 to 5 or 5 to 0 from good to bad depending on the particular standards). Removal of flaked portions of coating film is made by a brush. Under certain circumstances, and through agreement between interested parties, an adhesive tape is used for removal. In other standards this procedure is mandatory. The above data have been presumably obtained per ASTM-D-3359.

9. THERMAL CYCLING

Test conditions.

Pressure: 1,3 x 10^{-4} Pa

Temperature, Tmin: 123 K, Tmax: 373 K

Number of cycles: 200

Coating behavior.

	Appearance	Adhesion to scotch adhesive	ε	α_s
Before test	Matte	4/5 good	0,80±0,04	0,26±0,02
After Test	No change	4/5 good	0,80±0,04	0,29±0,04

Cummulative tests. Environmental + Thermal cycling.

After Test	No change	4/5 good	0,80±0,04	0,29±0,04

NOTE From Guillaumon & Blet (1982) [51], Guillaumon (1983) [49].

10. SOURCE

This coating, which has been developed by CNES, is commercialized by Société MASTER Peintures (ZI 09100 PAMIERS, France, Phone (61) 67.07.40).

11. COST

Not stated by supplier.

5.2.6 Silver vacuum deposited on fused Silica

1. COMPOSITION

Metallic Silver, vacuum deposited on one surface of fused silica. The silver is overcoated with dielectric or conductive materials to protect it from degradation.

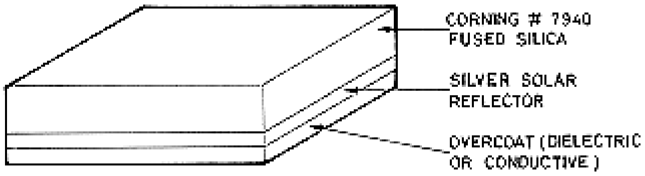

From OCLI (1980) [94].

The following description is given by Cunnington, Grammer & Smith (1969) [33].

Coating: Silver 10^{-7} m thick.

Overcoating: Inconel $5x10^{-8}$ m thick.

Both depositions made in the same chamber without breaking vacuum.

Fused Silica: Corning glass Works No. 7940, 0,008" ($2x10^{-4}$ m) thick.

3. USUAL DESIGNATION

Second Surface Thermal Control Mirror OCLI Type SI-100. Optical Coating Laboratory, Inc.

This coating system is also called Rigid Optical Solar Reflector (Rigid OSR), or Second Surface thermal control Mirror (SSM).

In the following the first designation is applied when the coating system is clearly identified in the reference, otherwise the more general designation, OSR fused silica, is used.

4. SUBSTRATE

Any clean substrate.

5. METHOD OF APPLICATION

The OSR fused silica mirrors can be bonded to the substrate with an adhesive or a double-backed tape. Silicone cements provide the most desirable characteristics.

5.1. Background. The OSR fused silica mirrors can be fabricated in a variety of shapes and sizes. The most common configuration presently in use is that of $2,54x10^{-2}$ m squares. Squares of $3,81x10^{-2}$ m have been also manufactured. Larger sizes can be produced while maintaining the fused silica thickness mentioned above, however, the breakage factor during fabrication and handling leads to increased costs. These larger sizes are available on request.

Special sizes and/or shapes are required for application on highly curved surfaces. Application to a $2,5x10^{-2}$ m diameter tube has been reported by Marshall & Breuch. (1968) [80].

5.1.1. Geometrical tolerances. Unless superseded by customer specifications, the fused silica substrates of the SI-100 mirrors are fabricated to the following tolerances:

	Dimensional Tolerance
Length	± 0,002" (5,08x10^{-5} m)
Width	± 0,002"
Thickness	± 0,002"
Perpendicularity of sides	90° ± 0° 15′
Edge Chips	± 0,010" (2,54x10^{-4} m) max. projection into face.
Parallelism of sides	± 0,002"

NOTE From OCLI (1980) [94].

5.1.2. Surface quality. F-F (80-50) or better per MIL-C-48497.

From OCLI (1980) [94].

5.1.3. Appearance. The coated surface gives the appearance of uniform coverage when observed through the fused silica substrate (face) by the unaided eye. The surface should be free of all metal deposition and other contamination. The overcoated surface (back) inherently has a distinct color when viewed under white light. This characteristic may be used to facilitate identification of the back face.

From OCLI (1980) [94].

5.2. Preparation of the surface for bonding. Depends on the substrate used. A detailed description of the several methods for preparing substrates for adhesive bonding can be found in Cagle (1968) [25]. Substrates considered are, among others, aluminium alloys, steels, titanium alloys, magnesium, copper and copper alloys, nickel and nickel base alloys, beryllium, chromium,... Manual methods for repairs, as well as methods for evaluating surface preparation are also given by Cagle.

5.3. Application. Detailed application procedures should be worked out for each case. Sometimes each mirror is applied individually. For other applications the mirrors are assembled in strings with tapes before transfer into the substrate. A small spacing between individual mirrors will allow for differences in thermal expansion between the mirrors and the substrate.

5.4. Curing process. Depends on the adhesive used. Table 5-27 gives a list of candidate adhesives, with pertinent outgassing data, as well as reference on past experience in the attachment of OSR silica mirrors.

See also THERMAL CYCLING, paragraph 9 of clause 5.2.6.

5.5. Quality of adhesive bonding. Mechanical stability could not be a reliable test of the bond. In some instances the thermal conductance between the mirror and the substrate and, thence, the effective thermal emittance of the system, decreased as a result of thermal cycling.

6. SOLVENT RESISTANCE

Fused silica is not attacked by solvents. Carbon tetrachloride, isooctane and xilene are silicone solvents. See clause 5.2.1.

Solvent cleaning for repairing purposes would only be used when there is no other alternative. Very little cleaning is achieved, and porous bond lines usually appear unless solvent completely before bonding.

Table 5-27: Candidate Adhesives for OSR Fused Silica Application

Adhesive	% TML [a]	% CVCM [b]	Cure Time [h]	Cure Temp. [K]	Vacuum Conditions	References	Comments
DC 58C [e]							Used in Helios. (Winkler & Stampfl (1975) [139]).
DC 6-1104 [e]	0,22 %RML: 0,14 [c]	0,01	72	298	$1,3x10^{-4}$ Pa – $1,3x10^{-5}$ Pa	ESTEC (1980) [39]	Prequalified by ESTEC for bonding CC-OSR fused silica on Aluminium Substrate. (Bosma & Levadou (1979) [16]).
DC 92-024 [e]							According to Marshall & Breuch (1968) [80], has proven to have excellent properties.
DC 93-500 [e] A/B as 11/1 by weight Silicone	0,09	0,01	168	298	Air	Campbell, Marriot & park (1978) [27].	Used in radiators, Beacon Experiment, CMSTAR satellites. (Hyman (1981) [62]).
DC 93-500 [e] A/B as 20/1 by weight Silicone	0,04	0,00	48	298	Air		
Eccobond 57C [f] A/B as 1/1 by weight	0,52	0,04	168	298	Air		Conductive Epoxy-Silver Adhesive. Used in SCATHA, ML12 experiment. (Hall & Fote (1979, 1980) [55] & [56]).
Eccobond 57C [f] A/B as 1/1 by weight	0,36	0,03	0,5	423	Air		

Adhesive	% TML [a]	% CVCM [b]	Cure Time [h]	Cure Temp. [K]	Vacuum Conditions	References	Comments
RTV-S 691 [g] A/B as 9/1 by weight G790 Primer/Al foil	0,25 %RML: 0,22 [c]	0,02	168	298	Below 1,3x10^{-4} Pa	ESTEC (1981) [40].	Qualified by AEG-TELEFUNKEN as solar cell adhesive (Koch (1978) [72]).
RTV 560/T-12 [h] as 0,1% T-12	2,22	0,49	3600	298	Air	Campbell, Marriot & Park (1978) [28].	Used in Boeing tests simulating HELIOS orbit. (Fodgall & Cannaday (1974) [42]). Used in HELIOS. (Winkler & Stampfl (1975) [139]).
RTV 560/T-12 [h] as 0,1% T-12	0,08	0,04	3600 [d] 24	298 398	Air 1,3x10^{-6} Pa		
RTV 560/577/T-12 [h] as 1/1/0,5% by weight Silicone	0,063	0,11	720 [d] 48	298 348	Air 1,3x10^{-6} Pa		
RTV 560/577/T-12 [h] as 1/9/0,5% by weight Silicone	3,30	0,57	720	298	Air		
RTV 560/577/T-12 [h] as 1/9/0,5% by weight Silicone	0,45	0,08	336 [d] 144	298 348	Air 1,3x10^{-6} Pa		
RTV 566 [h] 0,07% by weight Catalyst Silicone	0,12	0,00	168	298	Air		Used in Boeing tests simulating HELIOS orbit (Fodgall & Cannaday (1974) [42]). It was not used in HELIOS
RTV 566 [h] 0,075% by weight Catalyst Silicone	0,11	0,01	168	298	Air		

Adhesive	% TML[a]	% CVCM[b]	Cure Time [h]	Cure Temp. [K]	Vacuum Conditions	References	Comments
RTV 566[h] 0,08% by weight Catalyst Silicone	0,11	0,01	168	298	Air		because of technical problems. (Winkler & Sampfl (1975) [139]). Used in several USAF geosynchronous satellites. (Curran & Millard (1978) [34]).
RTV 566[h] 0,09% by weight Catalyst Silicone	0,10	0,01	168	298	Air		
RTV 566[h] 0,1% by weight Catalyst Silicone	0,10	0,02	168	298	Air		
RTV 566[h] 0,1% by weight Catalyst Silicone/DC 1200 Primer/Sandwich	0,12	0,01	4	353	Air		
RTV 566[h] 0,1% by weight Catalyst Silicone/GE 554155 Primer/Sandwich	0,13	0,01	4	353	Air		
RTV 615[h] GE SS4120 Primer							Good thermal cycling results. (Marshall & Breuch (1968) [80]). Used in USAF satellites. (Curran & Millard (1978) [34]).

[a] TML: Total Mass Loss.

[b] CVCM: Collected Volatile Condensable Materials.

[c] RML: Remainder Mass Loss. Per Specification ESA PSS-09/QRM-02T.

[d] Each one of these cures was used in the order given.

[e] Manufactured by Dow Corning Corporation, Midland, Michigan, USA.

[f] Manufactured by Emerson & Cuming, Incorporated, Canton, Massachusetts, USA.

[g] Manufactured by Wacker-Chemie GmbH, Munich, Germany.

[h] Manufactured by general Electric Company, Silicone Products Department, Waterford, New York, USA.

7. PHYSICAL PROPERTIES

7.1. Density. 2200 kg.m^{-3} (Cunnington, Grammer & Smith (1969) [33]).

The surface density, including adhesive, is (Marshall & Breuch (1968) [80]).

0,49 kg.m^{-2} for 0,008" (2x10^{-4} m) thick fused silica.

0,27 kg.m^{-3} for 0,004" thick fused silica.

7.2. Outgassing. Outgassing of adhesives, or of organic materials may degrade the optical properties of these mirrors.

Outgassing characteristics of adhesives given in Table 5-27 have been measured per ASTM E595-77.

7.3. Thermal radiation properties

7.3.1. Emittance.

7.3.1.1. Hemispherical total emittance: Figure 5-84.

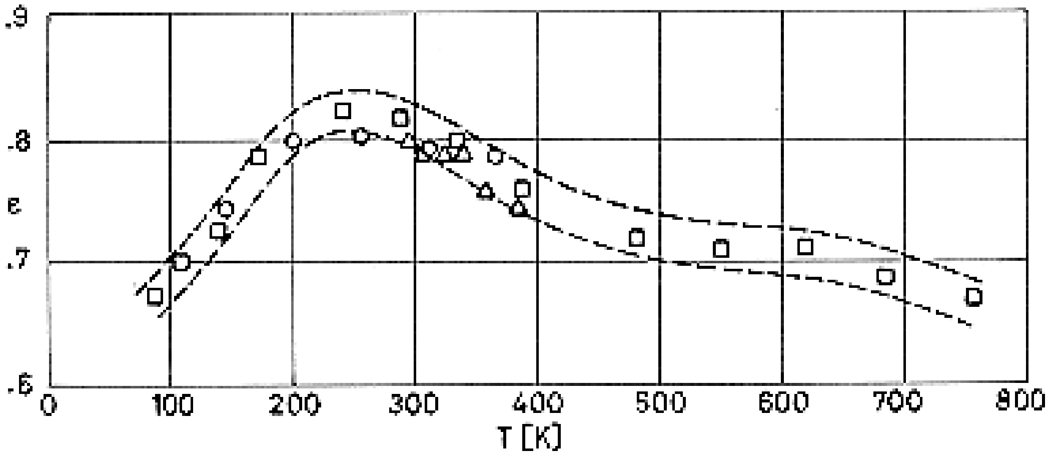

Note: non-si units are used in this figure

Figure 5-84: Hemispherical total emittance, ε, of OCLI Type SI-100 Thermal Control Mirrors as a function of temperature, T . ○ :> From Breuch (1967) [22]. □ :> From Marshall & Breuch (1968) [80]. △ :> From Cunnington, Grammer & Smith (1969) [33]. Uncertainty limits are from Marshall & Breuch (1968) [80].

7.3.1.2. Effects of the Space Environment on hemispherical total emittance.

7.3.1.2.1. Ultra-Violet Radiation. No significant change is anticipated. The following short table has been prepared using data from Cunnington, Grammer & Smith (1969) [33]

T [K]	t [h]	n	ε_0	ε_f	$\bar{\varepsilon}$	σ
339	2040	31	0,80	0,78	0,790	0,010

Degrading Source: $2\text{x}10^{-7}$ m to $4\text{x}10^{-7}$ m Xenon Lamp, 1 Sun Level.

Method of obtaining data: Calorimetric.

Chamber pressure: $1{,}33\text{x}10^{-5}$ Pa.

t, total exposure time. [h].

n, number of data points given in the source,

ε_0, ε_f, initial and after-exposure values of the hemispherical total emittance.

$\bar{\varepsilon}$, mean value.

$$\bar{\varepsilon} = \frac{\sum_{1}^{n} \varepsilon_i \Delta t_i}{t} \qquad [5\text{-}7]$$

σ, standard deviation.

$$\sigma = \sqrt{\frac{\sum_{1}^{n} (\varepsilon_i - \bar{\varepsilon})^2 \Delta t_i}{t-1}} \qquad [5\text{-}8]$$

7.3.2. Absorptance.

7.3.2.1. Solar Absorptance. according to Marshall & Breuch (1968) [80], values obtained from spectral reflectance data and the appropriate solar radiation intensity fall within the range,

$\alpha_s = 0{,}050 \pm 0{,}005$,

T from 180 K to 294 K.

OCLI (1980) [94] gives,

$\alpha_s \le 0{,}060$,

as deduced from spectral reflectance data (Cary 14 spectrophotometer) in the wavelength range $2{,}8\text{x}10^{-7}$ m to $2{,}5\text{x}10^{-6}$ m.

Slightly higher values can be found in the literature.

For example, Fogdall & Cannaday (1974) [43] quote

$\alpha_s = 0{,}065$,

$T = 153$ K,

from spectral reflectance data measured, at 100 selected wavelengths, in the range 2,5x10^{-7} m to 2,5x10^{-6} m, with in situ reflectometer and spectrophotometer outside the vacuum chamber.

7.3.2.3. Variation of solar absorptance with incidence angle. Figure 5-85a shows data (Stultz (1976) [123]) which correspond to:

1. Theoretical results, based on the electromagnetic wave theory and geometrical ray tracing, for the mirror geometries sketched in Figure 5-85b. The adhesive used to attach the mirrors is assumed to be totally absorbing, although the calculated α_s is based on that energy directly impinging on the fused silica. Because of the internal reflection at the non sunlit edge (Figure 5-85b) both configurations labeled A are equivalent, the same is true for B. In the analysis of configurations A both face and sunlit edge are taken into account, but only the face in the analysis B. Further details of the analysis are given in Stultz (1974) [122].

   It was seen during the analysis that for $\beta \geq 86°$ total capture of the refracted ray occurs if the first and second faces are out of parallel by as less as 0,13° (0,002" in 1"). Although these mirrors are out of standards (see paragraph 5.1.1 of clause 5.2.6), the probability of capture of the refracted ray increases when β becomes larger than 86°.

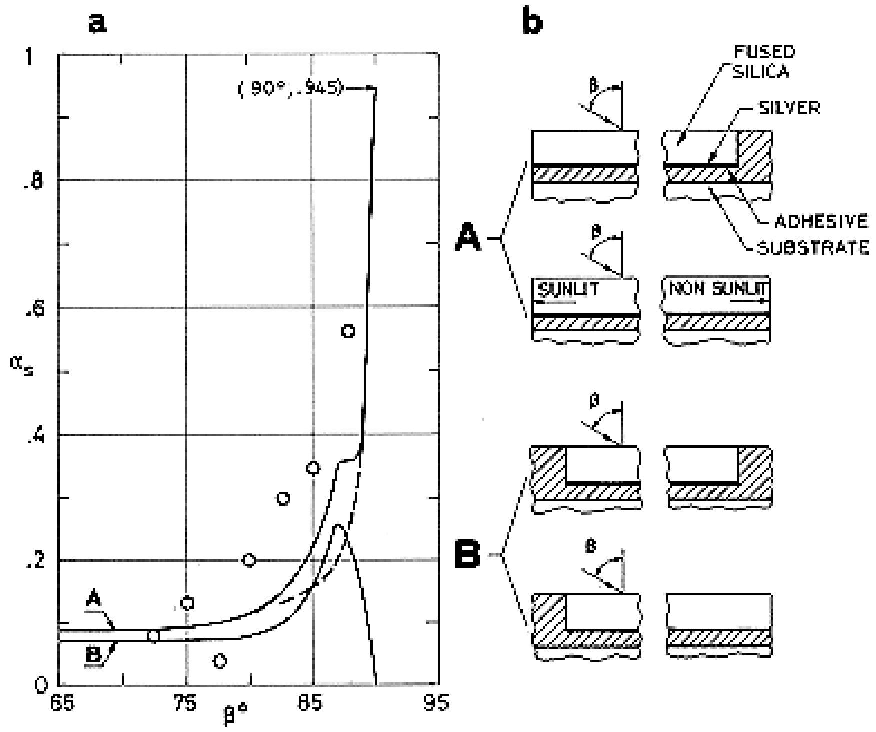

Note: non-si units are used in this figure

Figure 5-85: Solar absorptance, α_s, of OCLI Type SI-100 Thermal Control Mirrors vs. incidence angle, β. The full lines in *a* correspond to the analytical geometries sketched in *b*. Circles are from solar reflectance measurements, and the dotted line is based on flight temperatures of the NEMS radiator. From Stultz (1976) [123].

Mirrors of these geometrical characteristics would exhibit an α_s higher that shown in Figure 5-85a

2. Measurements made on a radiator, like those on board Nimbus E, Microwave Spectrometer (NEMS), which is covered by OSR fused silica mirrors. The JPL Celestarium was used for these measurements (Stultz (1974) [122]).

   These results are relative in the sense that they give the solar energy specularly reflected from a row of six mirrors. In order to locate the data points (circles in Figure 5-85a) it is assumed that the maximum reflected energy at β= 72,5° represents an average solar reflectance of ρ_s = 0,925 (α_s = 1–ρ_σ),and that the maximum values for other β angles are proportional to this reflectance.

3. The calculated solar absorptance for the NEMS radiator based upon the flight temperature data corresponding to a period of constant solar intensity (November 20, 1973 to February 7, 1974). Although outgassing contamination could increase α_s by at less 10% (see Figure 5-87), the trend of the dotted line in Figure 5-85a is similar to those of the other curves.

   Evidence of this β effect for smaller values of β has been reported by Hyman(1981) [62]. The analysis of radiator temperature data from COMSTAR satellites showed a seasonal increase and decay of α_s.

   Since a seasonal variation of β also occurred, the curves giving the solar absorptance, α_s, vs. time, t, were smoothed and the difference between original and smoothed curves was plotted as a function of the incidence angle, β. The results for COMSTAR D-1, D-2 and D-3 satellites are given in Figure 5-86. See also Figure 5-89. No explanation for the larger slope of D-1 is given by the author.

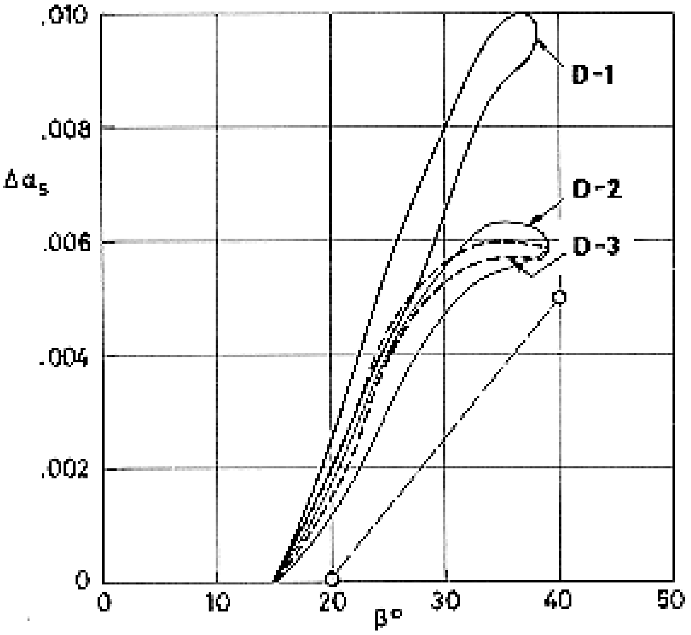

Note: non-si units are used in this figure

Figure 5-86: Change in solar absorptance, $\Delta\alpha_s$, of OCLI Type SI-100 Thermal Control Mirror vs. incidence angle, β, as deduced from data of COMSTAR D-1, D-2 and D-3 satellites. The envelopes contain all the data points. ○ :> Integrated sphere spectroreflectometer measurements made on a single mirror. From Hyman (1981) [62].

7.3.2.5. Effects of the Space Environment on absorptance.

OSR fused silica mirrors are very stable when exposed to space environment, although contamination may significantly compromise their stability and performance. It is due to this reason that considerable discrepancy arose in the past several years between earlier and recent data obtained from space borne experiments.

A list of test conditions under which no change in the solar absorptance of OSR fused silica mirrors was detected is given in Table 3 of Marshall & Breunch (1968) [80].

7.3.2.5.1. Ultra-Violet Radiation. Table 5-28 has been borrowed from Cunnington, Grammer & Smith (1969) [33].

Table 5-28: Ultra-Violet Radiation Effects on Spectral Absorptance of OCLI Type SI-100 Thermal Control Mirrors

T [K]	*t* [h]	α for Xenon Lamp					α_s
		Range of $\lambda x10^7$ [m]					
		2-4,1	4,1-6	6-8,5	8,5-	Total	
339	0	0,26	0,05	0,03	0,03	0,056	0,061
339	122	0,23	0,05	0,02	0,04	0,054	0,058
339	170	0,25	0,05	0,03	0,03	0,057	0,060
339	242	0,26	0,05	0,04	0,03	0,057	0,062
339	338	0,23	0,07	0,03	0,03	0,055	0,062
339	410	0,25	0,06	0,04	0,03	0,056	0,062
339	458	0,25	0,06	0,02	0,03	0,055	0,059
339	528	0,26	0,05	0,02	0,04	0,057	0,059
339	648	0,26	0,06	0,04	0,03	0,057	0,063
339	696	0,23	0,07	0,03	0,03	0,055	0,061
339	768	0,27	0,05	0,03	0,03	0,057	0,061
339	816	0,25	0,05	0,03	0,03	0,056	0,059
339	864	0,25	0,05	0,04	0,03	0,057	0,061
339	936	0,24	0,05	0,04	0,03	0,058	0,058
339	984	0,25	0,05	0,05	0,03	0,057	0,063
339	1032	0,25	0,05	0,04	0,03	0,056	0,061
339	1104	0,26	0,04	0,04	0,03	0,057	0,059
339	1152	0,23	0,07	0,03	0,03	0,055	0,062
339	1200	0,26	0,05	0,03	0,03	0,056	0,059
339	1272	0,24	0,06	0,03	0,03	0,056	0,060
339	1320	0,23	0,08	0,03	0,03	0,056	0,064
339	1468	0,22	0,08	0,02	0,03	0,054	0,061
339	1536	0,20	0,07	0,02	0,03	0,052	0,060

T [K]	t [h]	α for Xenon Lamp					α_s
		Range of $\lambda x10^7$ [m]					
		2-4,1	4,1-6	6-8,5	8,5-	Total	
339	1608	0,22	0,08	0,03	0,03	0,054	0,063
339	1656	0,25	0,05	0,03	0,03	0,056	0,059
339	1704	0,25	0,06	0,03	0,03	0,057	0,061
339	1776	0,24	0,07	0,03	0,03	0,056	0,063
339	1824	0,23	0,07	0,05	0,03	0,057	0,057
339	1944	0,24	0,06	0,05	0,03	0,058	0,063
339	1994	0,25	0,04	0,04	0,03	0,056	0,058
339	2040	0,24	0,06	0,05	0,03	0,059	0,063
Before Exposure [a]		0,25	0,05	0,03	0,01	0,052	0,055
After Exposure [a]		0,27	0,06	0,03	0,01	0,055	0,061

[a] Values deduced from spectral reflectance data. See Figure 5-94.

Degrading Source: $2x10^{-7}$ m to $4x10^{-7}$ m Xenon Lamp, 1 Sun level.

Method of obtaining data: Calorimetric in situ absorptance.

Chamber pressure: $1{,}33x10^{-5}$ Pa.

From Cunnington, Grammer & Smith (1969) [33].

The data presented seems to indicate that change in α_s due to ultra-violet radiation is negligible.

7.3.2.5.5. Contamination. Figure 5-87 gives data (curves of white circles and half black circles) which, being obtained under similar radiation exposures, substantially differ in the amount of contamination.

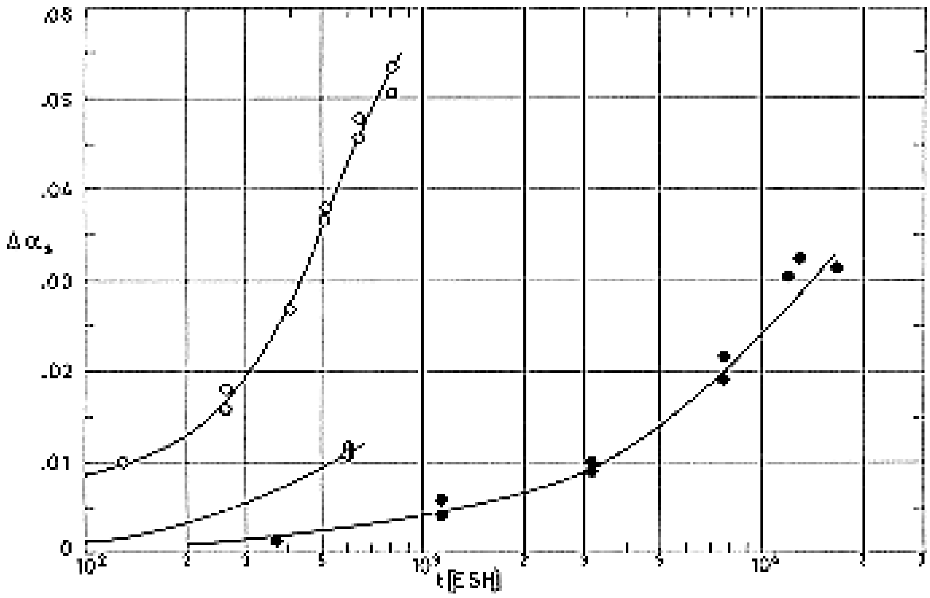

Note: non-si units are used in this figure

Figure 5-87: Change in solar absorptance, $\Delta\alpha_s$, of OCLI Type SI-100 Thermal Control Mirrors vs. exposure time, *t*.

Explanation

Key	Test Conditions					Comments
			Radiation Exposure			
				Charged Particles		
	Temp. [K]	Time [ESH]	UV [Suns]	Intensity [keV]	Integrated Flux [Particles.m^{-2}]	
○	153	up to 800	1	80	7x10^{17} p.m^{-2}	Adhesive migrates toward the mirrors contaminating them. The degradation can be increased by repolymerization of the silicone because of the subsequent impinging radiation. The original values of ρ'_λ and α_s are restored when the adhesive is removed from the faces.
				20-230	5x10^{18} e.m^{-2}	
◑	288	up to 600	1	80	5x10^{17} p.m^{-2}	Degradation rates are much

				20-230	4x10^{18} e.m^{-2}	lower since outgassed RTV is more effectively trapped on the cold samples than on those at room temperature.
●	448	up to 17x10^{3}	16	10	4x10^{20} p.m^{-2}	Intended to reproduce HELIOS orbit conditions at 0,25 AU. Samples bonded to the substrate were tested adjacent to like samples clipped bare. Space was left between all samples so that a fin-type cryogenic baffle could form walls between the samples in order to avoid cross-contamination. Nevertheless, a portion of the reported α_s changes may represent the influence of cross-contamination from other samples.
				25x10^{-3}	electron neutralization	

SAMPLE

Sample Description

OCLI Type SI-100 Mirror. Fused Silica, 0,009" (2,29x10^{-4} m) thick. Polished with Barnsite.

Initial solar absorptance, α_{so} = 0,065.

Sample Mounting

Sample was bonded to a copper substrate with RTV 560 or RTV 566 silicone adhesives.

CALCULATION METHOD

α_s deduced from spectral reflectance measured at 100 selected wavelengths, in the range 2,5x10^{-7} m to 2,5x10^{-6} m, with in situ reflectometer and a spectrophotometer outside the vacuum chamber.

Chamber pressure not given.

Reference: Fogdall & Cannaday (1974) [42].

7.3.2.5.6. Combined exposure. Results from in-orbit experiments are presented in the following. Typical exposures are given below. Data from both in-orbit and simulation experiments are summarized in Figure 5-92.

See also Table 5-29 and Table 5-30.

Orbit	**Satellite**	**Typical radiation Exposure**					**Comments**
		UV [Suns]	**Protons**		**Electrons**		
			Intensity [keV]	**Flux $[p.m^{-2}.s^{-1}]$**	**Intensity [keV]**	**Flux $[e.m^{-2}.s^{-1}]$**	
Near to Earth ~500 km altitude	OSO-III	1					The Earth's magnetosphere shields the satellite from charged particles.
Subsynchronous ~20200 km altitude	NAVSTAR	1	$<4x10^{3}$ $4x10^{3}$	10^{12} $<10^{6}$ (time dependent)	40 $1,5x10^{3}$	10^{10} 10^{17}	Crosses Van Allen radiation belt. Typical exposures estimated by the compiler after Johnson (1965) [66].
Geosynchronous 35800 km altitude	COMSTAR SCATHA	1	20	$5x10^{12}$	20	$2x10^{13}$	More than 76% of the charged particles are of low energy (<20 keV). See further details in Table 5-19 and Table 5-29.
Solar	HELIOS	up to 16	10	$2,5x10^{13}$			Also high temperatures *T*~450 K. Solar wind is the only source of particles. Solar flares could increase the quoted protons value. (Winkler & Brungs (1975) [136]).

OSO-III

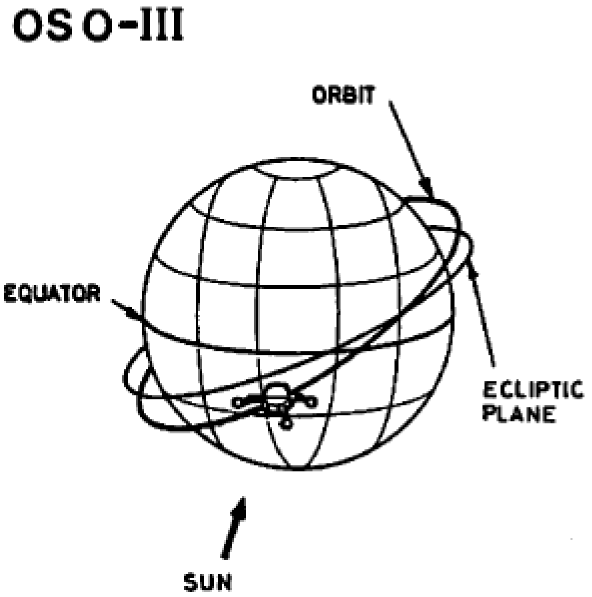

TEST CONDITIONS

Spacecraft & Programme

Third Orbiting Solar Observatory (OSO-III).

Thermal Control Coating Experiment (TCCE).

Orbit

Launched on March 8, 1967 into a near circular orbit with a latitude of about 550 km and an inclination of about 33° relative to the Equator.

Configuration

OSO satellites have two main parts: a lower section, consisting of a nine-sided wheel, which rotates to provide gyroscopic stabilization, and a stabilized semicircular upper section, or sail, aimed at the Sun. The plane of spin contains the satellite-Sun line.

Thermal Test

Test of this OSR fused silica mirror was part of an experiment involving twelve coating mounted on a single tray. This tray was located in the spinning wheel (about 3,9 $rad.s^{-1}$).

Data for the first year in orbit were reported by Millard (1969) [84]. Shortly after this year, the spacecraft tape recorders failed, but data to deduce $\Delta\alpha_s$ were still obtainable. Millard & Pearson (1973) [85] gave $\Delta\alpha_s$ up to June 1971, a little over four years in orbit.

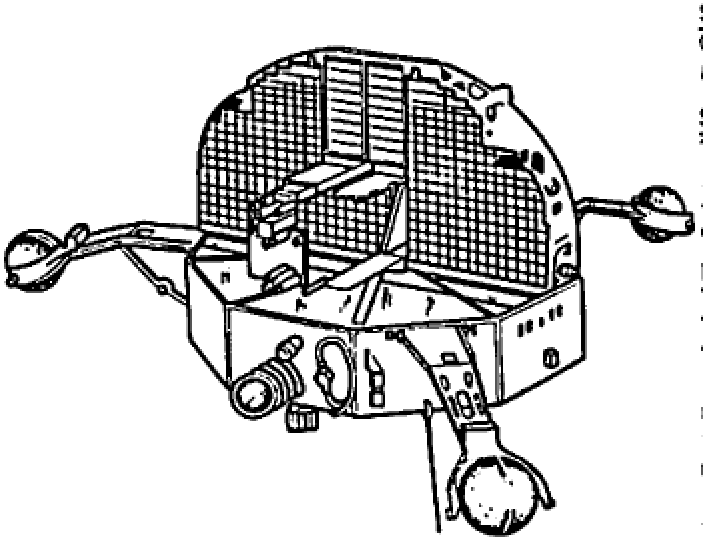

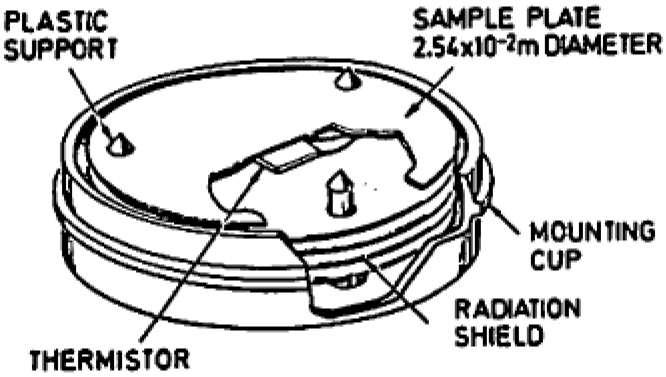

SAMPLE

Sample Description

OCLI Type SI-100 Mirror. It was furnished by Lockheed Missiles & Space Co.

Sample Mounting

The mirror is bonded to a thin aluminium disc, about $2{,}54 \times 10^{-2}$ m in diameter, which is mounted in a cup to minimize heat leaks to the back side of the disc.

"Sample plate" will henceforth indicate the mirror plus the support disc.

The details of the sample mounting area described by Neel (1964) [90].

The sample plate is supported by three small Kel-F supports.

The radiative coupling between the sample plate and the mounting cup is minimized by use of four radiation shields. All inner surfaces are polished and goldized to further reduce the radiant heat exchange. The temperature of the sample plate is measured by means of a thermistor soldered to the underside of the disc. The cups are in thermal contact with the tray base plate, whose temperature is measured with a thermistor. In order to evaluate the heat exchange between the sample plate and the mounting cups, it is assumed that the cups are at all times at the temperature of the tray base plate.

The tested thermal control surfaces alternatively view the Sun and the Earth, but their temperatures do not oscillate because of the relatively large thermal mass of the sample plates.

CALCULATION METHOD

α_s is measured calorimetrically from tray temperature, T_c, and sample plate temperature, T. The terms which appear in the heat balance equation are:

$c(T)dT/dt$, Sensible heat of the sample plate. It is, presumably, negligible. The temperature excursions in orbit of this sample plate remained in the range 210 K- 235 K, the narrowest among the twelve tested samples. In addition, the effect of this term can be minimized by taking the temperature data from a region of the orbit where time variations are small. This happens to be the case just before day-night transition when the sensor temperatures are near the maximum values.

$K(T_c^4-T^4)$, Radiation from the tray. K can be deduced as it is be indicated below.

$C(T_c-T)$, Conduction from the tray. It has been neglected.

$\varepsilon A\sigma(T_s^4-T^4)$, Radiation to outer space. The hemispherical total emittance, ε, of the sample plate is measured before launch. ε = 0,76 at 300 K. An evaluation of the different measurement techniques applied to nine of the coating in this experiment has been made by Millard & Streed (1969) [86]. The equivalent surrounding temperature, T_s, is assumed to be zero.

$\alpha_s FAS/\pi$, Radiation from the Sun. F is the view factor. S is the solar constant. The factor $1/\pi$ accounts for the fact that the sample is placed in the spinning wheel.

$\alpha_s F_a AaS$, Albedo radiation. F_a is the view factor, and a the mean albedo of the Earth. This term can be neglected provided that only data very near the terminator (day-night transition), when the satellite does not see the sunlit side of the Earth, are taken.

$\alpha_p F_{sp} AP$, Earth infrared radiation, α_p is the hemispherical Earth radiation absorptance of the sample plate ($\alpha_p \cong \varepsilon$). $F_{sp}$is the view factor, and $F_{sp}P$ the flux on the sample plate. This term was deduced from the balance equation for the day side of the orbit for a reference surface, which was a V-groove.

Another energy balance, this for the night side of the orbit (α_s = 0), would yield either ε or (if ε is assumed to be known) the radiative transfer coefficient, K.

The effect of the uncertainty of the several unknown variables on α_s has been analyzed following Millard (1968) [83]. In this particular case the uncertainty is of the order 0,05 α_s.

RESULTS

The laboratory value was α_s = 0,05.

The mirror exhibited no changes in α_s after 7500 ESH in orbit.

COMMENTS

No figure is given because, according to the reported results, $\Delta\alpha_s$ is practically zero.

References: Neel (1964) [90], Millard (1968, 1969) [83] & [84], Millard & Streed (1969) [86], Millard & Pearson (1973) [85].

NAVSTAR

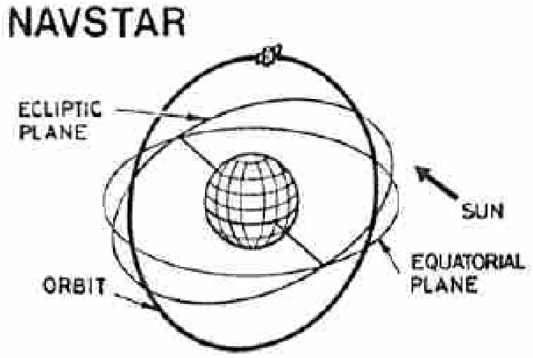
NAVSTAR
ECLIPTIC PLANE
SUN
EQUATORIAL PLANE
ORBIT

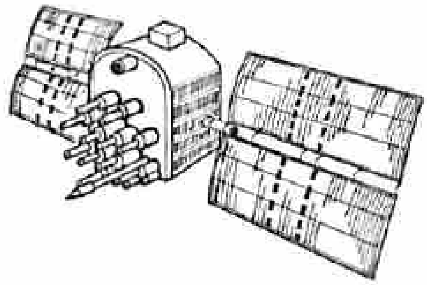

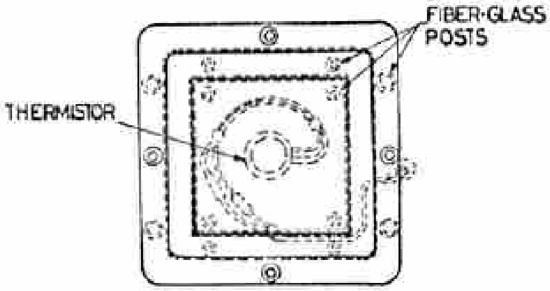
FIBER-GLASS POSTS
THERMISTOR

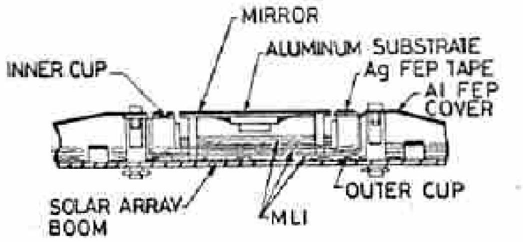
MIRROR
ALUMINUM SUBSTRATE
Ag FEP TAPE
Al FEP COVER
INNER CUP
OUTER CUP
SOLAR ARRAY BOOM
MLI

TEST CONDITIONS

Spacecraft & Programme

NavStar Global Positioning System (GPS).

Data in this item are from NavStar 5.

Orbit

NavStar satellites are being placed in subsynchronous, 12 h circular orbits of about 20170 km, in three orbital planes at 63° inclination, with eight satellites per ring. The complete system of 24 satellites should be operational by 1985 (Taylor (1979) [125]). NavStar provides three-dimensional position, velocity and time information to suitably equipped vehicles near or on the Earth's surface.

Six NavStar spacecraft were launched between February 1978 and April 1980.

NavStar 5 was launched on February 9, 1980 (Kruczynski (1980) [75]).

Configuration

The spacecraft uses three nickel-cadmium batteries operating within a very narrow temperature range (273 K to 303 K), while the other spacecraft components have less restrictive temperature limits. Thence the batteries are thermally insulated from the spacecraft main structure. Heat from the batteries is rejected to the outer space. Thermostatically controlled heaters provide heating as required.

Thermal Test

Analysis of the NavStar 1 to 4 battery temperature data showed that the radiator coating utilized (silvered Teflon), degraded much faster than anticipated. Thermal experiments on subsequent satellites aimed at evaluating alternate solar reflectors. In particular, OSR fused silica mirrors and $1{,}27\text{x}10^{-4}$ m silvered Teflon were tested on board NavStar 5.

The experiments were flown in pairs, one attached to each of two solar array booms. The sample holder contained $2{,}54\text{x}10^{-2}$ m square mirrors.

Once the spacecraft becomes 3-axis stabilized and the solar array are deployed, the booms are rotated so that the solar arrays (and thermal experiments) remain in full normal sunlight for the entire orbit.

SAMPLE

Sample Description

OSR fused silica mirror $2{,}54\text{x}10^{-2}$ m square. Not clearly identified in the reference.

Sample Mounting

The mirror is bonded to an aluminium substrate thermally insulated from the spacecraft. Substrate temperature is measured by a thermistor. Mirror and substrate form the sample plate.

The sample plate is partially surrounded by an inner aluminium cup. The gap between the sample plate and the edge of this cup, which was considered critical, was controlled to $1{,}27\text{x}10^{-4}$ m ± $0{,}51\text{x}10^{-4}$ m. The inner cup is shaped such that the solar radiation through the gap are absorbed inside. The sample plate is attached to the inner cup by 0,125" ($3{,}175\text{x}10^{-3}$ m) diameter hollow fiberglass support posts. The rear surface of the substrate and the inner cup were covered with goldized Kapton to minimize radiative heat transfer.

A glass epoxy outer cup is used both to insulate the inner cup, to which it contacts through a flange coated with $1{,}27\text{x}10^{-4}$ m silvered Teflon, and as an attachment point for the entire assembly to the spacecraft through fiber-glass posts. The interstices between inner and outer cup and between outer cup and spacecraft solar array boom are filled with MLI blankets. An outer MLI cover ($1{,}27\text{x}10^{-4}$ m aluminized Teflon) is attached to the outer cup by means of a double-faced tape (acrylic adhesive) and four screws.

The thermistor has leads gage No 22, as does the satellite wiring. To minimize heat leak through the leads, two pieces of constantan wire were spliced between the thermistor and the satellite wiring. The effect of the added electrical resistance on the accuracy level is negligible for α_s less than 0,5.

CALCULATION METHOD

The in orbit sample plate temperature was calculated by using a 44 lumped-capacity steady-state Rockwel General Thermal Analyzer Programme. Nodes are interconnected with 242 conduction and radiation couplings. Boundary nodes are used to represent the solar array boom, the main body of the spacecraft and the outer space. The use of the steady state approach is justified since the solar heating is nearly constant for non-eclipse orbits.

Parameters of the programme are:

1. Solar absorptance of the mirror and its hemispherical total emittance (which is assumed to be constant).
2. Solar absorptance of the inner cup, flange and MLI.
3. Radiation from the Sun, and
4. Temperature of the solar array boom. Albedo and infrared radiation from the Earth are neglected because only flight data when the mirror does not see the Earth are used.

Both pre-deployment of the solar array and in orbit configurations were modeled.

The output from the thermal model was compared to flight data. Small changes were made in the model values of the thermal conduction through the thermistor wires and through the fiber-glass posts, in the view factor from the mirrors to the remaining of the spacecraft, and in the effective emittance of the MLI in the cups. Using the same absorptance value for the beginning of the orbital life as for pre-deployment of the solar array, the calculated temperature values agreed with flight data to within 1 K.

Due to thermistor and telemetry errors the temperature readings have an uncertainty of 3,3 K, which means 0,01 uncertainty in α_s.

RESULTS

The solar absorptance, α_s, is plotted vs. orbital time, *t*. Since the mirrors remain in full normal sunlight for the entire orbit, orbital time in tantamount to ESH.

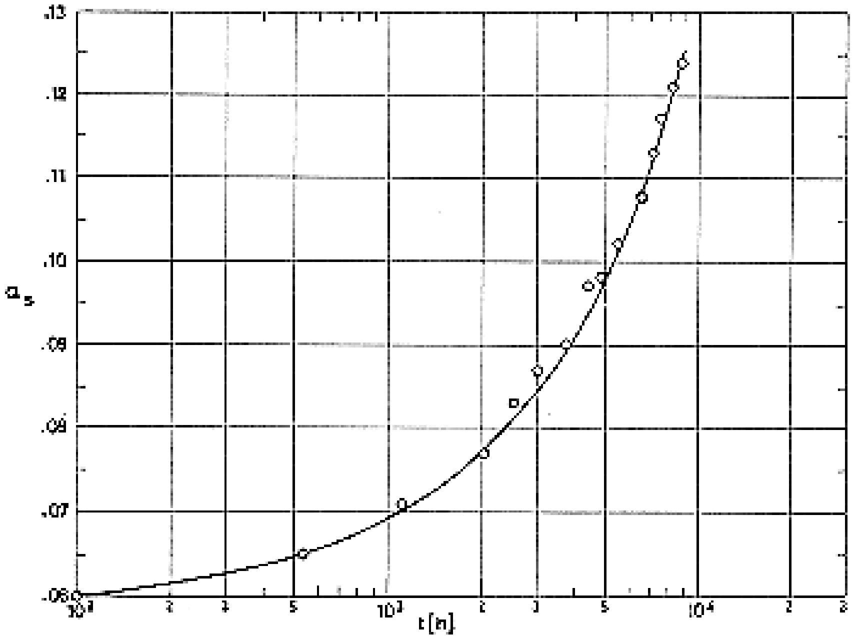

Note: non-si units are used in this figure

Figure 5-88: Solar absorptance, α_s, of OSR Fused Silica Mirrors vs. orbital time, *t*, as deduced from data of NavStar 5.

COMMENTS

Van Allen radiation is considered to be the most likely cause of the degradation experienced by these mirrors in orbital flight. The following reasons for ruling out contamination effects are quoted in the reference.

1. Any material used on NavStar should have a TML and CVCM below 0,1%.
2. NavStar satellites were assembled in a class 340000 clean room.

   Air cleanliness class 340000 implies at most 340000 particles per cubic feet 0,5 micron ($5x10^{-7}$ m) and larger, and at most 2380 particles per cubic feet 5 microns and larger (Fed. Std. No. 209a (1966)).
3. Each spacecraft was subjected to a 30 day thermal vacuum test prior to launch and no degradation in optical properties was observed.
4. Test samples were installed after thermal vacuum tests.
5. The most likely potential contamination sources namely, the solar cell array (cover slides and RTV silicone adhesive), and the apogee kick motor are out of the direct line of sight of the samples.
6. Contamination effects would be expected to be less pronounced with time and no such trend is observed in Figure 5-88.

References: All the data in this item, unless otherwise stated, are from Pence & Grant (1981) [99].

COMSTAR

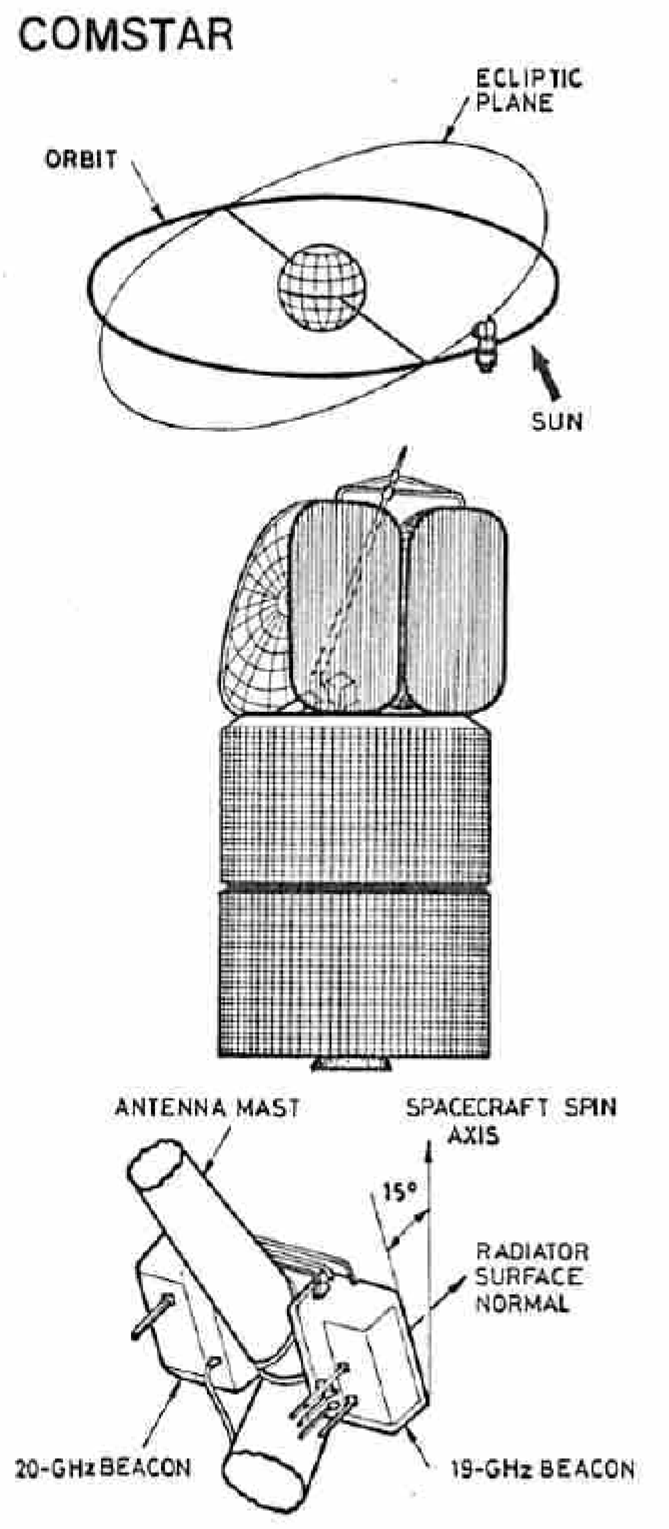
COMSTAR
ECLIPTIC PLANE
ORBIT
SUN
ANTENNA MAST
SPACECRAFT SPIN AXIS
15°
RADIATOR SURFACE NORMAL
20-GHz BEACON
19-GHz BEACON

TEST CONDITIONS

Spacecraft & Programme

COMSTAR D-1, D-2 and D-3.

Beacon Experiment.

Orbit

Data for the first three COMSTAR satellites are given in the following table.

Satellite	**Launching Date**	**Apogee [km]**	**Perigee [km]**	**Inclination [degrees]**	**Lifetime**
D-1	May 13, 1976	35810	35790	1	Unlimited
D-2	July 22, 1976	35795	35780	1	
D-3	June 29, 1978	35780	35470	0,08	

NOTE From Taylor (1977, 1979) [124] & [125].

Configuration

The Beacon Experiment was devised to investigate microwave propagation. It was not intended to study the performance of the radiator thermal control surface.

The beacon package as a means for α_s measurement consists of an OSR radiator surface attached to a base plate upon which components are mounted that produce uniformly distributed and constant heat dissipation.

The radiator surface views only the diurnal Sun.

Thermal Test

The beacon serves as a coating experiment which is more realistic than dedicated flight experiments. It represents large OSR radiators not subjected to the extreme control, care and cleaning given to sample coatings.

SAMPLE

Sample Description

OCLI Type SI-100 Mirror. 2,54x10^{-2} m square.

Sample Mounting

The surface radiator is a 0,257 m x 0,437 m rectangle, 98% covered by the OSRs bonded to the aluminium honeycomb substrate with DC 93-500 adhesive. Heat flow other than through the radiator is negligible due to an MLI blanket covering all other surfaces and to a low conductance mounting to the satellite mast. Heat dissipation, per package, is 29 W for D-1 and 32 W for D-2 and D-3, and is practically time-independent.

Temperature sensors within the beacon were provided for experiment performance evaluation.

CALCULATION METHOD

A thermal balance equation for the total package near temperature extremes (when $\partial / \partial t \cong 0$) contains the following terms.

Q(t), Net heat input from external sources other than via radiator. This contribution is small but can be easily estimated.

A 14 node thermal model, accounting for all sources and incorporating a thermal resistance between the radiator and the temperature sensor, was devised. The model was developed and improved after flight temperature data become available, making it possible to accurately introduce properties such as thermal mass, radiator to sensor thermal resistance, solar reflection from the insulator hump covering the mast and so on.

$\varepsilon A\sigma(T_s^4-T_r^4)$, Radiation to outer space. The hemispherical total emittance of the sample, ε, is measured before launch. $\varepsilon = 0{,}78$. The equivalent surrounding temperature, T_s, is assumed to be zero. Telemetry data revealed that change in temperature is very low near maximum, approximately 0,1 K.h^{-1}. Thence, it was assumed that maximum temperatures for the radiator, T_{rmax}, and the sensor, T_{max}, appeared simultaneously. It was also assumed that $T_{rmax} = T_{max}+\Delta T$ where ΔT, the temperature jump along the radiator-sensor thermal resistance, is the same throughout the year and for all values of α_s.

$\alpha_s AS(t)$, Radiation from the Sun. S is the solar flux, a known function of time.

Q_i, Internally dissipated power. It is kept constant at the above indicated values. This assumption has been confirmed through data of minimum temperatures. The thermal balance equation for the total package, when $\partial /\partial t = S(t) = 0$ and for couples of days exactly differing in one year (in order to eliminate the unknown $Q(t)$), indicates that over a one year interval $\Delta Q_i \cong 0{,}9$ W and that, even if Q_i is assumed to be constant, the maximum uncertainty in $\Delta\alpha_s$ per year usually ranges from 3,8% to 6,4%.

By using the balance equation for conditions near Tmax, and the above mentioned numerical model for Q(t), curves of $\partial T_{max}/\partial\alpha_s$ along the year for different values of α_s were produced, as well as a curve giving the predicted maximum temperature, T_{pr}, for the typical value $\alpha_s = 0{,}13$. Values of α_s for measured T_{max} differing from T_{pr} were calculated by the linear iterative formula

$\alpha_s = 0{,}13 + (T_{max}-T_{pr})/(\partial T/\partial\alpha_s)$,

where $\partial T/\partial\alpha_s$ was obtained from the curves for the previously derived α_s.

The random error introduced by this graphical data reduction process is estimated to be ± 0,02 K for temperature and 2% for $\partial T/\partial\alpha_s$. This is equivalent to an uncertainty of approximately 1% in $\Delta\alpha_s$/year.

Errors due to temperature measurements and to telemetry were considered negligible.

RESULTS

The results deduced by the above methods are shown as solid curves in Figure 5-89. All the curves exhibit an abrupt linear rise in α_s beginning at autumnal equinox, and an equally sharp decay at normal equinox. This is due to the incidence effect discussed in paragraph 7.3.2.3 of clause 5.2.6. The significance of this effect is estimated by first assuming a linear variation of α_s vs. time for normal incidence from autumnal equinox, following the general trend of the curves after excluding abnormal increases and decreases. The dashed curves are supposed to represent α_s vs. time corrected to normal incidence, and the difference is the effect of incidence. These last data fairly correlated (Particularly those from D-2 and D-3) with integrating sphere spectroreflectometer measurements made on an OSR sample at 20° and 40° from normal (Figure 5-86). No explanation of the larger deviation of D-1 data is given.

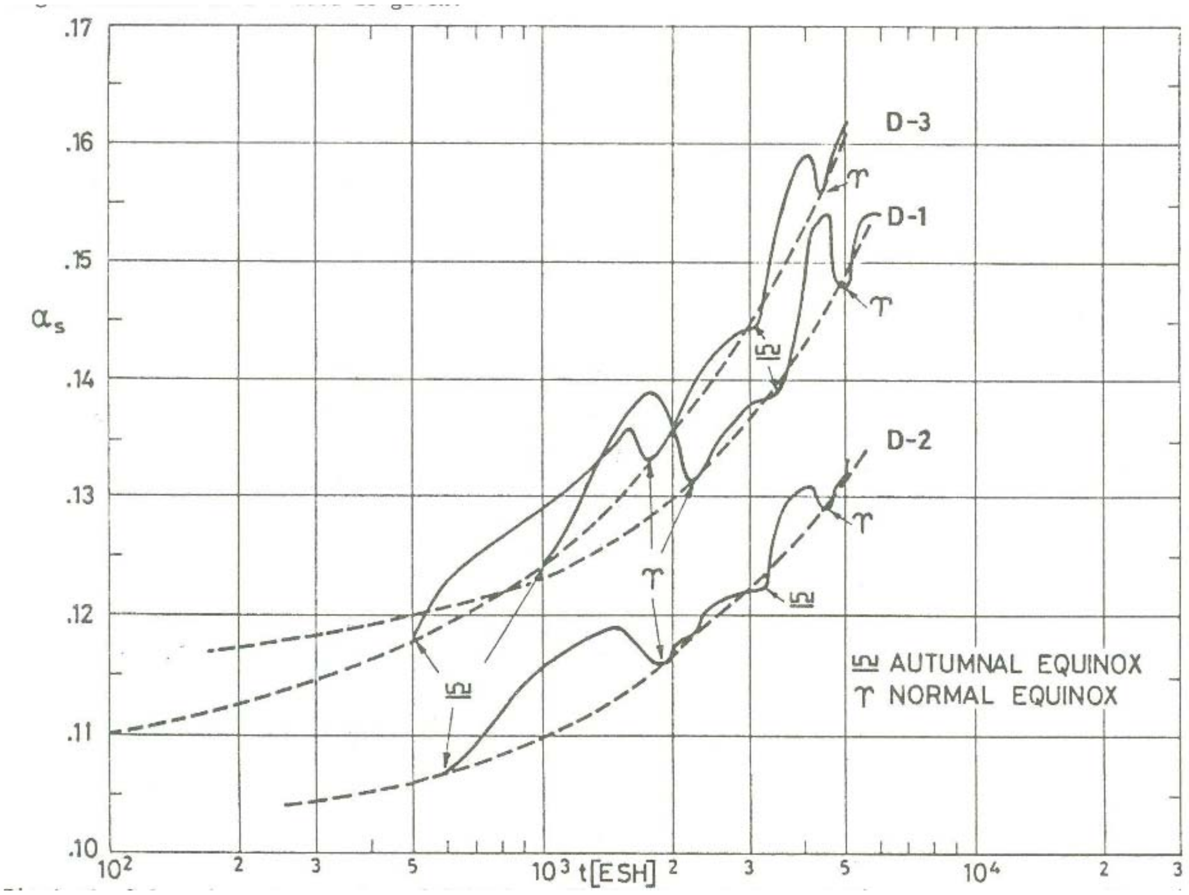

Note: non-si units are used in this figure

Figure 5-89: Solar absorptance, α_s, of OCLI Type SI-100 Thermal Control Mirrors vs. exposure time, *t*, as deduced from data of COMSTAR D-1, D-2 and D-3 satellites.
▬▬▬: Derived from> temperature telemetry.
▬ ▬: Corrected to> normal solar incidence.

COMMENTS

The curves corresponding to normal solar incidence given by Hyman (1981) [62] exhibit a high initial slope until approximately the first summer solstice (2000 to 3000 ESH), afterwards the slope decreases and remains constant. This cannot be appreciated in Figure 5-89 because of the logarithmic scale used in abscissa.

D-3 values are higher than the other two. The explanation could be based on the approximately 2 years longer storage time for D-3 mirrors. Although deposits on these mirrors were noticed, only standard cleaning procedures were used and cleaning effectiveness was not measured. According to Hyman (1981) [62], telemetry data from D-4 satellite (launched February 1981), where only one of the beacon radiators has been cleaned, should clear up the present uncertainties.

References: All the data in this item, unless otherwise stated, are from Hyman (1981) [62].

SCATHA

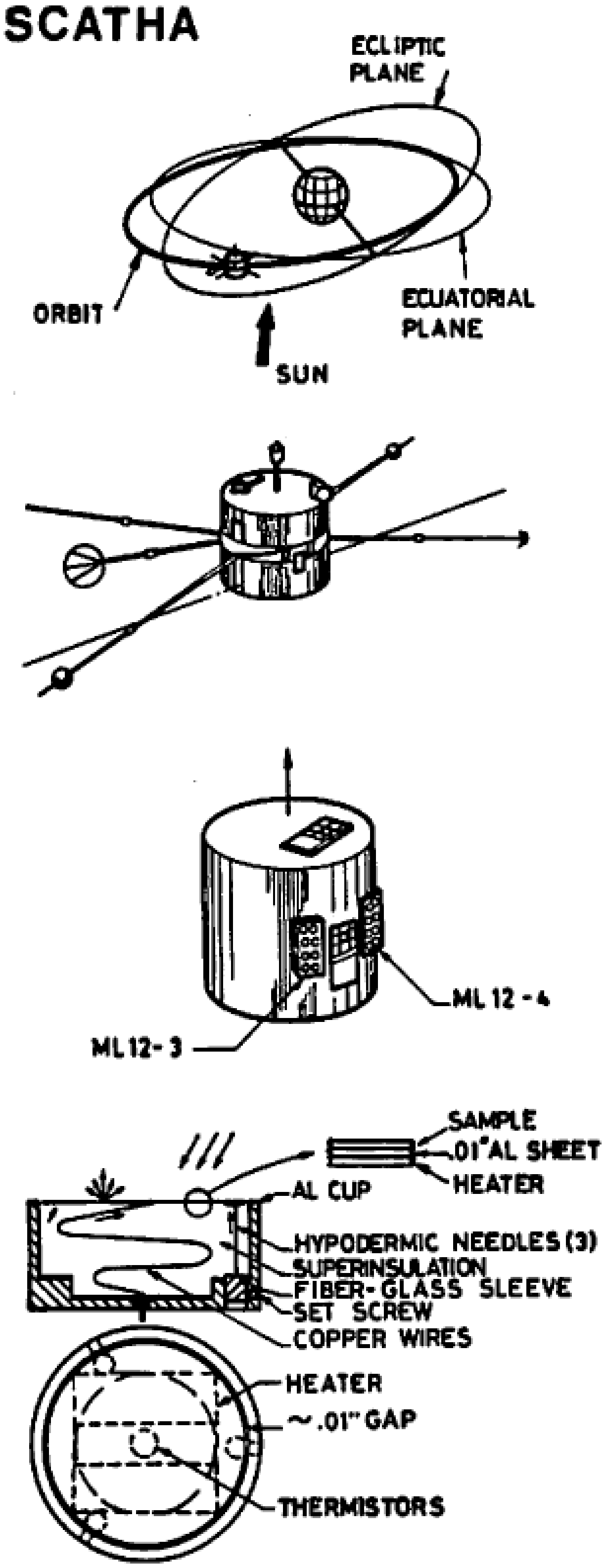
SCATHA
ECLIPTIC PLANE
ORBIT
EQUATORIAL PLANE
SUN
ML 12-4
ML 12-3
SAMPLE
.01"AL SHEET
HEATER
AL CUP
HYPODERMIC NEEDLES (3)
SUPERINSULATION
FIBER-GLASS SLEEVE
SET SCREW
COPPER WIRES
HEATER
~.01" GAP
THERMISTORS

TEST CONDITIONS

Spacecraft & Programme

Spacecraft Charging at High Altitudes (SCATHA).

USAP Space Test Programme (P78-2).

Orbit

Launched on January 30, 1979 into a 176 km by 43278 km transfer orbit. On February 2 it was injected into a 27600 km by 43300 km, 7,9° inclination final orbit. P78-2 passes through geosynchronous altitude (35786 km) twice per day and is always 23% of geosynchronism.

Configuration

The satellite is a circular cylinder approximately 1,75 m in both length and diameter. It spins with its axis approximately normal to the Sun line.

Thermal Test

Test of this OSR is a part of the ML12 experiment on board P78-2. The experiment consists of 16 calorimetrically mounted samples of thermal control coatings.

Another experiment concerning this OSR, among other coatings, has been performed on board P78-2 in the Satellite Surface Potential Monitor (SSPM) package which is devised to continually measure satellite frame to surface potential and bulk current of typical spacecraft thermal control materials (Koons, Mizera, Fennell & Hall (1980) [73]).

SAMPLE

Sample Description

OCLI Type SI-100 Mirror. 3,18x10^{-2} m diameter.

Sample Mounting

The mirror is mounted on an aluminium disc by means of diluted Eccobond EC 57C conductive epoxy. The disc is supported by three 0,014" (3,56x10^{-4} m) hypodermic needles, which are thermally insulated from the base of a cup by fiber-glass sleeving. The length and the diameter of the instrumentation leads to the disc were chosen to minimize conduction. The tubing and the wires together give approximately a thermal conductance of 9x10^{-4} W.K^{-1}. The volume enclosed by the sample plate and cup walls is filled with a combination of MLI and open-cell polyurethane insulation. The radiation coupling coefficient between sample plate and cup is approximately 7,9x10^{-12} W.K^{-4}. The underside of each sample plate carries two heaters in series and three thermistors. The heaters are used for preflight calibration and for allowing thermal desorption cleaning of the sample plate during flight. There are two trays, designated as ML12-3 and ML12-4 with eight samples each. This particular sample is placed on tray ML12-3. The trays were placed in the cylindrical surface of the satellite amid the end bases.

CALCULATION METHOD

α_s is measured calorimetrically from tray temperature, T_c, and sample plate temperature, T. The terms which appear in the heat balance are:

$c(T)dT/dt$, Sensible heat of the sample plate. The sample plate specific heat, c, is measured before launch.

$K(T_c^4-T^4)$, Radiation from the tray. K is measured before launch.

$C(T_c-T)$, Conduction from the tray. C is measured before launch.

$\varepsilon A\sigma(T_s^4-T^4)$, Radiation to outer space. ε measured before launch ($\varepsilon = 0{,}80$). the equivalent surrounding temperature, T_s, is assumed to be zero.

$\alpha_s FAS\sin\omega t$ for $0\leq \omega t\leq\pi$, and 0 for $\pi\leq \omega t\leq 2\pi$, Radiation from the Sun. F, shading factor from spacecraft booms, is calculated as a function of spacecraft attitude (resolution 1°). S is the solar flux for the day of the evaluated data.

Q_i, Power from sample heater, if applied.

α_s is calculated assuming that the sample plate temperature, T, weakly depends on time, t. A first approximation for α_s is obtained from the steady state equation ($\partial/\partial t = 0$) taking for T the measured instantaneous value, T_0. Then $T(t)-T_0$ is deduced by integration of the linearized ($T^4-T_0^4 \cong 4T_0^3(T-T_0)$) complete equation with the above α_s value. The process is repeated again with the new T.

An analysis of the expected degree of random errors has been performed. The results which are presented below are based on quick look data provided by the USAF Satellite Control Facility after one year in orbit.

The main sources of errors were, 1) Resolution of the telemetry system. The various input parameters which appear in the balance equation were varied by amounts equal to the resolution inherent in the telemetry processing, and the change in α_s was calculated. Reduction of the uncertainty may be possible by averaging large data sheets contained on magnetic tape. 2) Shading from the booms. The errors arise from the resolution of the table of shading values vs. attitude angle, and from the uncertainty of the angle at a given time. Reduction of the uncertainty is anticipated when more accurate spacecraft attitude data become available, and by selecting data from times when the knowledge of the spacecraft attitude is not highly critical.

RESULTS

Since the spacecraft spins around an axis normal to the Sun line, it takes π hours to accumulate one ESH of exposure. Thus, the ESHs abscissae in Figure 5-90 below have been deduced multiplying $24/\pi$ the times in julian days which appear in the references. This is not really justified for vacuum and energetic particle bombardment effects.

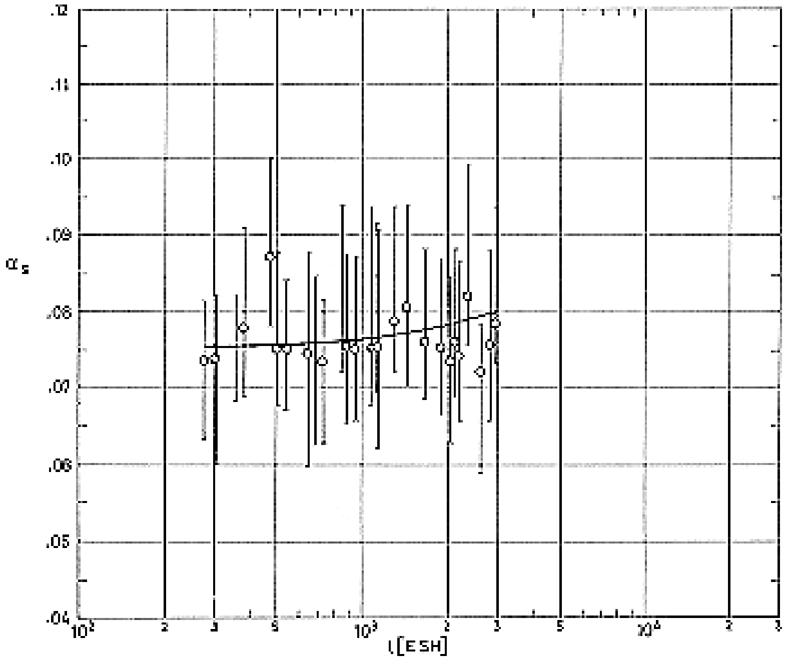

Note: non-si units are used in this figure

Figure 5-90: Solar absorptance, α_s, of OCLI Type SI-100 Thermal Control Mirrors vs. exposure time, t, as deduced from data of SCATHA spacecraft.

COMMENTS

α_s remained approximately constant over the year in orbit, which suggests that the coating is stable and that contamination effects were minor.

In order to calculate $\Delta\alpha_s$ plotted in the summary figure, Figure 5-92, the value α_{s0}= 0,075, resulting from the extrapolation to t = 0 of the curve in Figure 5-90, has been taken. This fairly large value (compare with those given in paragraph 7.3.2.1 of clause 5.2.6) seems to indicate that the initial degradation was relatively high.

References: All the data in this item, unless otherwise stated, are from Hall & Fote (1979, 1980) [55] & [56].

HELIOS

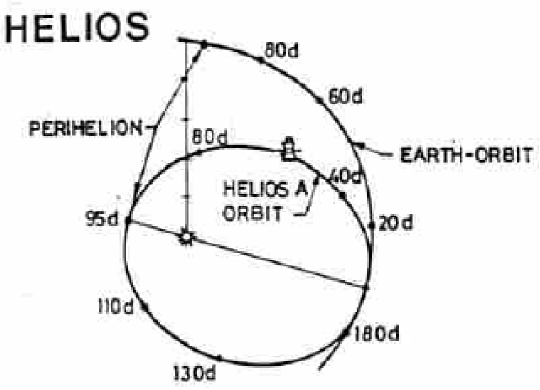
HELIOS
80d
60d
PERIHELION
80d
EARTH-ORBIT
40d
HELIOS A
ORBIT
95d
20d
110d
180d
130d

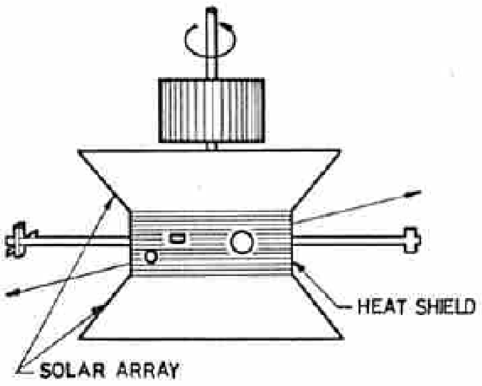
HEAT SHIELD
SOLAR ARRAY

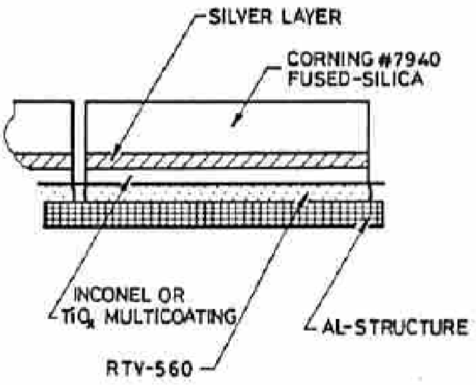
SILVER LAYER
CORNING #7940
FUSED-SILICA
INCONEL OR
TiO$_x$ MULTICOATING
AL-STRUCTURE
RTV-560

TEST CONDITIONS

Spacecraft & Programme

HELIOS-A and HELIOS-B solar probes.

Orbit

HELIOS-A was launched on December 12, 1974 on a highly eccentric elliptic solar orbit with a perihelion of 0,31 AU (1 AU = 1,495x10^{11} m). HELIOS-B was launched on January 15, 1976 on a slightly different orbit, perihelion of 0,29 AU.

Data presented here correspond to HELIOS-A first three orbits and HELIOS-B first orbit. Environmental conditions were similar to those assumed before launching (which correspond to black circles in Figure 5-87) although, according to measurements performed during HELIOS-Amission, the integrated flux of protons was 3,2x10^{20} p.m^{-2}. Solar flares were not detected, but an additional integrated flux of 2x10^{20}p.m^{-2} is estimated for an average Sun (1978-1980).

Configuration

HELIOS is an automatically-functioning solar probe. The basic structure is spool-shaped, with a cylindrical central compartment 1,75 in diameter by 0,55 m long. A conical solar array is attached to each end, completing the spool-shape.

The telecommunications antenna system is placed on the central body, within and protruding above the upper solar array. Two deployable double-hinged booms are fitted to carry experiments. Two other deployable booms, diametrically opposed, are used as antennae for radio-wave experiments.

Thermal Test

HELIOS was devised to investigate the solar wind, but temperatures in specific points were recorded for house-keeping purposes. The records were used for coating behavior evaluation. HELIOS-A and B were practically similar, only the ion guards of the horizontal antennae of HELIOS-B were modified and enlarged.

SAMPLE

Sample Description

OCLI Type SI-100 Mirror.

Sample Mounting

Sample was bonded on aluminium substrate, RTV 560 adhesive.

Data were deduced from a single temperature sensor (S2) placed at the upper edge of the heat shield, under the mirror substrate, within easy reach of the conical solar array IR radiation. This location, not chosen for reasons connected with sample monitoring, presents the following drawbacks. 1) High thermal coupling, both conductive and radiative, with the solar array. This effect is stronger the lower the temperature, in relative terms. 2) A thick contamination layer resulting from the sensor location near the corner. Thus $\Delta\alpha_s$, both initial and after the first perihelion was very pronounced in the particular case of this sample.

CALCULATION METHOD

A first estimate of α_s was made neglecting thermal couplings between spacecraft and sensor. Thence, $\alpha_s S = \varepsilon\sigma T$, were ε is assumed to be constant. Results from the first HELIOS-A orbit, as given by Winkler & Brungs (1975) [136], are shown in Figure 5-91. The estimated initial value of $\alpha_s$is $\alpha_s = 0{,}062$. Data near perihelion and near aphelion were lost since the measuring range of the sensor was limited to 233 K - 333 K.

The analysis of the results was mostly speculative at that stage both because of the above oversimplified calorimetric approach, and of the incomplete simulation of the following effects during ground tests. 1) Sample contamination, influenced by sources location, cold and hot surfaces,... 2) Sample degradation (physicochemical damage effects) which depends on the temperature. 3) Non-steady conditions (spin, varying Earth-Sun distance). 4) Combined effects.

Solar input data were considered reliable, and in fair agreement with those used for ground testing.

Errors due to the resolution of the telemetry system are, for instance, at aphelion: $\Delta\alpha_s = \pm\, 0{,}006$ for $\Delta T = \pm\, 1$ K.

Data from the first three orbits of HELIOS-A and the first orbit of HELIOS-B have been analyzed by Winkler (1977) [135]. The following effects have been considered. 1) Conductive thermal coupling between the spacecraft surface and the central compartment where the sensor is located. This introduces a correction which, for sensor S2, is $\Delta\alpha_s = 0{,}17\ (T_o - T_i)$, where T_o and T_i are outer and inner spacecraft temperatures, respectively. This correction accounts for most of the improvement in the analysis particularly near the perihelion. 2) Radiative thermal coupling and shading effects, which can be neglected for both HELIOS-A and B regarding this particular sample. 3) Influence of temperature on the hemispherical total emittance. 4) Degradation and contamination.

RESULTS

Results from Winkler & Brungs (1975) [136] and Winkler (1977) [135] are shown in Figure 5-91. Time in ESH has been calculated by assuming that the flux, for both UV and protons, varies as the square of the distance to the Sun.

Time for HELIOS-B has been compressed by a factor of 1,14, so that the perihelion and aphelion of both orbits correspond to the same ESH values.

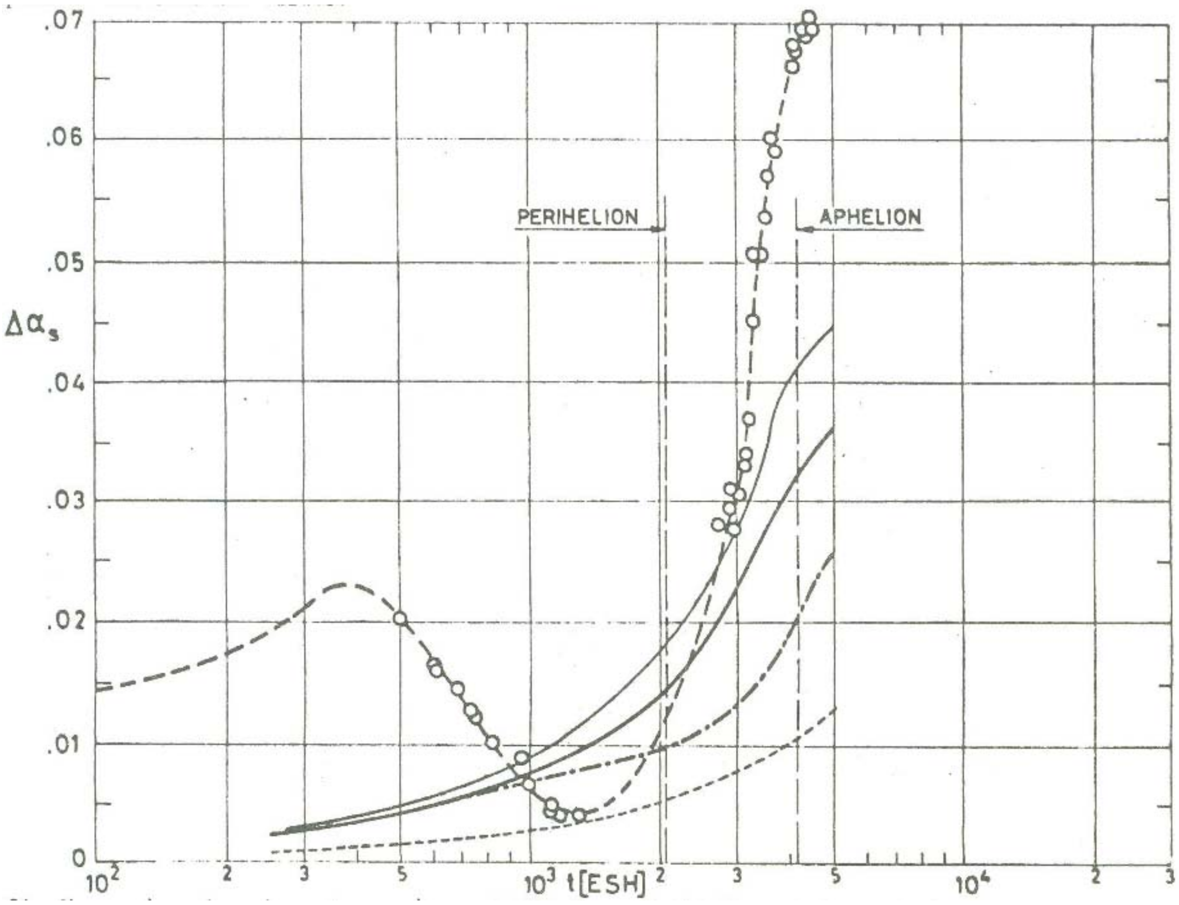

Note: non-si units are used in this figure

Line of circles	First HELIOS-A orbit. Simplified model of data analysis.
▬▬▬	Average of the> first three HELIOS-A orbits. Improved model of data analysis.
———	First HELIOS-B> orbit. Improved model of data analysis.
▬ ▬	Average of the> first three HELIOS-A orbits. Effect of degradation alone. Figure 5-87, α_{so} = 0,062.
▬·▬	Average of> the first three HELIOS-A orbits. Effect of contamination alone. Calculated.

Figure 5-91: Change in solar absorptance, $\Delta\alpha_s$, of OCLI Type SI-100 Thermal Control Mirrors vs. exposure time, *t*, as deduced from data of HELIOS-A and B spacecraft.

COMMENTS

In addition to the usual phenomena associated to outgassing under vacuum conditions, long time missions with extended periods at elevated temperatures, such as in HELIOS satellites, pose several peculiar problems.

1. Due to elevated temperatures a small fraction of the surrounding adhesive begins to creep into the surface sticking there. Incoming particles or high energy photons partially crack this creeping material. The resulting ions and neutral particles escape into open space (secondary outgassing). To estimate the influence of this effect on $\Delta\alpha_s$ it is assumed that, at least for the five or six first orbits, the rate of deposition on the spacecraft surface is constant. From the analysis of the results one can deduce that the thickness of the layer deposited in each orbit is $4{,}16\text{x}10^{-8}$ m.

2. Since the electric potential of the spacecraft surface is unevenly distributed and different from that of the undisturbed surrounding plasma, a boundary layer appears around the spacecraft whose thickness depends on the potential difference, and on plasma density and temperature. Outgassing material, which is ionized within the boundary layer, will rebound onto the surface creating a deposit of ionized molecules which increase α_s. One can estimate the thickness of the deposit on the basis of ad hoc values of the fraction of the ionized particles which build up the contamination layer, and of outgassing kinetic data (not readily available). Such processes as cracking, creeping, polymerization and others, leading to long term effects upon adhesives, are accounted for by means of an additional constant term.

The $\Delta\alpha_s$ value is related to the contamination thickness, Δt, by means of $\Delta\alpha_s = 1 - e^{B\Delta t}$ where $B = 1{,}2\text{x}10^5$ m^{-1}. Values calculated by Winkler (1977) [135] for the first three HELIOS-A orbits are:

1st orbit $\Delta t = 4{,}16\text{x}10^{-8}$ m + $8{,}50\text{x}10^{-8}$ m, $\Delta\alpha_s = 0{,}016$. The real value was $\Delta\alpha_s = 0{,}019$, because of sample position.

2nd orbit $\Delta t = 4{,}16\text{x}10^{-8}$ m + $12{,}76\text{x}10^{-8}$ m, $\Delta\alpha_s = 0{,}029$.

3rd orbit $\Delta t = 4{,}16\text{x}10^{-8}$ m + $16{,}92\text{x}10^{-8}$ m, $\Delta\alpha_s = 0{,}043$.

References: Winkler & Stampfl (1975) [139], Winkler & Brungs (1975) [136], Winkler (1977) [135].

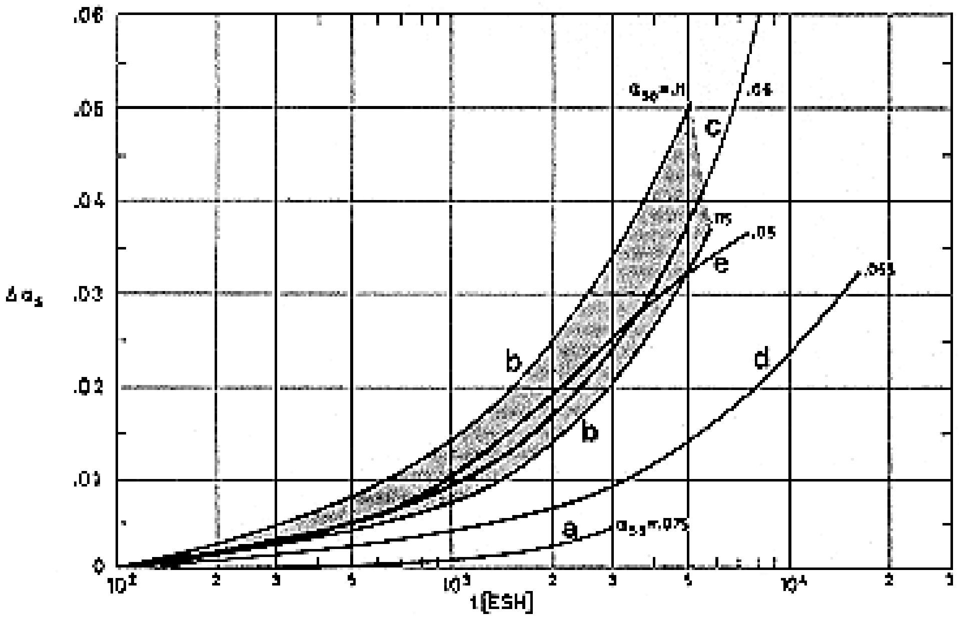

Note: non-si units are used in this figure

Figure 5-92: Summery data on the change in solar absorptance, *Δα*$_s$, of OCLI Type SI-100 Thermal Control Mirrors vs. exposure time, *t*.

The estimated values of the initial solar absorptance, α_{so}, are shown near each curve.
a From SCATHA. Partially geosynchronous orbit. α_{so} = 0,075.
b From COMSTAR. Geosynchronous orbit. Contaminated before launching.
α_{so} = 0,11 (COMSTAR D-3)
α_{so} = 0,115 (COMSTAR D-1)
See the description of COMSTAR in paragraph 7.3.2.5.6 of this clause.
c From NAVSTAR. Influenced by Van Allen radiation. α_{so} = 0,06
See the description of COMSTAR in paragraph 7.3.2.5.6 of this clause.
d Ground test. "Clean" simulation of HELIOS orbit. α_{so} = 0,065
See Figure 5-87.
e Ground test. Simulation of OTS orbit. α_{so}= 0,05
See paragraph 7.3.3.2.6 of clause 5.2.6.

The figure clearly shows the need for revised flight data acquisition procedures, improved satellite materials and careful ground-handling techniques, and the inadequacy of a data presentation in terms of the ultra-violet exposure time.

7.3.3. Reflectance.

7.3.3.1. Normal-hemispherical spectral reflectance. Data in Figure 5-93 are from Cunnington, Grammer & Smith (1969) [33].

Sample bonded to a 6061-T6 aluminium substrate. Adhesive not identified in the source.

Spectral reflectance in the wavelength range 2,7x10^{-7} m to 1,8x10^{-6} m was measured with a Cary Model 14 spectrophotometer with an integrating sphere operating in the indirect mode, i.e.: the sphere is illuminated from the external optics while the detector views the sample.

The Cary sphere is small and has relatively large apertures. This results in significant errors which can be minimized by calibration against known surfaces. A limited number of absolute measurements were made using a much larger integrating sphere, Gier-Dunkle Model SP 210, attached to a Perkin-Elmer Model 98 monochromator. When the Gier-Dunkle instrument is used to calibrate Cary measurements on identical samples, the accuracy in reflectance readings with the latter instrument is 0,02. Measurements in the wavelength range 2x10^{-6} m to 25x10^{-6} m were made with a Gier-Dunkle Model HC-300 heated cavity reflectometer in conjunction with a Perkin-Elmer Model 98 monochromator and a Brewer Model 129 chopper-amplifier system. The maximum relative error is, for most samples, no greater than ± 0,010. This instrument does not allow exactly normal ($\beta' = 0$) measurements with perfectly specular samples, since then the reflected flux from the sample originates from the viewing port itself.

Measurements were performed in ambient air.

See also data "before exposure" in Figure 5-94.

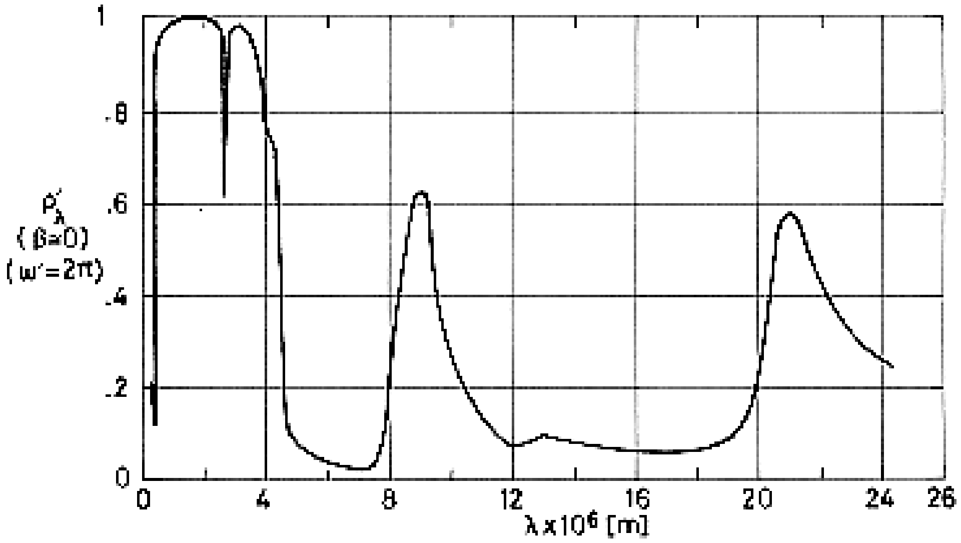

Note: non-si units are used in this figure

Figure 5-93: Normal-hemispherical spectral reflectance, ρ'_λ, of OCLI Type SI-100 Thermal Control Mirrors vs. wavelength, λ. From Cunnington, Grammer & Smith (1969) [33].

7.3.3.2. Effect of the Space Environment on reflectance.

7.3.3.2.1. Ultra-Violet Radiation. Data in Figure 5-94 are from Cunnington, Grammer & Smith (1969) [33]. The ultra-violet source was a 900 W Hanovia Xenon lamp, Model 530-CL. Uniformity of the source total irradiance was better than 10% within 10^{-2}m of the sample center.

A 1000 W, controllable and programmable tungsten iodide lamp, GE DXW, is used to heat the back of the substrate, so that the sample can be maintained at a given temperature or thermally cycled.

Radiation flux density at the sample level: 1 Sun.

Temperature: 339 K.

Chamber pressure: 1,33x10^{-5} Pa.

Exposure time: 2040h.

Spectral reflectance measured at ambient pressure and temperature, before and after irradiation.

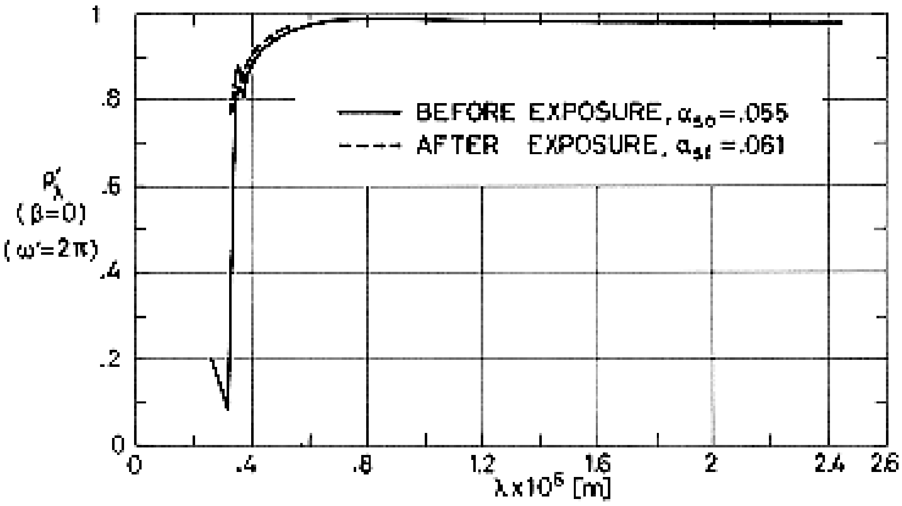

Note: non-si units are used in this figure

Figure 5-94: Effect of Ultra-Violet radiation on normal-hemispherical spectral reflectance, ρ'_λ, of OCLI Type SI-100 Thermal Control Mirrors vs. wavelength, λ. From Cunnington, Grammer & Smith (1969) [33].

7.3.3.2.6. Combined exposure. The following data are from Paillous (1975) [95], DERTS.

Sample on aluminium substrate. Three of the samples (labeled 1 to 3) were bonded with RTV 560 adhesive, and two more samples (4 and 5) were fastened bare.

Irradiation made under the following conditions:

Chamber pressure below 1,3x10^{-4} Pa.

Sample temperature: 363 K.

Reflectance measured in situ without breaking vacuum, unless otherwise stated.

Comments under CAUTION in paragraph 7.3.2.5.3 of clause 5.2.4 do not apply here because of the specular behavior of the mirrors.

The exposure is intended to simulate 7 years in geosynchronous orbit of the three-axis stabilized Orbital Test Satellite (OTS) north and south faces. The tests reproduced the simultaneous action of vacuum and temperature, and of ultra-violet, protons and electrons. The experimental facilities are those mentioned in paragraphs 7.3.3.2.3, 7.3.3.2.4 and 7.3.3.2.6 of clause 5.2.4. The procedures are also similar. See for further details Paillous (1975) [95].

Simulation time was controlled by the maximum achievable solar radiation flux density at the sample level, which was smaller than 3 Suns. Thence, protons and electrons, which could require shorter simulation times, were irradiated intermittently, whereas ultra-violet irradiation was performed continuously within the constraint of a correct simulation of the integrated fluxes at the end of the seven main steps of the test (Table 5-29).

Table 5-29: Test Conditions Simulating up to Seven Years in Geosynchronous Orbit

		Step A	**Step B**	**Step C**	**Step D**	**Step E**	**Step F**	**Step G**
Years in Orbit		0,17	1,11	2,05	3,15	4,05	5,40	7,14
Simulation Test Time [h]		96	612	1134	1740	2240	2982	3946
ESH		192	1224	2268	3480	4480	5964	7892
Protons Exposure 40 keV	Starting Time, First Run [h]	48	564	1110	1728	2228	2970	3934
	Stopping Time, Last Run [h]	96	612	1134	1740	2240	2982	3946
	Net Running Time [h]	48	48	24	12	12	12	12
	Flux [Protons.m^{-2}.s^{-1}]	4,05x10^{12}	2,26x10^{13}	4,86x10^{13}	1,07x10^{14}	9,03x10^{13}	1,32x10^{14}	1,67x10^{14}
	Integrated Flux [Protons.m^{-2}]	6,92x10^{17}	3,90x10^{18}	4,25x10^{18}	4,69x10^{18}	3,87x10^{18}	6,01x10^{18}	6,97x10^{18}
	Cumulative Integrated Flux [Protons.m^{-2}]	6,92x10^{17}	4,59x10^{18}	8,84x10^{18}	1,35x10^{19}	1,74x10^{19}	2,34x10^{19}	3,04x10^{19}
Protons Exposure 150 keV	Starting Time, First Run [h]	24	516	1086	1716	2216	2958	3922
	Stopping Time, Last Run [h]	48	564	1110	1728	2228	2970	3934
	Net Running Time [h]	24	48	24	12	12	12	12
	Flux [Protons.m^{-2}.s^{-1}]	2,90x10^{11}	7,52x10^{11}	1,49x10^{12}	3,68x10^{12}	3,01x10^{12}	4,47x10^{12}	5,65x10^{12}
	Integrated Flux [Protons.m^{-2}]	2,51x10^{16}	1,40x10^{17}	1,26x10^{17}	1,58x10^{17}	1,29x10^{17}	1,98x10^{17}	2,36x10^{17}
	Cumulative Integrated Flux [Protons.m^{-2}]	2,51x10^{16}	1,65x10^{17}	2,91x10^{17}	4,49x10^{17}	5,78x10^{17}	7,76x10^{17}	1,01x10^{18}
Electrons	Starting Time, First Run [h]	0	516	1086	1716	2216	2958	3922

		Step A	Step B	Step C	Step D	Step E	Step F	Step G
Exposure 200 keV	Stopping Time, Last Run [h]	96	612	1134	1740	2240	2982	3946
	Net Running Time [h]	96	96	48	24	24	24	24
	Flux [Electrons.$m^{-2}.s^{-1}$]	$4{,}05\text{x}10^{12}$	$2{,}28\text{x}10^{13}$	$4{,}83\text{x}10^{13}$	$1{,}06\text{x}10^{14}$	$9{,}03\text{x}10^{13}$	$1{,}38\text{x}10^{14}$	$1{,}66\text{x}10^{14}$
	Integrated Flux [Electrons.m^{-2}]	$1{,}43\text{x}10^{18}$	$7{,}92\text{x}10^{18}$	$8{,}44\text{x}10^{18}$	$9{,}13\text{x}10^{18}$	$7{,}70\text{x}10^{18}$	$1{,}19\text{x}10^{19}$	$1{,}44\text{x}10^{19}$
	Cumulative Integrated Flux [Electrons.m^{-2}]	$1{,}43\text{x}10^{18}$	$9{,}35\text{x}10^{18}$	$1{,}78\text{x}10^{19}$	$2{,}69\text{x}10^{19}$	$4{,}36\text{x}10^{19}$	$4{,}65\text{x}10^{19}$	$6{,}09\text{x}10^{19}$

NOTE From Paillous (1975) [95].

The following measurements were made:

1. Spectral reflectance at ambient conditions in air, before and after irradiation. An integrating sphere attached to the Beckman DK2A reflectometer was used.

Standards of polished aluminium. Total solar reflectances from these data, ρ_s, are given in Table 5-30.

2. In situ measurements of global reflectance, as in paragraph 7.3.3.2.6 of clause 5.2.4. The illuminating source was a solar-simulating high-pressure Xenon lamp, 75 W. Results appear in Table 5-30 as ρ.

3. In situ spectral reflectance, as in paragraph 7.3.3.2.3 of clause 5.2.4. The incident flux came from a Zeiss monochromator. The spectral measurements were made with two detectors attached to the integrating sphere: a photodiode for λ in the range $5{,}46\text{x}10^{-7}$ m to $1{,}5\text{x}10^{-6}$ m, and a photomultiplier for the range $2{,}75\text{x}10^{-7}$ m to $6{,}50\text{x}10^{-7}$ m. A limited amount of data are given in Figure 5-95 and Figure 5-96. The resulting spectral data were integrated against the solar spectral irradiance to obtain the reflectance for the different spectral bands (ultra-violet, visible, infrared and solar). Results appear in Table 5-30.

   An incident occurred during ultra-violet only irradiation between steps E and F, around the 2360 experiment hours (nearly 4,5 simulated years). One night the chamber pressure rose up to 1 Pa to 10 Pa. The damage was repaired the next morning. Duration of the malfunction was not determined.

The results look fairly insensitive to this incident.

Table 5-30: Combined Exposure Effects of Reflectance of OCLI Type SI-100. Thermal Control Mirrors.

	From Global Measurements				
	ρ for Xenon Lamp				
Sample	**1**	**2**	**3**	**4**	**5**
In Air before irradiation					
Under vacuum, <1,3x10^{-4} Pa. 293 K.	0,97	0,97	0,95	0,96	0,97
After 1 h under vacuum, <1,3x10^{-4} Pa. 363 K.	0,989	0,982	0,970	0,977	0,977
After 48 h under vacuum, <1,3x10^{-4} Pa. 363 K.	0,986	0,965	0,970	0,981	0,971
48 h after starting step A	0,982	0,974	0,984	0,987	0,972
After step A	0,989	0,969	0,979	0,975	0,969
Before step B	0,986	0,970	0,970	0,975	0,970
After step B	0,975	0,972	0,975	0,978	0,970
Before step C	0,980	0,975	0,975	0,965	0,967
After step C	0,969	0,964	0,971	0,974	0,971
Before step D	0,962	0,962	0,964	0,977	0,969
After step D	0,965	0,965	0,967	0,970	0,957

	From Global Measurements				
	ρ for Xenon Lamp				
Before step E	0,966	0,968	0,968	0,971	0,963
During step E (no details are given)	0,971	0,966	0,971	0,971	0,977
After step E	0,968	0,965	0,976	0,971	0,957
After vacuum pump incident (4800 ESH)	0,969	0,971	0,971	0,974	0,969
5300 ESH	0,963	0,964	0,971	0,986	0,967
Before step F	0,964	0,967	0,967	0,976	0,967
After step F	0,972	0,959	0,972	0,985	0,969
Before step G	0,970	0,951	0,969	0,983	0,970
After step G (First readings)	0,967	0,965	0,965	0,967	0,955
After step G (Second readings)	0,961	0,961	0,963	0,971	0,961
After Exposure, 12 h in Air at 293 K.	0,963	0,964	0,964	0,971	0,961
In Air after irradiation					

	From Spectral Measurements									
	ρ_{sUV} $2{,}35 \leq \lambda x10^{7}[m] \leq 3{,}80$					ρ_{sV} $2{,}95 \leq \lambda x10^{7}[m] \leq 7{,}30$				
Sample	1	2	3	4	5	1	2	3	4	5
In Air before irradiation										
Under vacuum $<1{,}3x10^{-4}$ Pa. 293 K.	0,48	0,46	0,46	0,47	0,47	0,89	0,88	0,89	0,92	0,91
After 1 h under vacuum $<1{,}3x10^{-4}$ Pa. 363 K.										
After 48 h under vacuum $<1{,}3x10^{-4}$ Pa. 363 K.	0,46	0,45	0,46	0,47	0,46	0,92	0,92	0,92	0,91	0,90
48 h after starting step A										
After step A	0,45	0,46	0,45	0,46	0,44	0,91	0,91	0,91	0,91	0,89
Before step B										
After step B										
Before step C										
After step C			0,42	0,43				0,89	0,89	
Before step D										
After step D	0,42	0,44	0,43	0,43	0,42	0,88	0,88	0,88	0,88	0,88
Before step E										

	From Spectral Measurements									
	ρ_{sUV} 2,35≤ λx10^{7}[m]≤ 3,80					ρ_{sV} 2,95≤ λx10^{7}[m]≤ 7,30				
During step E (no details are given)										
After step E										
After vacuum pump incident (4800 ESH)			0,43	0,43				0,87	0,87	
5300 ESH										
Before step F			0,42	0,42				0,87	0,86	
After step F			0,41	0,42				0,88	0,86	
Before step G			0,41	0,41				0,86	0,86	
After step G (First readings)	0,41	0,42	0,42	0,39	0,40	0,88	0,86	0,87	0,84	0,85
After step G (Second readings)	0,42	0,43	0,43	0,42	0,41	0,88	0,88	0,87	0,85	0,84
After Exposure, 12 h in Air at 293 K.			0,43	0,42				0,86	0,86	
In Air after irradiation										

	From Spectral Measurements									
	ρ_{sIR} 7,30≤ λx10^7[m]≤ 40					ρ_s				
Sample	1	2	3	4	5	1	2	3	4	5
In Air before irradiation						0,95	0,95	0,95	0,95	0,95
Under vacuum <1,3x10^{-4} Pa. 293 K.	0,97	0,95	0,96	0,97	0,96	0,93	0,92	0,93	0,95	0,93
After 1 h under vacuum <1,3x10^{-4} Pa. 363 K.										
After 48 h under vacuum <1,3x10^{-4} Pa. 363 K.	0,99	0,99	0,98	0,99	0,99	0,96	0,95	0,95	0,96	0,94
48 h after starting step A										
After step A	1,00	0,99	0,98	1,00	0,99	0,96	0,95	0,94	0,96	0,94
Before step B										
After step B										
Before step C										
After step C			0,98	1,00				0,94	0,94	
Before step D										
After step D	0,97	0,98	0,97	0,99	0,97	0,93	0,93	0,92	0,94	0,92
Before step E										

	From Spectral Measurements									
	ρ_{sIR} 7,30≤ λx10^{7}[m]≤ 40					ρ_{s}				
During step E (no details are given)										
After step E										
After vacuum pump incident (4800 ESH)			0,97	0,99				0,92	0,93	
5300 ESH										
Before step F			0,96	0,96				0,92	0,91	
After step F			0,97	0,99				0,93	0,92	
Before step G			0,97	0,99				0,92	0,93	
After step G (First readings)	0,97	0,98	0,97	0,97	0,96	0,92	0,92	0,92	0,91	0,91
After step G (Second readings)	0,98	0,98	0,98	1,00	0,98	0,93	0,93	0,93	0,93	0,91
After Exposure, 12 h in Air at 293 K.			1,02	1,00				0,94	0,93	
In Air after irradiation						0,94	0,94	0,94	0,94	0,94

NOTE From Paillous (1975) [95].

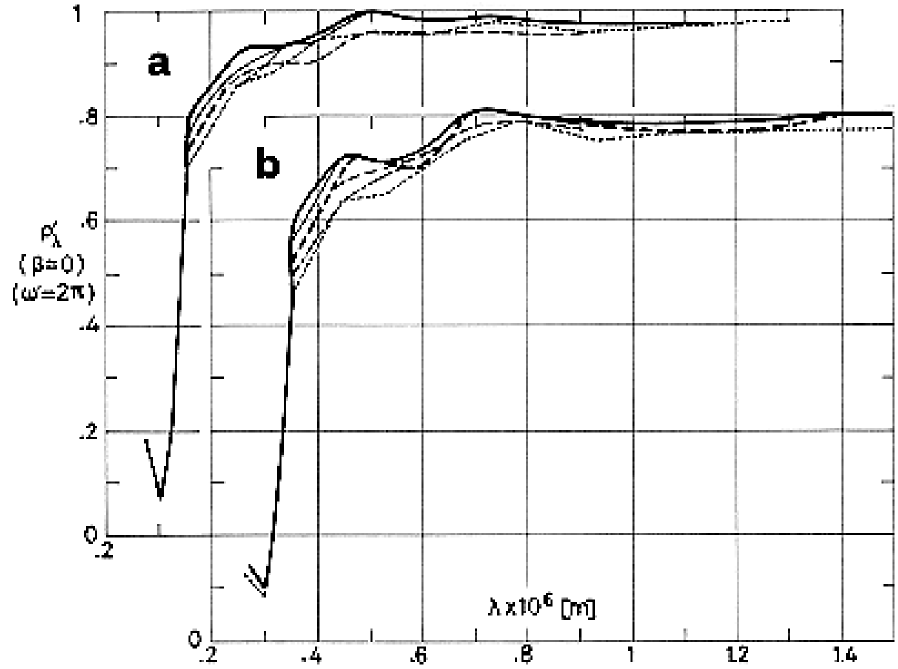

Note: non-si units are used in this figure

Figure 5-95: Effect of Combined Exposure, simulating up to seven years in geosynchronous orbit, on normal-hemispherical spectral reflectance, ρ'_λ, of OCLI Type SI-100 Thermal Control Mirrors vs. wavelength, λ. *a* Bonded sample. *b* Sample fastened bare. From Paillous (1975) [95].

Explanation

Key	Description	Comments
▬▬▬	After 48 h below 1,3x10^{-4} Pa pressure. T = 363 K.	
———	After step *A* (0,17 years in orbit). T = 363 K.	
▬ ▬	After step *C* (2,05 years in orbit). T = 363 K.	
— —	After step *D* (3,15 years in orbit). T = 363 K.	
▬·▬	After step *F* (5,4 years in orbit). T = 363 K.	After vacuum pump incident.
••••••••	After step *G* (7,14 years in orbit). T = 363 K.	

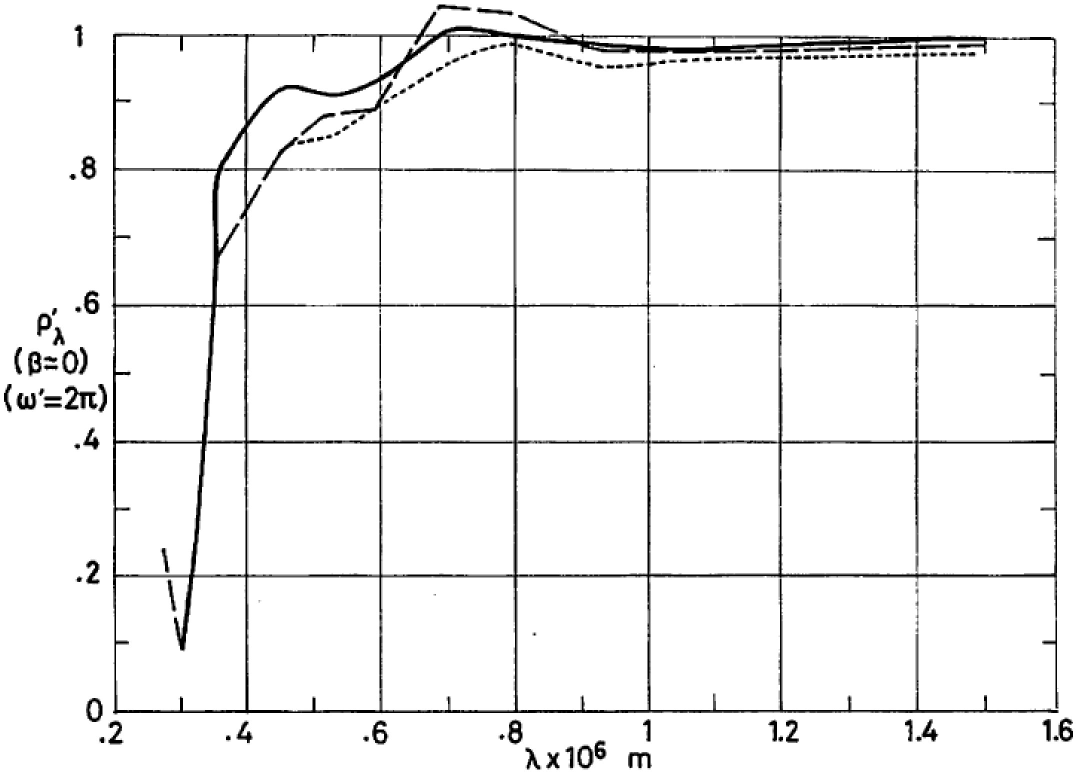

Note: non-si units are used in this figure

Figure 5-96: Effect of Combined Exposure, simulating up to seven years in geosynchronous orbit, on normal-hemispherical spectral reflectance, ρ'_{λ}, of OCLI Type SI-100 Thermal Control Mirrors vs. wavelength, λ. Sample fastened bare. From Paillous (1975) [95].

Explanation

Key	Description	Comments
▬▬	After 48 h below 1,3x10^{-4} Pa pressure. T = 363 K.	Same curves as in Figure 5-95.
••••••••	After step G (7,14 years in orbit). T = 363 K.	
▬ ▬	After Combined Exposure followed by 12 h in air at 293 K.	ρ'_{λ}1. Could give an estimate of the uncertainty level associated to data acquisition and handling.

7.4. Electrical resistance. OCLI Type SI-100 mirrors are nonconductive. Thence, the mirrors show a tendency to be charged electrostatically, particularly when the spacecraft becomes immersed in a substorm plasma.

7.4.3. Charging. The differential charging of the spacecraft components to a high voltage may generate a discharge (vacuum arc, arcing) if the voltage level exceeds the breakdown potential of the material.

The implications of these phenomena are:

1. On the thermal control mirrors.

   Charging might accelerate the deposition of contaminants.

   The discharges liberate contaminants.

   The discharges damage the mirrors.

2. On the onboard instrumentation.

   The components are irradiated by the electromagnetic waves associated with the vacuum arc.

   Transient pulses of sufficient magnitude to activate (or even burn) the circuits could result.

3. On the surrounding electric field.

   Electrical charges built up in the satellite would interfere with the space field.

   For an account of the phenomena involved in spacecraft charging and arcing see Rosen (1975) [108].

   Relevant test with OCLI Type SI-100 mirrors are presented in Table 5-31.

   The outcome from these tests can be summarized as follows.

Table 5-31: Charging-Arcing Tests with OCLI Type SI-100 Thermal Control Mirrors

1

Sample: Nine mirrors on an aluminium substrate, 6,5x10^{-2} m square. Overcoat not quoted. Furnished by ESTEC. RTV 560 adhesive (nonconductive).

Tests: The experimental facility has been described by Lévy (1976) [77]. An electron accelerator is connected to a vacuum chamber, where the sample holder and irradiation monitoring devices are placed. Uniformity of irradiation is held within 40% by diffusion of the beam through a 2x10^{-6} m thick aluminium foil. pressure not given. The energy of the impinging electron beam is increased from 5 keV to 30 keV, with current densities in the range 10^{-6} A.m^{-2} to 2x10^{-5} A.m^{-2}, until breakdown results. Thereafter irradiation is pursued for 40 h under constant conditions.

Ultra-violet irradiation was superposed to electron exposure for some time. No effect was detected.

Measurements. The substrate is grounded through electrical resistors and a nanoammeter, the output of which is recorded. Potential at a point in the grounding line is measured with an oscilloscope.

For each value of the electrons beam energy, the surface potential is related to the ratio of measured intensity to beam current. The surface potential-intensity ratio relationship was established by a previous calibration with a metal sheet, placed in the sample holder, to which known voltages were applied while reading the ammeter output.

Surface currents were measured with an intensity probe placed in a grounding line from the exposed face of the mirror. Peak amplitudes of the current pulses up to 25 A, with durations in the range 2x10^{-7} s to 4x10^{-7} s, were detected. Discharge intensities as large as 7x10^{3} A.m^{-2} resulted.

Beam Energy [keV]	Beam Current Density [A.m^{-2}]	Exposure Time [h]	Temp. [K]	Surface Potential [V]	Electrostatic Discharges			Voltage Breakdown [V]	Comments
					Occurrence	Rate [min^{-1}]	Total Number in 6 h		
25	2x10^{-5}	40						Between 4000 and 9000	Minimum conditions for breakdown. Estimated error in voltage readings was ± 1000 V.
30					Many		65		

From Lévy (1976) [77]

2

Sample. Nine mirrors on an aluminium substrate, 6,5x10^{-2} m square. Overcoat not quoted. Furnished by ESTEC. Conductive adhesive.

Tests. As above.

Measurements. As above. Surface currents at breakage were not measured.

Beam Energy [keV]	Beam Current Density [A.m^{-2}]	Exposure Time [h]	Temp. [K]	Surface Potential [V]	Electrostatic Discharges			Voltage Breakdown [V]	Comments
					Occurrence	Rate [min^{-1}]	Total Number in 6 h		
15	10^{-5}	0,5		5500					First run. One of the mirrors showed a transversal crack (not ascribable to the test). The breakdown occurs at lower energies than in table above, where a non-conductive adhesive was used.
20		1,33			Both small and large	1/5 to 1/7	60	6000	
25		0,6				1/4	90	5400	
20		1,43				2/7 to 2/9	90	4500	
25		0,42				2/7	100	4400	
25	2x10^{-5}	0,35				2/3	240	4000	
30	10^{-5}	0,73				1/3	120	4700	15 h since the end of the above run. Voltage breakdown decreases with beam energy.
30	2x10^{-5}	0,67				2/3 to 1/2	200	4600	
15	10^{-5}	0,75				1/15 to 1/20	20	7500	Same energy and flux as in the first run.

From Lévy & Sarrail (1976) [78].

3

Sample. Several mirrors (36 to 49) on a metal substrate. Neither overcoat nor adhesive are quoted.

Tests. An electron gun is used to irradiate a sample panel mounted on the floor of an evacuated chamber.

Measurements. The metal substrate of the sample panel is grounded through an ammeter. An electric field meter placed near the panel is used for measuring the field produced at its location by the surface charge on the sample. The relationship between (averaged) mirror surface potential and field meter output was established through calibration as in 1 above.

Surface potential and leakage current through the sample were recorded vs. time.

The electromagnetic field near the sample was explored, by use of suitable antennae, to look at the influence of the discharges on the vehicle circuitry. The tests indicate that negative charges can be expelled to distances of over 7x10^{-2} m from the mirror surface and, thence, noise pulses of considerable duration result.

Beam Energy [keV]	Beam Current Density [A.m^{-2}]	Exposure Time [h]	Temp. [K]	Surface Potential [V]	Electrostatic Discharges			Voltage Breakdown [V]	Comments
					Occurrence	Rate [min^{-1}]	Total Number in 6 h		
10	10^{-5}				One			3	
	3,3x10^{-5}				Several	1		3	
	6,7x10^{-5}				Small and large	3		2,5	Little changes resulted from small discharges.

From Adamo & Nanevicz (1976) [2].

4

Sample. Four mirrors on an aluminium substrate. inconel overcoating.

Conductive adhesive. RTV 566 with silver powder Cho-Bond 1029B (see paragraph 5.6 of clause 5.2.7).

Tests. Performed at DERTS (Toulouse) by use of the CEDRE substorm simulation facility (Bosma & Levadou (1979) [16]). Pressure below 6,5x10^{-3} Pa. Temperature between 260 K and 310 K. Uniformity of irradiation is achieved by diffusing the electron beam through a 7,5x10^{-7} m thick aluminium foil.

Measurements. Leakage current through the sample continuously monitored at constant electron energy and current density. Surface potential measured when cutting-off the electron beam at regular intervals.

A DC electrical breakdown tester was used to determine the breakdown voltages in air.

Beam Energy [keV]	Beam Current Density [A.m^{-2}]	Exposure Time [h]	Temp. [K]	Surface Potential [V]	Electrostatic Discharges			Voltage Breakdown [V]	Comments
					Occurrence	Rate [min^{-1}]	Total Number in 6 h		
5	10^{-5}	0,5	291	990					No hint to know when the electron beam is cut-off for surface potential measurements. Notice that surface potential depends on time when discharges occur. No voltage breakdown in air was observed up to 12 kV, upper limit of the breakdown tester used.
10				3420					
15				6840	One				
20				9300	Many				
10	5x10^{-5}			3530					
15				7200					
20				10360	Many	1 to 1/15			
10	5x10^{-5}	8							
20					Many				
5	10^{-5}	0,5	259	2630					No discharges were recorded. Apparently, the

10				5800					room temperature test affected the ability to discharge at low temperature. The large discharge could have been triggered by the potential probe.
15				10260					
20				13700	One large				
10	$5x10^{-5}$			5800					
15				10400					
20				14400					
From Bosma (1979) [13].									

1. Electrical charges on the mirror surface tend to discharge at a point of minimum resistance. This could be a discontinuity in the (nonconductive) adhesive, too narrow a gap between mirrors, or cracks in the mirror surface.

2. A typical discharge follows the mirror edge into the adhesive, through which it reaches the substrate.

3. Damage to the thermal control surface could appear as

3.1. Erosion of the adhesive from the joint between mirrors, and deposition on the quartz surface.

3.2. Defects in the silver layer such as cracks, local evaporation,...

3.3. Defects in the substrate.

3.4. Erosion of the quartz surface itself, near the edges, at high current levels.

4. Damages under 3.1 and 3.2 above become more severe when a conductive adhesive is used. This could be due to the fact that the discharge takes place at the mirror-adhesive interface instead of within the adhesive.

5. Damage under 3.3 results from nonconductive overcoatings. In that case the surge current through the silver discharges on the substrate, through the overcoating.

6. The rate of discharge occurrence is proportional to the beam current density, as in any relaxation oscillator. Nevertheless, the discharges tend to modify the later behavior of the sample in the most unpredictable way.

6.1. The discharge rate decreases with time.

6.2. the minimum beam energy for arcing depends on the history of the process. Evidence that many discharges contribute to lower the threshold energy, and evidence on the contrary are both available.

7. Conductive coated mirrors have been devised to avoid all these shortcomings. See clause 5.2.7.

8. ENVIRONMENTAL BEHAVIOR

8.1. Prelaunch. These mirrors are fragile and should be protected from mechanical damage during shipping and storage. Each mirror is individually wrapped in paper that does not scratch, leave a residue or corrode the metal surface. Surface contamination including finger-prints, oil, dust and atmospheric weathering does not cause permanent degradation after application. However, temporary contamination should be removed prior to launch.

From OCLI (1980) [94].

According to Winkler & Stampfl (1975) [139] Inconel overcoating is humidity-sensitive.

8.2. Postlaunch. Outgassing can be minimized by an appropriate curing process, see Table 5-27.

OSR panels have successfully passed sinusoidal and random vibration tests per "Lockheed Aircraft Corporation General Environmental Specification for Agena Satellite Programs".

8.2.1. Ascent. The effect of ascent heating on this rigid OSR is unknown. However no significant change in α_s is anticipated up to the upper operating temperature of the adhesive.

8.2.2. Orbital. Data on ultra-violet damage reveal no noticeable change in α_s due o near ultra-violet radiation. This rigid OSR is stable for extended missions up to two years in all space environments. It has been extensively investigated and has never been damaged. Nevertheless, many authors report space flight data, and laboratory results, indicating gradual degradation of α_s (see paragraph 7.3.2.5.6 of clause 5.2.6). In general, contamination adversely affects the thermophysical properties of the mirrors when the satellite is exposed to either ultra-violet or charged particles irradiations.

From Breuch (1967) [22], and Fogdall & Cannaday (1974) [42].

9. THERMAL CYCLING

According to the manufacturer, certification of thermal cycling is supplied after the following test: The temperature is lowered from ambient to 143 K ± 5 K, a dwell of 30 minutes, raising the temperature to 358 K ± 5 K, a dwell of 30 minutes, and returning the temperature to ambient. The cycle is repeated twice more. The rate of temperature change are not less than 2 $K.min^{-1}$. During the test, no condensation is allowed to form on the mirror. The mirror will show no evidence of degradation after this test.

From OCLI (1980) [94].

Factors limiting the useful temperature range of these mirrors are controlled by the methods used for attachment to the substrate.

Several rigid OSR samples bonded to aluminium substrate by use of GE-RTV 615 silicone adhesive were tested in a vacuum chamber at $1,3x10^{-3}$ Pa approximately. The test consisted of 20 cycles of near-sinusoidal temperature cycling between 166 K and 366 K. Each cycle had a period of approximately 20 min. Performance of these rigid OSRs and adhesive was satisfactory, with no mechanical failures occurring during the test.

From Marshall & Breuch (1968) [80].

10. SOURCE

Optical Coating Laboratory, Inc., 2789 Giffen Ave. P.O. Box 1599, Santa Rosa, California 95403, USA.

Manufacturing facilities serving Europe, OCLI Optical Coatings Limited.

621 London Road, High Wycombe, Buckinghamshire, HP11 1ET, England.

Telephone: High Wycombe (0494) 36286.

Telex: 83239.

Contact Person: Mr. J.A. Fawcett, Technical Products Manager.

11. COST

A large quantity price of 15000 US $\$.m^{-2}$ has been estimated on the basis of 1980 quotations. Adhesive is not included.

From Bosma (1981) [13].

12. SPATIAL EXPERIENCE

This rigid OSR was originally developed at Lockheed in 1964 for use an USAF satellite. It has been used in a number of satellites, some of them are listed in the following table. Additional sources of information, which has not been compiled in this item, are given in the mentioned table.

Spacecraft or Programme	Launching Date	Used or Tested	References
Lunar 1st Orbiter 5th	Aug. 10, 1966 Aug. 1, 1968	Used.	Marshall & Breuch (1968) [80].
OSO III	March 8, 1967	Tested, TCCE experiment. See paragraph 7.3.2.5.6 of clause 5.2.6.	Millard (1969) [84], Millard & Pearson (1973) [85].

Spacecraft or Programme	Launching Date	Used or Tested	References
Nimbus E	Dec. 11, 1972	Used in the radiator of the Nimbus E Microwave Spectrometer (NEMS). See paragraph 7.3.2.3 of clause 5.2.6.	Stultz (1974, 1976) [122] & [123].
ATS-F	May 30, 1974	Used in the radiator of the Advanced Thermal Control Flight Experiment (ATFE), and in the base plate of the Louvers (see ECSS-E-HB-31-01 Part 12 clause 5.2.3).	Kirkpatrick & Brennan (1973) [71], Kemp, Beynon, Luedke & Hall (1973) [69].
HELIOS A B	Dec. 12, 1974 Jan. 15, 1976	Used. Data available for analysis. See the description of HELIOS in paragraph 7.3.2.5.6 of clause 5.2.6.	Winkler & Brungs (1975, 1976) [136] & [137], Winkler (1975, 1977) [134] & [135].
Symphonie A B	Dec. 19, 1974 Aug. 26, 1975	Used in radiator.	Morelli (1974) [88].
INTELSAT IV A	Jan. 29, 1976	Used.	Rolfo (1981) [107].
COMSTAR D-1 D-2 D-3	May 13, 1976 July 22, 1976 June 29, 1978	Used. Data available for analysis. See the description of COMSTAR in paragraph 7.3.2.5.6 of clause 5.2.6.	Hyman (1981) [62].
OTS 2	May 11, 1978	Used, north & south faces. Data available for analysis.	Bouchez & Gülpen (1980) [17], Bouchez & Howle (1981) [18].
SCATHA	Jan. 30, 1979	Tested, ML12 and SSPM experiments. See the description of SCATHA in paragraph 7.3.2.5.6 of clause 5.2.6.	Hall & Fote (1979, 1980) [55] & [56].
ANIK B	Dec. 12, 1979	Used in radiators, north & south faces.	Rajagopalan & Willson (1980) [102].
NAVSTAR 5	Fev. 9, 1980	Tested. See the description of NAVSTAR in paragarph 7.3.2.5.6 of clause 5.2.6.	Pence & Grant (1981) [99].
USAF Geosynchronous	Several	Tested.	Curran & Millard (1978) [34].
LDEF	Scheduled for early 1984.	Experiment AO138-6 by A. Paillous & J.C. Guillaumon. Experiment S0010 by W.S. Slemp. Experiment S1002 by L. Preuss.	Preuss & Schäfer (1979) [100], Clark (1981) [30].

5.2.7 Silver vacuum deposited on fused Silica with a conductive coating

1. COMPOSITION

Metallic Silver, vacuum deposited on the second surface of fused silica with a transparent electrically conductive coating on the front surface. The silver is overcoated with dielectric or conductive materials.

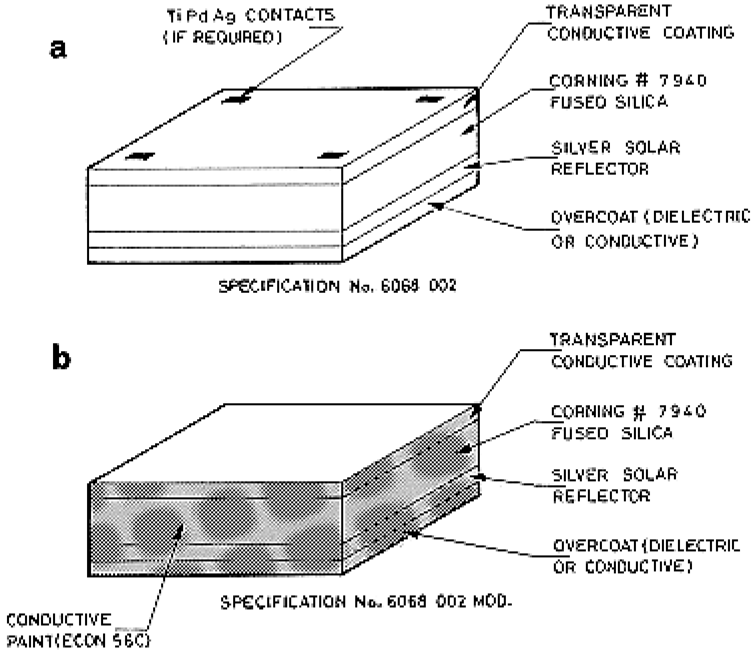
a
Ti Pd Ag CONTACTS (IF REQUIRED)
TRANSPARENT CONDUCTIVE COATING
CORNING # 7940 FUSED SILICA
SILVER SOLAR REFLECTOR
OVERCOAT (DIELECTRIC OR CONDUCTIVE)
SPECIFICATION No. 6068 002
b
TRANSPARENT CONDUCTIVE COATING
CORNING # 7940 FUSED SILICA
SILVER SOLAR REFLECTOR
OVERCOAT (DIELECTRIC OR CONDUCTIVE)
SPECIFICATION No. 6068 002 MOD.
CONDUCTIVE PAINT (ECON 56C)

From OCLI (1980) [94].

The protective overcoating could be either Incoel, Indium-Tin oxide, or a multicoating on TiO_x base. Incoel is humidity sensitive. The TiO_x based multicoating, on the other hand, exhibits an instability beyond 400 K leading to a substantial increase in solar absorptance, as discussed in connection with Figure 5-99.

Conductive coating: Tin-doped In_2O_3 1,3x10^{-8}m to 2,0x10^{-8} m thick.

From Winkler & Stampfl (1975) [139].

Electrical contacts as in *a* above are furnished on request (Specification No. 6068 002). *b* shows a recent development where the edges of the mirrors have been coated with a conductive paint (Specification No. 6068 002 Modified).

From Fawcett (1981) [41].

3. USUAL DESIGNATION

Conductive Coated Second Surface Thermal Control Mirror (CC-SSM or SSM/CC). Optical Coating Laboratory, Inc.

Also known as In_2O_3/rigid OSR or ITO/rigid OSR, as CC/rigid OSR or CC-OSR fused silica, and as OCLI Conductive Coating.

SSM/WC indicated a second surface mirror with conductive coating and welding or soldering contacts as in *a* above.

4. SUBSTRATE

Any clean surface

5. METHOD OF APPLICATION

5.1. Background. Typically square mirror substrates of 2x10^{-2} m side, 2x10^{-4} m thick are fabricated. The panels flown on the GEOS and ISEE-B satellites consisted of small individual units 2x10^{-2} m x 4x10^{-2} m (Bosma & Levadou (1979) [16]).

5.1.1. Geometrical tolerances. Typical fused silica substrates are fabricated to the following tolerances.

	Dimensional Tolerance
Length	± 5x10^{-5} m
Width	± 5x10^{-5} m
Thickness	± 5x10^{-5} m
Perpendicularity of sides	90º ± 0º 15′
Edge Chips	2,5x10^{-4} m max. projection into face.
Corner Chips	5x10^{-4} m max. length of leg,
	4x10^{-4} m max. projection into face.
Parallelism of sides	5x10^{-5} m

NOTE From OCLI (1974) [93].

5.1.1.1. Electrical contacts. The contacts show in *a* above may vary in size depending upon application. Typical dimensions and tolerances are as follows:

Width: 1,3x10^{-3} m ± 0,2x10^{-3} m

Length: 2,1x10^{-3} m ± 0,1x10^{-3} m

Thickness: 10^{-5} m ± 0,3x10^{-5} m

From OCLI (1974) [93].

5.1.2. Surface quality. 80-50 or better per MIL-O-13830A.

From OCLI (1974) [93].

5.1.3. Appearance. The coated surface gives the appearance of uniform coverage when viewed through the conductive coated substrate (front surface). The overcoated back surface has a distinct color when viewed under white light.

From OCLI (1974) [93].

5.2. Preparation of surfaces for bonding. As in clause 5.2.6.

5.3. Application. As in clause 5.2.6. See also Contacting.

5.4. Curing process. As in clause 5.2.6.

5.5. Quality of adhesive bonding. As in clause 5.2.6.

5.6. Contacting. A Titanium/Palladium/Silver contacting with the appropriate welding process and repair technique has been developed by AEG for the OCLI Conductive Coating used in HELIOS (Product Specification No. 6068 002. *a* in the figure of paragraph 1 of clause 5.2.7). the modules were interconnected through conductive contacts in the Indium oxide coating and electrically bonded by a silver string to the spacecraft structure.

The above mentioned technique, based in interconnecting individual units, is highly reliable from the electrostatic cleanliness point of view. It is, however, very expensive and involves considerable labour due to mounting and interconnection processes. A solution to avoid interconnection is the mounting of the mirror with a conductive adhesive, as in the next figure, which has been borrowed from Lehn (1979) [76]. See COST, paragraph 11 of clause 5.2.7 where a cost comparison between both contacting procedures is made.

In order to ease the contacting through the conductive adhesive, OCLI has recently developed a mirror with conductive coated edges (Product Specification No. 6068 002 Modified. *b* in the figure of paragraph 1 of clause 5.2.7). The edges of the mirror are coated with ECON 56C conductive paint. Optionally other paints may be requested.

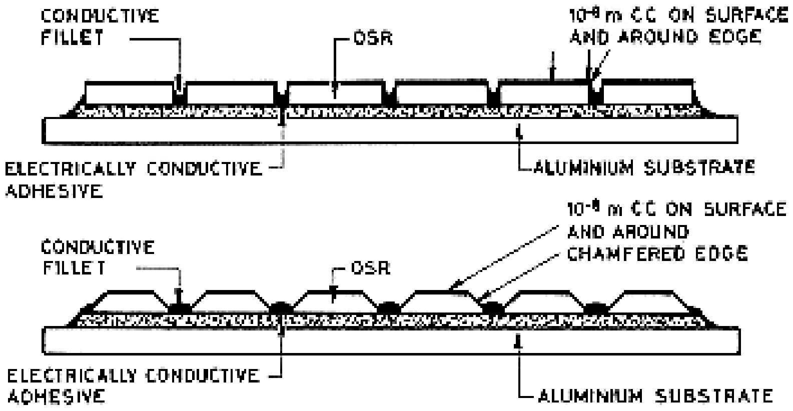
CONDUCTIVE FILLET
OSR
10⁻⁸ m CC ON SURFACE AND AROUND EDGE
ELECTRICALLY CONDUCTIVE ADHESIVE
ALUMINIUM SUBSTRATE
10⁻⁸ m CC ON SURFACE AND AROUND CHAMFERED EDGE
CONDUCTIVE FILLET
OSR
ELECTRICALLY CONDUCTIVE ADHESIVE
ALUMINIUM SUBSTRATE

A silicone-silver conductive adhesive based on,

Silicone rubber RTV 566. General Electric, USA, (General Electric Company. Silicone Products Department. Waterford, New York).

Silver powder Cho-Bond 1029B. Chomerics, USA, (Chromerics, Incorporated, Arlington, Massachusetts), has been prequalified by ESTEC for conductive adhesion of OSRs, both rigid and flexible. This formulation is not applicable as underlying adhesive (Bosma & Levadou (1979) [16]). The adhesive is prepared as follow (Benaïssa, Lévy, Paillous & Sarrail (1979) [11], Bosma & Froggatt (1980) [14]).

RTV 566A: 100 parts by weight,

Cho-Bond 1029B: 250 parts by weight.

Thorough mixing, then addition to the mixture,

RTV 566B catalyst: 0,15 parts by weight.

After further mixing, the adhesive is degassed under vacuum. Constant resistance of a 10^{-4} m thick layer between two aluminium plates is smaller than 10 Ω (Bosma & Levadou (1979) [16]). m^2 (see

Benaïssa, Lévy, Paillous & Sarrail (1979) [11], p. 22, or Bosma & Froggatt (1980) [14], p. 28), the resistivity of the conductive adhesive can be estimated as $\rho \cong 7$ Ω.m, i.e., $4x10^4$ times the resistivity of pure silver which, according to Weast (1976) [131], is $\rho = 1{,}6x10^{-4}$Ω.m.

Another conductive adhesive, quoted by Lehn (1979) [76], consists of silicone rubber filled with 13% by weight of chopped graphite fibers, as follows:

Silicone rubber RTV 566 or 560. General Electric, USA. $2{,}5x10^{-4}$ m chopped graphite fibers HERCULES HMS. Hercules, USA.

(Hercules, Incorporated, Wilmington, Delaware 19899. HMS calls for high modulus fibers).

The resistivity of this formulation is about 750 Ω.m. That of pure graphite is: $\rho = 0{,}138$ Ω.m (Weast (1976) [131]).

An epoxy-silver conductive adhesive has been used in SCATHA, ML12 experiment. See Table 5-27, paragraphs 7.3.2.5.6 of clauses 5.2.6 and 5.2.7.

6. SOLVENTS RESISTANCE

As in clause 5.2.6.

7. PHYSICAL PROPERTIES

7.1. Density

7.2. Outgassing. As in clause 5.2.6.

7.3. Thermal radiation properties

7.3.1. Emittance

7.3.1.1. Hemispherical total emittance. according to Lehn (1979) [76], the dependence of the hemispherical total emittance of OSR surfaces on the thickness of the Indium oxide conductive layer, in the range of layer thicknesses from 0 to $9x10^{-8}$ m, is small.

In the particular case of this rigid OSR, a slight decrease in emittance due to the Indium oxide layer has been consistently observed, as is shown below. Values measured calorimetrically by Hall & Fote (1980) [55] are:

$\varepsilon = 0{,}78$ for the CC-SSM,

contrasting with

$\varepsilon = 0{,}80$ for the SI-100 (uncoated).

Values in Table 5-32 correspond to normal total emittance, ε' ($\beta' = 0$), and solar absorptance, α_s, of several types of OCLI Type thermal control mirrors. Both ε' and α_s have been measured per Specification ESA PSS-16/QRM-09T. The maximum absolute error was ± 0,02, and the reproducibility ± 0,005, in all the cases.

Table 5-32: Normal Total Emittance, ε', and Solar Absorptance, α_s, of Several OCLI Type Thermal Control Mirrors

Description	ε' ($\beta' = 0$)	α_s
Specification No. 6068 002. Indium oxide top layer and Indium-Tin oxide rear side overcoating.	0,758	0,069
Specification No. 6068 002 Modified. Indium oxide top layer and Indium-Tin oxide rear side overcoating and ECON 56C conductive coated edges.	0,744	0,069
SI-100. Uncoated.	0,788	0,066
Uncoated. Indium-Tin oxide rear side overcoating.	0,785	0,063

NOTE From Bosma (1981) [13].

The influence of temperature has not been assessed.

7.3.2. Absorptance.

7.3.2.1. Solar absorptance. Values in Table 5-32, above, indicate that there is a small increase in solar absorptance dueto the Indium oxide layer.

Other values given in the literature are:

α_s = 0,06 Fogdall & Cannaday (1974) [42]. See Figure 5-99 below.

Hall & Fote (1979) [56]. See Figure 5-100 below.

α_s = 0,062 Winkler &Brungs (1975) [136]. See Figure 5-101 below.

A strong temperature influence above 400 K has been reported by Winkler& Stampfl (1975) [139], see also Figure 5-99 below. This effect, which has been attributed to thermal instability of TiO_x based rear sideovercoating, does not appear when using Incoel.

7.3.2.3. Variation of solar absorptance with incidence angle. Figure 5-97, from Winkler & Stampfl (1975) [139], shows the same trends as Figure 5-85, p. 1-114, for the uncoated mirror.

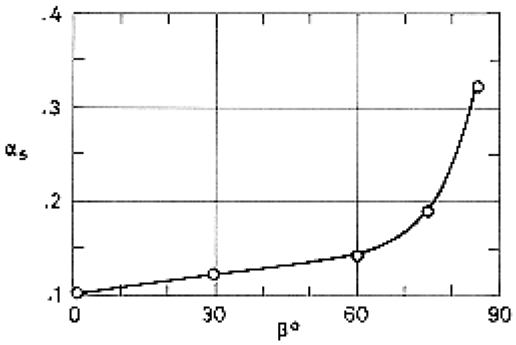

Note: non-si units are used in this figure

Figure 5-97: Solar absorptance, α_s, of OCLI Type CC-SSM vs. incidence angle, β. Circles are calculated values. From Winkler & Stampfl (1975) [139].

7.3.2.5. Effects of the Space Environment on solar absorptance.

7.3.2.5.6. Combined exposure. Data presented are:

1. Results from ground experiments simulating either geosynchronous orbit exposure of the OTS equatorial faces (Figure 5-98) or HELIOS orbit conditions at 0,25 AU (Figure 5-99 below).
2. Results from in orbit experiments. Those from a nearly geosynchronous orbit (SCATHA) are given in Figure 5-100 below, whereas those from HELIOS A and B appear in Figure 5-101 below.

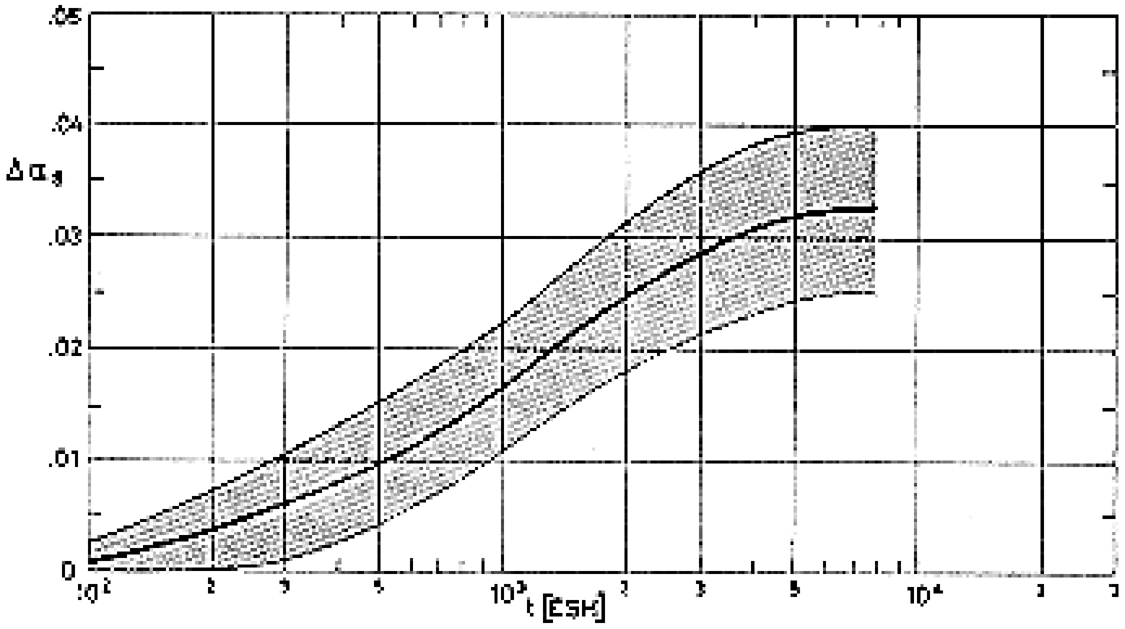

Note: non-si units are used in this figure

Figure 5-98: Estimated change in solar absorptance, *Δαs*, of OCLI Type CC-SSM vs. exposure time, *t*. The tests simulate geosynchronous orbit exposure of the Orbital Test Satellite (OTS) equatorial faces.

Table 5-33: Effects of Simulated Geosynchronous Orbit Exposure on Solar Absorptance of OCLI Type CC-SSM

Test Conditions	SAMPLE 1			SAMPLE 2			SAMPLE 3		
	Measured in situ		Corrected [a]	Measured in situ		Corrected [a]	Measured in situ		Corrected [a]
	α_s	$\Delta\alpha_s$	α_s	α_s	$\Delta\alpha_s$	α_s	α_s	$\Delta\alpha_s$	α_s
BEFORE IRRADIATION	0,065		0,090	0,050		0,090	0,053		0,090
AFTER *A* UNDER VACUUM	0,075	0,010	0,101	0,066	0,016	0,107	0,066	0,013	0,103
BEFORE *B*	0,069	0,004	0,094	0,074	0,024	0,113	0,054	0,001	0,091
AFTER *B*	0,075	0,010	0,101	0,079	0,029	0,119	0,067	0,014	0,104
AFTER PUMP DAMAGE	0,083	0,017	0,106	0,081	0,031	0,120	0,081	0,028	0,117
BEFORE *C*	0,083	0,018	0,107	0,085	0,035	0,124	0,081	0,028	0,117
AFTER *C*	0,081	0,016	0,105	0,082	0,032	0,121	0,076	0,023	0,112
BEFORE *D*	0,085	0,020	0,109	0,083	0,033	0,122	0,083	0,030	0,119
AFTER *D* UNDER VACUUM	0,080	0,015	0,104	0,077	0,027	0,117	0,088	0,035	0,124
AFTER *D* AND AIR EXPOSURE	0,074	0,009	0,099	0,077	0,027	0,117	0,077	0,024	0,113

[a] The correction has been made according to Paillous (1976) [96], as follows:

1) The initial value for OCLI Type CC-SSMs has been assumed to ba, $\alpha_{s0} = 0{,}09$. Measured in air.

2) $\Delta\alpha_{s\,corrected}$ has been related to $\Delta\alpha_{s\,in\,situ}$ as follows, $\Delta\alpha_{s\,corrected}/\Delta\alpha_{s\,in\,situ} = (1-\alpha_{s0})/(1-\alpha_{s0\,in\,situ}) = 0{,}91/0{,}94$

Reference: Paillous (1976) [96]

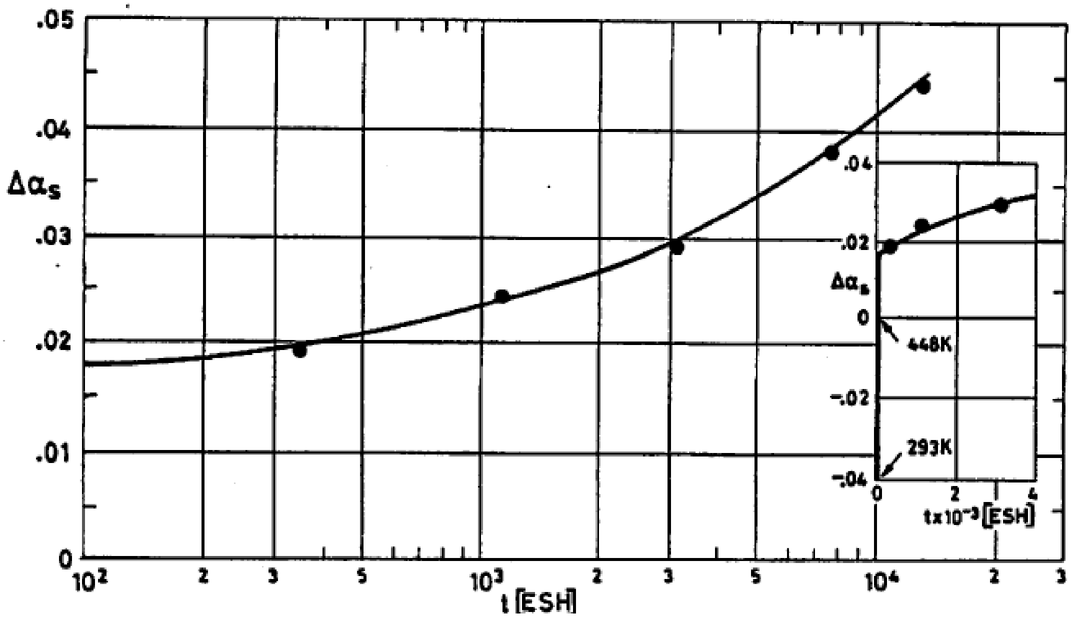

Note: non-si units are used in this figure

Figure 5-99: Change in solar absorptance, $\Delta\alpha_s$, of OCLI Type CC-SSM vs. exposure time, *t*. The insert shows the changes in α_s which suddenly results when ultra-violet exposure, at 16 Suns, begins.

Explanation

Key	Test Conditions					Comments
	Temp. [K]	Time [ESH]	Radiation Exposure			
			UV [Suns]	Charged Particles		
				Intensity [keV]	Integrated Flux [Particles.m^{-2}]	
●	448	up to 17×10^3	16	10	4×10^{20} p.m^{-2}	Intended to reproduce HELIOS orbit conditions at 0,25 AU. The zero line for $\Delta\alpha_s$ in Figure 5-99 corresponds to unexposed samples at 448 K (α_s = 0,10 to 0,11).The figure indicated that illumination with 16 Suns solar radiation as exposure begins, raises the sample temperature sufficiently to produce a quasi-initial α_s value of perhaps 0,115. This effect has been attributed by Winkler &
				25×10^{-3}	electron neutralization	

					Stampfl (1975) [139] to thermal instability of the rear side overcoating. The instability appears beyond 400 K and is due to the multicoating on TiO_x base. This multicoating seems to stabilize by diffusion and chemical reaction at high temperature, creating free activated oxygen atoms, which react with the silver forming black silver oxide.

SAMPLE

Sample Description

OCLI Type CC-SSM. Details not given.

Initial solar absorptance, α_{so} = 0,06.

Sample Mounting

Sample was bonded to a copper substrate with RTV 560 or RTV 566 silicone adhesives.

CALCULATION METHOD

α_s deduced from spectral reflectance measured at 100 selected wavelengths, in the range 2,5x10^{-7} m to 2,5x10^{-6} m, with in situ reflectometer and a spectrophotometer outside the vacuum chamber.

Chamber pressure not given.

Reference: Fogdall & Cannaday (1974) [42].

SCATHA

Details concerning TEST CONDITIONS, Sample Mounting and CALCULATION METHOD for the OCLI Type SI-100 thermal control mirrors (uncoated) can be seen in the description of SCATHA in paragraph 7.3.2.5.6 of clause 5.2.6.

The main distinguishing features of the bearing upon the CC-SSMs are summarized in the following.

SAMPLE

Sample Description

OCLI Type CC-SSM. 3,18x10^{-2} m in diameter.

Sample Mounting

The sample is placed on tray ML12-4.

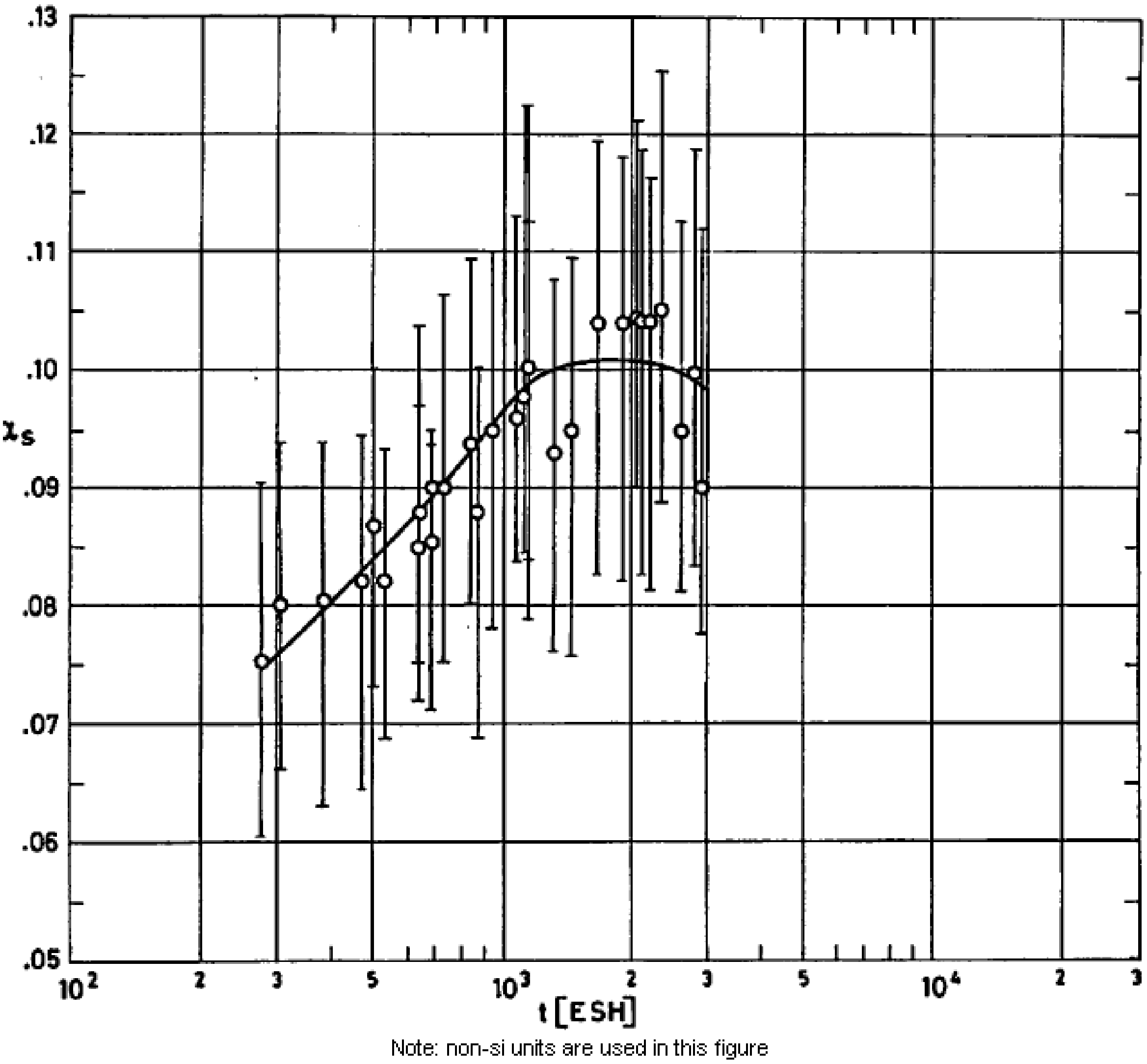

Figure 5-100: Solar absorptance, α_s, of OCLI Type CC-SSM vs. exposure time, *t* as deduced from data of SCATHA spacecraft.

COMMENTS

The data seems to indicate that the conductive coated mirrors degrade more rapidly than their uncoated counterparts. Compare Figure 5-100 above with Figure 5-90.

An initial value α_{so} =0,06 results from extrapolation to $t = 0$ of the α_s vs. t curve given by the authors.

References: Hall & Fote (1979, 1980) [55] & [56].

HELIOS

The information given in paragraph 7.3.2.5.6 of clause 5.2.6 is relevant here, unless otherwise stated.

SAMPLE

Sample description

OCLI Type CC-SSM. Inconel overcoating.

Sample Mounting

Data were deduced from a single temperature sensor (S1) placed on the center of the heat shield, underneath the mirror substrate. These data are deemed to be fairly reliable.

CALCULATION METHOD

Simplified model of data analysis as in paragraph 7.3.2.5.6 of clause 5.2.6.

The following effects were considered in the analysis of the first three orbits of HELIOS-A and the first orbit of HELIOS-B (Winkler (1977) [135]).

1. Conductive thermal coupling between the spacecraft surface and the central compartment, where the sensor is placed. This effect is, in this case, small but not quite negligible; near perihelion, $\Delta\alpha_s$ = 0,005, and near aphelion $\Delta\alpha_s$ = 0,0006.
2. Radiative input from the two solar array cones (already included in the simplified model).
3. Shading effects from the ion guard in HELIOS-B. This shading prevents 1/3 of the expected flux from reaching the surface, and distorts the temperature field, particularly near the perihelion, around the sensor location.
4. Influence on the hemispherical total emittance.
5. Degradation and contamination.

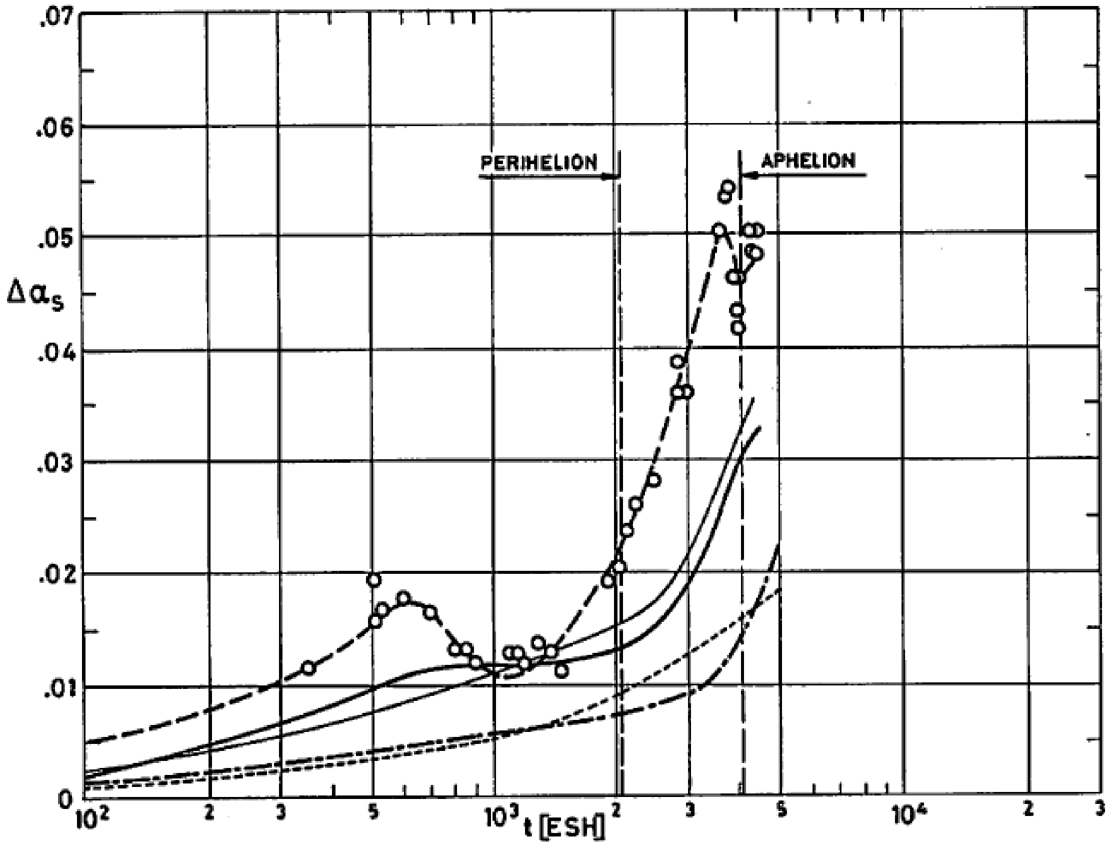

Note: non-si units are used in this figure

Figure 5-101: Change in solar absorptance, $\Delta\alpha_s$, of OCLI Type CC-SSM vs. exposure time, *t* as deduced from data of HELIOS-A and B spacecraft. Line of circles: First HELIOS-A orbit. Simplified model of data analysis.

Explanation:

▬: Average of the> first three HELIOS-A orbits. Improved model of data analysis.

——: First HELIOS-B> orbit. Improved model of data analysis.

▬ ▬: Average of the> first three HELIOS-A orbits. Effect of degradation alone.

Tests akin to Figure 5-99, α_s = 0,062.

▬•▬: Average of> the first three HELIOS-A orbits. Effect of contamination alone. Calculated by the compiler.

References: Winkler & Brungs (1975) [136], Winkler (1977) [135].

The results shown in the above figures are summarized in Figure 5-102, below.

The data are presented in terms of the change in solar absorptance, $\Delta\alpha_s$, based on an initial value α_{so}. This value results to be very large (α_{so} = 0,115) in the case of HELIOS ground tests (curve *d* in Figure 5-102) because of the initial degradation at high temperature which has been mentioned in paragraphs 7.3.2.1 and 7.3.2.5.6 of clause 5.2.7.

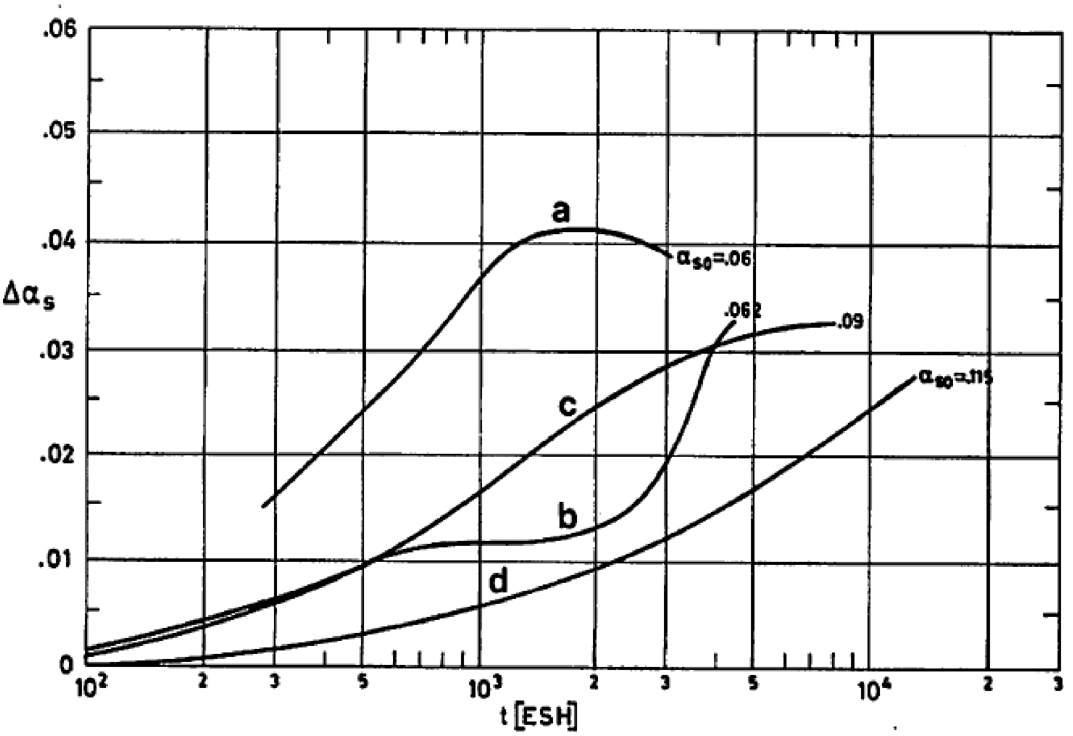

Note: non-si units are used in this figure

a : From SCATHA. Partially geosynchronous orbit, α_{so} = 0,06
b : From HELIOS-A. Solar orbit, α_{so} = 0,062. See paragraph 7.3.2.5.6 of clause 5.2.7.
c : Ground test. Simulation of OTS orbit, α_{so} = 0,09. See Table 5-33.
d : Ground test. "clean" simulation of HELIOS orbit, α_{so} = 0,115. See Figure 5-99.

Figure 5-102: Summary on the change in solar absorptance, $\Delta\alpha_s$, of OCLI Type CC-SSM vs. exposure time, *t*. The estimated values of the initial solar absorptance, α_{so}, are shown near each curve.

7.3.3. Reflectance.

7.3.3.2. Effects of the Space Environment on reflectance.

7.3.3.2.6. Combined exposure. Figure 5-103 from DERTS.

Sample: Three OCLI Type CC-SSMs, $2x10^{-2}$ m x $5x10^{-2}$ m, bonded with DC C6 1104 Adhesive to aluminium substrate. Irradiation and measurements in paragraph 7.3.3.2.6 of clause 5.2.6. Data in Figure 5-103 are related to those in Table 5-33.

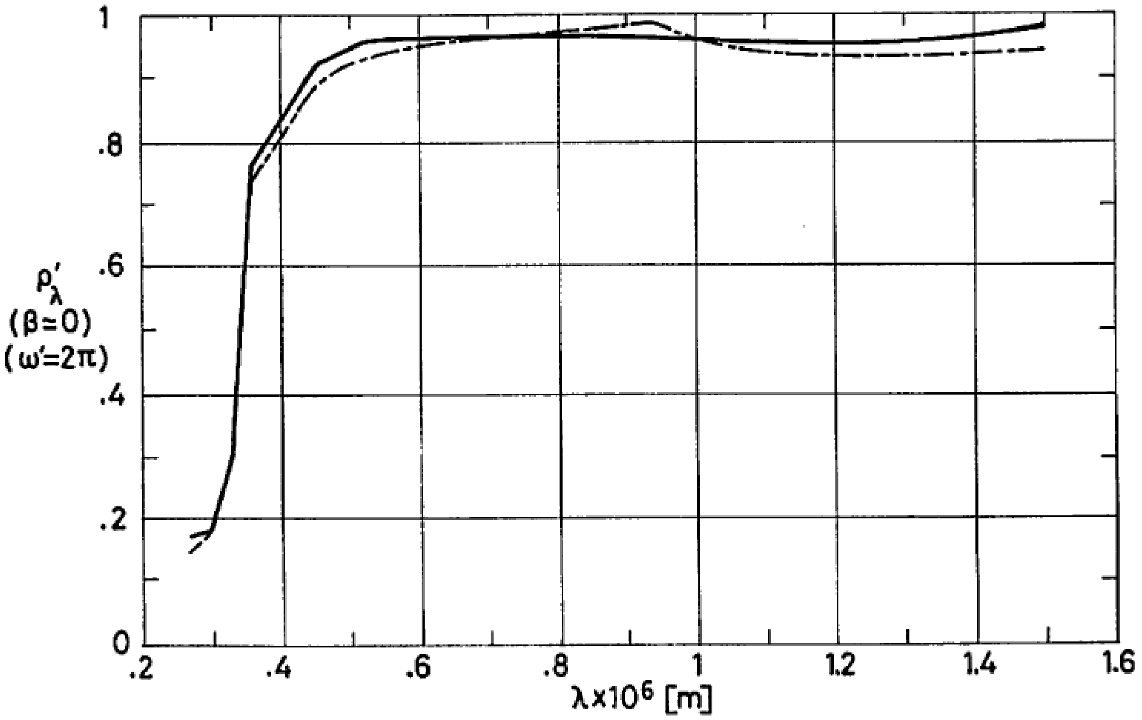

Note: non-si units are used in this figure

Figure 5-103: Effect of Combined Exposure, simulating up to three years in geosynchronous orbit, on normal-hemispherical spectral reflectance, ρ'_λ, of OCLI Type CC-SSMs vs. wavelength, λ. From Paillous (1976) [96].

Explanation

Key	Description	Comments
▬	After 125 h below $1,3x10^{-4}$ Pa pressure. $T = 363$ K.	
▬•▬	After step *D* (3 years in orbit). $T = 363$ K.	After pump damage. Influence is minimal.

7.4. Electrical resistance.

Fused silica is an insulator, thus it shows a tendency to be charged electrostatically in space. This may cause problems such as: coating degradation, transfer of contaminants, malfunction of electrical circuits,... (see paragraph 7,4 of clause 5.2.6). Particularly acute are the problems faced by the sun probe Helios (Winkler & Stampfl (1974, 1975) [138] & [139]) which was developed with the aim of measuring low energy particle (in the 10-100 eV) fluxes and their distribution function in space. Perturbations because of electrical charges built up in the sunlit and in the shadowed part of the satellite disturbs the field being measured, unless rapid charge exchange between the different parts of the spacecraft occurs through a conductive coating.

The electrical resistance of conductive coated second surface thermal control mirrors is considered in the following.

7.4.1. Effects of temperature on electrical resistance.

Figure 5-104a shows the sheet resistance as a function of temperature for several samples of CC-SSM. Electrical contacts were placed either in mode A or in mode B as in Figure 5-104b The results are interpreted as the electrical resistance of the surface, in Ω/square, although strictly speaking this property should be measured under conditions assuring that the electric field is uniform and one-dimensional.

Values given in Figure 5-104 conflict with the 40 kΩ quoted by Winkler & Stampfl (1975) [139]. Nevertheless, these authors also mention values of the order of 2-3 kΩ for temperatures above 373 K. They attribute this change in electrical resistance to two effects.

1. Influence of the contact resistance between the Ti/Pd/Ag-contacts and the In_2O_3 coating, and
2. Change of the coating behavior from semi-conducting to metallic. (See also Table 2 in Bentlage, Spanier & Wilkens (1976) [12], where changes in R with thermal load (573 K) in a high vacuum are reported).

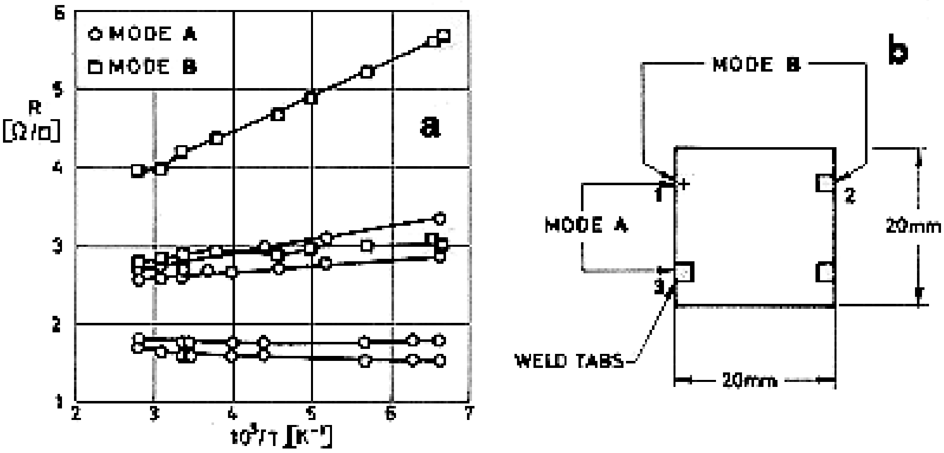

Figure 5-104: *a*. Electrical resistance, R, of six CC-SSM samples as a function of temperature, *T*. *b* shows the two alternative configurations of the electrical contacts set for performing the measurements. From Joslin & Kan (1975) [67].

7.4.2. Effects of the Space Environment on electrical resistance.

7.4.2.1. Ultra-Violet Radiation.

The sample consisted of Corning 7940 fused silica, $2,54x10^{-2}$ m by $2,15x10^{-2}$ m and about $1,5x10^{-4}$ m thick, with Indium oxide conductive coating, 10^{-7} m thick, on the front surface, and a blue reflector coating, $8x10^{-7}$ m thick, on rear surface. Although this sample is a solar cell-cover slide, the data are believed to be relevant for the purpose of evaluating space environment effects on the electrical resistance of the CC-SSM.

Irradiated in vacuum: Chamber pressure not given.

Sample temperature: 418 K ± 10 K.

Degrading source: General Electric AH-6 Mercury-Argon lamp.

Radiation flux density at the sample level: 16 Suns.

Exposure time: 800 ESH.

Sheet resistance measured, in air, with a Cambridge Four Point Probe, accuracy ± 2%.

The comparison of the values measured before and after test indicated that the sheet resistance decreased from about 0,9 kΩ/square to about 0,8 kΩ/square.

From Fry & Nicoletta (1972) [44].

7.4.2.3. Protons only exposure.

Data in Table 5-34, below, have been obtained with the same samples as above. All samples were exposed in vacuum at approximately 1,3x10^{-4} Pa. A 300 keV Texas Nuclear accelerator was used for the two lower fluxes, and an ORTEC RF source in the third case. Sheet resistance measured as above.

Electrons only exposure effects are also given in the table.

The values in the table indicate that a large jump in sheet resistance results from the 10^{20} e.m^{-2} exposure. The next table correspond to two strings of six conductive coated Corning 7940 substrates connected in series, furnished by AEG Telefunken. One string was shielded and used as control, whereas the other string was exposed to radiation. Resistance was measured with a General Radio resistance bridge, Model GR 1650 A, accuracy ± 1%.

Although the contact resistance between elements is not given, it is presumably both negligible and insensitive to degradation effects. Thus, changes in electrical resistance can be traced back to the degradation of the coating. Notice that values given in Table 5-35, once divided by six, are comparable to those in Figure 5-104 and in Table 5-34.

Table 5-34: Protons (Electrons) Only Exposure Effects on Sheet Resistance of OCLISolar Cell Cover Slides

Radiation Exposure		**Sheet Resistance [kΩ/square]**	
Intensity [keV]	**Integrated Flux [Particles.m^{-2}]**	**Before Exposure**	**After Exposure**
4	10^{16}	0,9	1,1
Protons	10^{18}	1	1,2
	10^{20}	0,8	1,3
4,5	10^{16}	0,8	1
Electrons	10^{18}	1	1,7
	10^{20}	1	3,6

NOTE From Fry & Nicoletta (1972) [44].

Table 5-35: Protons (Electrons) Only Exposure Effects on Resistance of Conductive Coated Fused Silica

Radiation Exposure		Electrical Resistance [Ω]		Comments
Intensity [MeV]	**Integrated Flux [Particles.m⁻²]**	**Shield Sample**	**Exposed Sample**	
1 Protons	Initial	12,4	11,5	In vacuum. Sample removed from machine for each resistance measurement.
	10^{15}	11,1	10,2	
	10^{16}	10,8	10,0	
	10^{17}	10,7	10,2	
	10^{18}	10,4	10,2	
	10^{19}	12,5	11,0	
1 Protons	Initial	9,8	10,5	In vacuum. Resistance measured simultaneously with irradiation. 167 minutes to reach 10^{19} p.m^{-2}.
	10^{16}	9,8	10,5	
	10^{17}	9,8	10,4	
	10^{18}	9,8	10,4	
	$2{,}5 \times 10^{18}$	9,8	10,4	
	5×10^{18}	9,8	10,3	
	$7{,}5 \times 10^{18}$	9,8	10,3	
	10^{19}	9,8	10,4	
1 Electrons	Initial	12,8	11,8	In air. Sample removed from machine for each resistance measurement.
	10^{15}	12,8	12,2	
	10^{16}	12,8	12,5	
	10^{17}	12,8	12,1	
	10^{18}	12,5	12,0	
	2 h after exposure	12,5	11,8	
	16 h after exposure	12,5	11,9	

Radiation Exposure		Electrical Resistance [Ω]		Comments
Intensity [MeV]	**Integrated Flux [Particles.m^{-2}]**	**Shield Sample**	**Exposed Sample**	
	10^{19}	12,6	11,2	
	2 h after exposure	12,6	10,9	
	16 h after exposure	12,7	10,8	
1 Electrons	Initial	12,5	11,0	In vacuum. Sample removed from machine for each resistance measurement.
	10^{16}	12,3	10,1	
	10^{17}	12,1	10,3	
	10^{18}	12,0	10,4	
	10^{19}	11,8	10,4	
1 Electrons	Initial	13,6	11,4	In vacuum. Resistance measured simultaneously with irradiation. 110 minutes to reach 10^{19} e.m^{-2}.
	$1{,}4\text{x}10^{18}$	13,6	11,6	
	$2{,}7\text{x}10^{18}$	13,6	11,6	
	$4\text{x}10^{18}$	13,6	11,6	
	$5{,}4\text{x}10^{18}$	13,6	11,7	
	$6{,}7\text{x}10^{18}$	13,5	11,7	
	$8\text{x}10^{18}$	13,4	11,5	
	$9{,}5\text{x}10^{18}$	13,4	11,6	
	10^{19}	13,4	11,6	
	10^{17}	13,6	11,4	

NOTE From Fry & Nicoletta (1972) [44].

7.4.2.4. Electrons only exposure.

Effects of the electron exposure on electrical resistance of conductive coated fused silica substrates are given in Tables 5-25 and Table 5-35.

Data on charging of simulated heat shields consisting of OCLI Type CC-SSMs appear in Charging, paragraph 7.4.3 of clause 5.2.7.

7.4.2.5. Contamination.

When outgassing products from several sources collect on the conductive coating, the electrical path goes through the deposited layer toward the coating. Thence, the effect of contamination is measured in terms of the electrical resistance perpendicular to the

Relevant results are given in Table 5-36 below.

The contaminating source is silicone Silastic 35 rubber material with several admixtures. The target is the conductive coating, the surface area of which is $4x10^{-4}$ m^2. Changes in the specific electrical cross resistance of the conductive coating are measured in situ with the simultaneous microgravimetric determination of the build up contaminating layers due to outgassing material. Measurements are performed by means of a diode measuring apparatus whose anode, the target, is hung on the load side of a special electronic microbalance.

Chamber pressure below $1,3x10^{-4}$ Pa.

Both source and target temperatures can be monitored independently from each other.

Table 5-36: Change in the Specific Electrical Cross Resistance, ρ_c, of OCLI Type CC-SSMs by Outgassing Silastic Materials

Outgas Material	Source Temp. [K]	% TML	% CVCM	Target Temp. [K]	Contaminant Mass on Target $m_s x10^5$ [$kgxm^{-2}$]	$\rho_c x10^{-2}$ [$\Omega.m^2$]	Comments
Silastic 35 with ZnO_2	573	10,5	2,8	373	135	42	
	573	10,4	2,9	373	141	52	
Silastic 35 with TiO	573	6,5	1,6	373	68,5	19,8	
	573	6,8	1,65	373	77,2	28,5	
Silastic treated with TiO	573	2,9	0,77	373	37,5	22	
	573	2,5	0,65	373	30,0	24	
	523	1,2	0,43	423	20,0	14	
	523	1,1	0,46	423	21,0	16	
	523	1,2	<0,05	443	<2,5	3,5	UV irradiation. 1,8 Suns
	523	1,1	0,09	443	5	No change	
	523	1,2	<0,05	443	<2,5	No change	

NOTE From Bentlage, Spanier & Wilkens (1976) [12].

The total mass loss, TML, in Table 5-36 was deduced by thoroughly weighting the contamination sample before and after test. The outgassing mass was about 1,8x10^{-4} kg differing somewhat from the sample, 1,7x10^{-4}kg up to about 2x10^{-4} kg, (Wilkens (1981) [133]).

The CVCM data are deduced from the contaminant mass on target, m_s, and the test geometry. Due to this geometry only 10% ± 1% of the outgassing products reached the target. Thus the CVCM was calculated as follows:

$\% \text{ CVCM} = 10^2 \text{x} 4 \text{x} 10^{-4} m_s/(\text{outgassing mass}/10)$

Three Hg high-pressure lamps are used as UV radiators. Neither these lamps nor the thermoionic cathode do affect the outgas specimen temperature. There is no interference between the electron current flowing from cathode to target and the contamination process, because of the relatively low electron energies (1,5 eV) used.

7.4.2.6. Combined exposure.

Data in Figure 5-105 correspond to three simulated years in geosynchronous orbit.

Sample: The same samples as in paragraphs 7.3.2.5.6 and 7.3.3.2.6 of clause 5.2.7.

Irradiations were performed as was indicated in paragraph 7.3.3.2.6 of clause 5.2.4. In order to perform the measurements, permanent electrical contacts were soldered to the front surface of the mirror. The position of the electrical contacts as well as that of the mirrors on the sample-holding plate are shown in Figure 5-105b below.

The electrical resistance is measured by establishing a voltage of 1V ± 10^{-4} V DC between the terminal for 1 min, reading the intensity with an ammeter.

Measurements were performed in air at 293 K before and after irradiation; in vacuum at 293 before irradiation, ad in vacuum at 363 K before and after the steps A to D which appear in Table 5-19.

Figure 5-105 indicates that the measured electrical resistance was, within experimental error, quite insensitive to the irradiation.

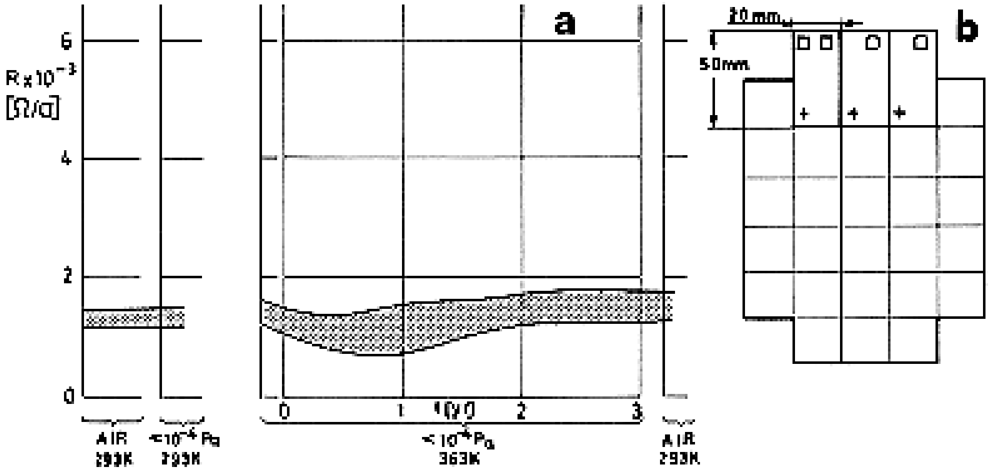

Figure 5-105: *a*. Sheet electrical resistance, *R*, of three OCLI Type CC-SSMs vs. time in simulated geosynchronous orbit, *t*.
***b*. Configuration of the electrical contacts and position of the mirrors on the sample holder for irradiation and measurements. From Paillous (1976) [96].**

7.4.3. Charging.

An isolated surface in plasma will charge to a potential depending on the characteristic of the impinging electrons, illumination of the surface, geometry,...

Two surfaces connected through a high-resistance bridge will charge to differential potentials. For a large enough potential buildup, a current discharge will occur.

To what extent should the electrical resistance be decreased to avoid charging is an open question because of the many variables involved. Thence, the charging of materials should be tested through appropriate simulation of the magnetic substorm conditions and realistic electric contacting and grounding of the surfaces.

Tests with OCLI Type CC-SSMs are summarized in Table 5-37.

Table 5-37: Charging Tests with OCLI Type CC-SSMs

1

Sample. Four mirrors on an aluminium substrate. Product Specification No. 6068 002. Indium-Tin oxide overcoating. Furnished by ESTEC.

Conductive adhesive. RTV 566 with silver powder Cho-Bond 1029B (see paragraph 5.6 of clause 5.2.7).

Tests. Performed at DERTS (Toulouse) by use of the CEDRE substorm simulation facility (Bosma & Levadou (1979) [16]). Pressure close to 10^{-3} Pa. Tests made successively at 323 K, 253 K and 223 K. Uniformity of irradiation better than ± 5% (on a 0,1 m x 0,1 m target), achieved by diffusing the electron beam through an $8x10^{-7}$ m thick aluminium foil.

Exposure time was of the order of 20 min for each set of values of ambient temperature, beam energy and beam current density. The electron beam was cutted-off at regular intervals for measuring the surface potential.

Once finished the above tests, which will be referred to as step A, the sample were exposed to air for three weeks. After that, tests at 323 K and 10^{-5} $A.m^{-2}$ (step B) were performed. These are followed by a long duration (8 h) exposure under the worst conditions (323 K, 20 keV, $5x10^{-5}$ $A.m^{-2}$) in order to detect long term degradation of the mirrors, which did not. The long exposure was followed by step C, tests at 323 K and 10^{-5} $A.m^{-2}$.

Measurements. Surface potential was measured by a TREK potential probe. The probe moves along an axis parallel to the mirrors surface, traveling straight over two side-by mirrors. The output of the probe directly feeds an XY plotter. Plotting resolution was better than 10 V. The probe can be calibrated with a metal sheet, placed on the sample holder, to which known voltages are applied.

In order to measure the leakage current through the sample, the metallic substrate is grounded through a microammeter, the output of which is continuously recorded by q two-channel recorder, second channel being used to record the beam current density.

Electrostatics discharges would be measured by an inductive probe, detecting the current pulses through a grounding connection from the substrate. The probe output would be recorded by a oscilloscope. No such discharges were detected.

Results of the tests performed at 373 K are given in the following. Similar tests at 253 K and 223 K were performed (step A only). In no case the surface potential exceeded 10 V. This surprising result, which is not new (see data from Bosma (1979) [15] in Table 5-31), is attributed by the authors to the enhanced electrical contacting between silver particles as a result of the adhesive contraction due to low temperatures.

T = 323 K															
Beam Energy [keV]	5			10				15				20			
Beam Current Density [$A.m^{-2}$]	10^{-5}			10^{-5}			$4x10^{-5}$	10^{-5}			$5x10^{-5}$	10^{-5}			$5x10^{-5}$
Step [a]	A	B	C	A	B	C	A	A	B	C	A	A	B	C	A
Exposure Time [min]	Maximum Surface Potential [V]														
0	<10	<10	<10	75	40	28	<10	55	50	50	15	55	55	75	40
0,5	60	55	40	160[b]	188	220	107	100	173	212	90	120	178	185	100
1,5	112	143	120	150	188	195	100	90	158	190	85	125	163	178	100
3,5	235	230	185	140	178	185	95	85	163	178	75	115	155	163	85
8,5	180	213	200	120	155	175	90	85	158	172	75	105	140	163	80
18,5	170	190	180	120	162	172	80	90	148	160	75	105	135	160	75

a Step *A*: Irradiation on samples as received.
B: After step A followed by three weeks of air exposure.
C: After step B followed by a long duration exposure under the worst achievable conditions.
b Value in p. 12 of the source is probably a misprint. Value given here is from Figure 5-7.

2 Sample. Four mirrors on an aluminium substrate. Product Specification No. 6068 002 modified. Indium-Tin oxide overcoating. Furnished by ESTEC. Conductive adhesive, Tests and Measurements as above. In no case the surface potential exceeded 10 V. No discharges were detected. The improved charging behavior is due to the conductive painting of the edges of these mirrors.

NOTE From Amartin & Paillous (1981) [5].

8. ENVIRONMENTAL BEHAVIOR

8.1. Prelaunch. As in clause 5.2.6.

8.2. Postlaunch. As in clause 5.2.6.

8.2.1. Ascent. As in clause 5.2.6.

8.2.2. Orbital. The in orbit behavior of these conductive coated mirrors seems to be quite similar to that of the non-conductive ones. Although data from SCATHA do indicate a faster degradation of the conductive mirrors (compare Figure 5-100 with Figure 5-90), "clean" tests performed at Boeing (Figure 5-87 and Figure 5-99) do not support this contention.

Really comparable degradation data for conductive uncoated mirrors are scanty.

9. THERMAL CYCLING

According to the manufacturer, certification of thermal cycling is supplied after the following test: The temperature is lowered from ambient to 143 ± 5 K, a dwell of 30 minutes, raising the temperature to 358 K ± 5 K, a dwell of 30 minutes, and returning the temperature to ambient. The cycle is repeated twice more. The rate of temperature change is not less than 2 K/min. During the test, no condensation is allowed to form on the mirror. The mirror will show no evidence of degradation after this test.

From OCLI (1974) [93].

Factors limiting the useful temperature range of this coating are controlled by the methods used for attachment to the spacecraft.

10. SOURCE

Optical Coating Laboratory, Inc., 2789 Giffen Ave., P.O. Box 1599, Santa Rosa, California 95403, USA.

Manufacturing facilities serving Europe, OCLI Optical Coatings Limited.

621 London Road, High Wycombe, Buckinghamshire, HP11 1ET, England.

Telephone: High Wycombe (0494) 36286.

Telex: 83239.

Contact Person: Mr. J.A. Fawcett, Technical Products Manager.

11. COST

In the case of type 6068 002, with TiPdAg contacts, a cost of 55000 US $\$.m^{-2}$ has been estimated.

When type 6068 002 modified is used, the estimated cost of the mirrors is 15000 US $\$.m^{-2}$. The cost of the conductive adhesive required (approximately 0,15 $kg.m^{-2}$) is close to 500 US $.

These estimates are based on 1980 quotations.

The balance will be even more favorable for the solution based on the 6068 002 modified mirrors when the manwork required for interconnecting the TiPdAg contacts is taken into account.

From Bosma (1981) [13].

12. PAST SPATIAL USE

This coating was originally developed for the German-USA HELIOS programme. It has been used in several satellites, as indicates in the following Table.

Spacecraft or Programme	Launching Date	Used or Tested	References
HELIOS A	Dec. 12, 1974 Jan. 15, 1976	Used. Data available for analysis. See paragraph 7.3.2.5.6 of clause 5.2.7.	Winkler & Brungs (1975, 1976) [136] & [137], Winkler (1975, 1977) [134] & [135].
GEOS	April 20, 1977	Used.	Bosma & Levadou (1979) [16], Morelli (1974) [88].
ISEE-B	Oct. 22, 1977	Used.	Bosma & Levadou (1979) [16].
SCATHA	Jan. 30, 1979	Tested, ML12 and SSPM experiments. See paragraph 7.3.2.5.6 of clause 5.2.7.	Hall & Fote (1979, 1980) [55] & [56].
USAF Geosynchronous	Satellite E (author's designation)	Tested.	Curran & Millard (1978) [34].

5.3 Total reflectors

5.3.1 Leafing Aluminium-Silicone

1. COMPOSITION

Pigment: Leafing Aluminium.

Vehicle: Silicone.

3. USUAL DESIGNATION

Fuller Aluminium Silicone Paint (172-A-1).

4. SUBSTRATE

Any clean, rigid, substrate which can withstand the cure cycle. (Breuch (1967) [22]).

5. METHOD OF APPLICATION

5.3. Application of paint. By any method.

5.4. Coating thickness. For internal applications, where emittance is the value of interest, a minimum thickness of $2{,}5\times10^{-5}$ m should be achieved. For external surfaces, where both ε and α_s are important, the minimum thickness for opacity is $7{,}5\times10^{-5}$ m (Breuch (1967) [22]).

5.5. Curing process. Baking at 514 K (Breuch (1967) [22]).

6. SOLVENTS RESISTANCE

The following data, concerning resistance of elestomeric silicones to chemical attack, have been reported.

	Volume Variation (per cent)
Solvents and fuels (after 7 d at room temperature)	
Acetone	15 to 25
Carbon tetrachloride	above 150
Ethyl alcohol	0 to 20
Isooctane	above 150
Xylene	above 150
B type fuel	above 150
JP-4 jet fuel	above 150
Oils (after 70 h at T = 423 K)	
ASTM No 1 Oil	5 to 10
ASTM No 3 Oil	35 to 60
Hydraulic fluid Mil-0-5606 (Univis J-43)	above 150
Oronite 8200 (silicate ester)	above 150

NOTE From DOW-CORNING (1970) [37].

7. PHYSICAL PROPERTIES

7.3. Thermal radiation properties

7.3.1. Emittance

7.3.1.1. Hemispherical total emittance: Table 5-37

7.3.1.3. Effects of the Space Environment on hemispherical total emittance.

7.3.1.3.1. Ultra-Violet Radiation.

The available information indicates that ε is unaffected after 600 ESH (Breuch (1967) [22]).

7.3.2. Absorptance.

7.3.2.1. Solar absorptance: Table 5-38.

Hemispherical Total Emittance and Solar Absorptance of Leafing Aluminium-Silicone

Table 5-38: Hemispherical Total Emittance and Solar Absorptance of Leafing Aluminium-Silicone

T [K]	**ε**	**α_s**	**References**
294	0,28± 0,07	0,25± 0,07	Breuch (1967)

7.3.2.5. Effects of the Space Environment on solar absorptance.

The available information indicates that α_s increases by $\Delta\alpha_{so}$ = 0,09 ± 0,04 after 600 ESH (Breuch (1967) [22]).

7.3.3. Reflectance.

7.3.3.1. Normal-hemispherical spectral reflectance: Figure 5-106.

7.3.3.2. Effects of the Space Environment on reflectance.

7.3.3.2.2. Gamma Radiation: Figure 5-107.

8. ENVIRONMENTAL BEHAVIOR

8.1. Prelaunch. The surface should be protected and carefully handled.

8.2. Postlaunch.

8.2.1. Ascent. No change has been detected in ε and α_s as a result of ascent heating with peak temperatures below 747 k.

8.2.2. Orbital. The primary source of degradation appears to be the near-ultraviolet portion of incident solar and albedo radiation.

From Breuch (1967) [22].

9. THERMAL CYCLING

The extreme temperatures at which this paint was tested without significantly changing its properties were:

T_{min} = 122 K

T_{max} = 294 K

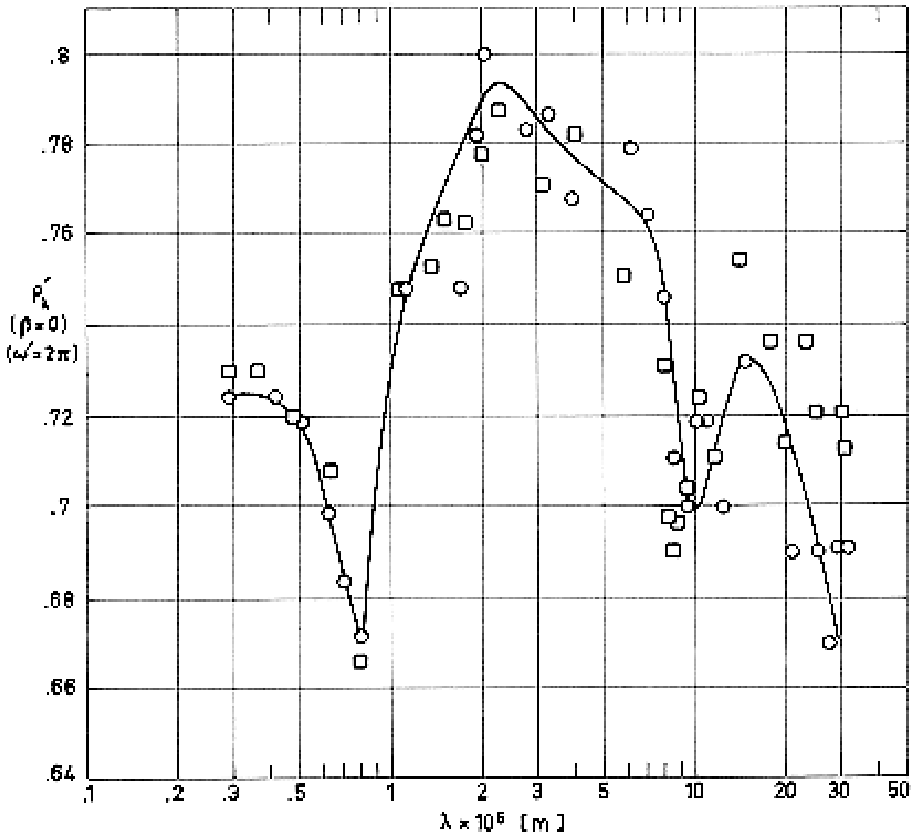

Note: non-si units are used in this figure

Figure 5-106: Normal-hemispherical spectral reflectance, ρ'_λ, of Fuller 172A1, vs. wavelength, λ. From Touloukian, DeWitt & Hernicz (1972) [126].

Explanation

Key	Description	Comments
○	2024 aluminium substrate.	T = 310 K. Measured in air soon after preparation
□	Same as ○.> Stored in dry chamber several days, then in N_2 several days.	T = 310 K.

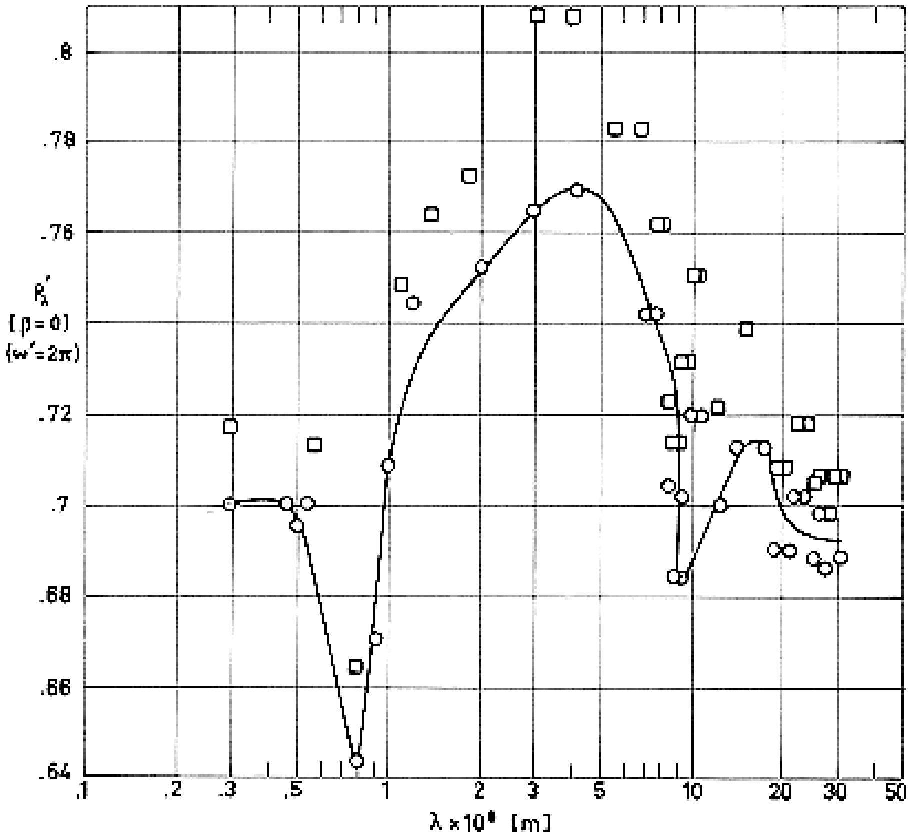

Note: non-si units are used in this figure

Figure 5-107: Normal-hemispherical spectral reflectance, ρ'_λ, of Fuller 172A1, exposed to gamma radiation, vs. wavelength, λ. From Touloukian, DeWitt & Hernicz (1972) [126].

Explanation

Key	Description	Comments
○	2024 aluminium substrate, exposed to gamma radiation. Sample stored in nitrogen for several days before measuring property in air.	T = 310 K. Gamma dose ~1,7x10^{6} J.kg^{-1}.K^{-1}. Exposure in vacuum (~1,33x10^{-4} Pa) maintained by diffusion pump. Property measured in air.
☐		

Cycling: 06 Cycles.min^{-1}.

From Rittenhouse & Singletary (1969) [105].

10. SOURCE

H.B. Fuller, Co. 1150 Eustis Street. St. Paul, Minn. 55108. USA.

5.4 Total absorbers

5.4.1 Carbon black-Acrylic resin

1. COMPOSITION

Pigment: Carbon black.

Vehicle: Acrylic resin.

3. USUAL DESIGNATION

Flat Black Kemacryl Lacquer M49BC12. Sherwin Williams Co.

4. SUBSTRATE

Any clean surface. Primer required (Breuch (1967) [22]).

5. METHOD OF APPLICATION

5.2. Preparation of surfaces for painting. The substrate should be primed with Sherwin Williams P40GC1, or Dow 17 on Mg alloy substrates (Breuch (1967) [22]).

5.3. Application of paint. By any method.

5.4. Coating thickness. Minimum thickness for opacity is $3,8x10^{-5}$ m (Breuch (1967) [22]).

5.5. Curing process. Satisfactory physical properties for most applications are obtained by an air drying cure of 8 h (PROCOLOR (1974) [101]). However, to avoid blistering during ascent heating, a minimum of 14 d at room temperature is recommended (Breuch (1967) [22]).

6. SOLVENTS RESISTANCE

Acrylic resins are soluble in Benzene, Toluene, ketones and in most acetates (Sidney Gross (1970) [115]).

7. PHYSICAL PROPERTIES

7.1. Density. As received: 1080 $kg.m^{-3}$. Solids content: 450y weight, 30,2% by volume.

7.3. Thermal radiation properties

Table 5-39 contains data concerning the following topics.

7.3.1. Emittance.

7.3.1.1. Hemispherical total emittance.

7.3.1.3. Effects of the Space Environment on hemispherical total emittance.

7.3.1.3.1. Ultra-Violet Radiation.

7.3.2. Absorptance.

7.3.2.1. Solar absorptance.

7.3.2.5. Effects of the Space Environment on solar absorptance.

7.3.2.5.1. Ultra-Violet Radiation.

Table 5-39: Hemispherical Total Emittance and Solar Absorptance of Carbon Black-Acrylic Resin

T [K]	ε	α_s	Comments	References
294	0,88± 0,03	0,93± 0,03		Breuch (1967) [22]
278	0,83	0,94	Substrate unknown. Value average on several determinations.	Touloukian, DeWitt & Hernincz (1972) [126]
278	0,81	0,94	Mg alloy substrate treated with Dow 17.	
278	0,79	0,92	Above specimen exposed to UV radiation in vacuum ($1,33 \times 10^{-4}$–$1,06 \times 10^{-3}$ Pa) from an argon-filled A-H6 high pressure Hg arc lamp for 80 h.	

7.3.3. Reflectance.

7.3.3.1. Normal-hemispherical spectral reflectance: Figure 5-108.

7.3.3.2. Effects of the Space Environment on reflectance.

7.3.3.2.2. Gamma Radiation: Figure 5-109.

8. ENVIRONMENTAL BEHAVIOR

8.1. Prelaunch. The surface is porous and requires protection from contamination.

8.2. Postlaunch. This paint requires a minimum of 14 days of room temperature curing to minimize blistering during ascent heating.

8.2.1. Ascent. This coating is not recommended for general use in locations reaching temperatures above 505 K. At peak temperatures above 517 K the paint blisters.

8.2.2. Orbital. No degradation has been detected.

From Breuch (1967) [22]).

9. THERMAL CYCLING

The extreme temperatures at which this paint was tested without significantly changing its properties were:

T_{min} = 172 K.

T_{max} = 294 K.

Cycling: 06 Cycles.min^{-1}

From Rittenhouse & Singletary (1969) [105].

10. SOURCE

Sherwin Williams Co. 101 Prospect Avenue. Cleveland, Ohio, 44101. USA.

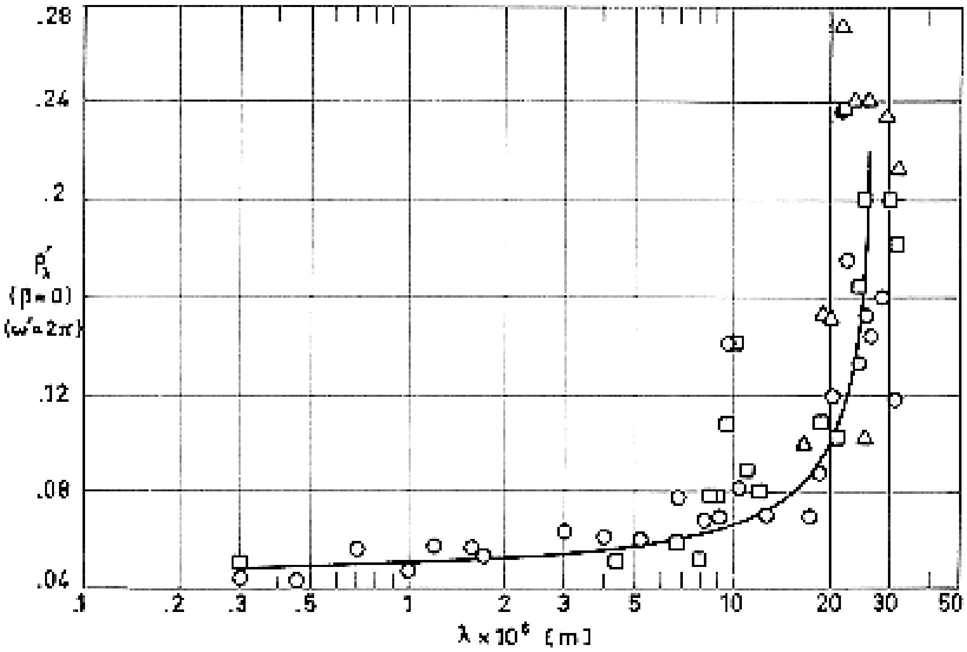

Note: non-si units are used in this figure

Figure 5-108: Normal-hemispherical spectral reflectance, ρ'_λ, of Kemacryl M49BC12, vs. wavelength, λ. From Touloukian, DeWitt & Hernicz (1972) [126].

Explanation

Key	Description	Comments
○	2024 Aluminium substrate primed with Sherwin-Williams P40GC1.	*T* = 310 K. Property measured in air soon after sample preparation. Representative values for 2 samples.
□	Same as ○ except store in dry chamber for several days, then in nitrogen for several days, then property measured.	
△	Same as □.	

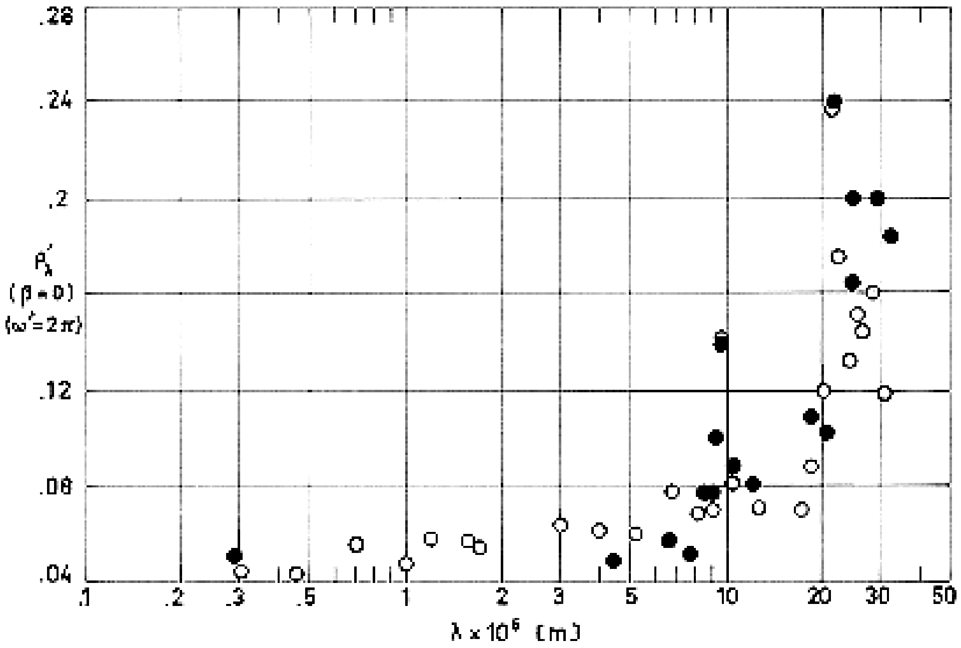

Note: non-si units are used in this figure

Figure 5-109: Normal-hemispherical spectral reflectance, ρ'_λ, of Kemacryl M49BC12, exposed to gamma radiation, vs. wavelength, λ. Points of white circles are those represented in Figure 5-108. From Touloukian, DeWitt & Hernicz (1972) [126].

Explanation

Key	Description	Comments
○	2024 Aluminium substrate primed with Sherwin-Williams P40GC1. Unexposed sample.	*T* = 310 K. Property measured in air soon after sample preparation. Representative values for 2 samples.
●	Same as ○ except exposed to gamma radiation. Sample stored in nitrogen for several days, then property measured.	*T* = 310 K. Gamma dose ~1,7x10^6 J.kg^{-1}.K^{-1}. Exposure in vacuum (~1,33x10^{-4} Pa) maintained by diffusion pump. Property measured in air.

6
Adhesive tapes

6.1 General

Pressure-sensitive adhesives can spread over a surface by mere pressure to make an adhesive bond, and are expected to be removed from the surface without leaving an adhesive residue. Pressure-sensitive adhesives, other than thermosetting types, do not change their physical state from the initial stage of adhesion upon wetting the surface to the final breaking of the adhesive bond.

Structural adhesives, on the contrary, are applied in the liquid state and set to the highly cohesive form by release of a solvent, by cooling of a hot melt, or by chemical reaction.

Pressure sensitive adhesive tapes can be used in aerospace as thermal control surfaces, for attaching multilayer insulations, as electrical insulators, and as temporary fasteners of sensors and wires during qualification test.

Primary emphasis is placed in this clause on adhesive tapes as thermal control coatings, but data concerning adhesive films and general purpose low-outgassing tapes are also included.

Compared with other thermal control coatings such as paints, plating or vacuum depositions, the tapes have the following advantages.

1. They are available in various widths and do not require setup or masking for application.
2. They are easy to remove. Damaged surfaces can easily be repaired in the field at any time, up to late prelaunch phases.
3. Mosaics can be prepared and easily changed by addition or removal of appropriate tapes.

6.1.2 Adhesive properties

The adhesive force of pressure sensitive tapes is commonly related to their peel strength.

The most popular of the methods used for performing the peel test is the 180° peel adhesion. This test is usually carried on pendulum machines using stainless steel panels to be adhered to the test sample. The adhesive force is measured as the force necessary for stripping the adhesive tape at an angle of 180º at a constant jaw separation rate.

As the test sample is noticeably deformed, peel strength depends on rate of peeling, peel angle, thickness of adhesive, width of tape, Young moduli of adhesive and backing materials, temperature, and so forth. Peel force becomes larger in proportion to the width of the sample, and increases to a maximum value when the thickness of adhesive increases.

Peel test is considered not to measure adhesion but rather a combination of adhesion and the viscoelastic properties of the adhesive.

Tack is the force required to separate the adhesive from an adherent after only a brief time of contact under low pressure application. Factors affecting tack are contact time, contact pressure, rate of separation, and temperature. Tack values also vary with modulus of backing film and thickness of adhesive, but the degree of these dependences is smaller than that of peel force value.

Tack is often measured by means of the Polyken probe tack tester (Toyama & Ito (1974) [127]) which way of working consists in bringing the tip of probes of various composition and surface texture into contact with the adhesive at controlled rates, contact pressure, contact time and temperature, and afterwards in breaking the tack bond thus formed at controlled rates. The tack value is the maximum force during separation.

In the rolling ball tack test the tack value is related to the distance between the initial contact point of a rolling ball on the surface of the sample adhesive tape and the point at which the ball stops. The initial rolling motion of the ball is imparted by means of a special incline. When care is taken in avoiding sliding, the ball losses momentum at a constant rate, so that in some tests the tack force is measured by the rate of momentum loss. Rolling ball tests are supposed to measure the resistance to detachment after a very short period of contact with the adhesive surface.

The three test methods of estimating adhesive characteristics appraise different aspects of adhesion. The peel force test mainly measures the viscoelastic properties of the adhesive, while the probe tack estimates the initial condition of adhesion in addition to the viscoelastic properties of the adhesive. The rolling ball tack may be mores sensitive to surface conditions as compared with the other test methods.

Several results obtained in a typical case are shown in Figure 6-1.

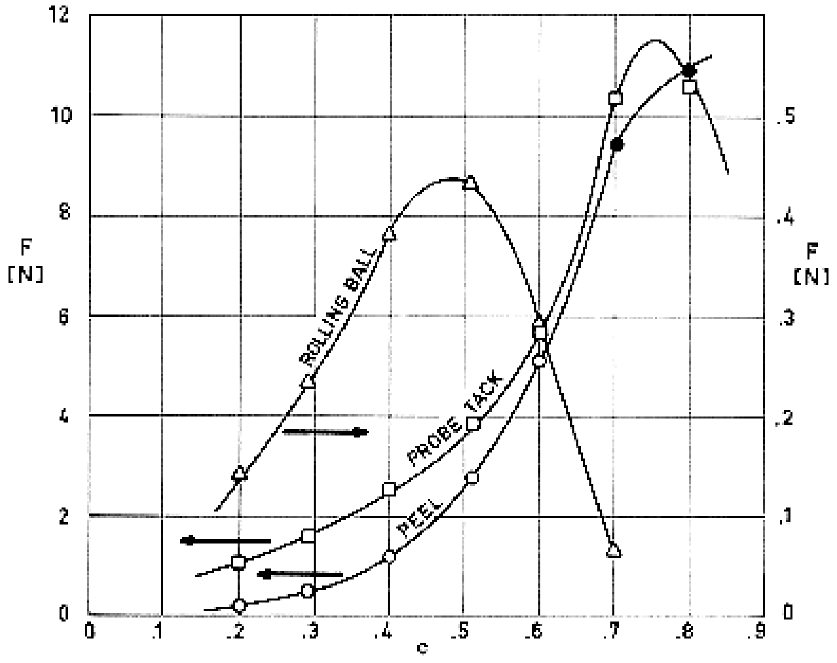

Note: non-si units are used in this figure

Figure 6-1: Peel force, probe tack and rolling ball tack, *F*, as functions of resin concentration, *c*, for a rubber adhesive on a polyethylene terephthalate (polyester) film.

Peel force has been measured at a rate of separation of $5x10^{-3}$ $m.s^{-1}$. Tape width is $1,2x10^{-2}$ m. Labels correspond to experimental points. Closed circles indicate that the cohesive failure occurs during measurements. Probe tack is measured by using a probe of $5x10^{-3}$ m diameter at $9,8x10^3$ Pa of contact pressure, 1 s of contact time and 10^{-2} $m.s^{-1}$ of rate of separation. Rolling ball tack is measured using No. 16 steel ball. The force given equals the rate of momentum loss of the rolling ball. From Toyama & Ito (1974) [127].

6.1.3 Curing of adhesive tapes

Generally, adhesives used in pressure sensitive adhesive tapes are thermoplastic. However, a small amount of curing agents may be added to the adhesive in order to increase heat resistance, cohesive strength, and solvent resistance. In the first two cases the adhesive tape is normally supplied with the adhesive already cross-linked (pre-cured adhesive). In the last case, where solvent resistance is achieving by cross-linking, it is more usual to cure the adhesive after the tape has been applied to the relevant surface. The adhesive is normally cross-linked by the application of heat and, once cured, pre-curing characteristics are lost.

Pre-curing is performed by the manufacturer before applying the adhesive on a backing by solvent coating and calendering spreading.

The curing process, when performed by the user is fairly troublesome and the main advantage of the adhesive tapes, which is ease of application, is lost.

Normally there is an optimum cure temperature for achieving a given purpose. Figure 6-2 illustrates the affect of cross-linking of a rubber based adhesive and the peel adhesion measured at 393 K. It can be seen that by increasing the curing temperature, the peel force increases to a maximum. This is due to the increase of cohesive strength of adhesive. After a maximum has been reached at 405 K, further increase in cure temperature or cross-linking results in a decrease in adhesion value.

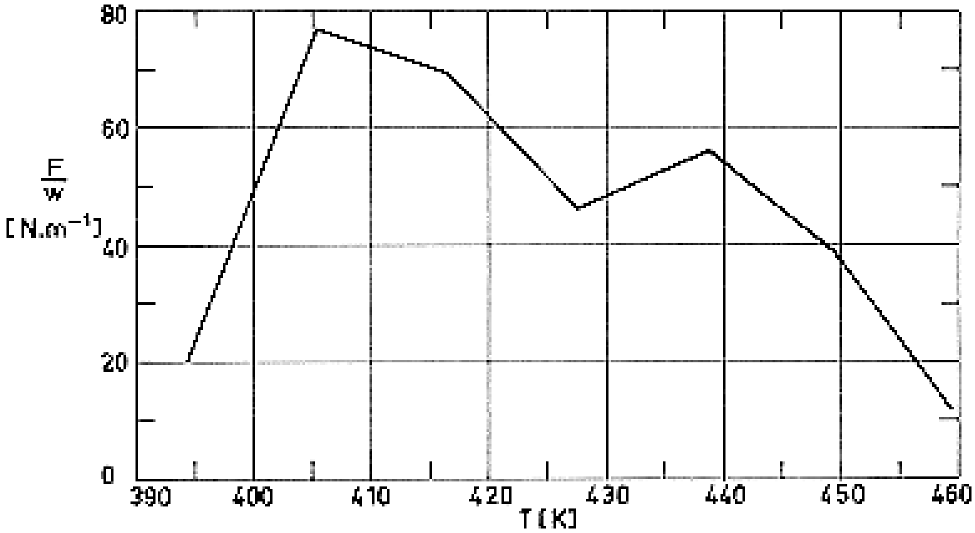

Figure 6-2: Peel adhesion, *F/w*, measured at 393 K as a function of curing temperature, *T*. Rubber based adhesive. From Toyama & Ito (1974) [127].

Table 6-1: Thermosetting Cure Cycles and Useful Temperature Range of Several MYSTIK Adhesive Tapes.

Adhesive	Cure Time [h]	Cure Temp. [K]	Tape No.	Backing	Useful Temp. Range [K]
Rubber	3	394	7321, 7322, 7323, 7351, 7352, 7355.	Polyester	233-436
	2	408			
	1	422			
Acrylic	3	394	7367.	Kapton	211-450
	2	408			
	1	422			
Silicone	3	533	7300,7331,	Polyester	211-469
			7361, 7362, 7366.	Kapton	193-561
			7502, 7503, 7505, 7510.	Teflon	193-505

NOTE From MYSTIK BRAND Insulation Tape Selector.

Obviously both the baking film and the adherent withstand the temperatures involved in the curing process. This condition introduces some coupling in the selection of the film and the adhesive, since it should be convenient that the optimum cross-linking temperature be as close as possible to the maximum operating temperature of the film. As an illustration Table 6-1 shows the suggested cure cycles for maximum cross-link density of several adhesives used in commercial tapes, together with the operating temperature range of the tape, as recommended by the manufacturer.

Unsupported adhesive tapes are normally thermoplastic. Although hand application of these tapes is easily accomplished, relatively high temperatures (of the order of 420 K)can be applied with a hand iron set. Thermoplastic adhesive tapes can be stored at room temperature for many months without deterioration.

Thermosetting adhesives are used sometimes to raise the service temperature of the system, the increase being of the order of 20 K. Thermosetting adhesive tapes are normally available upon request, they should be stored at 250-260 K, and have a shelf life of the order of 30 d.

Properties of several general purpose adhesive tapes are given in clause 6.1.3. Table 6-2 concerns double faced adhesive tapes, and Table 6-3 unsupported adhesive tapes.

6.1.4 General purpose adhesive tapes

Table 6-2: Properties of Double-Faced Adhesive Tapes[a]

Type		**3 M Co. 400**	**3 M Co. 404**	**3 M Co. 410**	**3 M Co. 411**
Description	**Backing**	Paper	Paper	Paper	Polyvinyl Chloride
	Adhesive			Natural Rubber	
	Liner (Detachable)			Paper	
Thickness, tx10^4 [m]	**Backing**				
	Adhesive (each face)				
	Liner				
	Total	1,27	1,14	1,14	3.81
Temp. Range [K]	**Intermit.**	Up to 368	Up to 403	Up to 368	Up to 338
	Continuous	Up to 338	Up to 378	Up to 338	Up to 318
Mechanical Properties	**Peel Strength (F/w)x10^{-2} [N.m^{-1}]**				
	Tack (F/w)x10^{-2} [N.m^{-1}]				

Type		**3 M Co. 400**	**3 M Co. 404**	**3 M Co. 410**	**3 M Co. 411**
Outgassing [d]	**%TWL**				
	%VCM				
	Cure *t* [h]				
	Cure *T* [K]				
	ATMOS.				
Comments		Excellent adhesion to rubber. Fair solvents resistance.	Resists temperature and plasticizers. Good solvents resistance.	Excellent adhesion. Fair solvents resistance. Easily strippable liner. Tape does not leave any residue upon removal. Standard lengths 10 m and 33 m.	Good resistance to plasticizers and solvents. Used for holding metallic plates.

Type		**3 M Co. 415**	**3 M Co. 4004**	**3 M Co. 4008**	**3 M Co. 4016**
Description	**Backing**	Polyester "Scotchpar"	Polyurethane Foam	Polyurethane Foam	Polyurethane Foam
	Adhesive	Synthetic Rubber	Acrylic	Acrylic	Acrylic
	Liner (Detachable)	Paper	Paper	Paper	Paper
Thickness, tx10^4	**Backing**	0,25			

Type		**3 M Co. 415**	**3 M Co. 4004**	**3 M Co. 4008**	**3 M Co. 4016**
[m]	**Adhesive (each face)**				
	Liner		4,25	4,25	4,25
	Total	4,77	60	32	16
Temp. Range [K]	**Intermit.**	Up to 393	Up to 463	Up to 463	Up to 463
	Continuous	Up to 353	Up to 368	Up to 368	Up to 368
Mechanical Properties	**Peel Strength $(F/w)\mathrm{x}10^{-2}$ [N.m^{-1}]**	5,46			
	Tack $(F/w)\mathrm{x}10^{-2}$ [N.m^{-1}]				
Outgassing [d]	**%TWL**	0,605			
	%VCM	0,118			
	Cure t [h]				
	Cure T [K]				
	ATMOS.				

Type	**3 M Co. 415**	**3 M Co. 4004**	**3 M Co. 4008**	**3 M Co. 4016**
Comments	High tack values to many materials (except untreated polyurethane). Fair solvents resistance. Good resistance to UV irradiation and ageing. Resists low temperatures, vibrations and shocks. "Scotchpar" allows an easy detachment of liner. Length 33 m.	Good solvents and moisture resistance. High tack values. Recommended temperature of application: 293 K to 313 K; once applied, low temperature do not impair the adhesive characteristics. Good ageing. Can be applied to rough surfaces. polyurethane foam insures good thermal insulating characteristics. Can be recommended as a vibration and noise damper.		

Type		**3 M Co. 4032**	**Mystik 5855**	**Mystik 5856**	**Mystik 6360**
Description	**Backing**	Polyurethane Foam	Cotton Cloth	Cotton Cloth	Paper
	Adhesive	Acrylic			
	Liner (Detachable)	Paper			
Thickness, $tx10^{4}$ [m]	**Backing**		2,41	2,03	1,40
	Adhesive (each face)				
	Liner	1,25			

Type		**3 M Co. 4032**	**Mystik 5855**	**Mystik 5856**	**Mystik 6360**
	Total	8	3,05	3,30	1,78
Temp. Range [K]	**Intermit.**	Up to 463			
	Continuous	Up to 368			
Mechanical Properties	**Peel Strength (F/w)x10^{-2} [N.m^{-1}]**		4,38 [e] 9,85 [f]	5,25 [e] 7,66 [f]	4,93 [e] 5,25 [f]
	Tack (F/w)x10^{-2} [N.m^{-1}]		1,31 [e] 4,38 [f]	0,015 [e] 0,012 [f] (Rolling ball)	2,41 [e] 3,06 [f]
Outgassing [d]	**%TWL**				
	%VCM				
	Cure t [h]				
	Cure T [K]				
	ATMOS.				
Comments		Same as 3M Co. 4004.	High adhesion one side, low adhesion other side. Recommended for blend fastening, carpet seaming, splicing and holding.	Carpet tape. High internal strength, good adhesion. Color: Blue.	High maneuverability. Strong moisture resistant. Excellent tear and creep resistance. Used for holding nameplates,

Type	**3 M Co. 4032**	**Mystik 5855**	**Mystik 5856**	**Mystik 6360**
		Color: White.		splicing paper, tabs or manifold forms. Color: White.

Type		**Mystik 6466**	**Mystik 7100**	**Mystik 7366**	**G.T. Schjeldahl Schjel-Bond GT 400**
Description	**Backing**	Polyester	Glass Cloth	Kapton	Polyester
	Adhesive		Silicone	Silicone	Polyester
	Liner (Detachable)			Cloth	
Thickness, tx10^4 [m]	**Backing**	0,25	1,17	0,25	0,51 [b]
	Adhesive (each face)				0,25 [b]
	Liner				
	Total	0,97	2,39± 0,13	1,24± 0,08	
Temp. Range [K]	**Intermit.**				Up to 400 [c]
	Continuous		193 to 561	193 to 561	Up to 355 [c]
Mechanical Properties	**Peel Strength (F/w)x10^{-2}**	3,72 [e]	2,19 Min. 3,28 Avg.[e]	1,75 Min. 2,19 Avg.[e]	7 [g]

Type		Mystik 6466	Mystik 7100	Mystik 7366	G.T. Schjeldahl Schjel-Bond GT 400
	[N.m^{-1}]	4,16[f]	2,19 Min. 3,17 Avg[f]	1,75 Min. 2,08 Avg[f]	
	Tack (*F*/*w*)x10^{-2} [N.m^{-1}]	2,63[e] 2,74[f]			
Outgassing[d]	**%TWL**		3,22 R 3,60 S	1,30 R 5,45 S	0,631
	%VCM		0,670 R 0,790 S	0,940 R 1,680 S	0,124
	Cure *t* [h]			72	0,083
	Cure *T* [K]			328 0	0,433
	ATMOS.			E-4	Air
Comments		High strength, excellent adhesion. Thermosetting and electrically non-corrosive. Color: Transparent.	Thermosetting. High-low temperature resistant, non-corrosive. Electrically pure. Does not shrink, rot or burn. High tensile strength, excellent thermal stability. Length 33 m	Thermosetting. High mechanical strength. retains dielectric strength at elevated temperatures. Stable over a wide temperature range. Length 33 m on	Used to bond plastic films, fibers, paper, metals, glass, ferrites, plastics and finishes. Thicker resin coatings are recommended for sealing porous materials. Also available as GT-401 with thermosetting adhesive.

Type	Mystik 6466	Mystik 7100	Mystik 7366	G.T. Schjeldahl Schjel-Bond GT 400
		on 7,62x10^{-2} m core. Color: White.	7,62x10^{-2} m core. Color: Amber.	Color: Milky-White; becomes clear when sealed.

[a] All data in this table, unless otherwise stated, are from manufacturer's bulletins.

[b] Typical values. For more details see Table below. 0 indicates that the configuration is not available for immediate delivery.

[c] Specific for individual base material, not necessarily same as for composite tape.

SCHJEL-BOND GT-400. Thermoplastic adhesive on both sides of polyester film. 7,62 m rolls.					
Adhesive x Mylar x Adhesive	**Width, wx10^2 [m]**				
Thickness, t x 10^4 [m]	1,3	2,5	5,1	10,2	53,3
0,13x0,13x0,13					
0,25x0,25x0,25					
0,25x0,51x0,25					
0,38x0,51x0,38	0			0	
0,38x1,27x0,38	0				

[d] Outgassing characteristics have been borrowed from Campbell, Marriott & Park (1973) [27].

TWL: Total Weight Loss

VCM: Volatile Condensable Materials (by weight)

R: Several layers of the tape were rolled on a glass Rod to permit outgassing at the edges.

S: The tape was placed on a Screen exposing the adhesive of the first layer.

E-4: Chamber pressure 10^{-4} torr = 0,013 Pa.

A zero indicates that cure conditions are unknown.

[e] Roll Side.

[f] liner Side.

[g] Bond adhesive to adhesive.

Table 6-3: Properties of Unsupported Adhesive Tapes [a]

Type		**3M Co. 465**	**3M Co. 467**	**G.T. Schjeldahl Schjel-Bond GT-100**
Description	**Adhesive**	Acrylic	Acrylic	Polyester
	Liner (Detachable)	Paper	Paper	Paper
Thickness, tx10^4 [m]	**Adhesive**	0,50		0,635 [b]
	Liner	0,75		
	Total			
Temp. Range [K]	**Intermittent**	Up to 393	Up to 478	Up to 400 [c]
	Continuous	Up to 353	Up to 448	Up to 355 [c]
Mechanical Properties	**Peel Strength (F/w)x10^{-2} [N.m^{-1}]**			7 [e]
	Tack (F/w)x10^{-2} [N.m^{-1}]			
Outgassing [d]	**%TWL**	0,840	1,320	0,250 [f]
	%VCM	0,209	0,080	0,082 [f]
	Cure t [h]	0	4	0,083
	Cure T [K]		311	422
	ATMOS.		AIR	AIR
Comments		Resistant to temperature, moisture and UV irradiation. Fair solvents resistance. High tack values. Excellent ageing. Can be applied to	Similar to above although it exhibits improved resistance to Sun irradiation and chemical attack. Excellent final adhesion. Can be applied to any	Used in bonding lap seams, constructing multi-layer circuits and joining parts and components. Also available as GT-101 with thermosetting adhesive on special order.

	any smooth surface such as cloth, crystal, metal, paper, plastic, wood. Length 55 m.	surface, except polyurethane.	Color: Milky-White; becomes clear when sealed.

[a] All data in this table, unless otherwise stated, are from manufacturer's bulletins.

[b] Typical value. For more details see Table below. 0 indicates that the configuration is not available for immediate delivery.

[c] Specific for individual base material, not necessarily same as for composite tape.

SCHJEL-BOND GT-100. Unsupported thermoplastic adhesive. 8,38 m rolls.

Adhesive Thickness, $t \times 10^4$ [m]	**Width, $w \times 10^2$ [m]**				
	1,3	**2,5**	**5,1**	**10,2**	**53,3**
0,13				0	
0,254				0	
0,635				0	

[d] Outgassing characteristics have been borrowed from Campbell, Marriott & Park (1973) [27].

TWL: Total Weight Loss

VCM: Volatile Condensable Materials (by weight).

A zero indicates that cure conditions are unknown.

[e] Bond adhesive to adhesive.

[f] Composite Mylar - GT-100 - Mylar.

6.2 Application and handling

6.2.1 Application

Thermal control tapes incorporate pressure sensitive adhesives such as acrylics, rubber or silicones which enable the tape to be positioned and set by applying pressure with a non-abrasive roller or ironing tool. Room-temperature-curing or elevated-temperature-curing adhesives are available.

Before applying the tapes it should be ensured that the adherent surface is clean enough, that the tape is regularly pressed, and that the adhesive surface is not damaged during the application.

Several commercially available metallic foils are protected with a nitrocellulose lacquer. This lacquer should be completely removed prior to application of the foil. The removal may be performed by wiping with a soft clean cloth, using the following solvents in this order (Breuch (1967) [22]):

1. Lacquer thinner or methyl-ethyl-ketone.
2. Isopropyl or ethyl alcohol.

The lacquer is almost invisible to eye. Any doubt concerning whether it has been removed or not can be dissipated by using an ohmmeter to measure the electrical resistance between points on the same foil face. If this resistance is large the lacquer has not been removed.

Films and foils can be applied to the substrate by using either a double faced or an unsupported adhesive tape. In these systems the film or foil is first attached to one adhesive side of the tape and subsequently applied by bringing the other side into contact with the substrate. This method is time-consuming and increases the chances for tape misalignment and air entrapment.

6.2.2 Cleaning

Foils and metallized films can be cleaned by lightly rubbing the surface with a soft cloth or cotton swab wetted with solvent. Choice of solvent depends upon: type of contaminant to be removed, and compatibility of the solvent with the adhesive. Special care should be employed during cleaning to avoid the scratching of the metallized surface. In addition, cleaning solvents can be absorbed into the adhesive, the tape, or both, diffusing out under vacuum conditions.

Adhesive tapes which are applied temporally contaminate the substrate which should be carefully cleaned after removal. On the other hand, when the tape is applied permanently it may be displaced by creep, leaving a dirty trace of its past position.

Solvents of relevant adhesives are listed in Table 6-4.

Table 6-4: Several Solvents of the Adhesives

Adhesive	Solvents	References
Acrylic	Glacial acetic acid. Methylene chloride.	Katz (1964) [68]
Rubber	Benzene.	Delmonte (1947) [35]
Silicone	Carbon tetracloride. Isooctane. Xylene.	DOW-CORNING (1970) [37]

6.2.3 Handling

Permanent damage to foils and metallized surfaces result from improper handling during installation or cleaning operation.

Data showing effects of abrading metallized surfaces are given in Table 6-5. Since the amount and degree of rubbing used in the tests was subjective, these data should be considered merely as qualitative.

Table 6-5: Rubbing Degradation of the Optical Properties of Aluminized Films

Material	Condition	α_s	ε [a]
First Surfaces			
Aluminized Mylar	As received Lightly rubbed Lightly rubbed Heavily rubbed	0,081 0,116 0,145 0,429	0,032 0,034 0,042 0,351
Aluminized Kapton	As received Lightly rubbed Lightly rubbed Heavily rubbed	0,096 0,162 0,273 0,192	0,032 0,067 0,100 0,075
Second Surfaces			
Aluminized FEP Teflon $1{,}27\mathrm{x}10^{-4}$ m thick	As received Lightly rubbed Lightly rubbed Heavily rubbed	0,134 0,137 0,147 0,138	0,805 0,809 0,808 0,807

[a] Infrared Emittance. measured by Gier-Dunkle Method. From Kordsmeier & Peters (1972) [74].

Additional recommendations concerning handling may be found under Terrestrial Degradation clause 6.3.2.

6.2.4 Repairing

Damaged surfaces can be removed and replaced.

6.3 Degradation

6.3.1 Introduction

The degradation in the thermal performance of the tapes depends on the materials, the construction, the application technique, the substrate, and the environment. The main degradation effects are: change in the thermo-optical characteristics of the surface, and loss of contact between the tape and the substrate.

General ideas concerning the degradation of adhesive tapes, which have been mainly borrowed from Brown & Merschel (1970) [23] are given in the following paragraphs.

6.3.2 Terrestrial degradation

1. Humidity Exposure.

   Emittance of almost all tapes having a metallic surface is seriously degraded.

   Absorptance increases slightly.

   Emittance and absorptance of the backing films are not affected.

   Comments. The effects of moisture, which are specially noteworthy in the case of aluminized coatings, can be minimized through use of protective packaging and control of storage and assembly environments.

   When environmental control cannot be exercised, substitution of goldized for aluminized films is recommended (Kordsmeier & Peters (1972) [74]).

2. Long Term Exposure to Air.

   Emittance increases slightly.

   Absorptance does not change significantly.

6.3.3 Space degradation

Thermo-optical properties of the first surface metallized films and metal foil tapes are essentially stable.

The second surface metallized and clear polyimide film tapes are relatively stable.

The second surface metallized and clear polyester film tapes exhibit large increases in solar absorptance.

FEP type A Teflon films are extremely resistant to damage from UV irradiation. Table 6-6 shows optical measurements and UV degradation data commercially available sheets of FEP type A Teflon, $1{,}27\text{x}10^{-4}$ m thick, coated on one side with vacuum deposited Silver plus a protective layer of evaporated Inconel. All samples have been obtained from sheets or tapes produced by G.T. Schjeldahl Company except sample identified as "control" which was coated by NASA Goddard Flight Center’s Engineering Applications Branch. Since the purpose of the study was to evaluate the acceptability of the commercially supplied coated film, several samples were cut from four different sheets as in indicated in the insert of Table 6-6. Roman numbers are used to distinguish between original sheets. In addition two tape rolls were tested which are identified as TI and TII.

Figure 6-3 gives the variation of solar absorptance in similar specimens as measured on board OSO-H, IMP-I and IMP-H satellites.

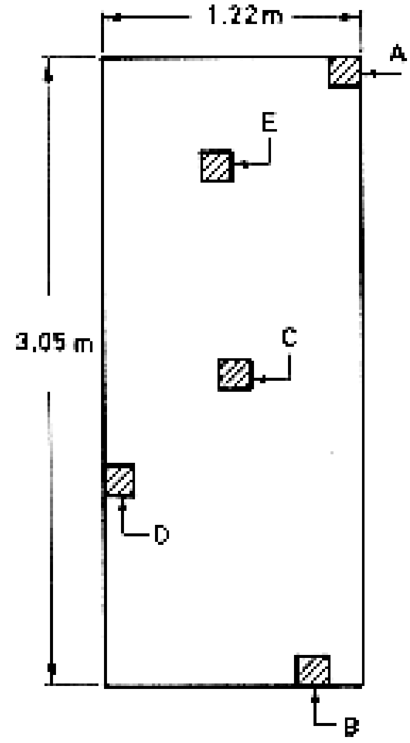

Note: non-si units are used in this figure

Table 6-6: Thermal radiation Properties of Second Surface Silver-Teflon (1,27x10^{-4} m thick)

Sample	α_s [a]	$\Delta\alpha_s$ [b]	ε' [c] (β~0)	ε [d]	α_s/ε
Control	0,085	+ 0,003	0,812	0,767	0,111
IA	0,085	+ 0,001	0,804	0,760	0,112
IB	0,082		0,805	0,761	0,108
IC	0,084		0,800	0,756	0,111
ID	0,080		0,799	0,757	0,106
IE	0,082	+ 0,001	0,802	0,759	0,108
IIA	0,097	0,000	0,809	0,765	0,127
IIB	0,087	– 0,002	0,806	0,762	0,114
IIC	0,084		0,802	0,759	0,111

Sample	α_s [a]	$\Delta\alpha_s$ [b]	ε' [c] (β'~0)	ε [d]	α_s/ε
IID	0,080		0,803	0,759	0,105
IIIA	0,084	– 0,002	0,807	0,763	0,110
IIIB	0,084		0,806	0,762	0,110
IIIC	0,083		0,807	0,763	0,109
IIID	0,091	– 0,001	0,803	0,759	0,120
IVA	0,082	– 0,008	0,795	0,755	0,109
IVB	0,094	– 0,002	0,801	0,757	0,124
IVC	0,088		0,806	0,762	0,115
IVD	0,079		0,806	0,762	0,104
TI-(¼ way in	0,087	+ 0,006	0,810	0,765	0,114
TI-End)	0,087		0,814	0,769	0,113
TII-Beginning	0,081	+ 0,002	0,807	0,763	0,106
TII-Middle	0,090		0,801	0,757	0,119

[a] From spectral reflectance data. Integrating sphere reflectometer used to cover the region $2{,}9\text{x}10^{-5}$ to $2{,}4\text{x}10^{-6}$ m, and hohlraum reflectometer to extend the range up to $8\text{x}10^{-6}$ m.
Precision: ± 0,003; Accuracy: ± 0,010.

[b] After 200 ESH UV irradiation from a filtered Xenon arc source (Spectrolab x-25).

[c] Measured at 300 K using a Gier-Dunkle DB-100 portable infrared reflectometer.
Precision: ± 0,005; Accuracy: ± 0,010.

[d] Calculated assuming $\varepsilon = 0{,}945\ \varepsilon'$.

NOTE From Heaney (1974) [59].

The OSO-H was in near earth orbit and was not subjected to charged particle irradiation, thence the data indicate that Silver-Teflon is not degraded by UV irradiation only. The initial value quoted in Figure 6-3 correspond to the 20th orbit. (20th orbit ≅ 20 ESH ≅ 30 orbital h) due to a malfunction in the tape recorder.

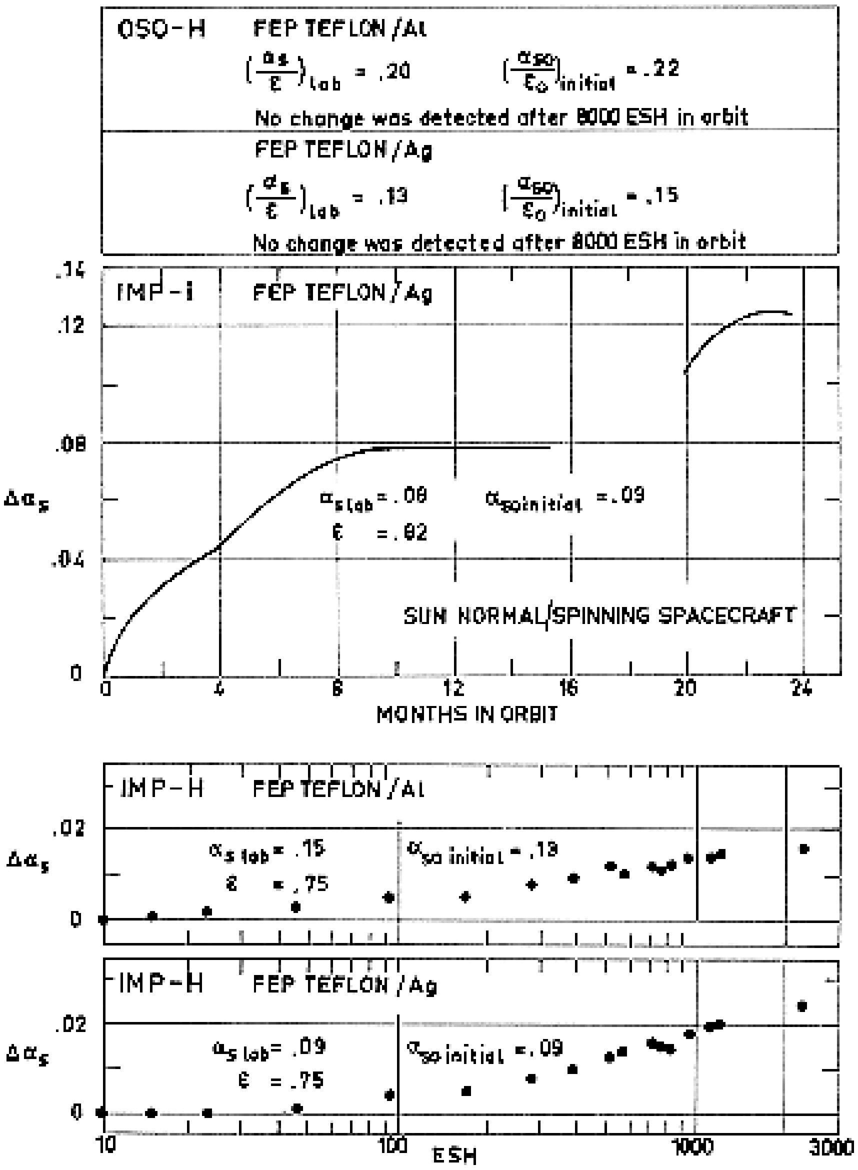

Note: non-si units are used in this figure

Figure 6-3: Space degradation of second surface mirrors based on $1,27x10^{-4}$ m thick FEP Teflon. All data are from Triolo (1973) [128] except those corresponding to IMP-I which are from Hoffman (1973) [61].

The degradation experienced by the Silver-Teflon coating in board IMP-I is considered to be the result of solar wind and high energy proton irradiation rather than solar UV irradiation. During the first 9 months in orbit, the temperature of the detector plate gradually rose from 202,5 K to 219 K, corresponding to an increase in the coating solar absorptance of 0,077. This value remained constant for another 7 months, at which time data keeping was ceased. Nearly 4 months later the spacecraft passed through an apogee shadow of almost 6 h duration. Data acquired again after this event shown that three was a sudden increase in detector plate temperature to 223 K with a continual rise thereafter, indicating that Teflon is susceptible to damage by charged particles. The estimated fluxes are given in the Table 6-7.

Table 6-7: Exposure Conditions of Silver-Teflon on IMP-I Spacecraft

Source	Intensity [MeV]	Integrated Flux [particles.m^{-2}]
Solar Wind		$3\text{x}10^{19}$
Electrons	All energies	10^{18}
Protons	0,1 – 5 4 – 50 Above 50	$3\text{x}10^{18}$ $3\text{x}10^{16}$ $3\text{x}10^{14}$

NOTE From Hoffman (1973) [61].

Concerning IMP-H, the initial α/ε values measured in flight were 50% larger than the laboratory values. The discrepancy has been attributed to blistering of Teflon (Triolo (1973) [128]). Data presented show again that Teflon may be damaged by charged particles.

6.3.4 Blistering

Blistering, Figure 6-4 occurs whenever the adhesive bond strength is locally exceeded by a lifting force. These forces are mainly due to:

1. Thermal expansion of air entrapped in the bond area.
2. Outgassing of the adhesive or substrate.

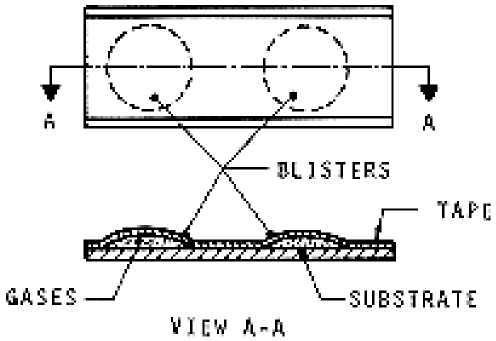

Figure 6-4: Sketch of a blistering tape. From Brown & Merschel (1970) [23].

Blistering of thermal control tapes inhibit the heat transfer through the tape-surface interface. When the purpose of the tape is to increase the emittance of a hot-plate, blistering would tend to create a partial shield between the plate and its surrounding. The added thermal resistance increases the substrate temperature which may in turn increase the blister size. Similarly, blistering may seriously affect the thermal behavior of tapes used as a solar collector surfaces.

Table 6-8 gives the blistering temperature of tapes applied to an aluminium substrate and exposed to 13,3 to 133 Pa pressure while temperature was being increased in steps of 7 K up to 385 K.

Table 6-8: Blistering Temperatures of Tapes Applied to an Aluminium Substrate [a]

Type	Description			Temperature [K]			
	Coating	Backing	Adhesive	T_1	T_2	T_3	T_4
3M Co. 53	Aluminium	Mylar	Rubber	361	364	378	
3M Co. 56		Mylar	Rubber	311			
3M Co. 425	Al. Foil			336		344	366
3M Co. 428 A	Al. Foil		Acrylic	> 383			341-389
3M Co. 850 S	Aluminium	Mylar	Acrylic	311	336	344	378
3M Co. 850 G	Gold	Mylar	Acrylic				383
3M Co. 853	Aluminium	Mylar		366	378		
3M Co. Y-9184 A	Gold	Kapton	Silicone	344	353	361	
Mystik 7390				<333			
Mystik 7402 L	Al. Foil		Silicone	311	319	328	
Mystik 7430	Lead Foil		Rubber	319	328	336	
Mystik 7453	Al. Foil		Acrylic	> 386			366
Mystik 7455	Al. Foil	Glass Cloth		300	311	319	
G.T. Schjeldahl GT 102000-4	Al. on nylon tulle	Kapton	Acrylic	328		336	364
G.T. Schjeldahl GT 103300	Aluminium	Kapton	Silicone	297	311 [b]	> 380	
TF-12				308		333	

NOTE T_1, Temperature at which blistering first occurred in thermal vacuum. Sample applied to a cleanser scrubbed aluminium sheet stock.
T_2, Temperature at which an increase in blister size was noted.
T_3, Temperature at which blisters were so large and numerous that almost entire tape area was delaminated.
T_4, Temperature at which blisters occurred on tapes tested after 10 d of humidity per MIL-STD-202, Method 106 B; applied to aluminium sheet conversion coated per MIL-C 5541.

[a] Single sample per tape.

[b] There was some increase in size and number of blisters at that temperature, but not further increase at higher temperatures.

NOTE From Brown & Merschel (1970) [23].

6.3.4.2 Precautions against blistering

Several rules to avoid blistering are given by Stevens (1971) [120]. Although these rules concern a particular tape (aluminium foil Mystik 7402 L), it is hoped that they can be applied in more general cases.

1. The use of too wide tapes should be avoided. Tapes of 5x10^{-2} m to 7,5x10^{-2} m width are recommended.

2. Whenever possible, the tapes should be baked in order to reduce outgassing.

   As quoted by Stevens, samples baked at 394 K for 24 h had a significantly reduced blistering, as compared with unbaked samples, when applied on a piece of 2020 Aluminium plate washed with detergent and then cleaned with xylene.

   The protective lacquer was removed before baking.

   Comments. There is some disagreement in connection with the usefulness of baking.

   (a) Brown & Merschel (1970) [23] reported no increase in the blistering resistance of 3 M Co. 850G tape after baking in vacuum at 366 K and 0,34x10^{4} to 1,4x10^{4} Pa for 24 h.

   (b) Baking does not appear to be a practical means to improve tape performance. If the baking process is performed by the manufacturer, larger quantities of tape would be ordered to achieve a reasonable price. On the other side, the use of special drying fixtures, vacuum ovens and high level clean room procedures would invalidate the main advantage of pressure sensitive adhesive tapes, which is the ease of application.

3. Tape application under vacuum conditions has been suggested by Brown & Merschel (1970) [23]. This process eliminates air entrapment reducing the cause of blister formation. However, taping under vacuum requires special tooling and equipment which makes the process expensive and cumbersome.

4. Performing the tape to open ways out to entrapped air, solvents or volatile constituents, could improve the blistering characteristics of tapes. Perforations having 8x10^{-4} m diameter on 1,5x10^{-2} m centers have been used by Stevens (1971) [120]. The thermo-optical characteristics of the coating are not seriously degraded by the presence of such a few small holes.

   Spiked rollers to perforate the tapes are available.

   In order to avoid introducing solvents within the adhesive, the protective lacquer (if present) should be removed prior to perforation of the foil.

5. Tests performed with different application pressures (13 N, 27 N and 45 N on approximately 4x10^{-3} m^{2}) shown that the tape should be just set on the substrate. In the experiments reported by Stevens only the lightly applied tapes remained free of blisters after the test. It is believed that the light application pressure kept the adhesive from sealing the gas escape paths.

   Light application of pressure is also required when using perforated tapes to avoid the flowing of adhesive towards the perforations thereby sealing them.

6. When the tape is applied externally it is advisable to provide mechanical fastening on both ends to prevent lifting forces from peeling the tape away from its substrate. (Breuch (1967) [22]).

7. As a general rule it should be said that rubber and silicone-based adhesives are unacceptable, because of poor outgassing behavior, unless baked at elevated temperatures (Kordsmeier & Peters (1972) [74]).

6.4 Relevant properties of thermal control tapes

Thermal radiation, adhesion and outgassing properties of widely used adhesive tapes are given in Table 6-9 to Table 6-11. Any tape whose solar absorptance, α_s,and total emittance, ε, are known to the compiler has been included in the pertinent table.

As an aid in the selection of the most appropriate tape, the thermal radiation properties from these tables have been plotted in Figure 6-5. The number next to each data point identify the tape in the tables. The first digit in these numbers, 1, 2 or 0, indicates whether the tape is first surface metallized (Table 6-9), second surface metallized (Table 6-10) or clear (Table 6-11), respectively.

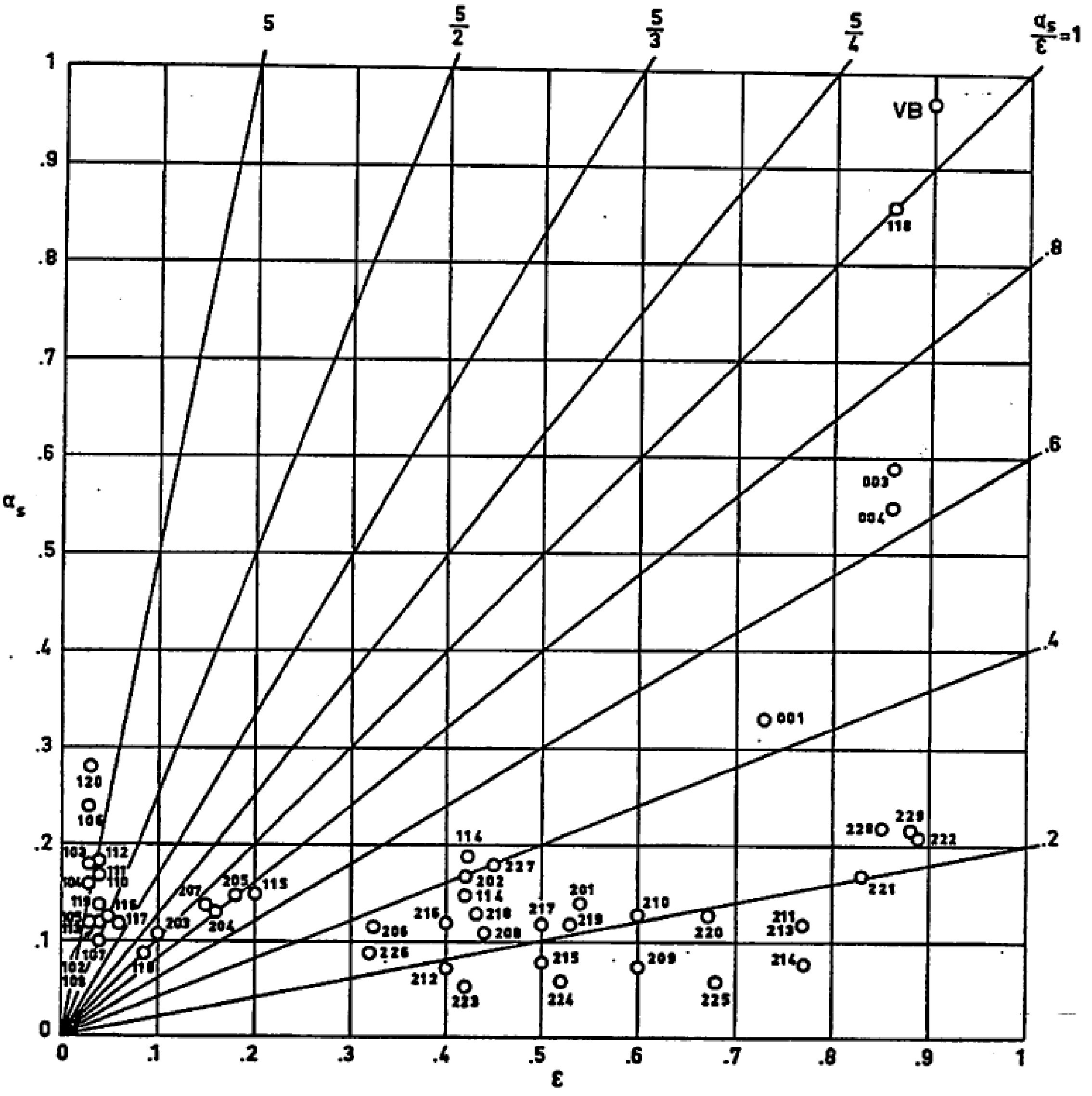

Note: non-si units are used in this figure

Figure 6-5: Solar absorptance, α_s, vs. total hemispherical emittance, ε, of several thermal control tapes.

Values of the mass/area ratio for several films and tapes are given in Table 6-12.

Table 6-13 presents data on general-purpose tapes which meet two criteria concerning outgassing: they have a maximum of 1,0 percent weight loss, and a maximum of 0,1 percent (in weight) of volatile condensable materials.

Availability of the tapes is not always indicated in the brochure sent by the manufacturers. Tape dimensions are generally from 10^{-2} to 0,5 m in width, and either 33 m or 66 m in length. normal sheets are 1,22 m wide by 3,05 m long.

Concerning costs, the following approximate figures have been quoted by Scollon & Carpitella (1970) [113]

Aluminized Teflon 45 US \$.m^{-2}.

Series Emittance 45-60 US \$.m^{-2}.

Table 6-9: Properties of First Surface Metallized Tapes [a]

Type		**101. Fasson S-277 I**	**102. Fasson S-277 II**	**103. 3M Co. 425**	**104. 3M Co. Y-9040**
Description	**Coating**	Al. Foil + Lacquer Coating	Aluminium Foil	Aluminium Foil	Aluminium Foil
	Backing				
	Adhesive	Acrylic S-277	Acrylic S-277	Acrylic [c]	Silicone
Thickness, tx10^{4} [m]	**Backing**	0,51 (metal foil)	0,51 (metal foil)	0,76 [c]	
	Total			1,27	0,51
Temp. Range [K]	**Intermittent**	464 [b]	464 [b]		
	Continuous			Up to 588 [c]	
Thermal Radiation Properties	α_s		0,12± 0,04 [b]	0,18	0,16
	ε	0,04± 0,02,0,01 [b]	0,04± 0,02,0,01 [b]	0,03	0,03
	α_s/ε		3,00	6,00	5,33
	Stability to Space Degradation			Good	Good
Mechanical	**Peel Strength**			7,00	

Type		**101. Fasson S-277 I**	**102. Fasson S-277 II**	**103. 3M Co. 425**	**104. 3M Co. Y-9040**
Properties	**(F/w)x10^{-2} [N.m^{-1}]**			10,00 [f]	
	Specifications			ASTM D1000	
Outgassing [d]	**%TWL**	1,367		0,240	1,120
	%VCM	0,421		0,030	0,640
	Cure t [h]	16		0	0
	Cure T [K]	338			
	ATMOS.	Air			
Comments					

Type		**105. 3M Co. Y-9050**	**106. 3M Co. Y-9184**	**107. 3M Co. Y-9360**	**108. Mystik 7402**
Description	**Coating**	Aluminium Foil	Gold vacuum deposited	Al. vacuum depos. both sides	Aluminium Foil
	Backing	Glass Cloth	Kapton	Mylar	
	Adhesive	Silicone	Silicone	Acrylic	Silicone
Thickness, tx10^4 [m]	**Backing**			0,25	0,51 (metal foil) [c]
	Total	1,52			1,12 [c]
Temp. Range [K]	**Intermittent**				700 (Internal) [b] 670 (External) [b]
	Continuous				
Thermal Radiation Properties	α_s	0,12	0,24 [e]	0,10	0,12± 0,04 [b]
	ε	0,03	0,03 [e]	0,04	0,04± 0,02,0,01 [b]
	α_s/ε	4,00	8,00	2,50	3,00

Type		**105. 3M Co. Y-9050**	**106. 3M Co. Y-9184**	**107. 3M Co. Y-9360**	**108. Mystik 7402**
	Stability to Space Degradation	Good	Good	Good	Good
Mechanical Properties	**Peel Strength (F/w)x10^{-2} [N.m^{-1}]**		1,75		4,71 [c] 3,85
	Specifications		ASTM D1000		MIL-T-81287 ASTM D1000
Outgassing [d]	**%TWL**	0,917	2,240	0,79 R 0,79 S	1,69 R 2,09 S
	%VCM	0,380	0,410	0,06 R 0,03 S	0,35 R 0,54 S
	Cure t [h]	0	0	0	0
	Cure T [K]				
	ATMOS.				
Comments					α_s = 0,07. From blackbody at 920 K [b]

Type		**109. Mystik 7430**	**110. Mystik 7452**	**111. Mystik 7453**	**112. Mystik 7455**
Description	**Coating**	Lead Foil	Aluminium Foil	Aluminium Foil	Aluminium Foil
	Backing				Glass Cloth
	Adhesive	Rubber	Acrylic	Acrylic	
Thickness, tx10^{4} [m]	**Backing**	1,27 (metal foil) [c]	0,51 (metal foil) [c]	0,76 (metal foil) [c]	1,14 [c]
	Total	1,65 [c]	0,94 [c]	1,30 [c]	1,30 [c]
Temp.	**Intermittent**				Up to 3600 short term [c]

Type		**109. Mystik 7430**	**110. Mystik 7452**	**111. Mystik 7453**	**112. Mystik 7455**
Range [K]	**Continuous**				194 to 560[c]
Thermal Radiation Properties	α_s		0,17	0,17	0,18
	ε	0,09	0,04	0,04	0,04
	α_s/ε		4,25	4,25	4,50
	Stability to Space Degradation	Good	Good	Good	Good
Mechanical Properties	**Peel Strength (*F*/*w*)x10^{-2} [N.m^{-1}]**	6,68[c] 10,70	6,57[c]	7,99[c] 6,48 9,63[f]	4,60[c] 6,48
	Specifications	HH-T-29 ASTM D1000		LT-80 ASTM D1000	ASTM D1000
Outgassing[d]	**%TWL**		0,37 0,25 R	0,092 R	3,820 1,710
	%VCM		0,04 0,03 R	0,003 R	2,620 1,340
	Cure *t* [h]		0	0	0 24
	Cure *T* [K]				0 423
	ATMOS.				Air
Comments					

Type		**113. Permacel EE6600**	**114. G.T. Schjeldahl G 101500**[d]	**115. G.T. Schjeldahl G 10200-4**	**116. G.T. Schjeldahl G 103300**
Description	**Coating**	Aluminium vacuum deposited	SiO$_x$ on Al. both vacuum deposited	Al. vacuum depos. over nylon tulle	Aluminium vacuum deposited

Type		**113. Permacel EE6600**	**114. G.T. Schjeldahl G 101500 [d]**	**115. G.T. Schjeldahl G 10200-4**	**116. G.T. Schjeldahl G 103300**
	Backing	Mylar	Kapton	Kapton	Kapton
	Adhesive	Rubber	Silicone	Acrylic	Silicone
Thickness, tx10^4 [m]	**Backing**		0,13	0,13	0,25
	Total				
Temp. Range [K]	**Intermittent**		88 to 533		88 to 533
	Continuous		88 to 422		88 to 422
Thermal Radiation Properties	α_s	0,12 [g]	<0,15	0,15± 0,03	<0,13
	ε	0,03 [g]	0,42	0,20± 0,07	0,05
	α_s/ε	4,00	0,35–0,45	0,75	2,50
	Stability to Space Degradation			Good	Good
Mechanical Properties	**Peel Strength (F/w)x10^{-2} [N.m^{-1}]**		1,10	3,15 5,43 [f]	1,75 [a] 1,10 [d]
	Specifications		ASTM D1000 (to Al.)	ASTM D1000	ASTM D1000 ASTM D1000 (to Al.)
Outgassing [d]	**%TWL**	>8.50			1,48 R
	%VCM	> 3,80			0,32 R
	Cure t [h]	0			0
	Cure T [K]				
	ATMOS.				
Comments					

Type		**117. G.T. Schjeldahl G 103500**	**118. G.T. Schjeldahl G 107000**	**119. G.T. Schjeldahl G 401000**	**120. G.T. Schjeldahl G 402600**
Description	**Coating**	Aluminium vacuum deposited	Thick film black	Aluminium vacuum deposited	Gold vacuum deposited
	Backing	Kapton	Kapton	Kapton	Kapton
	Adhesive	Silicone	Silicone	Acrylic	Silicone
Thickness, tx10^4 [m]	**Backing**	0,13	0,13	0,25	0,25
	Total				
Temp. Range [K]	**Intermittent**		88 to 422	88 to 505	88 to 505
	Continuous		88 to 380	88 to 395	88 to 395
Thermal Radiation Properties	α_s	0,10–0,14 [h]	0,86	0,14	0,25–0,28
	ε	<0,06	> 0,76	0,05	0,035
	α_s/ε	1,70–2,30 [h]	1,00	2,80	8,00
	Stability to Space Degradation				
Mechanical Properties	**Peel Strength (F/w)x10^{-2} [N.m^{-1}]**			2,19	1,10
	Specifications			ASTM D1000 (to Al.)	ASTM D1000 (to Al.)
Outgassing [d]	**%TWL**				
	%VCM				
	Cure t [h]				
	Cure T [K]				
	ATMOS.				

Type	**117.** **G.T.** **Schjeldahl** **G 103500**	**118.** **G.T.** **Schjeldahl** **G 107000**	**119.** **G.T.** **Schjeldahl** **G 401000**	**120.** **G.T.** **Schjeldahl** **G 402600**
Comments				

[a] All data in this table, unless otherwise stated, are from Brown & Merschel (1970) [23].

[b] From Breuch (1967) [22].

[c] Manufacturer's data.

[d] Data concerning G.T. Schjeldahl tapes are from bulletins issued by the producer, except those corresponding to GT 102000-4 which are given by Brown & Merschel (1970) [23].

[e] Outgassing characteristics have been borrowed from Campbell, Marriot & Park (1973) [27].
TWL: Total Weight Loss.
VCM: Volatile Condensable Materials (by weight).
A zero indicates that cure conditions are unknown.
R: Several layers of the tape were rolled on a glass Rod to permit outgassing at the edges.
S: The tape was placed on a Screen exposing the adhesive of the first layer.

[f] 90° peel strength of tape bonded to aluminium sheet exposed to 340 K in air for 30 d. From Brown & Merschel (1970) [23].

[g] From Kordsmeier & Peters (1972) [74].

[h] From Scollon & Carpitella (1970) [113].

Table 6-10: Properties of Second Surface Metallized Tapes [a]

Type		**201.** **3M Co. 850** **Silver**	**202.** **G.T.** **Schjeldahl** [c] **G 101500**	**203.** **G.T.** **Schjeldahl** **G 101600**	**204.** **G.T.** **Schjeldahl** **G 101701**
Description	**Plastic**	Mylar	Kapton	Kapton	Kapton
	Metal	Aluminium vacuum deposited	Al. vacuum deposited + SiO_x	Al. vacuum deposited + SiO_x	Al. vacuum deposited + SiO_x
	Adhesive	Acrylic	Silicone	Silicone	Silicone
Thickness, tx10^4 [m]	**Plastic**		0,13	0,13	0,13
	Total	0,63			
Temp. Range [K]	**Intermittent**		88 to 530		
	Continuous	223 to 423 [b]	88 to 420		
Thermal	α_s	0,14	<0,15		0,10–0,16 [f]

Type		**201. 3M Co. 850 Silver**	**202. G.T. Schjeldahl [c] G 101500**	**203. G.T. Schjeldahl G 101600**	**204. G.T. Schjeldahl G 101701**
Radiation Properties	ε	0,54	<0,42 [f]	0,06–0,14 [f]	0,11–0,21 [f]
	α_s/ε	0,26	0,35–0,45 [f]	1,00–1,20 [f]	0,70–1,00 [f]
	Stability to Space Degradation	Poor			
Mechanical Properties	**Peel Strength (F/w)x10^{-2} [N.m^{-1}]**	4,38 13,84 [e]			
	Specifications	ASTM D1000			
Outgassing [d]	**%TWL**	0,686			
	%VCM	0,097			
	Cure t [h]	0			
	Cure T [K]				
	ATMOS.				
Comments		Kordsmeier & Peters (1972) give $\alpha_s = 0{,}15$, $\varepsilon = 0{,}61$			

Type		**205. G.T. Schjeldahl G 101901**	**206. G.T. Schjeldahl G 101902**	**207. G.T. Schjeldahl G 102000**	**208. G.T. Schjeldahl G 107300**
Description	**Plastic**	Kapton	Kapton	Kapton + Nylon tulle	Kapton
	Metal	Al. vacuum deposited + SiO$_x$	Al. vacuum deposited + SiO$_x$	Aluminium vacuum deposited	Al. vacuum deposited + SiO$_x$
	Adhesive	Acrylic	Acrylic	Acrylic	
Thickness,	**Plastic**	0,25	0,25	0,13	0,25

Type		**205. G.T. Schjeldahl G 101901**	**206. G.T. Schjeldahl G 101902**	**207. G.T. Schjeldahl G 102000**	**208. G.T. Schjeldahl G 107300**
***t*x10⁴ [m]**	**Total**				
Temp. Range [K]	**Intermittent**				
	Continuous				
Thermal Radiation Properties	α_s	0,12–0,18 [f]	0,09–0,14 [f]	0,12–0,16 [f]	0,09–0,13 [f]
	ε	0,14–0,22 [f]	0,28–0,37 [f]	0,13–0,17 [f]	
	α_s/ε	0,70–1,00 [f]	0,32–0,48 [f]	0,70–1,20 [f]	0,19–0,31 [f]
	Stability to Space Degradation				
Mechanical Properties	**Peel Strength (F/w)x10^{-2} [N.m^{-1}]**				
	Specifications				
Outgassing [d]	**%TWL**				
	%VCM				
	Cure *t* [h]				
	Cure *T* [K]				
	ATMOS.				
Comments					

Type		**209. G.T. Schjeldahl G 400100**	**210. G.T. Schjeldahl G 400200**	**211. G.T. Schjeldahl G 400400**	**212. G.T. Schjeldahl G 400600**
Description	**Plastic**	FEP Teflon	FEP Teflon	Kapton	FEP Teflon
	Metal	Silver + Inconel both vacuum	Aluminium vacuum	Aluminium vacuum	Silver + Inconel both

Type		**209. G.T. Schjeldahl G 400100**	**210. G.T. Schjeldahl G 400200**	**211. G.T. Schjeldahl G 400400**	**212. G.T. Schjeldahl G 400600**
		dep.	deposited	deposited	vacuum dep.
	Adhesive	Acrylic	Acrylic	Acrylic	Acrylic
Thickness, tx10^{4} [m]	**Plastic**	0,51	0,51	1,27	0,13
	Total				
Temp. Range [K]	**Intermittent**	88 to 505	88 to 505	88 to 505	88 to 505
	Continuous	88 to 395	88 to 395	88 to 395	88 to 395
Thermal Radiation Properties	α_s	0,06–0,09	0,13	0,10–0,14	0,06–0,09
	ε	0,6	0,6	0,77	0,4
	α_s/ε	0,12	0,22	0,14	0,18
	Stability to Space Degradation				
Mechanical Properties	**Peel Strength (F/w)x10^{-2} [N.m^{-1}]**	2,19	2,19		
	Specifications	ASTM D1000 (to Al.)	ASTM D1000 (to Al.)		
Outgassing [d]	**%TWL**				
	%VCM				
	Cure t [h]				
	Cure T [K]				
	ATMOS.				
Comments					

Type		**213.** **G.T. Schjeldahl G 400800**	**214.** **G.T. Schjeldahl G 401900**	**215.** **G.T. Schjeldahl G 402500**	**216.** **G.T. Schjeldahl G 402800**
Description	**Plastic**	FEP Teflon	FEP Teflon	FEP Teflon	FEP Teflon
	Metal	Aluminium vacuum deposited	Silver + Inconel both vacuum dep.	Silver + Inconel both vacuum dep.	Aluminium vacuum deposited
	Adhesive	Acrylic	Acrylic	Acrylic	Acrylic
Thickness, tx10^4 [m]	**Plastic**	1,27	1,27	0,25	0,13
	Total				
Temp. Range [K]	**Intermittent**	88 to 505	88 to 505	88 to 505	88 to 505
	Continuous	88 to 395	88 to 395	88 to 395	88 to 395
Thermal Radiation Properties	α_s	0,10–0,14	0,06–0,10	0,06–0,10	0,10–0,14
	ε	0,77	0,77	0,50	0,40
	α_s/ε	0,18	0,09	~0,14	0,27
	Stability to Space Degradation				
Mechanical Properties	**Peel Strength (F/w)x10^{-2} [N.m^{-1}]**	2,19	2,19	2,19	2,19
	Specifications	ASTM D1000 (to Al.)	ASTM D1000 (to Al.)	ASTM D1000 (to Al.)	ASTM D1000 (to Al.)
Outgassing [d]	**%TWL**		0,335 R		
	%VCM		0,007 R		
	Cure t [h]		0		
	Cure T [K]				
	ATMOS.				

Type		**217. G.T. Schjeldahl G 402900**	**218. G.T. Schjeldahl Series Emittance Tape**	**219.**	**220. G.T. Schjeldahl Series Emittance Tape**
Description	**Plastic**	FEP Teflon	FEP Teflon		FEP Teflon
	Metal	Aluminium vacuum deposited	Aluminium vacuum deposited		Aluminium vacuum deposited
	Adhesive	Acrylic			
Thickness, tx10^4 [m]	**Plastic**	0,25	0,13	0,25	0,51
	Total				
Temp. Range [K]	**Intermittent**	88 to 505			
	Continuous	88 to 395			
Thermal Radiation Properties	α_s	0,10–0,14	0,13 [f]	0,12 [f]	0,13 [e]
	ε	0,50	0,43 [f]	0,53 [f]	0,67 [e]
	α_s/ε	0,22	0,30 [f]	0,23 [f]	0,19 [f]
	Stability to Space Degradation				$\Delta\alpha_s = 0$ [g] $\Delta\alpha_s = 0{,}07$ [h]
Mechanical Properties	**Peel Strength (F/w)x10^{-2} [N.m^{-1}]**	2,19			
	Specifications	ASTM D1000 (to Al.)			
Outgassing [d]	**%TWL**				
	%VCM				
	Cure t [h]				
	Cure T [K]				

Type		**217. G.T. Schjeldahl G 402900**	**218. G.T. Schjeldahl Series Emittance Tape**	**219.**	**220. G.T. Schjeldahl Series Emittance Tape**
	ATMOS.				
Comments					

Type		**221.**	**222.**	**223. G.T. Schjeldahl Series Emittance Tape**	**224.**
Description	**Plastic**	FEP Teflon	FEP Teflon	FEP Teflon	FEP Teflon
	Metal	Aluminium vacuum deposited	Aluminium vacuum deposited	Silver vacuum deposited	Silver vacuum deposited
	Adhesive				
Thickness, tx10^4 [m]	**Plastic**	1,27	2,54	0,13	0,25
	Total				
Temp. Range [K]	**Intermittent**				
	Continuous				
Thermal Radiation Properties	α_s	0,17 [e]	0,21 [e]	0,055 [e]	0,059 [e]
	ε	0,83 [e]	0,89 [e]	0,42 [e]	0,52 [e]
	α_s/ε	0,20 [f]	0,24 [f]	0,13 [f]	0,11 [f]
	Stability to Space Degradation				
Mechanical Properties	**Peel Strength (F/w)x10^{-2} [N.m^{-1}]**				
	Specifications				

Type		**221.**	**222.**	**223. G.T. Schjeldahl Series Emittance Tape**	**224.**
Outgassing [d]	**%TWL**				
	%VCM				
	Cure *t* [h]				
	Cure *T* [K]				
	ATMOS.				
Comments			Not included in G.T. Schjeldahl Bulletin		

Type		**225.**	**226.**	**227. G.T. Schjeldahl Series Emittance Tape**	**228.**
Description	**Plastic**	FEP Teflon	FEP Teflon	Polyvinyl butyral (Butvar)	Polyvinyl butyral (Butvar)
	Metal	Silver vacuum deposited	Silver vacuum deposited	Aluminium vacuum deposited	Aluminium vacuum deposited
	Adhesive				
Thickness, $tx10^{4}$ [m]	**Plastic**	0,51	1,27	0,19	0,81
	Total				
Temp. Range [K]	**Intermittent**				
	Continuous				
Thermal Radiation	α_s	0,059 [e]	0,090 [e]	0,18 [e]	0,22 [e]
	ε	0,68 [e]	0,82 [e]	0,45 [e]	0,85 [e]

Type		**225.**	**226.**	**227.** **G.T. Schjeldahl Series Emittance Tape**	**228.**
Properties	α_s/ε	0,087 [f]	0,11 [f]	0,40 [f]	0,26 [f]
	Stability to Space Degradation	$\Delta\alpha_s = 0$ [g]			
Mechanical Properties	**Peel Strength (F/w)x10^{-2} [N.m^{-1}]**				
	Specifications				
Outgassing [d]	**%TWL**				
	%VCM				
	Cure t [h]				
	Cure T [K]				
	ATMOS.				
Comments			Data on degradation in Table 6-6 (Samples TI & TII)		

Type		**229.**	**230.**
Description	**Plastic**	Polyvinyl butyral (Butvar)	Polyvinyl butyral (Butvar)
	Metal	Aluminium vacuum deposited	Aluminium vacuum deposited
	Adhesive		
Thickness, tx10^4 [m]	**Plastic**	1,65	2,03
	Total		

Type		**229.**	**230.**
Temp. Range [K]	**Intermittent**		
	Continuous		
Thermal Radiation Properties	α_s	0,22 [e]	0,17 [e]
	ε	0,88 [e]	
	α_s/ε	0,25 [f]	
	Stability to Space Degradation		$\Delta\alpha_s = 0$ [i] $\Delta\alpha_s = 0{,}25$ [j]
Mechanical Properties	**Peel Strength $(F/w)\mathrm{x}10^{-2}$ [N.m^{-1}]**		
	Specifications		
Outgassing [d]	**%TWL**		
	%VCM		
	Cure t [h]		
	Cure T [K]		
	ATMOS.		
Comments			

[a] All data in this table, unless otherwise stated, are from Brown & Merschel (1970) [23].

[b] Manufacturer's data. The tape remains flexible throughout the mentioned temperature range.

[c] Data concerning G.T. Schjeldahl tapes are from bulletins issued by the producer, unless otherwise stated.

[d] Outgassing characteristics have been borrowed from Campbell, Marriot & Park (1973) [27].
TWL: Total Weight Loss.
VCM: Volatile Condensable Materials (by weight).
A zero indicates that cure conditions are unknown.
R: Several layers of the tape were rolled on a glass Rod to permit outgassing at the edges.
S: The tape was placed on a Screen exposing the adhesive of the first layer.

[e] 90° peel strength of tape bonded to aluminium sheet exposed to 340 K in air for 30 d. From Brown & Merschel (1970) [23].

[f] From Scollon & Carpitella (1970) [113].

[g] 180 EUVSH+10^6 rads X-ray. From Scollon & Carpitella (1970) [113]. EUVSH: Equivalent Ultraviolet Sun Hours.

[h] 51 EUVSH+1,5x10^{20} protons.m^{-2} at 3 KEV. From Scollon & Carpitella (1970) [113].

[I] 250 EUVSH. From Scollon & Carpitella (1970) [113].

[j] 70 EUVSH+2,1x10^{20} protons.m^{-2} at 4 KEV. From Scollon & Carpitella (1970) [113].

Table 6-11: Properties of Clear Tapes [a]

Type		**001. 3M Co. 850**	**002. 3M Co. 853**	**003. 3M Co. X-1173**	**004. Mystik 7361**
Description	**Substrate**	Aluminium backside	Aluminium	low α_s Aluminium	Aluminium
	Plastic	Mylar	Mylar	Clear Kapton	Kapton
	Adhesive	Acrylic		Thermoset. Silicone	Silicone
Thickness, tx10^4 [m]	**Plastic**	0,51	0,25	0,51	0,25
	Total				0,51 ± 0,05 [c]
Temp. Range [K]	**Intermittent**				
	Continuous	223 to 423 [b]	223 to 453 [b]		195 to 560 [c]
Thermo-Optical Properties	α_s	0,33		0,59	0,55
	ε	0,73	0,76	0,86	0,86
	α_s/ε	0,45		0,69	0,64
	Stability to Space Degradation	Poor	Poor	Good	Good

Type		**001. 3M Co. 850**	**002. 3M Co. 853**	**003. 3M Co. X-1173**	**004. Mystik 7361**
Mechanical Properties	**Peel Strength (F/w)x10^{-2} [N.m^{-1}]**	2,74 [b]	4,38		1,42 Min. [c] 1,64 Avg. [c]
	Specifications	ASTM D 1000	ASTM D 1000		
Outgassing [d]	**%TWL**			2,150 R 3,040 S	1,150 1,380
	%VCM			0,580 R 1,390 S	0,200 0,550
	Cure t [h]			0	0
	Cure T [K]			0	0
	ATMOS.				
Comments		Roll Length: 66 m [c]	Roll Length: 33 m [c] 66 m [c]		Roll Length: 33 m Roll Width: 7,62x10^{-2} m [c]

Type		**005. G.T. Schjeldahl G 401100**	**Other Tapes**	
			3M Co. 53	**VB 3M Co. Y-9244**
Description	**Substrate**		Aluminium	
	Plastic	Kapton	Mylar	Velvet Black/Vinyl Film
	Adhesive	Acrylic	Thermoset. Rubber	Acrylic
Thickness, tx10^{4} [m]	**Plastic**	0,25	0,25	
	Total			
Temp. Range	**Intermittent**	88 to 505 [c]		

Type		**005. G.T. Schjeldahl G 401100**	**Other Tapes**	
			3M Co. 53	**VB 3M Co. Y-9244**
[K]	**Continuous**	88 to 395 [c]		
Thermo-Optical Properties	α_s			0,97
	ε		0,79	0,90
	α_s/ε			1,08
	Stability to Space Degradation		Poor	Good
Mechanical Properties	**Peel Strength (F/w)x10^{-2} [N.m^{-1}]**	2,19 [c]		
	Specifications	ASTM D1000 (to Al.) [c]		
Outgassing [d]	**%TWL**		1,026	6,760 R 1,660 S
	%VCM		0,131	0,840 R 0,160 S
	Cure t [h]		3	0 27
	Cure T [K]		394	0 383
	ATMOS.		Air	E-3
Comments				Additional outgassing data are given below [e]

[a] All data in this table, unless otherwise stated, are from Brown & Merschel (1970) [23].

[b] Manufacturer's data. The tape remains flexible throughout the mentioned temperature range.

[c] Manufacturer's data.

[d] Outgassing characteristics have been borrowed from Campbell, Marriot & Park (1973) [27].
TWL: Total Weight Loss.
VCM: Volatile Condensable Materials (by weight).
A zero indicates that cure conditions are unknown.
R: Several layers of the tape were rolled on a glass Rod to permit outgassing at the edges.
S: The tape was placed on a Screen exposing the adhesive of the first layer.
E-3: Chamber pressure 10^{-3} torr = 0,133 Pa.

[e] These data have been obtained by Scannapieco (1967) [109] by using the General Electric in-situ technique.

% TWL	**% VCM**	**CURE *t* [h]**	**CURE *T* [K]**	**ATMOS.**
4,8 ± 0,02	0,40 ± 0,11	24	Room	<1,33x10^{-3} Pa 341,5 ± 5
4,6 ± 0,02	0,20 ± 0,11	24	Room	<1,33x10^{-3} Pa 341,5 ± 5
		8	338 ± 5 Furnace pressure <1,33x10^{-3} Pa	

Table 6-12: Mass-Area Ratio of Several Foils and Tapes

Type	Description			Plastic Thicknessx10^4 [m]	(Mass/area)x10^2 [kg.m^{-2}]
	Metal	Plastic	Adhesive		
Mystik 7361		Kapton	Silicone	0,25	6,71
Mystik 7367		Kapton	Acrylic	0,25	9,72
Mystik 7375		Tedlar	Acrylic	0,51	11,92
G.T. Schjeldahl G 103300	Aluminium vacuum deposited	Kapton	Silicone	0,25	7,75
G.T. Schjeldahl G 400300	Silver+Inconel both vacuum dep.	FEP Teflon		0,51	10,85
G.T. Schjeldahl G 400900	Aluminium vacuum deposited	FEP Teflon		1,27	27,90
G.T. Schjeldahl G 401400	Silver+Inconel both vacuum dep.	FEP Teflon		0,25	6,20
G.T. Schjeldahl G 402000	Aluminium vacuum deposited	FEP Teflon		0,25	6,20
G.T. Schjeldahl G 402200	Silver+Inconel both vacuum dep.	FEP Teflon		0,25	6,20
G.T. Schjeldahl G 402300	Silver+Inconel both vacuum dep.	FEP Teflon		0,51	10,85

NOTE From manufacturer’s bulletins.

Table 6-13: Characteristics of Low-Outgassing Tapes [a]

Type		**3M Co. 425**	**3M Co. 850 Black**	**3M Co. 850 Silver**	**Mystik 7341**
Description	**Backing**	Aluminium	Mylar	Aluminized-Mylar	Mylar
	Adhesive	Acrylic	Acrylic	Acrylic	Acrylic
Thickness, tx10^4 [m]	**Backing**	0,76	0,25		
	Total	1,27	0,51	0,63	
Temp. Range [K]	**Intermittent**				
	Continuous	Up to 588	223 to 423	223 to 423	
Electrical	**Dielectric Strengthx10^{-3} [V]**				
Mechanical	**Peel Strength**	7,11 9,98 [c]	2,74	4,38 13,84 [c]	
	Tack				
Outgassing [b]	**%TWL**	0,240	0,770 R 0,650 R	0,686 R	0,238 R
	%VCM	0,030	0,020 R 0,090 R	0,097 R	0,041 R
	Cure t [h]	0	0	0	0
	Cure T [K]	0	0	0	0
	ATMOS.				
Comments		High temperature and reflectance qualities. Expands readily with thermal changes. Long ageing. Excellent moisture barrier.	Thermal, abrasion and solvent resistant. Long ageing. Bonds more firmly with time. Difficult to remove without adhesive transfer. Clear, red, white, and black tapes available.	Thermal and abrasion resistant. Good outdoor weathering. Excellent moisture barrier. Long ageing. Removal, after long bonding times, difficult without adhesive transfer. Length 66 m.	

Type		**Mystik 7367**	**Mystik 7375**	**Mystik 7420**
Description	**Backing**	Kapton	Tedlar	Copper
	Adhesive	Acrylic	Acrylic	Acrylic
Thickness, *t*x10⁴ [m]	**Backing**	0,25	0,51	0,41
	Total	0,76± 0,08	0,94± 0,10	0,89
Temp. Range [K]	**Intermittent**			
	Continuous	211 to 450	211 to 450	
Electrical	**Dielectric Strengthx10^{-3} [V]**	7,20 Min. 7,50 Avg.	4,90 Min. 5,20 Avg.	
Mechanical	**Peel Strength**	3,28 Min. 4,70 Avg.	5,58 Min. 6,79 Avg.	6,02
	Tack	1,42 Min. 1,75 Avg.	2,41 Min. 3,06 Avg.	1,14 m (Rolling ball)
Outgassing [b]	**%TWL**	0,639	0,341 R	0,215 R
	%VCM	0,049	0,007 R	0,010 R
	Cure *t* [h]	0	0	0
	Cure *T* [K]	0	0	0
	ATMOS.			
Comments		High temperature, solvent, and moisture resistant. Electrically pure with excellent dielectric strength. High adhesion. Length 33 m on 7,62x10^{-2} m core. Color: Amber.	Excellent outdoor weather-ability, solvent and moisture resistant. High adhesion, conformability and elongation, and good dielectric strength. Abrasion resistant. Length 66 m on 7,62x10^{-2} m core. Color: White.	Temperature resistant, solderable.

[a] All data in this table, unless otherwise stated, are from manufacturer's bullatins.

[b] Outgassing characteristics have been borrowed from Campbell, Marriot & Park (1973) [27].
TWL: Total Weight Loss.
VCM: Volatile Condensable Materials (by weight).
A zero indicates that cure conditions are unknown.
R: Several layers of the tape were rolled on a glass Rod to permit outgassing at the edges.
S: The tape was placed on a Screen exposing the adhesive of the first layer.

[c] From Brown & Merschel (1970) [23]. 90° pel strength of tape bonded to aluminium sheet exposed to 338,5 K in air for 30 d.

6.5 Past spatial use

Tapes are widely used in spacecraft as thermal control coatings. The following examples have been found. Launching date is given in parenthesis.

Explorers 12, 14, 15 and 26 - Energetic Particles Explorers (EPE).

(Aug. 16, 1961. Oct. 2 and 27, 1962. Dec. 21, 1964). Aluminized tape or foil tape. (Rittenhouse & Singletary (1969) [105]).

Mariner 2. (Aug. 27, 1962). Exposed wiring wrapped with Teflon-coated aluminium foil. (Rittenhouse & Singletary (1969) [105]).

ERS. (Environmental Research Satellite). (Sept. 17, 1962, failed).

External surface - Among other coatings, Gold vacuum deposited on Mylar tape 3M Co. Y-9181,and Aluminized foil tape 3M Co. 425, were used. (Rittenhouse & Singletary (1969) [105]).

Vela. (Oct. 17, 1963). Aluminium foil tape (3M Co. 425) and aluminized Mylar tape (3M Co. 850) used as thermal control coatings. (Rittenhouse & Singletary (1969) [105]).

Explorers 18, 21, and 28 - Interplanetary Monitoring Platform (IMP). (Nov. 27, 1963. Oct. 4, 1964. May 29, 1965). Small are covered with aluminized or foil tape. (Rittenhouse & Singletary (1969) [105]).

Ranger 6 through 9. (Jan. 30 and July 28, 1964. Feb. 17 and Mar. 21, 1965). Aluminized Mylar used for wrapping cable harnesses. (Rittenhouse & Singletary (1969) [105]).

Nimbus 1. (Aug. 8, 1964). Aluminized Mylar and aluminized Teflon tapes used to cover the truss structure of the louvers. Electrical cable harnesses covered with the same tapes. (Rittenhouse & Singletary (1969) [105]).

Pegassus 1 and 2. (Feb. 16 and May 25, 1965). Tubing near electronics boxes-wrapped with aluminized Mylar tape. (Rittenhouse & Singletary (1969) [105]).

Oscar 3. (Mar. 9, 1965). External surface - Non leafing aluminium paint on Mystik tape. (Rittenhouse & Singletary (1969) [105]).

ERS 15 and 16. (July 20, 1965). Aluminized Mylar wrap, 3M Co. 850 applied over the bodies of valves prepared to perform several cold-welding experiments. (Rittenhouse & Singletary (1969) [105]).

Apollo 1 through 15. (Feb. 26, 1966 - July 26, 1971). Gold tapes and aluminium tapes were used in the Command Module. (Rittenhouse & Singletary (1969) [105]).

Aluminized tapes were used to attach multilayer insulations in the cryogenic propulsion systems of Saturn S-II stage. (Schroeder (1973) [112]).

SERT II (Space Electric Rocket Test). (Feb. 3, 1970). About 27 m of $5x10^{-2}$ m wide Mystik 7402 L tape were used for thermal control. (Stevens (1971) [120]).

OSO-H (Orbiting Solar Observatory). (). The following coatings, among others, were tested in the Thermal Control Coatings Experiment:

1. FEP Teflon 1,27x10^{-4} m thick coated with Silver (≅ 10^{-7} m thick), vacuum deposited, plus a layer of Inconel, attached to Al substrate by Mystik 7366 double backed adhesive tape.
2. Same as above except Aluminium is deposited instead of Silver-Inconel. (Triolo (1973) [128]).

IMP-I (Interplanetary Monitoring Platform). (March 13, 1971). A second surface mirror, vapor deposited Silver on 1,27x10^{-4} m thick FEP Teflon, was used to minimize the effect of the incident solar energy on a detector of the Energy Particle Experiment. The coating was applied by use of the pressure sensitive double sided adhesive tape Mystik 7366. Inconel is vapor deposited over the silver backing to protect this film from possible degradation by the adhesive. Data concerning the space degradation of this coating were already presented under the heading Space Degradation (Hoffman (1973) [61]).

IMP-H (Interplanetary Monitoring Platform). (Sept. 22, 1972). The following coatings, among others, were tested in the Thermal Control Coatings Experiment:

1. FEP Teflon 1,27x10^{-4} m thick coated with Silver (≅ 10^{-7} m thick), vacuum deposited, plus a layer of Inconel, attached to Al substrate by Mystik 7366 double backed adhesive tape. (Metal side down).
2. Same as above except that Silver plus Inconel has been substituted for Aluminium. Preliminary results of the experiments undertaken during these two flights were compared with laboratory results in the paragraph dealing with Space Degradation. (Triolo (1973) [128]).

Meteosat. (Geostationary European Meteorological Satellite). The following tapes are included in the Thermal Control Material List:

Fasson Bright Solid Aluminium Foil, 0,51x10^{-4} m thick, with S-227 adhesive. Used as thermal control coating.

G.T. Schjeldahl G 400200. FEP Teflon on Aluminium with Acrylic adhesive. Used as a Second Surface Mirror.

Mystik 7300. Mylar film with Silicone Adhesive. Used for coating masks.

Mystik 7367. Kapton film with Acrylic Adhesive. Superinsulation assembly.

3M Co. 850. Mylar film with Acrylic Adhesive. Superinsulation assembly.

3M Co. 250. Adhesive tape, acrylic. Coating film adhesion.

Bibliography

[1] 3M Co., "Technical Data for Industry", Data Sheets D-14, D-20, D-21, D-22 and F-5. 3M Co., St. Paul, Minnesota 55101.

[2] Adamo, R.C., Nanevicz, J.E., "Spacecraft-Charging Studies of Voltage Breakdown Processes on Spacecraft Thermal Control Mirrors", in "Spacecraft Charging by Magnetospheric Plasmas", Progress in Astronautics and Aeronautics, Vol. 47, A. Rosen, Ed., The MIT Press, Cambridge, Massachusetts, 1976, pp. 225-235.

[3] Adams, V.W., "Prospero: The First Year in Orbit", RAE-TR-73 114, Royal Aircraft Establishment, Farborough, England, Sep. 1973.

[4] Ahern, J.E., Karperos, K., "Calorimetric Measurements of Thermal Control Surfaces on Operational Satellites", AIAA Paper No. 83-0075, AIAA 21st Aerospace Science Meeting, Reno, Nevada, Jan. 10-13, 1983.

[5] Amartin, M., Paillous, A., "Comportement de Deux Types d'OSR en Silice Argentés a Couche d'ITO sous Irradiation par Electrons de 5 a 20 keV", ONERA CERT DERTS EC 4134, Toulouse, France, Juillet, 1981.

[6] ASTRAL, "Revêtement de Contrôle Thermique -PSG 120-", Astral Peintures et Vernis, 164 Rue Ambroise Croizat, 93204 Saint-Dénis, France, Janv. 1976.

[7] ASTRAL, "Primaire P 123", Astral Peintures et Vernis, 164 Rue Ambroise Croizat, 93204 Saint-Dénis, France, Janv. 1976.

[8] ASTRAL, "Primaire P 128", Astral Peintures et Vernis, 164 Rue Ambroise Croizat, 93204 Saint-Dénis, France, Janv. 1976.

[9] ASTRAL, "PSZ 184", Astral Peintures et Vernis, 164 rye Ambroise Croizat, 93204 Saint-Dénis, France, Avril 1981.

[10] Bachofer, B.T., "Landsat D - Case Study in Spacecraft Design", AIAA Professional Study Series, AIAA Educational Programs, New York, Aug. 1979.

[11] Benaïsa, B., Lévy, L., Paillous, A., Sarrail, D., "Satellite Spacecraft Charging Control Materials", ONERA CERT DERTS Interim Scientific Report, Toulouse, France, July 1979.

[12] Bentlage, H., Spanier, H.P., Wilkens, W., "Changes in Electrical Cross-Resistance of Conductive Coatings Due to Contamination by Outgassing of Silicon Rubber Material Silastic", NASA TT F-16727, April 1976.

[13] Bosma, J., Private communication, ESTEC, Noordwijk, The Netherlands, Dec, 14, 1981.

[14] Bosma, J., Froggatt, M., "evaluation of a Conductive Adhesive System for the Grounding od Aluminised Kapton Coated with Indium/Tin Oxide", ESA STM-213, Aug. 1980.

[15] Bosma, S.J., "Microscopic Investigation of Electrostatic Discharge Phenomena on Nonconductive Optical Solar Reflectors with a Conductive Adhesive", ESA STM-211, March 1979.

[16] Bosma, S.J., Levadou, F., "Electrostatic Charging and Space Materials", in ESA SP-145, "Spacecraft Materials in Space Environment", J. Dauphin & T.D. Guyenne, Eds., Proceedings of a Symposium held at ESTEC, Noordwijk, The Netherlands, Oct. 2-5, 1979, pp. 189-207.

[17] Bouchez, J.P., Gülpen, J., "The European Geostationary Communication Satellite OTS - Two Years of Thermal Control Experience in Orbit", AIAA Paper No. 80-1500, , AIAA 15th Thermophysics Conference, Snowmass, Colorado, July 14-16, 1980.

[18] Bouchez, J.P., Howle, D., "The Orbital Test Satellite OTS-2-Two Years of Orbital Thermal Control Experience", ESA Bulletin, No. 26, May 1981, pp. 54-61.

[19] Bourrieau, J., "Irradiations par Protons et Irradiations par Electrons de Revêtements de Contrôle Thermique et de Films Polymériques. Tome 2 - Partie Théorique. Rapport Final", ONERA CERT DERTS EC 4059, Toulouse, France, 1978.

[20] Bourrieau, J., Paillous, A., "Effects of Radiations on Polymers and Thermal Control Coatings", in ESA SP-145, "Spacecraft Materials in Space Environment", J. Dauphin & T.D. Guyenne, Eds., Proceedings of a Symposium held at ESTEC, Noordwijk, The Netherlands, Oct. 2-5, 1979, pp. 227-245.

[21] Bourrieau, J., Paillous, A., Romero, M., "Degradations de Revêtements de Contrôle Thermique Sous L'Effect des Rayonements Ultraviolets et Particulaires. Rapport Final", ONERA CERT DERTS EC 4046, Toulouse, France, Oct. 1976.

[22] Breuch, R.A., "Handbook of Optical Properties for Thermal Control Surfaces", LMSC-A847882, Vol. III, Lockheed Missiles & Space Company, Sunnyvale, California, June 1967.

[23] Brown, G.L., Merschel, R.P., "Thermal Control Tapes for Spacecraft Applications", Proceedings of the Symposium on Thermodynamics and Thermophysics of Spacecraft Flight, Sponsored by USAF and Lockheed, Palo Alto, California, March, 23-25, 1970, pp. 221-228.

[24] Brown, R.R., Fogdall, L.B., Cannaday, S.S., "Electron-Ultraviolet Radiation Effects on Thermal Control Coatings", in "Thermal Design Principles of Spacecraft and Entry Bodies", Progress in Astronautics and Aeronautics, Vol. 21, J.T. Bevans, Ed., Academic Press, New York, 1969, pp. 697-724.

[25] Cagle, C.V., "Adhesive Bonding-Techniques and Applications", McGraw-Hill Book Company, New York, 1968, Chap. 5. Pp. 86-123.

[26] Caldwell, C.R., Nelson, P.A., "Thermal Control Experiments on the Lunar Orbiter Spacecraft", in "Thermal Design Principles of Spacecraft and Entry Bodies", Progress in Astronautics and Aeronautics, Vol. 21, J.T. Bevans, Ed., Academic Press, New York, 1969, pp. 819-852.

[27] Campbell, Jr. W.A., Marriott, R.S., Park, J.J., "A Compilation of Outgassing Data for Spacecraft Materials", NASA TN D-7362, Sept. 1973, pp. 82-88.

[28] Campbell, Jr., W.A., Marriott, R.S., Park, J.J., "An Outgassing Data Compilation of Spacecraft Materials", NASA RP 1014, Jan. 1978.

[29] Chalmers, D.R., Konzok, H.G., Bouchez, J.P., Howle, D., "OTS-2: Five Years of Thermal Testing on a Satellite in a Geostationary Orbit", in "Proceedings of the International Symposium on Environmental and Thermal Systems for Space Vehicles", T.D. Guyenne & J.J. Hunt, Eds., Toulouse, France, 4-7 Oct. 1983. ESA SP-200, Paris, 1983, pp. 425-436.

[30] Clark, L.G., "LDEF Mission 1 - Experiment Description", Preliminary Copy, Langley Research Center, NASA, Sept. 1981.

[31] Cull, R.A., Stevenson, G., Harada, Y., Mell, R., "Requalification of S-13 G/LO", AIAA Paper No. 84-1775, AIAA 19th Thermophysics Conferences, Snowmass, Colorado, June 25-28, 1984.

[32] Cunnington, G.R., Private communication, Lokheed, Palo Alto Research Laboratory, Palo Alto, California, Oct. 25, 1974.

[33] Cunnington, G.R., Grammer, J.R., Smith, F.J., "Emissivity Coatings for Low-Temperature Space Radiators", NASA CR-1420, (NAS 3-7630), Lockheed Missiles & Space Company, Sunnyvale, California, Sept. 1969.

[34] Curran, D.G.T., Millard, J.M., "Contamination/Degradation Measurements on Operational Satellite Thermal Control Surfaces", in "Heat Transfer and Thermal Control Systems", Progress in Astronautics & Aeronautics, Vol. 64, L.S. Fletcher, Ed., American Institute of Aeronautics and Astronautics, New York, 1978, pp. 236-289.

[35] Delmonte, J., "The Technology of Adhesives", Reinhold Publishing Corporation, New York, 1947, Chap. 8, pp. 178-228.

[36] Domingo, E., Private communication, Madrid, 30 Jan. 1987.

[37] DOW CORNING, "Les Elastomères Silicones Silastic au Service des Bureaux d'Etudes", Dow Corning Int, Ltd., Chaussée de la Hulpe, 177, B-1170, Brussels, Belgium, 1970.

[38] ESTEC, Private communication, Meteosat, Material List (Thermal Control), May 1974.

[39] ESTEC, "Co-ordination of Materials Studies", Data Sheet No. 28, 4th Quarter 1980, ESTEC, Noordwijk, The Netherlands, 1980.

[40] ESTEC, "Co-ordination of Materials Studies", Data Sheet No. 30, 2nd Quarter 1981, ESTEC, Noordwijk, The Netherlands.

[41] Fawcett, J.A., Private communication, OCLI Europe, High Wycombe, Buckinghamshire, England, June, 1981.

[42] Fodgall, L.B., Cannaday, S.S., "Radiation Effects on Second Surface Mirrors", in "Evaluation de l'Action de l'Environnement Spatial sur les Materiaux", Centre National d'Etudes Spatiales, Toulouse, France, June 1974, pp. 549-560.

[43] Fogdall, L.B., Cannaday, S.S., Brown, R.R., "Electron Energy Dependence for in Vacuum Degradation and Recovery in Thermal Control Surfaces", in "Thermophysics: Applications to Thermal Design of Spacecraft", Progress in Astronautics and Aeronautics, Vol. 23, J.T. Bevans, Ed., Academic Press, New York, 1970, pp. 219-248.

[44] Fry, J., Nicoletta, C.A., "Ultraviolet and Charged Particle Irradiation of Proposed Solar Cell Coverslide Materials and Conductive Coatings for the Helios Spacecraft", NASA TM X-65945, June 1972.

[45] Gilligan, J.E., Harada, Y., Gates, D.W., "Current Technology for Development of Low α_s/ε Coatings", in "Evaluation de l'Action de l'Environnement Spatial sur les Materiaux", Centre National d'Etudes Spatiales, Toulouse, France, June 1974, pp. 567-587.

[46] Gilligan, J.E., Zerlaut, G.A., "The Space Environment Stability Problem in White Pigmented Coatings", 17th Annual Meeting Institute of Environmental Sciences, Los Angeles, California, April 1971, pp. 447-457.

[47] Gilligan, J.E., Zerlaut, G.A., "Thermal Control Materials and Technology in the 1970s", Transactions of the ASME, Journal of Engineering for Industry, Vol. 95, Series B, No. 4, Nov. 1973, pp. 1065-1068.

[48] Guillaumon, J.C., "Development du Nouveaux Revêtements de Contrôle Thermique pour les Vehicles Spatiaux", in "Spacecraft Materials in Space Environment", A. Rolfo, J. Dauphin & T.D. Guyenne, Eds., ESA SP-178, Paris, 1982, pp. 21-26.

[49] Guillaumon, J.C., "Peinture Blanche Conductrice (PCBZ CNES). Qualification de l'Application Directe (Sans P128) sur les Alliages Legers", CNES Report CT/DRT/SST/TH/2326, Oct. 1983.

[50] Guillaumon, J.C., Private communication, Toulouse, 25 Feb. 1986.

[51] Guillaumon, J.C., Blett, L., "Peinture Blanche Conductrice (PCBZ CNES - Compte Rendu de Qualification", CNES Report CT/PRT/SST/TH/331, Dec. 1982.

[52] Guillaumon, J.C., Guillin, J., "Paints, Potting Compounds and Silicone Varnishes with Low Outgassing in Space Environment", in ESA SP-145, "Spacecraft Materials in Space Environment", J. Dauphin & T.D. Guyenne, Eds., Proceedings of a Symposium held at ESTEC, Noordwijk, The Netherlands, Oct. 2-5, 1979, pp. 63-66.

[53] Guillaumon, J.C., Guillin, M.J., "Development of Low Outgassing Resins and Electrical Conductive Paints for Thermal Control and Space Applications", AIAA Paper No. 81-1182. AIAA 16th Thermophysics Conference, Palo Alto, California, June 23-25, 1981.

[54] Guillette, R.B., Brown, R.R., Seiler, R.F., Sheldon, W.R., "Effect of protons and Alpha Particles on Thermal Properties of Spacecraft and Solar Concentrator Coatings", in "Thermophysics and Temperature Control of Spacecraft and Entry Vehicles", Progress in Astronautics and Aeronautics, Vol. 18, G.B. Heller, Ed., Academic Press, New York, 1966, pp. 413-440.

[55] Hall, D.F., Fote, A.A., "Preliminary Flight Results from P78-2 (SCATHA) Spacecraft Contamination Experiment", in ESA SP-145, "Spacecraft Materials in Space Environment", J. Dauphin & T.D. Guyenne, Eds., Proceedings of a Symposium held at ESTEC, Noordwijk, The Netherlands, Oct. 2-5, 1979, pp. 81-90.

[56] Hall, D.F., Fote, A.A., "α_s/ε Measurements of Thermal Control Coatings on the P78-2 (SCATHA) Spacecraft", AIAA Paper No. 80-1530, , AIAA 15th Thermophysics Conference, Snowmass, Colorado, July 14-16, 1980. Also published in "Heat Transfer and Thermal Control", Progress in Astronautics & Aeronautics, Vol. 78, A.L. Crosbie, Ed., American Institute of Aeronautics and Astronautics, New York, 1981, pp. 467-486.

[57] Harada, Y., Private communication. IITRI, Chicago, Illinois, Jan. 30, 1981.

[58] Harada, Y., Wilkes, D.R., "Inorganic Zn_2TiO_4 Thermal Control Coatings", in "The Enigma of the Eighties: Environment, Economics, Energy", SAMPE National Business Office, Azusa, California, 1979, Vol. 24, Book 2, pp. 936-944.

[59] Heaney, J.B., "Evaluation of Commercially Supplied Silver Coated Teflon for Spacecraft Temperature Control Usage", NASA TM-X70588, Jan, 1974.

[60] Henninger, J.H., "Solar Absorptance and Thermal Emittance of Some Common Spacecraft Thermal-Control Coatings", NASA RP 1121, Apr. 1984.

[61] Hoffman, R.H., "Spaceflight Performance of Silver Coated FEP Teflon as a Thermal Control Surface on the IMP-I Spacecraft", NASA TM X-66242, April 1973.

[62] Hyman, N.L., "Solar Absorptance Degradation of OSR Radiators on the COMSTAR Satellites", AIAA Paper No. 81-1185. AIAA 16th Thermophysics Conference, Palo Alto, California, June 23-25, 1981.

[63] IITRI, "Price Schedule for IITRI Services in Spacecraft Thermal Control Materials", IIT Research Institute, Chicago, Illinois 60616, July 1974.

[64] INTA, "S-13 G/LO Coating. Outgassing Test No. I-305", Private communication. Test Performed on Aug. 2, 1976.

[65] INTA, "PCB Z Coating. Outgassing Test", Private communication. Test Performed on March 12, 1984.

[66] Jonhson, F.S., "Satellite Environment Handbook", 2nd ed. Stanford University Press, Stanford, California, 1965, Chap. 3, pp. 64-76.

[67] Joslin, D.E., Kan, H.K.A., "Properties of Conductive Coatings for Thermal Control Mirrors and Solar Cell Covers", in NASA SP-379, "Eight Conference Space Simulation", Proceedings of a Symposium held at Silver Spring, Maryland, Nov. 3-5, 1975, pp. 187-193.

[68] Katz, I., "Adhesive Materials, Their Properties and Usage", Foster Publishing Company, Long Beach, California, 1964, Part I, Chap. 6, pp. 44-54.

[69] Kemp, R.F., Beynon, J.C., Luedke, E.E., Hall, D.F., "Effects of Cesium Ions and Cesium Vapor on Selected ATS-F Samples", AIAA Paper No. 73-1099, AIAA 10th Electric Propulsion Conference, Lake Tahoe, Nevada, Oct. 31-Nov. 2, 19973.

[70] Keyte, G.E., "The Prospero Thermal Control Surfaces Experimental-Investigation of Thermal Control Surface Materials in Space Environment", RAE-TR-75123, Royal Aircraft Establishment, Farnborough, England, Dec. 1975.

[71] Kirkpatrick, J.P., Brennan, P.J., "The Advanced Thermal Control Flight Experiment", AIAA Paper No. 73-757, AIAA 8th Thermophysics Conference, Palm Springs, California, July 16-18 1973. Also Published in "Thermophysics and Spacecraft Thermal Control", Progress in Astronautics and Aeronautics, Vol. 35, R.G. Hering, Ed., The MIT Press, Cambridge, Massachusetts, 1974, pp. 409-430.

[72] Koch, J., "Some Current Developments in Solar Array Technology at AEG-Telefunken", in ESA SP-140, "Photovoltaic Generators in Space", K. Bogus & T.D. Guyenne, Eds., Proceedings of a Symposium held at ESTEC, Noordwijk, The Netherlands, Sept. 11-13, 1978, pp. 33-40.

[73] Koons, H.C., Mizera, P.F., Fennell, J.F., Hall, D.F., "Spacecraft Charging-Results from the SCATHA Satellite", Astronautics & Aeronautics, Vol. 18, No. 11, Dec. 1980, pp. 44-47.

[74] Kordsmeier, N.H., Peters, S.T., "Materials and Processes for Thermal Control Surfaces", in "Non-Metallic Materials Selection, Application and Environmental Effects", 4th National SAMPE Technical Conference and Exhibition, Palo Alto, California, 17-19 Oct. 1972, pp. 79-90.

[75] Kruczynski, L.R., "Astrodynamics", Astronautics & Aeronautics, Vol. 18, No. 12, Dec. 1980, pp. 32-33.

[76] Lehn, W.L., "New Space Materials Developments in the United States", in ESA SP-145, "Spacecraft Materials in Space Environment", J. Dauphin & T.D. Guyenne, Eds., Proceedings of a Symposium held at ESTEC, Noordwijk, The Netherlands, Oct. 2-5, 1979, pp. 37-47.

[77] Lévy, L., "Irradiations par Electrons de Revêtements de Contrôle Thermique", ONERA CERT DERTS EC 4050, Toulouse, France, Oct. 1976.

[78] Lévy, L., Sarrail, D., "Essai de Claquage sur un Echantillon de Paneau OSR de 65 mm x 65 mm Collés aves un Adhésif Conducteur", ONERA CERT DERTS EC 4052, Toulouse, France, Oct. 1976.

[79] Lewis, D.W., Thostesen, T.O., "Mariner-Mars Absorptance Experiment", in "Thermophysics and Temperature Control of Spacecraft and Entry Vehicles", Progress in

Astronautics and Aeronautics, Vol. 18, G.B. Heller, Ed., Academic Press, New York, 1965, pp. 441-457.

[80] Marshall, K.N., Breuch, R.A., "Optical Solar Reflector: A Highly Stable Low α_s/ε Spacecraft Thermal Control Surface", Journal of Spacecraft and Rockets, Vol. 5, No. 9, Sept. 1968, pp. 1051-1056.

[81] MASTER, "Departement Aerospatial", Master Peintures Pamiers, June, 1985.

[82] McCargo, M., Spradley, L.W., Greenberg, S.A., McDonald, S.L., "Review of the Transient Degradation/Contamination of Thermal Coatings", LMSC-D1778, (NAS 8-26004), Lockheed Missiles & Space Company, Sunnyvale, California, 1971.

[83] Millard, J.P., "An Uncertainty Analysis for Satellite Calorimetric Measurements", NASA TN D-4354, 1968.

[84] Millard, J.P., "Results from the Thermal Control Coatings Experiment on OSO-III", in "Thermal Design Principles of Spacecraft and Entry Bodies", Progress in Astronautics and Aeronautics, Vol. 21, J.T. Bevans, Ed., Academic Press, New York, 1969, pp. 769-795.

[85] Millard, J.P., Pearson, Jr., B.D., "Optical Stability of Coatings Exposed to Four Years Space Environment on OSO-III", AIAA Paper No. 73-734, AIAA 8th Thermophysics Conference, Palm Springs, California, July 16-18 1973. Also Published in "Thermophysics and Spacecraft Thermal Control", Progress in Astronautics and Aeronautics, Vol. 35, R.G. Hering, Ed., The MIT Press, Cambridge, Massachusetts, 1974, pp. 249-262.

[86] Millard, J.P., Streed, E.R., "A Comparison of Infrared-Emittance Measurements and Measurement Techniques", Applied Optics, Vol. 8, No. 7, July 1969, pp. 1485-1492.

[87] Miller, R.A., Campbell, F.J., "Effects of Low Energy Protons on Thermal Control Coatings", in "Thermophysics and Temperature Control of Spacecraft and Entry Vehicles", Progress in Astronautics and Aeronautics, Vol. 18, G.B. Heller, Ed., Academic Press, New York, 1966, pp. 399-412.

[88] Morelli, D., Private communication, OCLI, Santa Rosa, California, Oct. 23, 1974.

[89] MYSTIK, "Mystik Brand Industrial Tape Selector", and "Mystik Brand Insulation Tape Selector", Mystik Tape Division, Winnetka, Illinois 60093.

[90] Neel, C.B., "Measurement of Thermal-Radiation Characteristics of Temperature-Control Surfaces During Flight in Space", ISA Trans., Vol. 3, No. 2, pp. 108-122, April, 1964.

[91] Neel, C.B., "Role of Flight Experiments in the Study of Thermal-Control Coatings for Spacecraft", in "Thermophysics of Spacecraft and Planetary Bodies", Progress in Astronautics and Aeronautics, Vol. 20, G.B. Heller, Ed., Academic Press, New York, 1967, pp. 411-438.

[92] NFT 30-0 14, "Détermination du Temps d'Écoulement des Peintures, Vernis et Préparations Assimilées au Moyen des Coupes Françaises", Sept. 1983.

[93] OCLI, "Conductive Coated Second Surface Thermal Control Mirror - Product Specification 6068 002", OCLI Inc., P.O.B., 1599, Santa Rosa, California 95403, July 1974.

[94] OCLI, "Second Surface Thermal Control Mirror (Standard Type) - Product Specification 6065 002", OCLI Inc., P.O.B. 1599, Santa Rosa, California 95403, June 1980.

[95] Paillous, A., "Qualification des Revêtements de Contrôle Thermique aux Rayonnements Ultra-Violets et Parculaires de l'Espace. Rapport Final". ONERA CERT DERTS EC 4025, Toulouse, France, 1975.

[96] Paillous, A., "Degradation de Revêtements de Contrôle Thermique par Irradiations Ultravioletes et Particulaires", ONERA CERT DERTS EC 4047, Toulouse, France, Oct. 1976.

[97] Paillous, A., Amat, M.T., Marco, J., Panabiere, G., "Irradiations par Protons et Irradiations par Electrons de Revêtements de Contrôle Thermique et de Films Polymériques. Tome 1 - Partie Expérimentale. Rapport Final", ONERA CERT DERTS EC 4059, Toulouse, France, 1977.

[98] Paillous, A., Millan, Ph., "Irradiation Ultraviolette des Peintures Blanches Conductrices PCB-Z et PCB-T", ONERA CERT DERTS EC 4169, Toulouse, France, Mars, 1983.

[99] Pence, W.R., Grant, T.J., "α_s Measurements of Thermal Control Coatings on Navstar Global Positioning System Spacecraft", AIAA Paper No. 81-1186. AIAA 16th Thermophysics Conference, Palo Alto, California, June 23-25, 1981.

[100] Preuss, L., Schäfer, W., "Coating and Contamination Experiment on LDEF", in ESA SP-145, "Spacecraft Materials in Space Environment", J. Dauphin & T.D. Guyenne, Eds., Proceedings of a Symposium held at ESTEC, Noordwijk, The Netherlands, Oct. 2-5, 1979, pp. 71-80.

[101] PROCOLOR, Private communication, Procolor, Madrid, Oct. 28, 1974.

[102] Rajagopalan, R., Willson, W.J., "Thermal Performance of Anik-B Satellite on Orbit", AIAA Paper No. 80-1498, , AIAA 15th Thermophysics Conference, Snowmass, Colorado, July 14-16, 1980.

[103] Reichard, P.J., Triolo, J.J., "Preflight Testing of the ATS-1 Thermal Coatings Experiment", in "Thermophysics of Spacecraft and Planetary Bodies", Progress in Astronautics and Aeronautics, Vol. 20, G.B. Heller, Ed., Academic Press, New York, 1967, pp. 491-513.

[104] RHONE-POULENC, "Rhodorsil RTV 121", Informations Silicones Rhodorsil E-09-6, Rhone-Poulec, Département Silicones, 33, rue Jean Goujon, 75008 Paris, Cedex 08, Sept. 1978.

[105] Rittenhouse, J.B., Singletary, J.B., "Space Materials Handbook", 3rd ed., NASA SP-3051, 1969, pp. 485-493.

[106] Rolfo, A., "In Flight Results of a Cryogenic Cooler Designed for Meteosat", IAF 76-210, XXVII Congress International Astronautical Federation, Anaheim, California, Oct. 10-16, 1976.

[107] Rolfo, A., "In Flight Contamination and Charges in Thermo Optical Properties Measurements", AIAA Paper No. 81-1184. AIAA 16th Thermophysics Conference, Palo Alto, California, June 23-25, 1981.

[108] Rosen, A., "Large discharges and Arcs on Spacecraft", Astronautics & Aeronautics, Vol. 13, No. 6, June 1975, pp. 36-44.

[109] Scannapieco, J.F., "Final Report of Thermal Vacuum Weight Loss Study of Cat-a-Lac and 3M Velvet Black Paints", Radnor Project 73PO57, General Electric, Missile and Space Division, Philadelphia, Pensylvania, Feb. 1967.

[110] Schafer, C.F., Bannister, T.C., "Thermal Control Coating Degradation Data from the Pegasus Experiment Packages", in "Thermophysics of Spacecraft and Planetary Bodies", Progress in Astronautics and Aeronautics, Vol. 20, G.B. Heller, Ed., Academic Press, New York, 1967, pp. 457-473.

[111] SCHJELDAHL, Data Sheets G 4001, G 4002, G 4008, G 4015 and G 4019, "Capability Bulletin - Thermal Control Materials", Schjel-Bond, Product Bulletin No. EP-301, G.T. Schejeldahl Company, Northfield, Minnesota 55057.

[112] Schroeder, C.J., "Insulation Commonality Assessment (Phase 1), Vol. 2", NASA CR-124473, Feb. 1973, clause 16.9, pp. 12-36.

[113] Scollon, T.R., Carpitella, M.J., "Long Life High Reliability Thermal Control Systems Study Data Handbook", Contract NAS 8-26252, Space Systems Organization, General Electric Company, Valley Forge Space Technology Center, Philadelphia, Pennsylvania, 1970.

[114] Seidenberg, B., Park, J.J., Clatterbuck, C., "Achievement of a Low-Outgassing White Paint System for Spacecraft Thermal Control", NASA TN D-6892, August 1972.

[115] Sidney Gross, "Modern Plastics Encyclopedia", McGraw-Hill Publications Company, New York, 1970, pp. 868-869.

[116] Siliconas Hispania, Private communication, Barcelona, 1 Oct. 1985.

[117] Simon, J., "Actions des Ultra-Violets sur les Materiaux de Controle Thermique et Confrontation des Essais en Laboratoire avec les Performances Enregistréss en Vol", Séminaire International Simulation et Espace, Toulouse, France, Sept. 10-14, 1973.

[118] Simon, J., "Influence de la Temperature sur la Degradation des Revêtements de Contrôle Thermique Soumis a des Radiations Ultra-Violettes sous Vide", in "Evaluation de l'Action de l'Environnement Spatial sur les Materiaux", Centre National d'Etudes Spatiales, Toulouse, France, June 1974.

[119] Spisz, E.W., Jack, J.R., "Thermal and Radiative Property Measurement of Thermal-Control Coatings by Cyclic Radiation", NASA TN D-6316, Apr. 1971.

[120] Stevens, N.J., "Application of Sert II Thermal Control Coatings", NASA TM X-2155, Feb. 1971.

[121] Stevens, N.J., Smolak, G.R., "Report on the Flight Performance of the Z-93 White Paint Used in the Sert II Thermal Control System", in "Fundamental of Spacecraft Thermal Design", Progress in Astronautics and Aeronautics, Vol. 29, J.W. Lucas, Ed., The MIT Press, Cambridge, Massachusetts, 1972, pp. 189-204.

[122] Stultz, J.W., "Solar Absorptance of Second Surface Mirrors for High Angles of Incidence", AIAA Paper No. 74-670, AIAA-ASME 1974 Thermophysics and Heat Transfer Conference, Boston, Massachusetts, July 15-17, 1974.

[123] Stultz, J.W., "Solar Absorptance of Second Surface Mirrors for High Angles of Incidence", Journal of Spacecraft and Rockets, Vol. 13, No. 1, Jan. 1976, pp. 57-59.

[124] Taylor, J.W.R., Jane's all the World's Aircraft, 1977-1978", MacDonald and Jane's Publishers Ltd., London, 1977, pp. 745-746.

[125] Taylor, J.W.R., "Jane's all the World's Aircraft", 1979-1980", MacDonald and Jane's Publishers, Ltd., London, 1979, pp. 677 and 680.

[126] Touloukian, Y.S., DeWitt, D.P., Hernicz, R.S., "Thermal Radiative Properties. Coatings", Thermophysical Properties of Matter, Vol. 9, IFI/Plenum, New York, 1972.

[127] Toyama, M., Ito, T., "Pressure-Sensitive Adhesives", in "Polymer-Plastics Technology and Engineering", Vol. 2, L. Naturman, Ed., Marcel Dekker, Inc., New York, 1974, pp. 161-230.

[128] Triolo, J.J., "General Aspects of Space Simulation Validity and Comparison between Laboratory and In-Flight Degradation", Séminaire International Simulation et Espace, Toulouse, France, Sept. 10-14, 1973.

[129] Triolo, J.J., Heaney, J.B., Hass, G., "Coatings in Space Environment", SPIE Vol. 121, Optics an Adverse Environment, Proceedings of the Seminar, San Diego, California, Aug. 25-26, 1977. Society of Photo-Optical Instrumentation Engineers, Bellingham, Washington, 1978, pp. 45-66.

[130] Van Wazer, J.R., Lyons, J.W., Kim, K.Y., Colwell, R.E., "Viscosity and Flow Measurement", Interscience Publishers, New York, 1963, Chap. 4, pp. 258-262.

[131] Weast, R.C., "Handbook of Chemistry and Physics", 57th ed., CRC Press, Inc., Cleveland, Ohio, 1976, p. F-170.

[132] Westcott, M., "The Measurement of Solar Absorptance and Thermal Emittance", ESRO TN-23 (ESTEC), Jan. 1968.

[133] Wilkens, W., Private communication, DFVLR, Braunschweig, Germany, March 19, 1981.

[134] Winkler, W., "Helios Surface Materials, Test-Predictions and Test-Results of Orbit Conditions Compared with Mission Results", in NASA SP-379, "Eight Conference on Space Simulation", Proceedings of a Symposium held at Silver Spring, Maryland, Nov. 3-5, 1975, pp. 51-61.

[135] Winkler, W., "Improved Model for Performance of Spacecraft Materials", Acta Astronautica, Vol. 4, No. 5-6, May-June 1977, pp. 709-726.

[136] Winkler, W., Brungs, W., "Helios Surface Materials Prediction for Orbit and Mission Results", IAF 75-021, XXVI Congress International Astronautical Federation, Lisbon, Sept. 21-27, 1975. Also published in Acta Astronautica, Vol. 3, No. 5-6, May-June 1976, pp. 395-406.

[137] Winkler, W., Brungs, W., "Helios Surface Materials, Predictions for Orbit and Mission Results", Acta Astronautica, Vol. 3, No. 5-6, May-June 1976, pp. 395-406.

[138] Winkler, W., Stampfl, P., "Conductive Coatings (CC) a Concept to Achieve Electrostatic Cleanliness (ESC) on Satellites Completely Covered with Dielectric Materials. Scientific Requirements and Practical Approach on the Sunprobe Helios", in "Evaluation de l'Action de l'Environnement Spatial sur les Materiaux", Centre National d'Etudes Spatiales, Toulouse, France, June 1974, pp. 45-55.

[139] Winkler, W., Stampfl, W., "Conductive Coatings: Problem of Electrostatic Clealiness", Acta Astronautica, Vol. 2, No. 7-8, July-August 1975, pp. 745-754.

[140] Zerlaut, G.A., Courtney, W.J., "Space-Simulation Facility for In Situ Reflectance Measurements", in "Thermophysics of Spacecraft and Planetary Bodies", Progress in Astronautics and Aeronautics, Vol. 20, G.B. Heller, Ed., Academic Press, New York, 1967, pp. 349-369.

[141] Zerlaut, G.A., Gilligan, J.E., Ashford, N.A., "Space Radiation Environmental Effects on Reactively Encapsulated Zinc Orthotitanates and Their Paints", in "Fundamentals of Spacecraft Thermal Design", Progress in Astronautics and Aeronautics, Vol. 29, J.W. Lucas, Ed., The MIT Press, Cambridge, Massachusetts, 1972, pp. 3-32.

[142] Zerlaut, G.A., Harada, Y., Tompkins, E.H., "Ultraviolet Irradiation of White Spacecraft Coatings in Vacuum", in NASA SP-55, "Symposium on Thermal Radiation of Solids", Proceedings of a Symposium held at San Francisco, California, March 4-6, 1964, pp. 391-420.

[143] Zerlaut, G.A., Noble, G., Rogers, F.O., "Development of Space Stable Thermal Control Coatings", Report No. IITRI-U6002-59, (NAS 8-5379), ITT Research Institute, Chicago, Illinois, 1968.

[144] Zerlaut, G.A., Rogers, F.O., Noble, G., "The Development of S-13 G-Type Thermal Control Coatings", in "Thermal Design Principles of Spacecraft and Entry Bodies", Progress in Astronautics and Aeronautics, Vol. 21, J.T. Bevans, Ed., Academic Press, New York, 1969, pp. 741-766.

[145] Zwaal, A., Private communication, Noordwijk, 13 March 1986.